THE MICROBIAL MODULATION OF AUTOIMMUNE PROCESSES AND PROINFLAMMATORY PATHWAYS

EDITED BY: Elias Adel Rahal, Margret Shirinian and Daniele Dessì
PUBLISHED IN: Frontiers in Cellular and Infection Microbiology

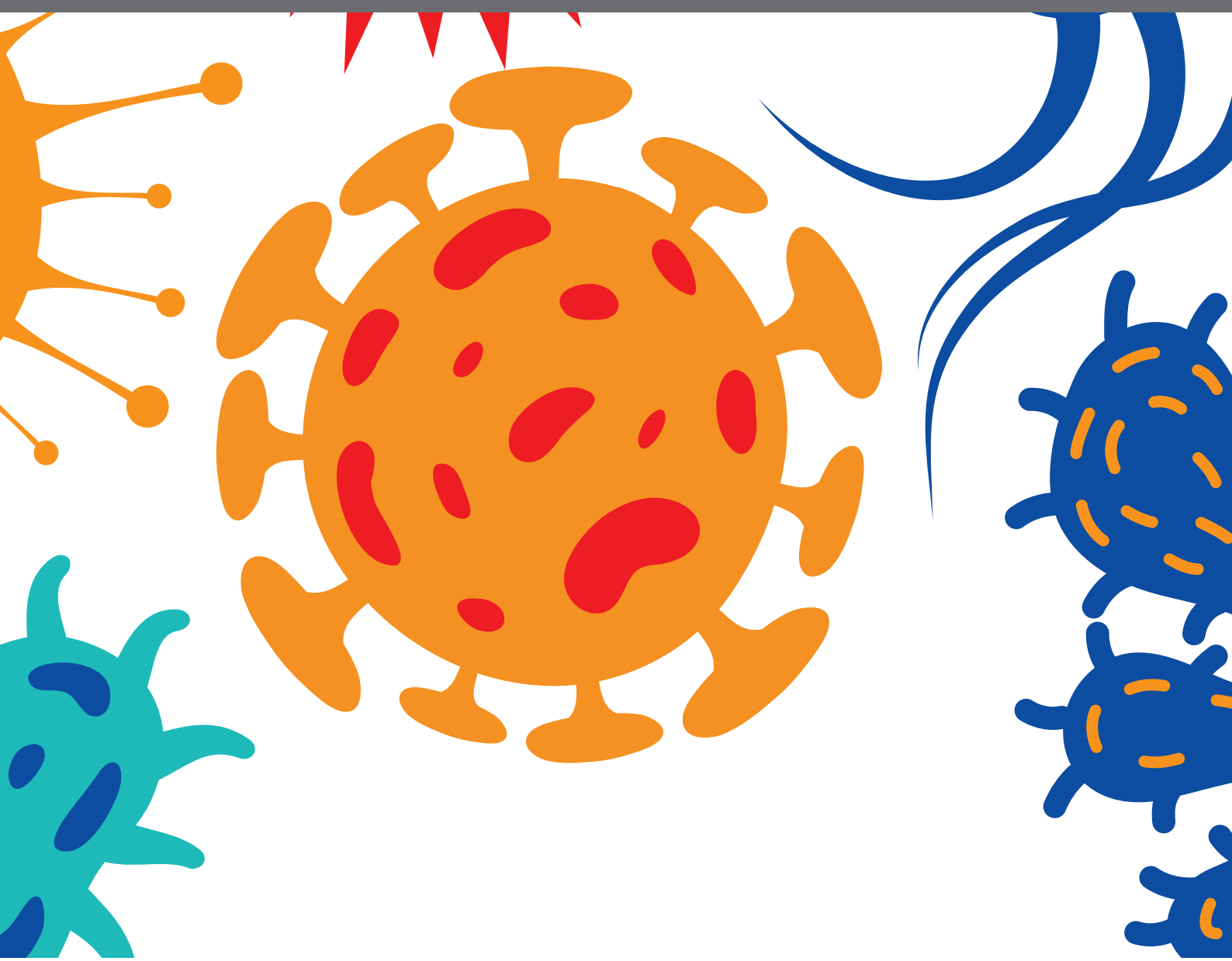

frontiers Research Topics

frontiers

ISSN 1664-8714
ISBN 978-2-88976-932-2
DOI 10.3389/978-2-88976-932-2

About Frontiers

Frontiers is more than just an open-access publisher of scholarly articles: it is a pioneering approach to the world of academia, radically improving the way scholarly research is managed. The grand vision of Frontiers is a world where all people have an equal opportunity to seek, share and generate knowledge. Frontiers provides immediate and permanent online open access to all its publications, but this alone is not enough to realize our grand goals.

Frontiers Journal Series

The Frontiers Journal Series is a multi-tier and interdisciplinary set of open-access, online journals, promising a paradigm shift from the current review, selection and dissemination processes in academic publishing. All Frontiers journals are driven by researchers for researchers; therefore, they constitute a service to the scholarly community. At the same time, the Frontiers Journal Series operates on a revolutionary invention, the tiered publishing system, initially addressing specific communities of scholars, and gradually climbing up to broader public understanding, thus serving the interests of the lay society, too.

Dedication to Quality

Each Frontiers article is a landmark of the highest quality, thanks to genuinely collaborative interactions between authors and review editors, who include some of the world's best academicians. Research must be certified by peers before entering a stream of knowledge that may eventually reach the public - and shape society; therefore, Frontiers only applies the most rigorous and unbiased reviews.
Frontiers revolutionizes research publishing by freely delivering the most outstanding research, evaluated with no bias from both the academic and social point of view. By applying the most advanced information technologies, Frontiers is catapulting scholarly publishing into a new generation.

What are Frontiers Research Topics?

Frontiers Research Topics are very popular trademarks of the Frontiers Journals Series: they are collections of at least ten articles, all centered on a particular subject. With their unique mix of varied contributions from Original Research to Review Articles, Frontiers Research Topics unify the most influential researchers, the latest key findings and historical advances in a hot research area! Find out more on how to host your own Frontiers Research Topic or contribute to one as an author by contacting the Frontiers Editorial Office: frontiersin.org/about/contact

THE MICROBIAL MODULATION OF AUTOIMMUNE PROCESSES AND PROINFLAMMATORY PATHWAYS

Topic Editors:
Elias Adel Rahal, American University of Beirut, Lebanon
Margret Shirinian, American University of Beirut, Lebanon
Daniele Dessì, University of Sassari, Italy

Citation: Rahal, E. A., Shirinian, M., Dessì, D., eds. (2022). The Microbial Modulation of Autoimmune Processes and Proinflammatory Pathways.
Lausanne: Frontiers Media SA. doi: 10.3389/978-2-88976-932-2

Table of Contents

frontiers | Frontiers in Cellular and Infection Microbiology

TYPE Editorial
PUBLISHED 02 August 2022
DOI 10.3389/fcimb.2022.969610

OPEN ACCESS

EDITED AND REVIEWED BY
Annemarie H. Meijer,
Leiden University, Netherlands

*CORRESPONDENCE
Elias A. Rahal
er00@aub.edu.lb
Margret Shirinian
ms241@aub.edu.lb
Daniele Dessì
danieled@uniss.it

SPECIALTY SECTION
This article was submitted to Microbes and Innate Immunity, a section of the journal Frontiers in Cellular and Infection Microbiology

RECEIVED 15 June 2022
ACCEPTED 24 June 2022
PUBLISHED 02 August 2022

CITATION
Rahal EA, Shirinian M and Dessì D (2022) Editorial: the microbial modulation of autoimmune processes and proinflammatory pathways. *Front. Cell. Infect. Microbiol.* 12:969610. doi: 10.3389/fcimb.2022.969610

Editorial: The microbial modulation of autoimmune processes and proinflammatory pathways

Elias A. Rahal[1,2]*, Margret Shirinian[1,2]* and Daniele Dessì[3]*

[1]Department of Experimental Pathology, Immunology and Microbiology, American University of Beirut, Beirut, Lebanon, [2]Center for Infectious Disease Research, American University of Beirut, Beirut, Lebanon, [3]Dipartimento di Scienze Biomediche, Università Degli Studi di Sassari, Sassari, Italy

KEYWORDS

dysbiosis, inflammation, autoimmune diseases, microbiome, infection

Editorial on the Research Topic
The microbial modulation of autoimmune processes and proinflammatory pathways

Microbial agents, whether they are part of the human microbiome or extrinsic organisms, can modulate immune processes, potentially resulting in exacerbated inflammatory responses or their amelioration; microbial products can also play similar roles. This may favor or curb the initiation of a proinflammatory disorder or alter the course of an ongoing disease. Mirroring the effect of microbial agents on modulation of immune responses, an inflammatory disease may shape an individual's microbiome, resulting in modification of the disease state (Belkaid and Hand, 2014). Hence, a two-way street exists between the organisms we harbor and our immune processes. With the Research Topic "*The Microbial Modulation of Autoimmune Processes and Proinflammatory Pathways*," we aimed at examining the various facets of how microbial organisms and inflammatory conditions affect each other. The Research Topic comprises eight papers that investigate the roles played by members of the microbiota in modulating inflammation and vice versa, pathways that play a role in these processes, alterations in immune processes induced by microbial products, and the prognostic value of particular markers of inflammation in certain infections.

The study by Yu et al. examines the fecal microbiome of rheumatoid arthritis (RA) patients and controls using 16S rDNA sequencing. The authors also used liquid chromatography–tandem mass spectrometry (LC-MS/MS) to conduct metabolic profiling of the fecal samples. While previous studies have focused on the roles that butyrate and short-chain fatty acids may play in decreasing the severity of arthritis (Rosser et al., 2020; Martinsson et al., 2022), this is the first study to systematically examine the full spectrum of changes in the gut flora as well as the metabolomic profile in RA. The study reveals alterations in the abundances of several genera and in the levels of a number of metabolites; data indicate that dysbiosis and dysregulation of several

pathways, including those of the metabolism of tryptophan, alpha-linolenic acid, and glycerophospholipid, may play a significant role in the development of RA. This may highlight novel biomarkers as well as therapeutic avenues for this disease.

On the other hand, Toyofuku et al. studied the effect of haploinsufficiency of A20 (HA20) on the gut microbiome of affected subjects. HA20 is a relatively recently described autoinflammatory disorder resulting from dysregulation of NF-kB signaling (Aeschlimann et al., 2018). Not only did the study included in the Research Topic at hand show dysbiosis in HA20 patients, the severity of the disease was also associated with a lower number of operational taxonomic units (OTUs). Moreover, the study revealed that *Streptococcus mutans* and *Lactobacillus salivarius* may increase in patients with autoantibodies compared with those who do not have such autoantibodies. The implications of these finding on the management or prognosis of HA20 require further investigations.

The study by Khadka et al. demonstrates that administration of curcumin monoglucuronide (CMG) to the experimental autoimmune encephalomyelitis (EAE) mouse model of multiple sclerosis modulated the disease state. Moreover, this treatment altered the fecal and ileal microbiota. A correlation between the severity of EAE and the ileal microbiota was also noted. The administration of curdlan to the same mouse model by Sato et al. worsened the disease condition, resulting in enhanced central nervous system infiltration and increased proinflammatory cytokine levels. In contrast, administration of curdlan to the viral mouse model of MS, the Theiler's murine encephalomyelitis virus-induced demyelinating disease (TMEV-IDD) model, ameliorated the disease severity. These studies may indicate that the specific underlying cause of a disease should be considered when developing a management plan. The implication here is that two patients with the same inflammatory disorder may not respond in a similar manner depending on the disease triggering or exacerbating conditions.

In exploring the roles ASB17 plays in immune processes, Wan et al. observed that it mediates NF-kB signal activation and subsequent cytokine production; this occurs *via* stabilizing TRAF6 by inhibiting the latter's ubiquitination. The indicated observations were made in bone marrow–derived dendritic cells (BMDCs) stimulated with lipopolysaccharide (LPS). ASB17 is an ankyrin repeat and SOCS box-containing protein (ASB) family member whose biological roles are still under investigation; hence, this study sheds light on this mediator, revealing its relevant role in the regulation of cytokine production in response to microbial products. The immunomodulatory effects of another microbial product, Shiga toxin type 2a (Stx2a), were examined by Rosso et al. This bacterial toxin is usually produced by particular strains of *Escherichia coli* that can result in bloody diarrhea and hemolytic uremic syndrome (HUS), a kidney-affecting, potentially fatal disorder (Joseph et al., 2020). In the study by Rosso et al., Stx2a-stimulated human glomerular endothelial cells activated γδ T cells and induced the production of proinflammatory cytokines by these T cells as well as favored their differentiation toward a Th1-like profile. This is the first report to describe a possible role for human γδ T cells in the pathogenesis of Shiga toxin–associated HUS.

On the other hand, a study by Zheng et al. shows that higher blood D-dimer (D-d) levels correlate with disease severity in children with *Mycoplasma pneumoniae* pneumonia (MPP). D-d is a fibrinolysis product that is often correlated with inflammatory conditions (Ala et al., 2019; Ge et al., 2019; Zhang et al., 2021; Feng et al., 2022). Not only did the levels of D-d correlate with the length of hospital stay and the duration of fever in these patients, levels of this marker also correlated with those of inflammatory mediators, such as IL-6 and IFN-γ. On the other hand, the study by Qi et al. demonstrates that higher blood levels of acetic acid correlate with mortality in *Pseudomonas aeruginosa* ventilator-associated pneumonia. Increased acetic acid levels were also associated with decreased blood levels of lymphocytes and monocytes; this may provide some mechanistic insight as to how acetic acid results in a poor prognosis, which merits further exploration. Hence, both of these studies provide novel prognostic markers that may reflect the inflammatory status as well as the severity of particular types of pneumonia.

Overall, the collection of papers in this Research Topic highlight various novel means by which microbes or their products and immune responses shape each other. Such studies often suggest intervention modes that may prove useful in the alleviation of inflammatory disease conditions triggered or exacerbated by microbial agents.

Author contributions

All authors listed have made a substantial, direct, and intellectual contribution to the work and approved it for publication.

Funding

ER is supported by grants from the American University of Beirut-Medical Practice Plan (MPP), the Lebanese National Council for Scientific Research (L-CNRS) and the Asmar Fund. MS is funded by the American University of Beirut-Medical Practice Plan (MPP), the Lebanese Council for Scientific Research (CNRS) and the King Hussein Cancer Research Award. DD is supported by University of Sassari, Grant FAR 2020.

Acknowledgments

We would like to thank the authors of the papers included in this Research Topic as well as the reviewers who contributed to assessing these studies. We also wish to thank the Frontiers

editorial team, particularly members of the Frontiers in Cellular and Infection Microbiology editorial office, for their hard work.

Conflict of interest

The authors declare that the research was conducted in the absence of any commercial or financial relationships that could be construed as a potential conflict of interest.

Publisher's note

References

Aeschlimann, F. A., Batu, E. D., Canna, S. W., Go, E., Gul, A., Hoffmann, P., et al. (2018). A20 haploinsufficiency (HA20): Clinical phenotypes and disease course of patients with a newly recognised NF-kB-mediated autoinflammatory disease. *Ann. Rheum Dis.* 77 (5), 728–735. doi: 10.1136/annrheumdis-2017-212403annrheumdis-2017-212403

Ala, C. K., Banerjee, K., Chahine, J., Verma, B., Kumar, A., Furqan, M., et al. (2019). D-dimer as a novel marker of inflammation in pericarditis. *J. Am. Coll. Cardiol.* 73 (9), 984–984. doi: 10.1016/S0735-1097(19)31591-8

Belkaid, Y., and Hand, T. W. (2014). Role of the microbiota in immunity and inflammation. *Cell* 157 (1), 121–141. doi: 10.1016/j.cell.2014.03.011S0092-8674(14)00345-6

Feng, J. Q., Li, J., Li, Y. X., Jin, Y. Y., Du, F., and Chen, X. X. (2022). Elevated serum d-dimer may reflect the presence of gut inflammation in spondyloarthritis. *Front. Med.* 8. doi: 10.3389/Fmed.2021.816422

Ge, Y. L., Liu, C. H., Wang, N., Xu, J., Zhu, X. Y., Su, C. S., et al. (2019). Elevated plasma d-dimer in adult community-acquired pneumonia patients is associated with an increased inflammatory reaction and lower survival. *Clin. Lab.* 65 (1-2), 131–138. doi: 10.7754/Clin.Lab.2018.180720

Joseph, A., Cointe, A., Mariani Kurkdjian, P., Rafat, C., and Hertig, A. (2020). Shiga toxin-associated hemolytic uremic syndrome: A narrative review. *Toxins (Basel)* 12 (2), E67. doi: 10.3390/toxins12020067toxins12020067

Martinsson, K., Durholz, K., Schett, G., Zaiss, M. M., and Kastbom, A. (2022). Higher serum levels of short-chain fatty acids are associated with non-progression to arthritis in individuals at increased risk of RA. *Ann. Rheum Dis.* 81 (3), 445–447. doi: 10.1136/annrheumdis-2021-221386annrheumdis-2021-221386

Rosser, E. C., Piper, C. J. M., Matei, D. E., Blair, P. A., Rendeiro, A. F., Orford, M., et al. (2020). Microbiota-derived metabolites suppress arthritis by amplifying aryl-hydrocarbon receptor activation in regulatory b cells. *Cell Metab.* 31 (4), 837–851.e810. doi: 10.1016/j.cmet.2020.03.003

Zhang, W., Sang, L., Shi, J. R., Zhong, M., Jiang, L., Song, B., et al. (2021). Association of d-dimer elevation with inflammation and organ dysfunction in ICU patients with COVID-19 in wuhan, China: a retrospective observational study. *Aging-Us* 13 (4), 4794–4810. doi: 10.18632/aging.202496

frontiers in Cellular and Infection Microbiology

ORIGINAL RESEARCH
published: 29 April 2021
doi: 10.3389/fcimb.2021.669409

Association of Increased Circulating Acetic Acid With Poor Survival in *Pseudomonas aeruginosa* Ventilator-Associated Pneumonia Patients

Xiaoling Qi†, Li Zhang†, Jing Xu, Zheying Tao, Xiaoli Wang, Yuzhen Qiu, Tingting Pan, Zhaojun Liu, Hongping Qu, Ruoming Tan and Jialin Liu**

Department of Critical Care Medicine, Ruijin Hospital, Shanghai Jiao Tong University School of Medicine, Shanghai, China

OPEN ACCESS

Edited by:
Elias Adel Rahal, American University of Beirut, Lebanon

Reviewed by:
Benjamin G. Wu, New York University, United States
Huma Ali, Jinnah Sindh Medical University, Pakistan
Laurent Gorvel, INSERM U1068 Centre de Recherche en Cancérologie de Marseille (CRCM), France

***Correspondence:**
Jialin Liu
ljl11243@rjh.com.cn
Ruoming Tan
sandratan37@hotmail.com

†These authors have contributed equally to this work

Specialty section:
This article was submitted to Microbes and Innate Immunity, a section of the journal Frontiers in Cellular and Infection Microbiology

Received: *18 February 2021*
Accepted: *14 April 2021*
Published: *29 April 2021*

Citation:
Qi X, Zhang L, Xu J, Tao Z, Wang X, Qiu Y, Pan T, Liu Z, Qu H, Tan R and Liu J (2021) Association of Increased Circulating Acetic Acid With Poor Survival in Pseudomonas aeruginosa Ventilator-Associated Pneumonia Patients. Front. Cell. Infect. Microbiol. 11:669409. doi: 10.3389/fcimb.2021.669409

Background: We previously found that microbial disruption in *Pseudomonas aeruginosa* ventilator-associated pneumonia (PA-VAP) patients are long-lasting. Long-term microbial dysbiosis may lead to changes in metabolites. Short-chain fatty acids (SCFAs) are microbial fermentation products and show beneficial effects in patients with pneumonia. In this study, we aimed to explore the association between circulating SCFA levels and clinical outcomes in patients with PA-VAP.

Methods: In this study, we analyzed SCFAs in the serum of 49 patients with PA-VAP by gas chromatography-mass spectrometry analysis. Twenty of these patients died, and 29 survived. The correlation between serum SCFAs and patient survival and immune parameters was analyzed.

Results: We developed a partial least squares discriminant analysis (PLS-DA) model to examine differential SCFAs in 49 patients with PA-VAP. Among the seven SCFAs, only acetic acid was increased in non-survivors ($P = 0.031$, VIP > 1). Furthermore, high levels of acetic acid (>1.96ug/ml) showed increased 90-day mortality compared to low levels of acetic acid (<1.96ug/ml) in Kaplan-Meier survival analyses ($P = 0.027$). Increased acetic acid also correlated with reduced circulating lymphocyte and monocyte counts.

Conclusion: Our study showed that increased circulating acetic acid is associated with 90-day mortality in PA-VAP patients. The decrease in lymphocytes and monocytes might be affected by acetic acid and involved in the poor prognosis.

Keywords: *Pseudomonas aeruginosa*, ventilator-associated pneumonia, short-chain fatty acid, lymphocyte, monocyte

Abbreviations: PA-VAP, *Pseudomonas aeruginosa* ventilator-associated pneumonia; SCFAs, short-chain fatty acids; PCA, Principal Component Analysis; PLS-DA, partial least squares discriminant analysis; VAP, ventilator-associated pneumonia; ICUs, intensive care units; CBA, cytometric bead array; VIP, Variable Importance in Projection; HDACs, histone deacetylases; BMI, body mass index; SOFA, Sequential Organ Failure Assessment; APACHE, Acute Physiology and Chronic Health Evaluation; CPIS, clinical pulmonary infection score; MCP-1, Monocyte chemotactic protein-1; RANTES, regulated upon activation of normal T cells expressed and secreted; VEGF, vascular endothelial growth factor.

INTRODUCTION

Pseudomonas aeruginosa (PA) is a common cause of ventilator-associated pneumonia (VAP) (Sader et al., 2014; Borgatta et al., 2017). It was reported that 10%-20% of patients with PA colonization might develop VAP (Köhler et al., 2010). Only approximately 70% of PA-VAP cases can be cured despite optimizing current antimicrobial strategies (Crandon et al., 2016). In addition, patients harboring multidrug-resistant PA in the respiratory tract have a higher risk of death than those with PA colonization (Borgatta et al., 2017). These observations suggest the need for a reassessment of the treatment for PA-VAP.

In our previous study, we found that the lung microbiota of patients with PA-VAP changes significantly (Qi et al., 2018). Recent studies have also found that gut microbial dysbiosis occurs in most critically ill patients, including VAP patients (Dickson, 2016; Shimizu et al., 2018). Microbial dysbiosis in patients with VAP is characterized by decreased diversity and the disappearance of beneficial commensals (Ruppé et al., 2018), and the degree of microbial dysbiosis is related to the prognosis of the patient (Guarner and Malagelada, 2003; Shimizu et al., 2011). Multi-omic analysis has shown that microbial-derived metabolites usually drive microbiota changes in patients with a respiratory infection (Stewart et al., 2018; Bowerman et al., 2020), suggesting changes in microbial-derived metabolites might have an impact on the outcome of these patients.

Short-chain fatty acids (SCFAs) are the products of colonic microbial fermentation and can be absorbed in the gut and then drain into the circulation (Zaiss et al., 2019). They play an essential role in local microbiome balance and are likely to have a broad impact on the host immune system (Koh et al., 2016). SCFAs act on a variety of immune cells, including neutrophils, dendritic cells (Trompette et al., 2014), macrophages (Wu et al., 2020), T lymphocytes (Trompette et al., 2018), and B lymphocytes (Sanchez et al., 2020). They can reduce the recruitment and migration of dendritic cells and macrophages, and inhibit the proliferation and cytokine secretion of T cells (Gonçalves et al., 2018; Yao et al., 2020). Because SCFAs can dampen immune responses, they have a protective effect on various chronic inflammatory diseases, such as asthma and inflammatory bowel disease (Gonçalves et al., 2018).

Recent studies have shown that the anti-inflammatory properties of SCFAs could also reduce lung damage during respiratory infections (Trompette et al., 2018; Li et al., 2021). In addition, it was reported that SCFAs enhanced the effects of CD8+ T cells and macrophages to protect against respiratory infection (Trompette et al., 2018; Wu et al., 2020). These results suggested that SCFAs could also enhance the immune response. However, the role of SCFAs in the immune response was regulated by their concentration. Different from the enhancing effect of low dose-SCFAs, high-dose SCFAs can dampen innate and adaptive immune response during infections (Ciarlo et al., 2016; Sanchez et al., 2020). Besides, a recent study observed that SCFAs increase in chronic rhinosinusitis patients infected with PA (Cho et al., 2020). It was proved that SCFAs could promote pathogenically (PA and Escherichia coli) growth (Zumbrun et al., 2013; Ciarlo et al., 2016; Cho et al., 2020). Given the multiple effects of SCFAs, it is difficult to define whether they are beneficial or detrimental during bacterial infection. Clinical research is needed to clarify the role of SCFAs in those patients. Therefore, we conducted a prospective study to explore the association between serum SCFA levels and clinical outcomes in patients infected with PA.

METHODS

Subjects

This prospective study was conducted in intensive care units (ICUs) between March 2016 and March 2020. Patients diagnosed with PA-VAP met the following criteria: (1) mechanical ventilation for more than 48 hours; (2) met at least two of the following: body temperature > 38°C or < 36°C; peripheral white blood cell count > 10 × 10^9/L or < 4 × 10^9/L; or purulent secretions; (3) new or progressive chest infiltrates, and a second evaluation was conducted for patients with underlying cardiopulmonary disease; (4) secretions of lower respiratory tract cultured PA at least +2 growth using semi-quantitative measurements. Exclusion criteria included: (1) age below 18 years; (2) pregnant women; (3) secretions of lower respiratory tract positively cultured PA before or within 48 hours of mechanical ventilation; (4) patients with structural lung disease. The clinical data collection started at hospital admission and ended at study withdrawal, discharge, or death. Healthy people were also included as a control group. Written informed consent was obtained from enrolled patients or their guardians. This study was approved by the Ruijin Hospital Ethics Committee of Shanghai Jiao Tong University School of Medicine (approval number 2012-82).

Sample Collection

Peripheral venous blood was collected in vacutainer tubes on the first day of PA-VAP diagnosis. After blood collection, the serum of samples was collected by centrifugation (2,000 rpm, 10 min, 4°C) and stored at -80°C for SCFA and cytokine analysis.

SCFA Analysis

For SCFA analysis, 50% H_2SO_4 (50 μL) was added to serum (50 μL) for acidification, and an internal standard (2-Methylvaleric acid) was used for gas chromatography-mass spectrometry (GC-MS) analysis. An Agilent 7890B gas chromatograph system coupled with an Agilent 5977B mass spectrometer fitted with a capillary column (HP-FFAP 30 m × 250 μm × 0.25 μm) was used for GC-MS analysis. An Agilent chemstation was used for chromatographic peak extraction and quantitative analysis. The standard curve of SCFA concentration was calculated according to the ratio of SCFAs and the internal standard chromatographic peak area. Seven SCFAs, acetic acid, propionic acid, isobutyric acid, butyric acid, isovaleric acid, valeric acid, and hexanoic acid were quantified.

Immune Cell Quantification and Cytokine Detection

Immune cell quantification was conducted by Beckman Coulter LH750. Cytometric bead array (CBA) was used to detect cytokines in the serum of patients with PA-VAP. CBA kits of cytokines (IL-2, IL-6, IL-7, IL-8, IL-10, MCP-1, RANTES, VEGF) were provided by BD Biosciences (BD Biosciences, Franklin Lakes, NJ, USA). The standard was diluted to eight different concentrations, and one blank was prepared. The standard and the serum sample (50 μL) were mixed with the microspheres and incubated for 1 h at room temperature. PE-labelled cytokine antibody was added to all samples and incubated for 1 h at room temperature in the dark. All samples were washed and suspended for detection using an Accuri C6 system (BD Biosciences, Franklin Lakes, NJ, USA).

Statistical Analysis

The difference of SCFAs was calculated using unsupervised Principal Component Analysis (PCA) and supervised Partial Least Square-Discriminant Analysis (PLS-DA). The variable projection importance (VIP) is calculated by the PLS-DA model to measure each metabolite's impact on the classification and discrimination of each group of samples, thereby assisting screening metabolic markers. VIP values >1.0 suggest that the metabolite has significant differences between groups. VIP values and the Mann-Whitney U test were both used to assist in the screening of differential SCFAs. Clinical data were processed using SPSS version 23 (IBM Corp., Armonk, NY, USA). Differences between the two groups were tested using a two-tailed t-test, Mann-Whitney U test, or Chi-squared test as appropriate, and the significance level was set at 0.05 (2-tailed). The correlation between SCFA and clinical data and immune parameters was calculated using Spearman correlation analysis. Figures were created using GraphPad Prism version 6.0.

RESULTS

Patient Characteristics

A total of 49 PA-VAP patients were included in this study, of which 20 patients died in the ICU and 29 patients survived (**Figure 1**). Baseline characteristics of all patients were collected during the first 24 hours of PA-VAP diagnosis (**Table 1**). Within the PA-VAP patients, 21 patients were admitted to the ICU due to medical diseases, 26 patients following surgery, and two patients following trauma. The type of disease at admission showed a significant difference between survivors and non-survivors (P = 0.031). The APACHE II score of non-survivors was slightly higher than that of survivors at the time of PA-VAP diagnosis (survivors vs. non-survivors, 11.48 ± 3.78 vs. 13.55 ± 4.06, P = 0.074). We also found that the number of lymphocytes and monocytes were both sharply reduced in the non-survivors (lymphocytes: survivors vs. non-survivors [1.46 ± 0.69] × 10^9/L vs. [0.92 ± 0.50] × 10^9/L, P = 0.005; monocytes: survivors vs. non-survivors 0.52 [0.39, 0.70] × 10^9/L vs. 0.32 [0.23, 0.44] × 10^9/L, P = 0.005). Among the non-survivors, 17 died of sepsis, two died of respiratory failure, and one died of circulatory failure.

Circulating Acetic Acid Change in Relation to Survival

Ten healthy people were recruited as control group. All of SCFAs significantly decreased in PA-VAP patients compared to healthy people (**Supplementary Table S1** and **Supplementary Figure S1**). To explore the impact of circulating SCFAs on survival, all SCFAs were subjected to supervised PLS-DA and unsupervised PCA analysis. Samples from the survivors and non-survivors showed significant differences in the PLS-DA model but not in the PCA analysis (**Figures 2A, B** and **Supplementary Figure S2**). VIP scores were also calculated to identify differential SCFAs. The VIP scores of acetic acid and propionic acid were both > 1, while only the P value of acetic acid was < 0.05 (survivors vs. non-survivors 1.69[1.51,2.88] vs. 1.73 [1.46,2.60], P = 0.031) (**Figures 2C, D**). This suggests that decreased circulating acetic acid is associated with survival.

90-Day Mortality Was Associated With Circulating Acetic Acid

As shown in **Figure 2**, only acetic acid was increased in non-survivors among the seven circulating SCFAs. We, therefore, performed Kaplan-Meier survival analyses according to the level of acetic acid. Patients with acetic acid in the fourth quartile (Q4, >1.96 ug/ml) versus those in the first to third quartiles(Q1-Q3, <1.96ug/ml) showed significantly higher 90-day mortality (P = 0.027) (**Figure 3A**). The degree of disease severity of all patients was evaluated on the day of diagnosis of PA-VAP. Among the three evaluation systems, we observed higher APACHE II scores in patients with acetic acid in the fourth quartile compared to the first to third quartiles (AA<1.96ug/ml vs. AA>1.96ug/ml 11.57 ± 3.78 vs. 14.67 ± 3.85, P = 0.018). CPIS score (P = 0.869) and SOFA score (P = 0.053) were not significantly different between the two groups (**Figure 3B**). We also conducted Kaplan-Meier survival analyses according to the level of other six SCFAs. Conversely, compared with the first to third quartiles (Q1-Q3, <0.333ug/ml), propionic acid in the fourth quartile (Q4,> 0.333ug/ml) showed a trend of lower 90-day mortality) (P = 0.079) (**Supplementary Figure S3**). There is no significant correlation between the levels of the other five SCFAs and the 90-day mortality rate of PA-VAP patients) (**Supplementary Figure S3**).

Correlation of Circulating Acetic Acid and Host Immune Response

As shown in **Table 1**, non-survivors had lower blood lymphocyte and monocyte counts. We, therefore, performed a Spearman correlation analysis between acetic acid and circulating immune parameters. Lymphocyte and monocyte counts were both negatively correlated with acetic acid (**Table 2** and **Supplementary Figures S4A, B**). However, no significant correlation was observed between white blood cell count, neutrophil count, neutrophil-lymphocyte ratio, and acetic acid (**Table 2**). We also explored the dynamic changes in immune

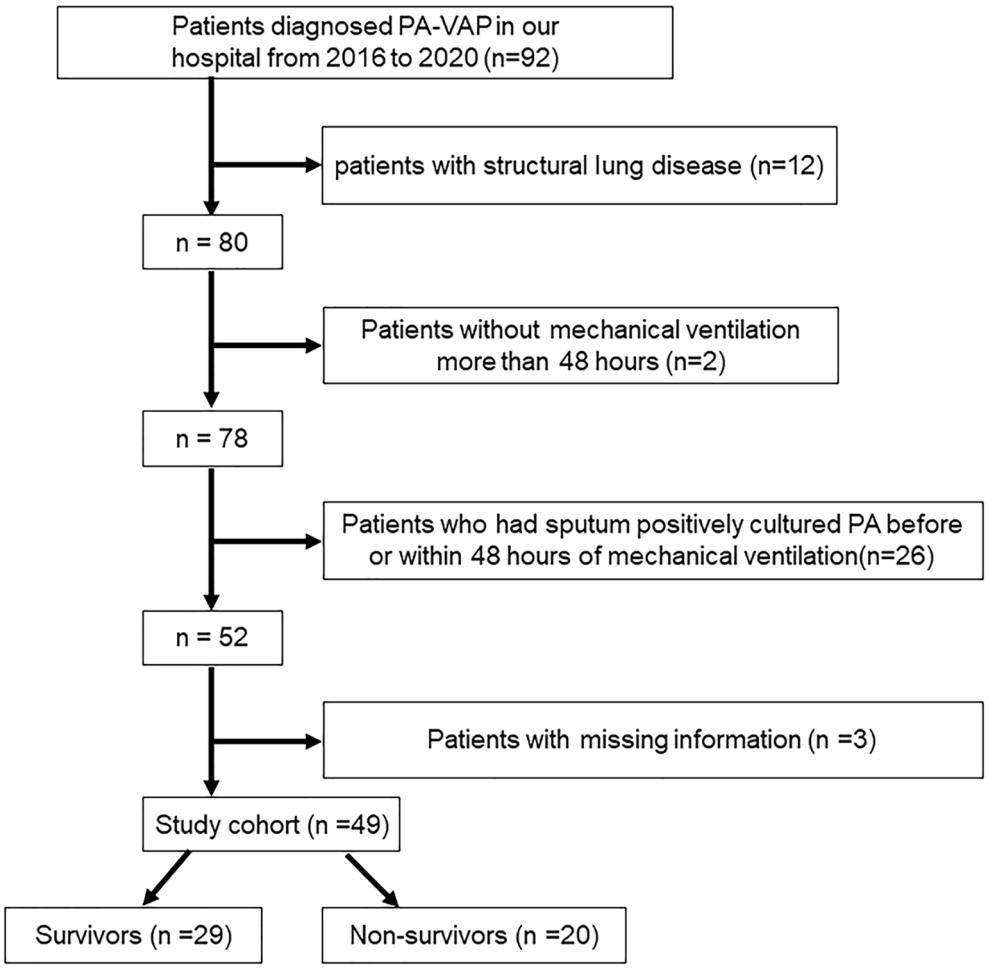

FIGURE 1 | Study flow chart.

cells within seven days after the diagnosis of PA-VAP, grouped by acetic acid quartile. White blood cell and neutrophil counts showed no significant difference between the two groups (**Figures 4A, B**), while patients with acetic acid in the fourth quartile (Q4, >1.96 ug/ml) showed continuous lower lymphocyte and monocyte counts compared to those in the first to third quartiles (Q1-3, <1.96 ug/ml) (**Figures 4C, D**). We also found that patients with acetic acid in the fourth quartile (Q4, >1.96 ug/ml) showed a continuously higher trend in the neutrophil-lymphocyte ratio (**Figure 4E**). We then asked whether circulating acetic acid was associated with systemic inflammation, as measured on the diagnosis day. Only IL-2 was significantly negatively correlated with circulating acetic acid ($P = 0.022$, $R = -0.455$) (**Supplementary Table S2** and **Supplementary Figure S4C**). On the other hand, we conducted a Spearman correlation analysis to explore the correlation between acetic acid and clinical parameters. We found that platelet counts were negatively correlated with circulating acetic acid ($P = 0.005$, $R = -0.397$) (**Supplementary Table S3**).

Effects of ICU Related Factors on Circulating Acetic Acid Concentration

Acetic acid is produced by intestinal microbiota digesting specific dietary components, mainly dietary fiber. Within the whole cohort, 36 (73.5%) patients received enteral nutrition, two (4.1%) patients received parenteral nutrition, six (12.2%) patients fasted, and five (10.2%) patients received a normal diet. According to the composition of enteral nutrition, we divided the patients who received enteral nutrition into a dietary fiber-containing group and a dietary fiber-free group. Acetic acid showed similar concentrations in the dietary fiber-containing and dietary fiber-free groups ($P=0.89$) (**Figure 5A**). Considering the impact of abdominal surgery on intestinal microbiota, we divided the whole cohort into no surgery, abdominal surgery, and non-abdominal surgery groups to explore the effect of surgery on circulating acetic acid. Acetic acid showed no significant difference among the three groups ($P = 0.94$) (**Figure 5B**). It is reported that lactate is also a precursor of SCFAs, so we conducted Spearman correlation

TABLE 1 | Baseline characteristics of PA-VAP patients.

Characteristics	Survivors (n=29)	Non-survivors (n=20)	P value
Demographic data			
Male, n (%)	18(62%)	13(65%)	0.834
Age, years	62.83±18.88	70.40±9.84	0.074
BMI, kg/m^2	23.95±4.73	21.70±4.39	0.099
Current smoker, n (%)	5(17%)	5(25%)	0.508
Admission type			
Medical, n (%)	16(55%)	5(25%)	0.031
Surgical, n (%)	11(38%)	15(75%)	
Trauma, n (%)	2(7%)	0(0%)	
Charlson Comorbidity Index	2.86±1.51	3.30±1.30	0.296
Disease severity			
CPIS score	7[5. 9]	7[6, 8]	0.322
APACHE II score	11.48±3.78	13.55±4.06	0.074
SOFA score	4[2. 6.5]	5.5[3, 7]	0.154
Laboratory indicators			
White blood cell, 10^9/L	9.52[6.99, 15.11]	8.37[6.69, 12.26]	0.314
Neutrophils, 10^9/L	6.68[4.84, 11.62)	6.48[5.00, 10.40]	0.919
Lymphocytes, 10^9/L	1.46±0.69	0.92±0.50	0.005
Monocytes, 10^9/L	0.52[0.39, 0.70]	0.32[0.23, 0.44]	0.005
PaO2/FiO2	262.38±79.21	249.91±90.06	0.611
Cause of death			
Sepsis	/	17	
Respiratory failure	/	2	
Circulatory failure	/	1	

BMI, body mass index; SOFA, Sequential Organ Failure Assessment; APACHE, Acute Physiology and Chronic Health Evaluation; CPIS, clinical pulmonary infection score.

analysis to observe the association between lactate and SCFAs. In PA-VAP patients, there was a significant positive correlation between isobutyric acid and serum lactate (P=0.035, R=0.334), while the other six SCFAs have no significant correlation with lactate levels (**Supplementary Table S4**). Considering that dietary fiber can affect the level of SCFAs, we re-analyzed the correlation between lactate levels and SCFAs in PA-VAP patients without dietary fiber intake. We found that acetic acid, butyric acid, and isobutyric acid showed a significant positive correlation with lactate levels (acetic acid: P=0.015, R=0.421) (**Supplementary Table S4** and **Figure 5C**).

DISCUSSION

SCFAs are the main products of the microbial fermentation of dietary fiber and can have various effects on host physiology (Koh et al., 2016). PA-VAP is a common complication in critically ill patients with obvious "imbalanced microbiota" and "imbalanced immunity". However, little is known about the relationship between SCFAs and clinical outcomes in PA-VAP patients. In this study, we found that high serum acetic acid levels were associated with disease severity and poor prognosis in PA-VAP patients. We also observed that high acetic acid levels might be related to immunosuppression, which mainly showed a negative correlation between acetic acid concentrations and lymphocyte counts and monocyte counts. Previous studies have also shown that persistent low circulating lymphocytes and monocytes are associated with a poor prognosis of lung infection (Ceccato et al., 2019; Feng et al., 2019). These findings indicate that high levels of serum acetic acid may have detrimental effects on PA-VAP patients.

Firstly, we found that serum acetic acid increased in non-surviving PA-VAP patients, and the increased serum acetic acid was associated with disease severity and mortality. Although it is generally believed that SCFAs have various benefits rather than detriments, SCFAs have not shown obvious beneficial effects on bacterial infections. SCFAs could inhibit cytokines and nitric oxide production by monocytes/macrophages and not improve the survival of pulmonary-sepsis (Ciarlo et al., 2016). Furthermore, recent studies found that excessive SCFAs have detrimental effects on the host (Zumbrun et al., 2013; Cho et al., 2020). It has been reported that a high-fiber diet (producing more SCFAs) promotes pathogenic Escherichia coli O157:H7 strain colonization and increases mortality (Zumbrun et al., 2013). In addition, SCFAs, especially acetic acid, could also promote the proliferation of PA. The high concentration of acetic acid in sinusitis mucus was a risk factor for chronic rhinosinusitis with PA infection (Cho et al., 2020). On the other hand, some clinical studies also found that SCFAs may be detrimental (Kurilshikov et al., 2019; Behary et al., 2021). It was reported that SCFAs were associated with poorer clinical outcomes in hepatocellular carcinoma patients (Behary et al., 2021). Since most of the protective effects of SCFAs have been found in mice, more clinical studies are needed to clarify the role of SCFAs in bacterial pneumonia.

Then we found that PA-VAP patients with high acetic acid levels had lower numbers of monocytes and lymphocytes in the peripheral blood compared to those with low levels of acetic acid. Acetic acid is an inhibitor of histone deacetylases (HDACs) and plays an essential role in immunosuppression (Koh et al., 2016).

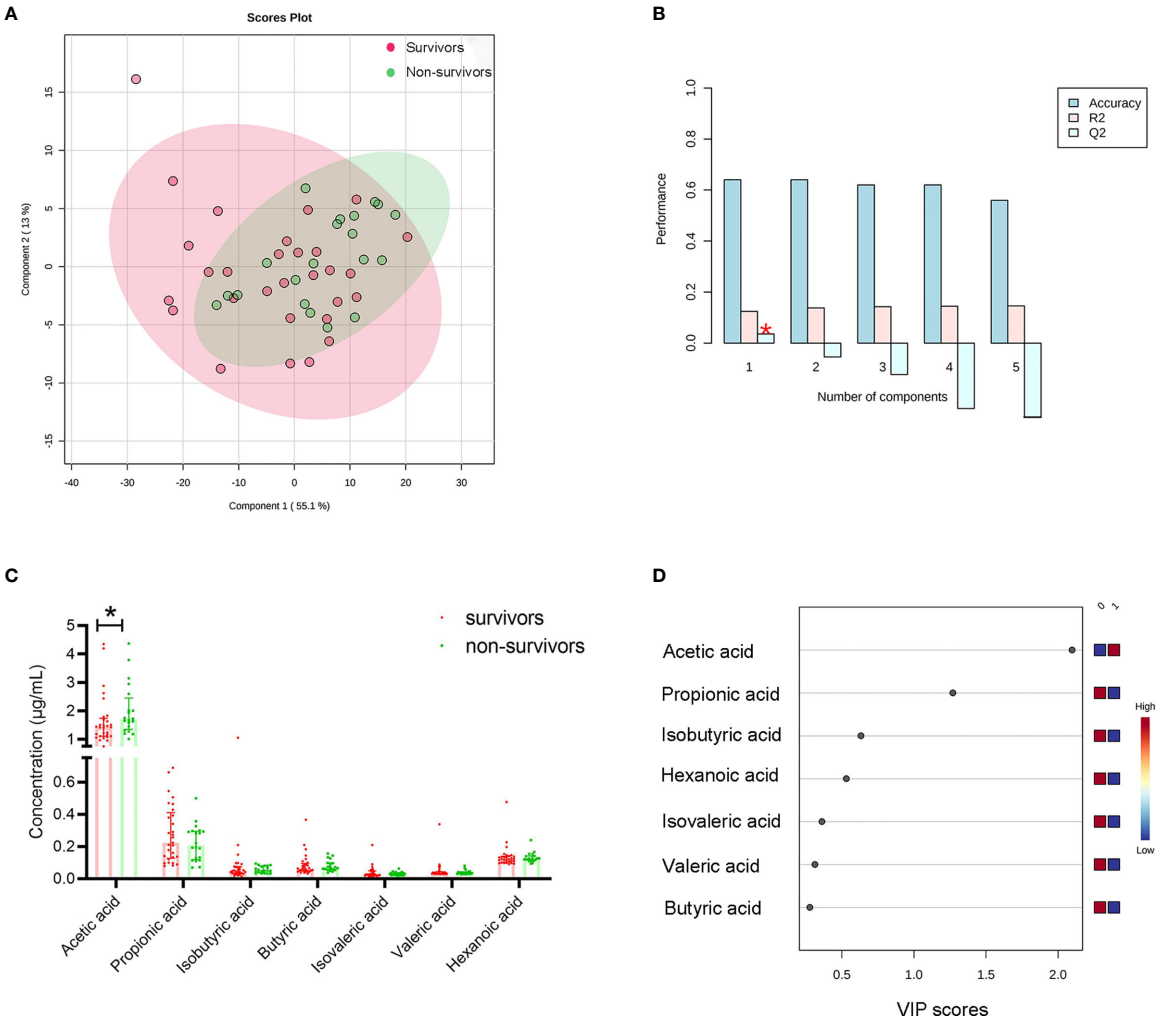

FIGURE 2 | Differential SCFA analysis between survivors and non-survivors with PA-VAP. **(A)** Supervised clustering conducted by partial least squares discriminant analysis (PLS-DA) revealed that the SCFAs were different between the two groups. **(B)** Cross-validation test for PLS-DA model. **(C)** Mann Whitney analysis demonstrated that only acetic acid was significantly different between the two groups. **(D)** The Variable Importance in Projection score of acetic acid and propionic acid were both > 1. PA-VAP, *Pseudomonas aeruginosa* ventilator-associated pneumonia; SCFAs, short chain fatty acids; *P < 0.05.

It was reported that acetic acid damages the T-dependent immune responses and prevents the activation of effector B cells (Azizov et al., 2020). Acetic acid can also directly inhibit the production of cytokines by human monocytes under inflammatory stimuli (Cox et al., 2009; Ang et al., 2016). The immunosuppressive effect of acetic acid on human monocytes was mediated by P38 phosphorylation mediated by G protein-coupled receptors 41/G protein-coupled receptors 43 (Ang et al., 2016). However, the immunosuppressive effect of acetic acid on human monocytes did not appear in mice (Ang et al., 2016). These findings suggest that additional clinical studies are needed to investigate the role of acetic acid. On the other hand, it is worth noting that different concentrations of SCFAs can induce different effects. High-dose SCFAs reduced the expression of AID and Blimp1 in B cells, inhibit class-switch DNA recombination, somatic hypermutation, and plasma cell differentiation, thereby inhibiting local and systemic antibody responses in mice. At the same time, low-dose SCFAs could promote local and systemic antibody responses (Sanchez et al., 2020). As is known, butyric acid can provide energy for colon cells and prevent infection. However, butyric acid at physiological concentration can inhibit intestinal stem cells' proliferation (Kaiko et al., 2016). In this study, we found that high concentration of acetic acid may have immunosuppressive effects in PA-VAP patients. It suggested that high levels of acetic acid may be detrimental to patients who have already developed PA-VAP.

We also found that patients with high levels of serum acetic acid had higher mortality. Those patients showed a continuously lower level of monocytes and lymphocytes and a higher neutrophil-lymphocyte ratio in the peripheral blood.

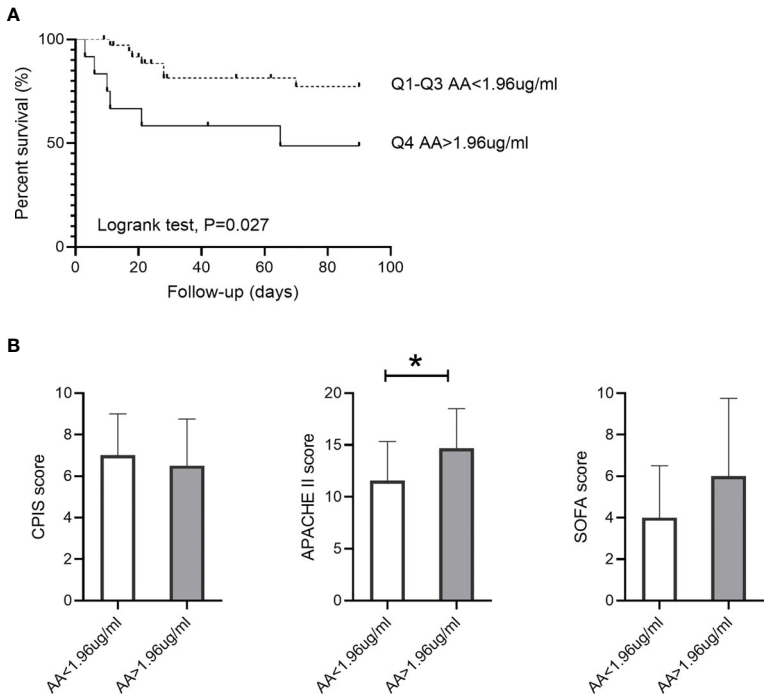

FIGURE 3 | Association between circulating acetic acid concentration and 90-day mortality. **(A)** Kaplan-Meier survival analysis grouped by acetic acid quartile in PA-VAP patients. **(B)** Comparison of the CPIS score, APACHE II score, and SOFA score between high acetic acid concentration group (Q4, >1,96ug/ml) and low acetic acid concentration group (Q1-Q3, <1.96ug/ml) in PA-VAP patients. PA-VAP, *Pseudomonas aeruginosa* ventilator-associated pneumonia; AA, acetic acid; SOFA, Sequential Organ Failure Assessment; APACHE, Acute Physiology and Chronic Health Evaluation; CPIS, clinical pulmonary infection score; *P < 0.05.

TABLE 2 | Correlation between acetic acid and circulating immune cells in PA-VAP patients.

Immune parameters	R	P
White blood cell, 10^9/L	-0.107	0.46
Neutrophils, 10^9/L	0.025	0.86
Lymphocytes, 10^9/L	-0.288	0.045
Neutrophils/Lymphocytes	0.255	0.077
Monocyte, 10^9/L	-0.367	0.009

As reported, continuous lymphocytopenia and a high neutrophil-lymphocyte ratio can predict mortality in patients with ICU-acquired pneumonia (Akilli et al., 2014; Ceccato et al., 2019; Feng et al., 2019). On the other hand, even with appropriate antibiotic therapy, lymphocytopenia occurring during the day of diagnosis may increase the risk of treatment failure in VAP patients (Gursel et al., 2008). IL-2 plays an important role in promoting lymphocyte proliferation. It was reported that the severity of pneumonia in critically ill patients was associated with IL-2-induced lymphocytopenia (Shi et al., 2020). Consistent with the effects of IL-2, we found that IL-2 concentration and the number of lymphocytes were both negatively related to serum acetic acid, which suggests that serum acetic acid may decrease the number of lymphocytes via the IL-2 signaling pathway.

SCFAs are the products of colonic microbial fermentation. Acetic acid, propionate, and butyrate are the major SCFAs. Butyrate is an important energy source for colonocytes and is locally consumed in the colon, while acetic acid and propionate are absorbed into the peripheral circulation. SCFAs are regulated mainly by diet and gut microbiota (Koh et al., 2016). The microbiota of critically ill patients changes dramatically, including decreasing microbial diversity, loss of commensal, and potentially pathogenic species (McDonald et al., 2016). Interventions in the ICU, such as antibiotics, invasive devices, and enteral nutrition, could profoundly affect the microbiota. In this study, we found that the intake of fiber and gastrointestinal surgery had no significant effects on serum acetic acid level. This may be relevant to the different dietary fiber intakes. As is known, lactate can also be converted into SCFAs (Koh et al., 2016). In this study, we observed that levels of acetic acid and butyric acid showed a significant positive correlation with lactate levels in PA-VAP patients without dietary fiber intake. It suggested that the elevated acetic acid in the non-survivors with PA-VAP may be related to excessive lactate.

This study had some limitations. Firstly, the sample size was limited. Secondly, the gut microbiota, fecal SCFAs, and intestinal permeability markers were not measured simultaneously in this study. These parameters may provide a better understanding of why circulating acetic acid levels increased in non-survivors. Thirdly, as there was no record of daily dietary fiber intake in PA-VAP patients before sampling, a prospective cohort should be conducted to identify the causal relationship between dietary

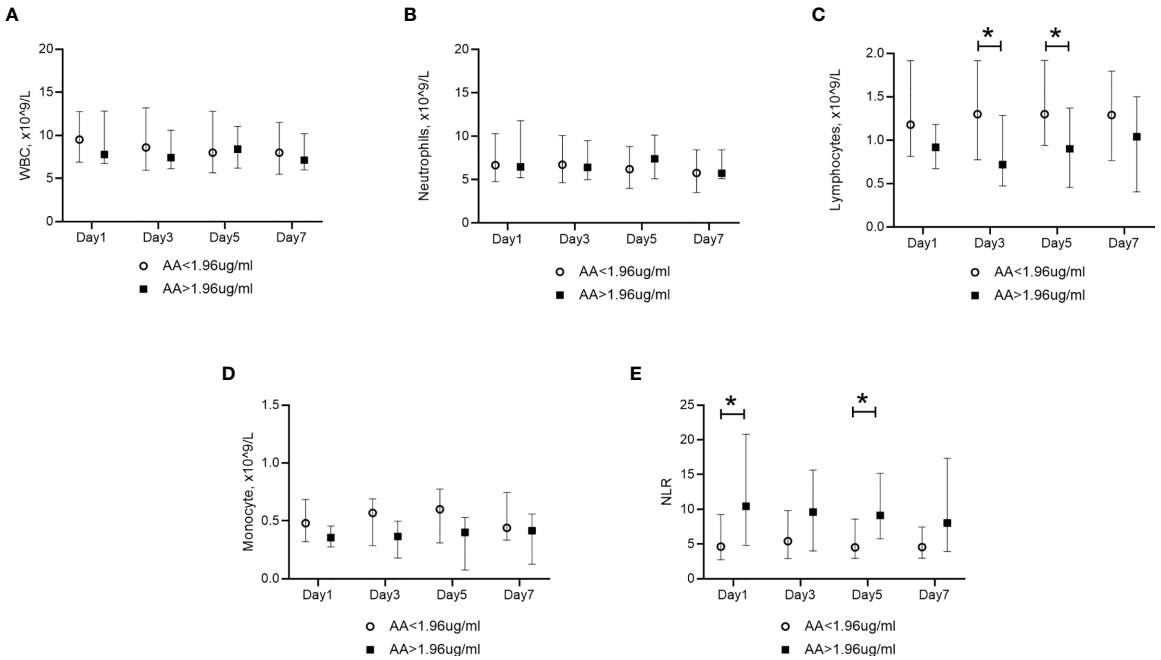

FIGURE 4 | Dynamic changes in blood immune cells in PA-VAP patients. Grouping depended on the acetic acid quartile. **(A, B)** Similar levels of WBCs and neutrophils in the high acetic acid concentration group (Q4, >1,96ug/ml) and low acetic acid concentration group (Q1-Q3, <1.96ug/ml) within the 7-day observation period. **(C, D)** Higher levels of lymphocytes and monocytes were found in the high acetic acid concentration group (Q4, >1,96ug/ml). **(E)** lower level of NLR was found in the high acetic acid concentration group (Q4, >1,96ug/ml). PA-VAP, *Pseudomonas aeruginosa* ventilator-associated pneumonia; AA, acetic acid; WBC, white blood cell; NLR, neutrophil-lymphocyte ratio; *P < 0.05.

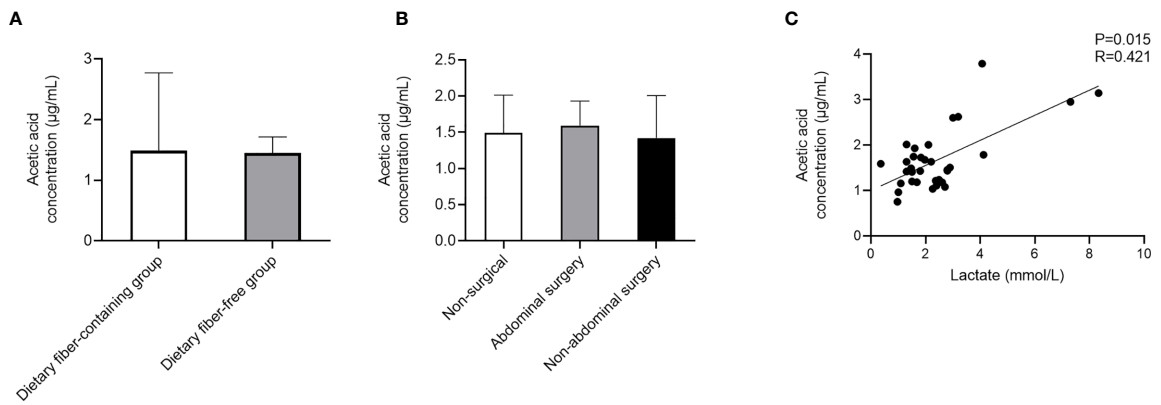

FIGURE 5 | Analysis of factors affecting acetic acid level in PA-VAP patients. **(A)** The concentration of acetic acid was not significantly different between the dietary fiber-containing and dietary fiber-free groups. **(B)** Level of acetic acid was similar among the no surgery group, abdominal surgery group, and non-abdominal surgery group. **(C)** Serum acetic acid showed a significant positive correlation with serum lactate in PA-VAP patients without dietary fiber intake. PA-VAP, *Pseudomonas aeruginosa* ventilator-associated pneumonia.

fiber and circulating acetic acid levels in PA-VAP patients. Fourthly, since the antibiotic strategies of PA-VAP patients showed significant interpersonal differences, we cannot perform statistical analysis to obtain the impact of antibiotics on the level of SFCAs. Although we have found that acetic acid may be related to immunosuppression in PA-VAP patients, further mechanical experiments are needed to verify this association.

In summary, the level of acetic acid in serum was negatively correlated with lymphocytes and monocytes in PA-VAP patients. These results suggest that higher serum acetic acid levels in patients with PA-VAP may lead to immunosuppressive

and dampen anti-infection immunity responses, which may increase mortality.

DATA AVAILABILITY STATEMENT

The raw data supporting the conclusions of this article will be made available by the authors, without undue reservation.

ETHICS STATEMENT

The studies involving human participants were reviewed and approved by Ruijin Hospital Ethics Committee Shanghai Jiao Tong University School of Medicine. The patients/participants provided their written informed consent to participate in this study.

AUTHOR CONTRIBUTIONS

JL, XQ, and RT contributed to the study design. ZL, XW, TP, and HQ contributed to the subject recruitment and the sample collection. XQ, LZ, JX, and ZT, performed the experiments. JL, XQ, and YQ contributed to data analysis. JL, XQ, RT, and LZ contributed to data interpretation. All authors contributed to the article and approved the submitted version.

FUNDING

This study was supported by the National Natural Science Foundation of China (81770005) and (81970005) awarded to JL, Medical-engineering Cross Foundation of Shanghai Jiao Tong University grant "2019-nCoV research project" (YG2020YQ30) awarded to JL, Talent development project for Three-years action plan of Shanghai public health system construction (GWV-10.2-XD03) awarded to JL, National Key R&D Program of China (2017YFC1309700, 2017YFC1309705) awarded to HQ, National Natural Science Foundation of China (81801885) awarded to TP. Shanghai Sailing Program (18YF1413800) awarded to TP.

SUPPLEMENTARY MATERIAL

The Supplementary Material for this article can be found online at: https://www.frontiersin.org/articles/10.3389/fcimb.2021.669409/full#supplementary-material

Supplementary Figure 1 | Unsupervised clustering was conducted by Principal Component Analysis (PCA) in the whole cohort. The composition of serum SCFAs in PA-VAP patients was significantly different from that of healthy people. PA-VAP, *Pseudomonas aeruginosa* ventilator-associated pneumonia; SCFAs, short chain fatty acids.

Supplementary Figure 2 | Unsupervised clustering conducted by Principal Component Analysis (PCA) revealed that the level of SCFAs were similar between surviving PA-VAP patients and non-surviving PA-VAP patients. PA-VAP, *Pseudomonas aeruginosa* ventilator-associated pneumonia; SCFAs, short chain fatty acids.

Supplementary Figure 3 | Association between circulating SCFAs concentration and 90-day mortality. A Kaplan-Meier survival analysis grouped by propionic acid **(A)**, isobutyric acid **(B)**, butyric acid **(C)**, isovaleric acid **(D)**, valeric acid **(E)**, and hexanoic acid **(F)** quartile in PA-VAP patients. PA-VAP, *Pseudomonas aeruginosa* ventilator-associated pneumonia; SCFAs, short chain fatty acids.

Supplementary Figure 4 | Correlation between acetic acid and circulating immune cells **(A, B)** and IL-2 **(C)** in PA-VAP patients. PA-VAP, *Pseudomonas aeruginosa* ventilator-associated pneumonia.

REFERENCES

Akilli, N. B., Yortanlı, M., Mutlu, H., Günaydın, Y. K., Koylu, R., Akca, H. S., et al. (2014). Prognostic importance of neutrophil-lymphocyte ratio in critically ill patients: short- and long-term outcomes. *Am. J. Emerg. Med.* 32, 1476–1480. doi: 10.1016/j.ajem.2014.09.001

Ang, Z., Er, J. Z., Tan, N. S., Lu, J., Liou, Y.-C., Grosse, J., et al. (2016). Human and mouse monocytes display distinct signalling and cytokine profiles upon stimulation with FFAR2/FFAR3 short-chain fatty acid receptor agonists. *Sci. Rep.* 6, 34145. doi: 10.1038/srep34145

Azizov, V., Dietel, K., Steffen, F., Dürholz, K., Meidenbauer, J., Lucas, S., et al. (2020). Ethanol consumption inhibits T cell responses and the development of autoimmune arthritis. *Nat. Commun.* 11 (1), 1998. doi: 10.1038/s41467-020-15855-z

Behary, J., Amorim, N., Jiang, X.-T., Raposo, A., Gong, L., McGovern, E., et al. (2021). Gut microbiota impact on the peripheral immune response in non-alcoholic fatty liver disease related hepatocellular carcinoma. *Nat. Commun.* 12, 187. doi: 10.1038/s41467-020-20422-7

Borgatta, B., Gattarello, S., Mazo, C. A., Imbiscuso, A. T., Larrosa, M. N., Lujàn, M., et al. (2017). The clinical significance of pneumonia in patients with respiratory specimens harbouring multidrug-resistant Pseudomonas aeruginosa: a 5-year retrospective study following 5667 patients in four general ICUs. *Eur. J. Clin. Microbiol. Infect. Dis.* 36, 2155–2163. doi: 10.1007/s10096-017-3039-z

Bowerman, K. L., Rehman, S. F., Vaughan, A., Lachner, N., Budden, K. F., Kim, R. Y., et al. (2020). Disease-associated gut microbiome and metabolome changes in patients with chronic obstructive pulmonary disease. *Nat. Commun.* 11, 5886. doi: 10.1038/s41467-020-19701-0

Ceccato, A., Panagiotarakou, M., Ranzani, O. T., Martin-Fernandez, M., Almansa-Mora, R., Gabarrus, A., et al. (2019). Lymphocytopenia as a Predictor of Mortality in Patients with ICU-Acquired Pneumonia. *J. Clin. Med.* 8 (6), 843. doi: 10.3390/jcm8060843

Cho, D.-Y., Skinner, D., Hunter, R. C., Weeks, C., Lim, D. J., Thompson, H., et al. (2020). Contribution of Short Chain Fatty Acids to the Growth of in Rhinosinusitis. *Front. Cell Infect. Microbiol.* 10, 412. doi: 10.3389/fcimb.2020.00412

Ciarlo, E., Heinonen, T., Herderschee, J., Fenwick, C., Mombelli, M., Le Roy, D., et al. (2016). Impact of the microbial derived short chain fatty acid propionate on host susceptibility to bacterial and fungal infections in vivo. *Sci. Rep.* 6, 37944. doi: 10.1038/srep37944

Cox, M. A., Jackson, J., Stanton, M., Rojas-Triana, A., Bober, L., Laverty, M., et al. (2009). Short-chain fatty acids act as antiinflammatory mediators by regulating prostaglandin E(2) and cytokines. *World J. Gastroenterol.* 15, 5549–5557. doi: 10.3748/wjg.15.5549

Crandon, J. L., Luyt, C.-E., Aubry, A., Chastre, J., and Nicolau, D. P. (2016). Pharmacodynamics of carbapenems for the treatment of Pseudomonas aeruginosa ventilator-associated pneumonia: associations with clinical outcome and recurrence. *J. Antimicrob. Chemother.* 71, 2534–2537. doi: 10.1093/jac/dkw200

Dickson, R. P. (2016). The microbiome and critical illness. *Lancet Respir. Med.* 4, 59–72. doi: 10.1016/S2213-2600(15)00427-0

Feng, D.-Y., Zhou, Y.-Q., Zhou, M., Zou, X.-L., Wang, Y.-H., and Zhang, T.-T. (2019). Risk Factors for Mortality Due to Ventilator-Associated Pneumonia in a Chinese Hospital: A Retrospective Study. *Med. Sci. Monit.* 25, 7660–7665. doi: 10.12659/MSM.916356

Gonçalves, P., Araújo, J. R., and Di Santo, J. P. (2018). A Cross-Talk Between Microbiota-Derived Short-Chain Fatty Acids and the Host Mucosal Immune System Regulates Intestinal Homeostasis and Inflammatory Bowel Disease. *Inflammation Bowel. Dis.* 24, 558–572.10.1093/ibd/izx029. doi: 10.1093/ibd/izx029

Guarner, F., and Malagelada, J.-R. (2003). Gut flora in health and disease. *Lancet* 361, 512–519. doi: 10.1016/S0140-6736(03)12489-0

Gursel, G., Aydogdu, M., Ozyilmaz, E., and Ozis, T. N. (2008). Risk factors for treatment failure in patients with ventilator-associated pneumonia receiving appropriate antibiotic therapy. *J. Crit. Care* 23, 34–40. doi: 10.1016/j.jcrc.2007.12.015

Kaiko, G. E., Ryu, S. H., Koues, O. I., Collins, P. L., Solnica-Krezel, L., Pearce, E. J., et al. (2016). The Colonic Crypt Protects Stem Cells from Microbiota-Derived Metabolites. *Cell* 167, 1137. doi: 10.1016/j.cell.2016.10.034

Koh, A., De Vadder, F., Kovatcheva-Datchary, P., and Bäckhed, F. (2016). From Dietary Fiber to Host Physiology: Short-Chain Fatty Acids as Key Bacterial Metabolites. *Cell* 165, 1332–1345. doi: 10.1016/j.cell.2016.05.041

Köhler, T., Guanella, R., Carlet, J., and van Delden, C. (2010). Quorum sensing-dependent virulence during Pseudomonas aeruginosa colonisation and pneumonia in mechanically ventilated patients. *Thorax* 65, 703–710. doi: 10.1136/thx.2009.133082

Kurilshikov, A., van den Munckhof, I. C. L., Chen, L., Bonder, M. J., Schraa, K., Rutten, J. H. W., et al. (2019). Gut Microbial Associations to Plasma Metabolites Linked to Cardiovascular Phenotypes and Risk. *Circ. Res.* 124, 1808–1820. doi: 10.1161/CIRCRESAHA.118.314642

Li, J., Richards, E. M., Handberg, E. M., Pepine, C. J., and Raizada, M. K. (2021). Butyrate Regulates COVID-19-Relevant Genes in Gut Epithelial Organoids From Normotensive Rats. *Hypertension* 77, e13–e16. doi: 10.1161/HYPERTENSIONAHA.120.16647

McDonald, D., Ackermann, G., Khailova, L., Baird, C., Heyland, D., Kozar, R., et al. (2016). Extreme Dysbiosis of the Microbiome in Critical Illness. *mSphere* 1 (4), e00199-16. doi: 10.1128/mSphere.00199-16

Qi, X., Qu, H., Yang, D., Zhou, L., He, Y.-W., Yu, Y., et al. (2018). Lower respiratory tract microbial composition was diversified in Pseudomonas aeruginosa ventilator-associated pneumonia patients. *Respir. Res.* 19, 139. doi: 10.1186/s12931-018-0847-3

Ruppé, É., Lisboa, T., and Barbier, F. (2018). The gut microbiota of critically ill patients: first steps in an unexplored world. *Intensive Care Med.* 44, 1561–1564. doi: 10.1007/s00134-018-5309-3

Sader, H. S., Farrell, D. J., Flamm, R. K., and Jones, R. N. (2014). Antimicrobial susceptibility of Gram-negative organisms isolated from patients hospitalised with pneumonia in US and European hospitals: results from the SENTRY Antimicrobial Surveillance Progra-2012. *Int. J. Antimicrob. Agents.* 43, 328–334. doi: 10.1016/j.ijantimicag.2014.01.007

Sanchez, H. N., Moroney, J. B., Gan, H., Shen, T., Im, J. L., Li, T., et al. (2020). B cell-intrinsic epigenetic modulation of antibody responses by dietary fiber-derived short-chain fatty acids. *Nat. Commun.* 11, 60. doi: 10.1038/s41467-019-13603-6

Shimizu, K., Ogura, H., Hamasaki, T., Goto, M., Tasaki, O., Asahara, T., et al. (2011). Altered gut flora are associated with septic complications and death in critically ill patients with systemic inflammatory response syndrome. *Dig. Dis. Sci.* 56, 1171–1177. doi: 10.1007/s10620-010-1418-8

Shimizu, K., Yamada, T., Ogura, H., Mohri, T., Kiguchi, T., Fujimi, S., et al. (2018). Synbiotics modulate gut microbiota and reduce enteritis and ventilator-associated pneumonia in patients with sepsis: a randomized controlled trial. *Crit. Care* 22, 239. doi: 10.1186/s13054-018-2167-x

Shi, H., Wang, W., Yin, J., Ouyang, Y., Pang, L., Feng, Y., et al. (2020). The inhibition of IL-2/IL-2R gives rise to CD8 T cell and lymphocyte decrease through JAK1-STAT5 in critical patients with COVID-19 pneumonia. *Cell Death Dis.* 11, 429. doi: 10.1038/s41419-020-2636-4

Stewart, C. J., Hasegawa, K., Wong, M. C., Ajami, N. J., Petrosino, J. F., Piedra, P. A., et al. (2018). Respiratory Syncytial Virus and Rhinovirus Bronchiolitis Are Associated With Distinct Metabolic Pathways. *J. Infect. Dis.* 217, 1160–1169.10.1093/infdis/jix680. doi: 10.1093/infdis/jix680

Trompette, A., Gollwitzer, E. S., Pattaroni, C., Lopez-Mejia, I. C., Riva, E., Pernot, J., et al. (2018). Dietary Fiber Confers Protection against Flu by Shaping Ly6c Patrolling Monocyte Hematopoiesis and CD8 T Cell Metabolism. *Immunity* 48 (5), 992-1005.e8. doi: 10.1016/j.immuni.2018.04.022

Trompette, A., Gollwitzer, E. S., Yadava, K., Sichelstiel, A. K., Sprenger, N., Ngom-Bru, C., et al. (2014). Gut microbiota metabolism of dietary fiber influences allergic airway disease and hematopoiesis. *Nat. Med.* 20, 159–166. doi: 10.1038/nm.3444

Wu, T., Li, H., Su, C., Xu, F., Yang, G., Sun, K., et al. (2020). Microbiota-Derived Short-Chain Fatty Acids Promote LAMTOR2-Mediated Immune Responses in Macrophages. *mSystems* 5 (6), e00587-20. doi: 10.1128/mSystems.00587-20

Yao, Y., Cai, X., Fei, W., Ye, Y., Zhao, M., and Zheng, C. (2020). The role of short-chain fatty acids in immunity, inflammation and metabolism. *Crit. Rev. Food Sci. Nutr.* 1, 1–12. doi: 10.1080/10408398.2020.1854675

Zaiss, M. M., Jones, R. M., Schett, G., and Pacifici, R. (2019). The gut-bone axis: how bacterial metabolites bridge the distance. *J. Clin. Invest.* 129, 3018–3028. doi: 10.1172/JCI128521

Zumbrun, S. D., Melton-Celsa, A. R., Smith, M. A., Gilbreath, J. J., Merrell, D. S., and O'Brien, A. D. (2013). Dietary choice affects Shiga toxin-producing Escherichia coli (STEC) O157:H7 colonization and disease. *Proc. Natl. Acad. Sci. U. S. A.* 110, E2126–E2133. doi: 10.1073/pnas.1222014110

Conflict of Interest: The authors declare that the research was conducted in the absence of any commercial or financial relationships that could be construed as a potential conflict of interest.

frontiers in Cellular and Infection Microbiology

ORIGINAL RESEARCH
published: 15 July 2021
doi: 10.3389/fcimb.2021.687391

The Level of D-Dimer Is Positively Correlated With the Severity of *Mycoplasma pneumoniae* Pneumonia in Children

Yan Zheng[1,2], *Lingling Hua*[1,3], *Qiannan Zhao*[1], *Mengyao Li*[1], *Meixia Huang*[1], *Yunlian Zhou*[1], *Yingshuo Wang*[1], *Zhimin Chen*[1*] and *Yuanyuan Zhang*[1*]

[1] Department of Pulmonology, Children's Hospital Zhejiang University School of Medicine, National Clinical Research Center for Child Health, Hangzhou, China, [2] Department of Pediatrics, The Quzhou Affiliated Hospital of Wenzhou Medical University, Quzhou People's Hospital, Quzhou, China, [3] Department of Pediatrics, Ningbo Women and Children's Hospital, Ningbo, China

OPEN ACCESS

Edited by:
Elias Adel Rahal, American University of Beirut, Lebanon

Reviewed by:
Tongqiang Zhang, Tianjin Children's Hospital, China
James Daubenspeck, University of Alabama at Birmingham, United States

***Correspondence:**
Yuanyuan Zhang
chzyy@zju.edu.cn
Zhimin Chen
zmchen@zju.edu.cn

Specialty section:
This article was submitted to Microbes and Innate Immunity, a section of the journal Frontiers in Cellular and Infection Microbiology

Received: *29 March 2021*
Accepted: *28 June 2021*
Published: *15 July 2021*

Citation:
Zheng Y, Hua L, Zhao Q, Li M, Huang M, Zhou Y, Wang Y, Chen Z and Zhang Y (2021) The Level of D-Dimer Is Positively Correlated With the Severity of Mycoplasma pneumoniae Pneumonia in Children. Front. Cell. Infect. Microbiol. 11:687391. doi: 10.3389/fcimb.2021.687391

Objective: *Mycoplasma pneumoniae* pneumonia (MPP) is an important disease in children. Studies have demonstrated that the levels of D-dimer are elevated in some children with MPP, especially those with thrombotic complications. However, the potential association between MPP and D-dimer remains unclear. In our study, we sought to explore the relationship between the levels of plasma D-dimer and clinical characteristics of MPP patients.

Methods: Retrospective analysis was conducted on 356 patients who were hospitalized in our hospital for MPP between January 1, 2017, and December 31, 2019. According to the peak value of D-dimer, patients were divided into three groups: the normal group (D-dimer<0.55 mg/L), the mild-moderately elevated group (D-dimer 0.55–5.5 mg/L) and the severely elevated group (D-dimer >5.5 mg/L). The demographic and clinical information, radiological findings, laboratory data, and treatments of patients were compared among different groups.

Results: 106 patients were in the normal group, 204 patients were in the mild-moderately elevated group, and 46 patients were in the severely elevated group. More severe clinical and radiographic manifestations, longer length of fever, hospital stay and antibiotic therapy duration, higher incidences of extra-pulmonary complications, refractory MPP (RMPP), severe MPP (SMPP) were found in the elevated group, when compared with the normal group (P<0.01). Meanwhile, we found that the percentage of neutrophil (N%) and CD_8^+ lymphocyte (CD_8^+%), C-reactive protein (CRP), lactate dehydrogenase (LDH), interleukin (IL)-6, IL-10, and interferon-gamma (IFN-γ) trended higher with increasing D-dimer, whereas the percentage of lymphocyte (L%) and prealbumin (PAB) trended lower (P<0.01). In addition, the proportions of patients requiring oxygen therapy, glucocorticoid, bronchoscopy, immunoglobulin use, thoracentesis, or ICU admission were significantly higher in the severely elevated group than those in the other two groups (P<0.01). Correlation analysis showed that N%, L%, CRP, LDH, IL-10, length of

fever, length of stay, and length of antibiotic therapy had strong correlations with the level of D-dimer.

Conclusions: MPP patients with higher levels of D-dimer had more severe clinical manifestations and needed longer duration of treatment, which might be closely related to the severity of lung inflammation after MP infection.

Keywords: *Mycoplasma pneumoniae*, pneumonia, D-dimer, children, severity

INTRODUCTION

Mycoplasma pneumoniae (MP) is one of the most important microorganisms that caused community-acquired pneumonia (CAP) in children (Jain et al., 2015; Meyer Sauteur et al., 2020). It may be responsible for about 4% to 8% of CAP during periods of endemicity, whereas it could cause up to 20% to 40% of CAP in the general population during epidemics (Waites et al., 2017). In general, *Mycoplasma pneumoniae* pneumonia (MPP) is recognized as a self-limited disease, but recently, some researchers reported that it could cause pulmonary and extra-pulmonary complications, or even life-threatening situations, such as necrotizing pneumonitis, myocarditis, hemolytic anemia, acute pancreatitis, and so on (Poddighe, 2018). Furthermore, several recent studies show that MPP patients could have concurrent pulmonary embolism, cerebral infarction, spleen infarction, and other systemic thrombotic diseases (Park et al., 2012; Kang et al., 2016; Mélé and Turc, 2018; Chen et al., 2020). The pathogenic mechanisms of MP infection may be related to the cytoadherence, intracellular localization, cytotoxicity, inflammation, and so on, which is still elusive (Waites and Talkington, 2004).

D-dimer is a soluble fibrin degradation product that results from the ordered breakdown of thrombi by the fibrinolytic system (Weitz et al., 2017). Numerous studies have reported that elevated D-dimer is associated with thrombotic diseases (Goldenberg et al., 2004; Nowak-Göttl et al., 2004). Consequently, D-dimer has been extensively used for the diagnosis of venous thromboembolism (VTE) (Adam et al., 2009). Recently, it has also been reported that the levels of D-dimer are related to the severity of coronavirus disease 2019 (COVID-19) (Sakka et al., 2020). However, few people had concentrated on the relationship between clinical manifestations of MPP and D-dimer.

In this study, we retrospectively analyzed the clinical characteristics of MPP patients with different degrees of D-dimer who were hospitalized in our hospital between January 1, 2017, and December 31, 2019, and explore the relationship between the levels of D-dimer and clinical characteristics of MPP patients.

METHODS

Study Population

In this study, we retrospectively collected the clinical data of patients with MMP who were admitted to Children's hospital, Zhejiang University School of Medicine between January 1, 2017, and December 31, 2019. The criteria for enrolling patients were as follows: (1) signs and symptoms indicative of CAP, including fever, cough, abnormal lung auscultation and new infiltrate(s) on chest radiograph; (2) had both positive results for MP RNA polymerase chain reaction (PCR) tests and positive results for MP-IgM (Witmer et al., 2007; Waites et al., 2017). Exclusion criteria were the follows (Zhang et al., 2014; Jin et al., 2018): (1) had positive results for other pathogens; (2) had received corticosteroids, intravenous immunoglobulin (IVIG), and anticoagulation therapy before admission; (3) with underlying diseases, such as chronic cardiac and pulmonary disease, rheumatic diseases, and immunodeficiency; (4) had incomplete medical records.

Data Collection

Demographic and clinical information, radiological findings, laboratory data, such as blood routine test, C-reactive protein (CRP), lactate dehydrogenase (LDH), D-dimer, prealbumin (PAB), subpopulations of T lymphocytes, immunoglobulins, cytokines were retrospectively collected from all patients by reviewing their electronic medical records. During the hospitalization, clinical signs and symptoms of patients were obtained, including body temperature, respiratory rates, extra-pulmonary complications (Poddighe, 2018,) (Witmer et al., 2007; Zhou et al., 2014), and so on. All patients underwent chest radiography during the illness, confirming unequivocal focal or segmental infiltration with or without pleural effusion. Although patients had progressive symptoms, suspected complications, clinical deterioration, or persistent fever after appropriate antibiotic therapy, chest CT scans were performed. The large lesion was defined as the extent of infiltration on chest imaging more than one third of the lung (Uehara et al., 2011).

Severe MPP (SMPP) was defined as MPP with any one of the follows: (1) a poor general condition; (2) fastidium or dehydration; (3) disturbance of consciousness; (4) an increased respiratory rate (infants > 70 breaths/min and older children > 50 breaths/min); (5) dyspnea; (6) cyanosis; (7) extent of infiltration on chest X-ray ≥2/3 of one lung or multilobe involvement; (8) extra-pulmonary complications; (9) pleural effusion; (10) oxygen saturation in room air ≤92% (Subspecialty Group of Respiratory Diseases, 2013). Refractory MPP (RMPP) was diagnosed based on the presence of persistent fever and clinical, as well as radiological deterioration after azithromycin treatment for 7 days or longer (Tamura et al., 2008; Subspecialty Group of Respiratory Diseases, 2013). The indications for oxygen

therapy, bronchoscopy, glucocorticoid, and mechanical ventilation were evaluated according to the guidelines for management of community-acquired pneumonia in children in China (Subspecialty Group of Respiratory Diseases, 2013).

Sample Detection

Nasopharyngeal aspirate/swab specimens were routinely tested within 24 hours after admission. Peripheral blood samples were obtained on admission for detecting the laboratory data, and the abnormal values of D-dimer and inflammatory indicators, such as WBC, CRP, cytokines, and so on, were detected every 3 to 5 days thereafter.

Serum cytokines were routinely measured because this would be, to some extent, helpful for therapy decisions, and the costs were not expensive. We detected the concentrations of interleukin (IL)-2, IL-4, IL-6, IL-10, tumor necrosis factor-alpha (TNF-α), and interferon-gamma (IFN-γ) in serum by a CBA HumanTh1/Th2 Cytokine Kit II (BD Biosciences, San Diego, CA, USA). The value of D-dimer was determined *via* INNOVANCE D-dimer (SIEMENS, Marburg, Germany), the normal value was less than 0.55 mg/L. The MP IgM was determined *via* a specific Anti-MP ELISA assay (EUROIMMUN, Luebeck, Germany), the absorbance above 1.1 was determined positive. MP RNA detection was performed on an ABI 7500 detection system *via* SAT-MP Assay Kit (Rendu Biotechnology Co., Ltd, Shanghai, China). All steps were performed according to the manufacturer's instructions and previous studies (Zhang et al., 2016; Li et al., 2017).

Ethics

The study was approved by the ethics committee of the Children's Hospital, Zhejiang University School of Medicine (2019-RIB-058). And the data from patients were collected anonymously.

Statistical Analysis

SPSS 20.0 (IBM Corp., Armonk, NY, USA) was used for statistical analysis. Continuous data are shown as median (25th to 75th percentile). Categorical data were shown as number (%). The Kruskal-Wallis-H(K-W-H) method was used to compare differences in continuous variables among multiple groups. The Mann-Whitney U-test was used to compare differences in continuous variables between two groups. Pearson's chi-square test was used to analyze differences between categorical variables. Spearman rank-correlation coefficients were used to describe the association between different variables and D-dimer. Statistical significance was defined as $P<0.05$.

RESULTS

General Information of Patients

From January 1, 2017, to December 31, 2019, a total of 356 patients admitted to our hospital for MPP were enrolled in the study. All patients had positive MP PCR tests and serological detection. According to the peak value of D-dimer (Huang et al., 2021), they were divided into three groups, the normal group (D-dimer <0.55 mg/L, n=106), the mild-moderately elevated group (D-dimer 0.55–5.5 mg/L, n=204) and the severely elevated group (more than 10 times higher than the normal range, D-dimer >5.5 mg/L, n=46). As shown in **Table 1**, the median age in the normal group was 4.1 years (range, 2.1–6.1), younger than that in the mild-moderately elevated group 5.8 years (range, 4.3–7.0) and the severely elevated group 6.1 years (range, 4.6–8.0) ($P<0.01$), but no difference was found in gender distribution ($P>0.05$).

Clinical Characteristics of Patients

The most common symptoms of MPP were cough (100.0%) and fever (98.0%). Chest pain (1.7%) was rare, and 62 patients (17.4%) presented with wheezing. As shown in **Table 1**, the higher incidence of fever and the lower incidence of wheezing were found in the mild-moderately or severely elevated group than those in the normal group ($P<0.01$). We also found that the total length of fever, the total length of antibiotic therapy, the length of stay, and the incidences of RMPP and SMPP were significantly different among the three groups ($P<0.01$). Interestingly, there were 14 patients (13.2%) with extra-pulmonary complications in the normal group, 72 patients (35.3%) in the mild-moderately elevated group, and 33 patients (71.7%) in the severely elevated group, which showed significant differences among these three groups ($P<0.01$). Moreover, the total length of fever, the total length of antibiotic therapy, the length of stay, and the incidence of extra-pulmonary complications, RMPP, SMPP were increased with the level of D-dimer ($P<0.01$).

Laboratory Findings of Patients

Laboratory findings of patients on admission were shown in **Table 2**. Besides D-dimer, the WBC, percentage of peripheral neutrophils (N%) and lymphocytes (L%), platelet (PLT), CRP, LDH, PAB, percentage of CD_4^+ and CD_8^+ T lymphocytes (CD_4^+%, CD_8^+%), IgA, IL-6, IL-10, TNF-α, IFN-γ also differed significantly among the three groups ($P<0.01$), but there were no statistically significant differences in hemoglobin, percentage of CD_3^+ T lymphocytes (CD_3^+%), IL-2, IL-4, IgG, IgM, and IgE ($P>0.05$). Furthermore, we found that N%, CRP, LDH, CD_8^+%, IL-6, IL-10, and IFN-γ were significantly increased in the elevated group, especially in the severely elevated group than those in the normal group, which were in line with the levels of D-dimer; whereas the L% and PAB decreased with the levels of D-dimer.

Radiographic Features of Patients

As shown in **Table 3**, we found that there were significant differences in radiographic features among the three groups ($P<0.01$). With the increase of D-dimer, the incidences of pleural effusion (26.4% *vs.* 64.2% *vs.* 93.5%, $P<0.01$), lobar atelectasis (3.8% *vs.* 33.3% *vs.* 63.0%, $P<0.01$), pulmonary consolidation (22.6% *vs.* 57.8% *vs.* 87.0%, $P<0.01$), large lesions (18.9% *vs.* 33.5% *vs.* 55.6%, $P<0.01$) were all significantly increased. As for necrotizing pneumonia, we found that it was likely to occur in the severely elevated group (23.9%, $P<0.01$), and there was no difference between the normal group and the

TABLE 1 | Demographic and clinical characteristics of patients with MPP.

Clinical information	Normal group (n=106)	Mild-moderately elevated group (n=204)	Severely elevated group (n=46)	*P*-value
Sex (male/female)	56/50	91/113	21/25	0.397
Age, years	4.1 (2.1~6.1)	5.8 (4.3~7.0) [a#]	6.1 (4.6~8.0) [b#]	0.000
Clinical presentation, n (%)				
Fever	100 (94.3%)	203 (99.5%) [a#]	46 (100.0%) [b#]	0.010
Cough	106 (100.0%)	204 (100.0%)	46(100.0%)	1.000
Wheezing	34 (32.1%)	25 (12.3%) [a#]	3 (6.5%) [b#]	0.000
Chest pain	2 (1.9%)	3 (1.5%)	1 (2.2%)	1.000
Extra-pulmonary complications, n (%)	14 (13.2%)	72 (35.3%) [a#]	33 (71.7%) [b#,c#]	0.000
Digestive system	7 (6.6%)	45 (22.1%)	12 (26.1%)	
Cardiovascular system	2 (1.9%)	9 (4.4%)	5 (10.9%)	
Neurologic system	2 (1.9%)	4 (2.0%)	2 (4.3%)	
Hematologic system	1 (0.9%)	2 (1.0%)	3 (6.5%)	
Skin and Mucosae	1 (0.9%)	3 (1.5%)	0 (0.0%)	
Multi-systems	1 (0.9%)	9 (4.4%)	11 (23.9%)	
Length of fever, days	7.3±3.9	10.2±3.1 [a#]	14.5±4.8 [b#,c#]	0.000
Length of stay, days	6.0 (4.0~7.0)	7.0 (5.0~10.0) [a#]	13.0 (10.0~18.0) [b#,c#]	0.000
Length of antibiotic therapy days	10.5 (8.0~13.3)	12.0 (10.0~16.0) [a#]	19.0 (15.0~25.0) [b#,c#]	0.000
RMPP, n (%)	7 (6.6%)	85 (41.7%) [a#]	40 (87.0%) [b#,c#]	0.000
SMPP, n (%)	68 (64.2%)	176 (86.3%) [a#]	46 (100.0%) [b#,c#]	0.000

Data are presented as median (25^{th}~75^{th} percentile), or number (percentage). #P < 0.01; [a]compared between normal group and mild-moderately elevated group; [b]compared between normal group and severely elevated group; [c]compared between mild-moderately elevated group and severely elevated group.

Digestive system complications: hepatic impairment, hepatomegaly.

Cardiovascular system complications: myocardial damage, pericardial effusion, Kawasaki disease.

Neurologic system complications: encephalitis, Guillain–Barre's syndrome.

Hematologic system complications: anemia, cytopenia.

Skin and Mucosae complications: unspecific rashes, Stevens-Johnson syndrome.

RMPP, Refractory mycoplasma pneumonia pneumonia; SMPP, Severe mycoplasma pneumonia pneumonia.

TABLE 2 | Laboratory findings of patients with MPP on admission.

Laboratory information	Normal group (n=106)	Mild-moderately elevated group (n=204)	Severely elevated group (n=46)	*P*-value
Routine blood test				
White blood cell ($\times10^9$/L)	7.72 (6.28~9.79)	7.33 (5.79~9.36)	8.22 (6.72~10.65) [c*]	0.048
Neutrophil, %	57.7 (43.5~65.2)	65.4 (55.9~71.8) [a#]	75.9 (66.8~81.2) [b#,c#]	0.000
Lymphocyte, %	31.2 (25.9~44.8)	24.7 (18.9~32.5) [a#]	17.2 (12.6~25.7) [b#,c#]	0.000
Hemoglobin, g/L	122 (113~128)	122 (116~129)	119 (114~129)	0.197
Platelet ($\times10^9$/L)	336 (267~405)	288 (222~361) [a#]	262 (197~336) [b#]	0.000
CRP, mg/L	3.4 (0.5~12.7)	15.1 (6.2~37.0) [a#]	56.2 (23.4~95.3) [b#,c#]	0.000
LDH, IU/L	334 (272~438)	440 (348~591) [a#]	678(542~944) [b#,c#]	0.000
PAB, g/L	0.11 (0.10~0.14)	0.10 (0.08~0.13) [a#]	0.08 (0.06~0.12) [b#,c#]	0.000
Subpopulations of T lymphocytes, %				
CD_3	65.55 (58.48~74.84)	66.68 (59.92~74.23)	63.55 (54.74~72.39)	0.156
CD_4	36.98 (31.64~43.66)	36.15 (29.90~42.09)	28.23 (23.76~36.60) [b#,c#]	0.000
CD_8	20.92 (16.70~26.28)	23.33 (19.44~28.99) [a#]	26.48 (22.95~33.09) [b#,c#]	0.000
Total Immunoglobulin (Ig)				
IgG, g/L	8.80 (7.10~10.73)	8.95 (7.60~10.70)	8.35 (7.18~10.63)	0.475
IgA, g/L	1.02 (0.69~1.37)	1.28 (0.87~1.78) [a#]	1.25 (0.99~1.64) [b#]	0.000
IgM, g/L	1.57 (1.16~2.03)	1.65 (1.22~2.24)	1.55 (0.99~2.40)	0.229
IgE, IU/ml	96.9 (37.6~218.5)	93.9 (38.4~290.5)	99.9 (51.1~287.3)	0.855
Cytokines, pg/ml				
IL-2	1.4 (1.1~1.7)	1.4 (1.1~1.7)	1.6 (1.1~2.4)	0.190
IL-4	2.0 (1.7~2.3)	2.0 (1.6~2.5)	2.2 (1.4~2.8)	0.593
IL-6	16.9 (7.9~43.4)	26.7 (13.3~57.8) [a*]	59.5 (24.2~120.3) [b#,c#]	0.000
IL-10	5.5 (4.4~7.6)	8.5 (6.0~12.0) [a#]	9.4 (7.1~16.0) [b#,c*]	0.000
TNF-α	2.5(1.8~4.6)	2.3(1.8~4.1)	1.7 (1.0~2.6) [b#,c#]	0.000
IFN-γ	3.2 (2.2~4.8)	5.1 (2.8~10.8) [a#]	8.4 (4.0~40.1) [b#,c*]	0.000
D-dimer, mg/L	0.37 (0.25~0.44)	1.26 (0.82~2.07) [a#]	7.68 (6.22~14.16) [b#,c#]	0.000

*Data are presented as the median (25^{th}-75^{th} percentile). *P < 0.05, #P < 0.01; [a]compared between normal group and mild-moderately elevated group; [b]compared between normal group and severe elevated group; [c]compared between mild-moderately elevated group and severely elevated group. CRP, C-reactive protein; LDH, Lactate dehydrogenase; PAB, Prealbumin; IL-2, Interleukin 2; IL-4, Interleukin 4; IL-6, Interleukin 6; IL-10, Interleukin 10; TNF-α, Tumor necrosis factor-alpha; IFN-γ, Interferon-gamma.*

TABLE 3 | Radiographic features of patients with MPP.

Radiological features, n (%)	Normal group (n=106)	Mild-moderately elevated group (n=204)	Severely elevated group (n=46)	*P*-value
Pleural effusion	28 (26.4%)	131 (64.2%) $^{a\#}$	43 (93.5%) $^{b\#,c\#}$	0.000
Lobar atelectasis	4 (3.8%)	68 (33.3%) $^{a\#}$	29 (63.0%) $^{b\#,c\#}$	0.000
Pulmonary consolidation	24 (22.6%)	118 (57.8%) $^{a\#}$	40 (87.0%) $^{b\#,c\#}$	0.000
Large lesions	20 (18.9%)	66 (33.5%) $^{a\#}$	30 (55.6%) $^{b\#,c\#}$	0.000
Necrotizing pneumonia	1 (0.9%)	7 (3.4%)	11 (23.9%) $^{b\#,c\#}$	0.000
Embolism	0 (0.0%)	0 (0.0%)	0 (0.0%)	1.000

Data are presented as number (percentage). $^{\#}P < 0.01$; ^{a}compared between normal group and mild-moderately elevated group; ^{b}compared between normal group and severely elevated group; ^{c}compared between mild-moderately elevated group and severely elevated group.
Large lesion was defined as the extent of infiltration on chest imaging more than 1/3 of the lung.

TABLE 4 | Treatments of patients with MPP.

Treatments, n (%)	Normal group (n=106)	Mild-moderately elevated group (n=204)	Severely elevated group (n=46)	*P*-value
Oxygen therapy	28 (26.4%)	46 (22.5%)	24 (52.2%) $^{b\#,c\#}$	0.000
Glucocorticoid	51 (48.1%)	150 (73.5%) $^{a\#}$	44 (95.7%) $^{b\#,c\#}$	0.000
Bronchoscope	21 (19.8%)	110 (53.9%) $^{a\#}$	40 (87.0%) $^{b\#,c\#}$	0.000
immunoglobulin	3 (2.8%)	10 (4.9%)	14 (30.4%) $^{b\#,c\#}$	0.000
ICU	0 (0.0%)	2 (1.0%)	8 (17.4%) $^{b\#,c\#}$	0.000
Mechanical ventilation	0 (0.0%)	0 (0.0%)	0 (0.0%)	1.000
Thoracentesis	0 (0.0%)	15 (7.4%) $^{a\#}$	19 (41.3%) $^{b\#,c\#}$	0.000

Data are presented as number (percentage). $^{\#}P < 0.01$; ^{a}compared between normal group and mild-moderately elevated group; ^{b}compared between normal group and severely elevated group; ^{c}compared between mild-moderately elevated group and severely elevated group.

mild-moderately elevated group (0.9% *vs.* 3.4%, $P>0.05$). However, none of the patients developed embolism in our study.

Treatment of Patients

In addition to antibiotics, patients received other treatments depending on the disease severity, such as oxygen therapy, glucocorticoid, bronchoscopy, immunoglobulin, thoracentesis, or ICU admission (as shown in **Table 4**). In our study, we found that patients in the severely elevated group received a higher proportion of oxygen therapy, glucocorticoid, bronchoscopy, immunoglobulin, thoracentesis, and ICU admission when compared with the other two groups ($P<0.01$). Meanwhile, the usage rates of glucocorticoid, bronchoscopy and thoracentesis were likewise higher in the mild-moderately elevated group than those in the normal group ($P<0.01$). None of the patients needed mechanical ventilation. All the children recovered and were discharged from the hospital without death.

Correlation Analysis of the Level of D-dimer With Different Variables

Using the Spearman correlation test, we analyzed the relationships between the level of D-dimer and different variables. As shown in **Figure 1**, we found that the following variables showed significant positive correlations with the level of D-dimer ($P<0.01$): N%, CRP, LDH, CD_8^+%, IL-6, IL-10, IFN-γ, age, length of fever, length of stay, and length of antibiotic therapy. Meanwhile, L%, PLT, PAB, CD_4^+%, and TNF-α were negatively correlated with the level of D-dimer ($P<0.01$). Among these variables, N%, L%, CRP, LDH, IL-10, length of fever, length of stay, and length of antibiotic therapy had particularly strong correlations with D-dimer.

DISCUSSION

Mycoplasma pneumoniae (MP) is one of the most common pathogens of CAP in children. In some cases, MP infection will cause severe pneumonia with a variety of complications (Poddighe, 2018). Recently, a few researchers have also reported that thrombotic diseases could occur in patients with MPP, which is thought to be associated with the elevated level of D-dimer (Li et al., 2017; Liu et al., 2020; Mirijello et al., 2020). The elevation of D-dimer is widespread in patients with MPP, but the incidence of thrombosis is not high, and no case of embolism was found, as well as in our study. Furthermore, to the best of our knowledge, there is little published literature focusing on the significance of elevated D-dimer in patients with MPP. So, in the present study, we retrospectively enrolled 356 MPP patients with different degrees of D-dimer and analyzed the relationship between the levels of D-dimer and clinical characteristics.

In our study, more severe signs and symptoms, higher incidence of extra-pulmonary complications, RMPP, SMPP, and longer process of disease were found in the elevated groups, especially in the severely elevated group. And there were more severe pulmonary lesions and higher levels of inflammatory biomarkers, such as CRP, LDH, N%, CD_8^+%, IL-6, IL-10, and IFN-γ, which were in line with the increase of D-dimer, whereas the L% and PAB decreased with the levels of D-dimer. Furthermore, we found that N%, L%, CRP, LDH, IL-10, length of fever, length of stay, and length of antibiotic therapy had strong correlations with D-dimer.

D−dimer was originally known as a specific fibrin degradation product, as well as a specific marker of the fibrinolytic system, which can reflect the coagulation function and fiber activity of the body (Zhang et al., 2020). However,

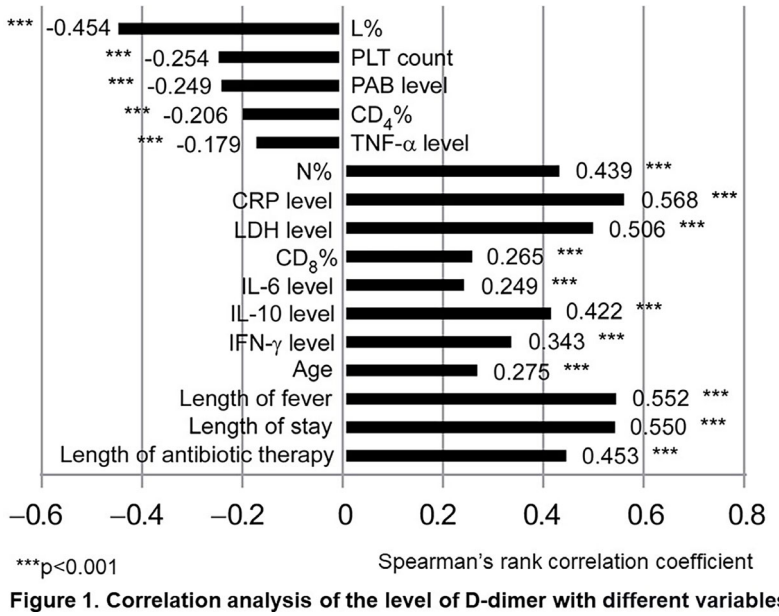

FIGURE 1 | Correlation analysis of the level of D-dimer with different variables. Spearman rank-correlation coefficients were used to describe the association between different variables and D-dimer. Statistical significance was defined as $P < 0.05$, ***$P < 0.001$. N, neutrophil; L, lymphocyte; PLT, Platelet; CRP, C-reactive protein; LDH, Lactate dehydrogenase; PAB, Prealbumin; IL-6, Interleukin 6; IL-10, Interleukin 10; TNF-α, Tumor necrosis factor-alpha; IFN-γ, Interferon-gamma.

recently, it has also been recognized as an indicator for evaluating the severity of CAP (Snijders et al., 2012). The results in our study showed that MPP patients with higher levels of D-dimer had more severe clinical manifestation and needed a longer duration of treatment, which might help to confirm other research's finding that D-dimer could act as an indicator for evaluating the severity of disease.

Cell-mediated immunological response plays a major role in the progression of MPP (Waites et al., 2017). Our preceding study and several other studies have demonstrated that inflammatory cytokines and some serum biomarkers were involved in the immunopathogenesis of MP infection (Tanaka et al., 2002; Narita and Tanaka, 2007; Lu et al., 2015; Choi et al., 2019; Ling et al., 2020). Furthermore, with the progress of MPP, immune cells release different kinds of inflammatory mediators, such as IL-1β, IL-8, TNF-α, and then aggravate the injury of vascular endothelial cells, leading to a significant increase of D-dimer (Iturriaga et al., 2015; Mishra et al., 2015; Jin et al., 2018). In this study, we found that some cytokines and inflammatory markers (CRP, LDH, N%, CD_8^+%, IL-6, IL-10, and IFN-γ) were significantly increased in the elevated groups, and there were highly positive correlations between the levels of D-dimer and some inflammatory markers (N%, CRP, LDH, IL-10). These results implied that higher levels of D-dimer might be associated with stronger inflammation, which was consistent with other reports (Yu et al., 2020).

MP is well recognized for producing a broad array of extra-pulmonary manifestations. More interestingly, our study found that the incidence of extra-pulmonary complications was much higher in the elevated groups than that in the normal group, and the incidence of extra-pulmonary complications was increased with the level of D-dimer. To our knowledge, this is the first report showing the relationship between the level of D-dimer and the extra-pulmonary complications in MPP patients. The mechanisms of MPP causing extra-pulmonary complications, by far, are not fully understood. Some studies have shown that it might be a direct effect of the MP that presents at the site of inflammation mediated by cytokine release by the host (Waites et al., 2017). Some researchers considered that it might be a direct or indirect effect by the production of vasculitis or thrombosis as a result of cytokines and chemokines or by immunomodulation through mediators, such as complement and fibrin D-dimers (Narita, 2009; Li et al., 2017; Waites et al., 2017). The latter might be the underlying mechanisms of the phenomenon in our study that the higher the incidence of extra-pulmonary complication was, the higher the D-dimer value was. Recent medical literature also suggested that increased IgE levels (atopy) might be associated with extra-pulmonary manifestations in children with MPP (Wang et al., 2019). However, we found that there were no significant differences in IgE levels among all three groups in our study. This might be because that different age ranges of patients among groups caused different normal ranges of IgE.

There were several limitations in our study. First, our study was a single-center retrospective study, which might have introduced a selection bias. The results reported in our study cannot be extrapolated to other areas of China. Thus, a prospective multicenter study is needed in the future. Second,

there might be some patients who had coinfection with other pathogens, which could not be detected precisely and might therefore lead to the elevation of D-dimer. Third, we did not monitor dynamic changes of D-dimer. Therefore, it may result in some omissions of hypercoagulable states.

In conclusion, MPP patients with higher levels of D-dimer might have more severe clinical manifestation and need a longer duration of therapy, which was perhaps closely related to the degree of inflammation of MPP. These findings might help physicians to have deeper insights into MPP and provide proper treatment for MPP patients with higher levels of D-dimer.

DATA AVAILABILITY STATEMENT

The original contributions presented in the study are included in the article/supplementary material. Further inquiries can be directed to the corresponding authors.

AUTHOR CONTRIBUTIONS

Conceived and designed the experiments: YYZ and ZMC. Wrote the manuscript: YZ and YYZ. Collected and analyzed the data: YZ, LLH, QNZ, MYL, YSW, YLZ and MXH. All authors contributed to the article and approved the submitted version.

FUNDING

This work was supported by grants from National Natural Science Foundation (81871264).

ACKNOWLEDGMENTS

We are grateful to colleagues in the Department of Pulmonology for taking care of patients and collecting the clinical data. We would like to thank the support of Zhejiang Provincial Key Laboratory of Immunity and Inflammatory diseases.

REFERENCES

Adam, S. S., Key, N. S., and Greenberg, C. S. (2009). D-dimer antigen: current concepts and future prospects. *Blood* 113 (13), 2878–2887. doi: 10.1182/blood-2008-06-165845

Chen, S., Ding, Y., Vinturache, A., Gu, H., Lu, M., and Ding, G. (2020). Pulmonary Embolism Associated With Mycoplasma in a Child. *Lancet Infect. Dis.* 20 (11), 1347. doi: 10.1016/S1473-3099(20)30253-X

Choi, Y. J., Jeon, J. H., and Oh, J. W. (2019). Critical Combination of Initial Markers for Predicting Refractory Mycoplasma Pneumoniae Pneumonia in Children: A Case Control Study. *Respir. Res.* 20 (1), 193. doi: 10.1186/s12931-019-1152-5

Goldenberg, N. A., Knapp-Clevenger, R., and Manco-Johnson, M. J. (2004). Mountain States Regional Thrombophilia Group. Elevated plasma factor VIII and D-dimer levels as predictors of poor outcomes of thrombosis in children. *N Engl. J. Med.* 351 (11), 1081–1088. doi: 10.1056/NEJMoa040161

Huang, X., Li, D., Liu, F., Zhao, D., Zhu, Y., and Tang, H. (2021). Clinical Significance of D-Dimer Levels in Refractory Mycoplasma Pneumoniae Pneumonia. *BMC Infect. Dis.* 21 (1), 14. doi: 10.1186/s12879-020-05700-5

Iturriaga, R., Moya, E. A., and Del Rio, R. (2015). Inflammation and Oxidative Stress During Intermittent Hypoxia: The Impact on Chemoreception. *Exp. Physiol.* 100 (2), 149–155. doi: 10.1113/expphysiol.2014.079525

Jain, S., Williams, D. J., Arnold, S. R., Ampofo, K., Bramley, A. M., Reed, C., et al. (2015). Community-acquired pneumonia requiring hospitalization among U.S. children. *N Engl. J. Med.* 372 (9), 835–845. doi: 10.1056/NEJMoa1405870

Jin, X., Zhu, Y., Zhang, Y., Chen, J., Rong, L., and Zhao, X. (2018). Assessment of Levels of D-Dimer and Interferon-γ in Pediatric Patients With Mycoplasma Pneumoniae Pneumonia and its Clinical Implication. *Exp. Ther. Med.* 16 (6), 5025–5030. doi: 10.3892/etm.2018.6873

Kang, B., Kim, D. H., Hong, Y. J., Son, B. K., Lim, M. K., Choe, Y. H., et al. (2016). Complete Occlusion of the Right Middle Cerebral Artery Associated With Mycoplasma Pneumoniae Pneumonia. *Korean J. Pediatr.* 59 (3), 149–152. doi: 10.3345/kjp.2016.59.3.149

Li, W., Fang, Y. H., Shen, H. Q., Yang, D. H., Shu, Q., and Shang, S. Q. (2017). Evaluation of a Real-Time Method of Simultaneous Amplification and Testing in Diagnosis of Mycoplasma Pneumoniae Infection in Children With Pneumonia. *PloS One* 12 (5), e0177842. doi: 10.1371/journal.pone.0177842

Ling, Y., Zhang, T., Guo, W., Zhu, Z., Tian, J., Cai, C., et al. (2020). Identify Clinical Factors Related to Mycoplasma Pneumoniae Pneumonia With Hypoxia in Children. *BMC Infect. Dis.* 20 (1), 534. doi: 10.1186/s12879-020-05270-6

Liu, J., He, R., Wu, R., Wang, B., Xu, H., Zhang, Y., et al. (2020). Mycoplasma Pneumoniae Pneumonia Associated Thrombosis at Beijing Children's Hospital. *BMC Infect. Dis.* 20 (1), 51. doi: 10.1186/s12879-020-4774-9

Li, T., Yu, H., Hou, W., Li, Z., Han, C., and Wang, L. (2017). Evaluation of Variation in Coagulation Among Children With Mycoplasma Pneumoniae Pneumonia: A Case-Control Study. *J. Int. Med. Res.* 45 (6), 2110–2118. doi: 10.1177/0300060517709613

Lu, A., Wang, C., Zhang, X., Wang, L., and Qian, L. (2015). Lactate Dehydrogenase as a Biomarker for Prediction of Refractory Mycoplasma Pneumoniae Pneumonia in Children. *Respir. Care* 60 (10), 1469–1475. doi: 10.4187/respcare.03920

Mélé, N., and Turc, G. (2018). Stroke Associated With Recent Mycoplasma Pneumoniae Infection: A Systematic Review of Clinical Features and Presumed Pathophysiological Mechanisms. *Front. Neurol.* 9, 1109. doi: 10.3389/fneur.2018.01109

Meyer Sauteur, P. M., Theiler, M., Buettcher, M., Seiler, M., Weibel, L., and Berger, C. (2020). Frequency and Clinical Presentation of Mucocutaneous Disease Due to Mycoplasma Pneumoniae Infection in Children With Community-Acquired Pneumonia. *JAMA Dermatol.* 156 (2), 144–150. doi: 10.1001/jamadermatol.2019.3602

Mirijello, A., La Marca, A., D'Errico, M. M., Curci, S., Vendemiale, G., Grandone, E., et al. (2020). Venous Thromboembolism During Mycoplasma Pneumoniae Infection: Case Report and Review of the Literature. *Eur. Rev. Med. Pharmacol. Sci.* 24 (19), 10061–10068. doi: 10.26355/eurrev_202010_23223

Mishra, K. P., Ganju, L., and Singh, S. B. (2015). Hypoxia Modulates Innate Immune Factors: A Review. *Int. Immunopharmacol* 28 (1), 425–428. doi: 10.1016/j.intimp.2015.07.008

Narita, M. (2009). Pathogenesis of Neurologic Manifestations of Mycoplasma Pneumoniae Infection. *Pediatr. Neurol.* 41 (3), 159–166. doi: 10.1016/j.pediatrneurol.2009.04.012

Narita, M., and Tanaka, H. (2007). Cytokines Involved in the Severe Manifestations of Pulmonary Diseases Caused by Mycoplasma Pneumoniae. *Pediatr. Pulmonol* 42 (4), 397. doi: 10.1002/ppul.20445

Nowak-Göttl, U., and Kosch, A. (2004). D-Dimer, and Thromboembolism in Children. *N Engl. J. Med.* 351 (11), 1051–1053. doi: 10.1056/NEJMp048150

Park, S. J., Lee, Y. M., Lee, C. H., Cho, J. H., and Lee, J. H. (2012). A case of splenic infarction possibly attributable to Mycoplasma pneumoniae infection without accompanying pneumonia. *J. Infect. Chemother.* 18 (6), 945–947. doi: 10.1007/s10156-012-0390-y

Poddighe, D. (2018). Extra-Pulmonary Diseases Related to Mycoplasma Pneumoniae in Children: Recent Insights Into the Pathogenesis. *Curr. Opin. Rheumatol* 30 (4), 380–387. doi: 10.1097/BOR.0000000000000494

Sakka, M., Connors, J. M., Hékimian, G., Martin-Toutain, I., Crichi, B., Colmegna, I., et al. (2020). Association Between D-Dimer Levels and Mortality in Patients With Coronavirus Disease 2019 (COVID-19): A Systematic Review and Pooled Analysis. *J. Med. Vasc.* 45 (5), 268–274. doi: 10.1016/j.jdmv.2020.05.003

Snijders, D., Schoorl, M., Schoorl, M., Bartels, P. C., van der Werf, T. S., and Boersma, W. G. (2012). D-dimer levels in assessing severity and clinical outcome in patients with community-acquired pneumonia. A secondary analysis of a randomised clinical trial. *Eur. J. Intern. Med.* 23 (5), 436–441. doi: 10.1016/j.ejim.2011.10.019

Subspecialty Group of Respiratory Diseases (2013). The Society of Pediatrics, Chinese Medical Association; Editorial Board, Chinese Journal of Pediatrics. [Guidelines for Management of Community Acquired Pneumonia in Children (the Revised Edition of 2013) (I)]. *Zhonghua Er Ke Za Zhi* 51 (10), 745–752.

Tamura, A., Matsubara, K., Tanaka, T., Nigami, H., Yura, K., and Fukaya, T. (2008). Methylprednisolone Pulse Therapy for Refractory Mycoplasma Pneumoniae Pneumonia in Children. *J. Infect.* 57 (3), 223–228. doi: 10.1016/j.jinf.2008.06.012

Tanaka, H., Narita, M., Teramoto, S., Saikai, T., Oashi, K., Igarashi, T., et al. (2002). Role of Interleukin-18 and T-Helper Type 1 Cytokines in the Development of Mycoplasma Pneumoniae Pneumonia in Adults. *Chest* 121 (5), 1493–1497. doi: 10.1378/chest.121.5.1493

Uehara, S., Sunakawa, K., Eguchi, H., Ouchi, K., Okada, K., Kurosaki, T., et al. (2011). Japanese Guidelines for the Management of Respiratory Infectious Diseases in Children 2007 With Focus on Pneumonia. *Pediatr. Int.* 53 (2), 264–276. doi: 10.1111/j.1442-200X.2010.03316.x

Waites, K. B., and Talkington, D. F. (2004). Mycoplasma Pneumoniae and its Role as a Human Pathogen. *Clin. Microbiol. Rev.* 17 (4), 697–728. doi: 10.1128/CMR.17.4.697-728.2004

Waites, K. B., Xiao, L., Liu, Y., Balish, M. F., and Atkinson, T. P. (2017). Mycoplasma Pneumoniae From the Respiratory Tract and Beyond. *Clin. Microbiol. Rev.* 30 (3), 747–809. doi: 10.1128/CMR.00114-16

Wang, Z., Sun, J., Liu, Y., and Wang, Y. (2019). Impact of Atopy on the Severity and Extrapulmonary Manifestations of Childhood Mycoplasma Pneumoniae Pneumonia. *J. Clin. Lab. Anal.* 33 (5), e22887. doi: 10.1002/jcla.22887

Weitz, J. I., Fredenburgh, J. C., and Eikelboom, J. W. (2017). A Test in Context: D-Dimer. *J. Am. Coll. Cardiol.* 70 (19), 2411–2420. doi: 10.1016/j.jacc.2017.09.024

Witmer, C. M., Steenhoff, A. P., Shah, S. S., and Raffini, L. J. (2007). Mycoplasma Pneumoniae, Splenic Infarct, and Transient Antiphospholipid Antibodies: A New Association? *Pediatrics* 119 (1), e292–e295. doi: 10.1542/peds.2006-1340

Yu, B., Li, X., Chen, J., Ouyang, M., Zhang, H., Zhao, X., et al. (2020). Evaluation of Variation in D-Dimer Levels Among COVID-19 and Bacterial Pneumonia: A Retrospective Analysis. *J. Thromb. Thrombolysis* 50 (3), 548–557. doi: 10.1007/s11239-020-02171-y

Zhang, Y., Chen, Y., Chen, Z., Zhou, Y., Sheng, Y., Xu, D., et al. (2014). Effects of Bronchoalveolar Lavage on Refractory Mycoplasma Pneumoniae Pneumonia. *Respir. Care* 59 (9), 1433–1439. doi: 10.4187/respcare.03032

Zhang, Y., Mei, S., Zhou, Y., Huang, M., Dong, G., and Chen, Z. (2016). Cytokines as the Good Predictors of Refractory Mycoplasma Pneumoniae Pneumonia in School-Aged Children. *Sci. Rep.* 6, 37037. doi: 10.1038/srep37037

Zhang, L., Yan, X., Fan, Q., Liu, H., Liu, X., Liu, Z., et al. (2020). D-dimer levels on admission to predict in-hospital mortality in patients with Covid-19. *J. Thromb. Haemost.* 18 (6), 1324–1329. doi: 10.1111/jth.14859

Zhou, Y., Zhang, Y., Sheng, Y., Zhang, L., Shen, Z., and Chen, Z. (2014). More Complications Occur in Macrolide-Resistant Than in Macrolide-Sensitive Mycoplasma Pneumoniae Pneumonia. *Antimicrob. Agents Chemother.* 58 (2), 1034–1038. doi: 10.1128/AAC.01806-13

Conflict of Interest: The authors declare that the research was conducted in the absence of any commercial or financial relationships that could be construed as a potential conflict of interest.

frontiers in Cellular and Infection Microbiology

BRIEF RESEARCH REPORT
published: 25 November 2021
doi: 10.3389/fcimb.2021.765941

Human Glomerular Endothelial Cells Treated With Shiga Toxin Type 2 Activate γδ T Lymphocytes

*David Antonio Rosso[1], Micaela Rosato[1], Fernando Daniel Gómez[2], Romina Soledad Álvarez[2], Carolina Maiumi Shiromizu[1], Irene Angélica Keitelman[1], Cristina Ibarra[2], María Marta Amaral[2] and Carolina Cristina Jancic[1,3]**

[1] Instituto de Medicina Experimental–Consejo Nacional de Investigaciones Científicas y Técnicas (CONICET)–Academia Nacional de Medicina., Buenos Aires, Argentina, [2] Laboratorio de Fisiopatogenia, Departamento de Fisiología, Instituto de Fisiología y Biofísica Bernardo Houssay (IFIBIO Houssay–Consejo Nacional de Investigaciones Científicas y Técnicas (CONICET)), Facultad de Medicina, Universidad de Buenos Aires, Buenos Aires, Argentina, [3] Departamento de Microbiología, Parasitología e Inmunología, Facultad de Medicina, Universidad de Buenos Aires, Buenos Aires, Argentina

The hemolytic uremic syndrome associated with diarrhea, a consequence of Shiga toxin (Stx)-producing *Escherichia coli* infection, is a common cause of pediatric acute renal failure in Argentina. Stx type 2a (Stx2a) causes direct damage to renal cells and induces local inflammatory responses that involve secretion of inflammatory mediators and the recruitment of innate immune cells. γδ T cells constitute a subset of T lymphocytes, which act as early sensors of cellular stress and infection. They can exert cytotoxicity against infected and transformed cells, and produce cytokines and chemokines. In this study, we investigated the activation of human peripheral γδ T cells in response to the incubation with Stx2a-stimulated human glomerular endothelial cells (HGEC) or their conditioned medium, by analyzing in γδ T lymphocytes, the expression of CD69, CD107a, and perforin, and the production of TNF-α and IFN-γ. In addition, we evaluated by confocal microscopy the contact between γδ T cells and HGEC. This analysis showed an augmentation in cellular interactions in the presence of Stx2a-stimulated HGEC compared to untreated HGEC. Furthermore, we observed an increase in cytokine production and CD107a expression, together with a decrease in intracellular perforin when γδ T cells were incubated with Stx2a-treated HGEC or their conditioned medium. Interestingly, the blocking of TNF-α by Etanercept reversed the changes in the parameters measured in γδ T cells incubated with Stx2a-treated HGEC supernatants. Altogether, our results suggest that soluble factors released by Stx2a-stimulated HGEC modulate the activation of γδ T cells, being TNF-α a key player during this process.

Keywords: γδ T cells, hemolytic uremic syndrome, Shiga toxin type 2, inflammation, Th1-like profile

OPEN ACCESS

Edited by:
Elias Adel Rahal, American University of Beirut, Lebanon

Reviewed by:
Mona Elgazzaz, Louisiana State University, United States
Moo-Seung Lee, Korea Research Institute of Bioscience and Biotechnology (KRIBB), South Korea

***Correspondence:**
Carolina Cristina Jancic
cjancic@fmed.uba.ar
orcid.org/0000-0001-9222-9571

Specialty section:
This article was submitted to Microbes and Innate Immunity, a section of the journal Frontiers in Cellular and Infection Microbiology

Received: *27 August 2021*
Accepted: *19 October 2021*
Published: *25 November 2021*

Citation:
Rosso DA, Rosato M, Gómez FD, Álvarez RS, Shiromizu CM, Keitelman IA, Ibarra C, Amaral MM and Jancic CC (2021) Human Glomerular Endothelial Cells Treated With Shiga Toxin Type 2 Activate γδ T Lymphocytes. Front. Cell. Infect. Microbiol. 11:765941. doi: 10.3389/fcimb.2021.765941

INTRODUCTION

Hemolytic uremic syndrome (HUS) is a late acute onset of symptoms that can appear after an initial intestinal infection with Shiga Toxin (Stx)-producing *Escherichia coli* (STEC). While some STEC strains can cause severe diseases, others are only associated with mild diarrhea or no disease at all (Coombes et al., 2011). This is due in part to the variations in the genetic background of the virulence genes in the different strains. STEC O157:H7 has been considered the strain most associated with HUS outbreaks (Carter et al., 2021), but there are other serotypes such as STEC O145 that are associated with human disease and have also been the cause of reported outbreaks worldwide (Carter et al., 2021). As well, *Escherichia coli* strain belonging to serotype O104:H4 was responsible for the outbreak of HUS and bloody diarrhea that began in northern Germany, which spread rapidly locally (Bielaszewska et al., 2011; Frank et al., 2011) and subsequently in 15 other countries (Rasko et al., 2011). The particular features of this outbreak were that it affected mainly adult women and provoked severe neurological complications and, it has been reported, several fatal cases (Frank et al., 2011). Of mention, the O104:H4 outbreak strain was an enteroaggregative *Escherichia coli* strain rather than a typical enterohemorrhagic one (Rasko et al., 2011). In addition, a series of outbreaks of infection with enterohemorrhagic *Escherichia coli* O157:H7 occurred in Japan in 1996, the largest outbreak occurring in primary schools in Osaka Prefecture, where more than 7,500 cases were reported (Terajima et al., 2014). The condition of Japan infection was not exactly the same as in continental Europe, where non-O157 STEC serotypes were more common than infections with O157:H7 STEC (Blanco et al., 1992; Caprioli and Tozzi, 1998). In addition, between 2000 and 2012, there were 12 other outbreaks that appear to have resulted from consumption of contaminated foods. Interestingly, other than O157:H7 STEC were characterized, such as O111:H8 (Terajima et al., 2014). In accordance with the data described, in Argentina, HUS is highly prevalent, being the most common cause of acute renal failure and the second cause of chronic renal failure in children younger than 5 years old (Repetto, 1997). Furthermore, it is one of the leading causes of renal transplants in childhood, having STEC O157:H7 as the main pathogen involved. Stx type 1 and type 2 (Stx1 and Stx2) produced by STEC O157:H7 and other strains are considered the main and essential virulence factors associated with HUS that trigger kidney damage in patients. Of mention, STEC strains expressing Stx2 are the most common etiologic pathogen responsible for severe cases of HUS in Argentina, and the subtype Stx2a causes more serious illnesses than strains encoding Stx2c (Fitzgerald et al., 2019). Of note, Stx2 is classified into several subtypes (i.e., Stx2a, Stx2b, Stx2c, Stx2d, Stx2e, Stx2f, and Stx2g) (Scheutz et al., 2012). STEC with Stx2a was more frequently isolated from HUS patients than the strains with the other Stx2 subtypes (Friedrich et al., 2002; Persson et al., 2007). Regarding the toxin structure, the Stxs contain two subunits, A and B, organized as a pentameric ring of identical B-subunits non-covalently associated with a single A-subunit (Lee et al., 2016). The B-subunits allow the interaction with Stx receptor, and the A-subunit has the enzymatic activity involved in the toxic effect. Once the toxin interacts with its receptor, the membrane glycolipid, globotriaosylceramide (Gb3, also known as CD77), the toxin is internalized and suffers a retrograde intracellular trafficking. By the interaction with the pentameric B-subunits, Gb3 cross-linking, it is thought to trigger receptor-mediated endocytosis (Sandvig et al., 2014). Following the internalization, the toxin is sequentially delivered from an early endosome to the trans-Golgi network, then to the Golgi apparatus, and finally to the endoplasmic reticulum (Sandvig et al., 1992). During the transport to the endoplasmic reticulum, Stx A-subunits dissociate from the B-subunits through a mechanism that involves proteolysis and disulfide bond reduction (Garred et al., 1995). Once dissociated, fragments of the A-subunits associate with chaperones present in the endoplasmic reticulum and then retrotranslocate to the cytosol (LaPointe et al., 2005). Once in the cytoplasm, toxin A-fragments appear to re-fold into their active conformation (Hazes and Read, 1997). All this process results in host cell protein synthesis inhibition, activation of the ribotoxic and endoplasmic reticulum stress responses, and in the induction of apoptosis (of epithelial, endothelial, lymphoid and myeloid cells), autophagy and increased expression of pro-inflammatory cytokines and chemokines (Johannes and Römer, 2010), which contribute to tissue damage in the colon and the development of HUS and central nervous system complications. HUS is clinically characterized by microangiopathic hemolytic anemia, thrombocytopenia, and variable degrees of kidney injury (Alconcher et al., 2018). During the hemorrhagic colitis stage, disruption of the mucosa allows the Stx to enter the bloodstream and to target tissues expressing its receptor, which is present in the microvasculature of several organs, mainly the kidney and central nervous system (Boyd and Lingwood, 1989; Fujii et al., 2008). Of note, the kidney is the most affected organ by Stx2a due to its high expression of Gb3 receptor and its physiological function of filtering large volumes of blood in which the toxin could be present, increasing the probability of contact between Stx2a and Gb3 (Obrig, 2010). Once in contact with the glomerular endothelial cells, Stx2a activates them and causes a switch into a proinflammatory state by increasing the expression of adhesion molecules and the secretion of cytokines and chemokines, thus promoting the recruitment of leukocytes (Ramos et al., 2007). Interestingly, macropinocytosis increases toxin endocytosis by intestinal epithelial cells and also stimulates toxin transcellular transcytosis. Thus, macropinocytosis might be responsible for toxin uptake by Gb3-free intestinal epithelial cells and transcytosis (Malyukova et al., 2009). Once within the bloodstream, most of the toxin circulate associated to blood cells such as leukocytes (Te Loo et al., 2011), platelets, and aggregates between these cells (Ståhl et al., 2009), and red blood cells (Arvidsson et al., 2015). Also, it has been reported that the binding of toxin to blood cells activates them and induces the shedding of microvesicles, which are pro-inflammatory, pro-thrombotic (Arvidsson et al., 2015), and, importantly, transport the toxin to its target organ. This has been suggested to be one of the

main mechanisms of toxin-induced systemic and targeted organ injury (Karpman et al., 2017). Regarding the innate cells participating in the pathogenesis of HUS, it has been reported that monocytes, NK cells, and neutrophils are involved (Ramos et al., 2007; Ramos et al., 2016). Nevertheless, there is no evidence in humans about the role of γδ T cells, which are lymphocytes of the innate and adaptive immune response. γδ T cells represent 1–10% of the total T cell population in peripheral blood (Fonseca et al., 2020), and those expressing Vγ9Vδ2 TCR constitute the main circulating γδ T cell subset in healthy humans (Silva-Santos et al., 2015). As other innate immune cells, γδ T lymphocytes can infiltrate tissues (Fay et al., 2016), and in kidney injury, γδ T cells can be potentially recruited as they express the fractalkine receptor CX3CR1 (Nishimura et al., 2002), which was demonstrated to be involved in the recruitment of NK cells and monocytes to this organ (Malyukova et al., 2009). Interestingly, Vγ9Vδ2 T cells do not recognize antigens presented in the context of the major complex histocompatibility molecules. Instead, these cells display a unique response to non-peptide prenyl-pyrophosphate antigens, called phosphoantigens, such as isopentenyl pyrophosphate (IPP), which is produced by eukaryotic cells, and they can also recognize those that are produced by prokaryotic cells such as (E)-4-hydroxy-3-methyl-but-enyl pyrophosphate (HMBPP) (Poupot and Fournié, 2004). IPP is overexpressed by cells suffering malignant transformation, allowing them to be targeted by Vγ9Vδ2 T cells, after the interaction with the molecule BTN3A1 (Harly et al., 2015). Apart from the phosphoantigens, γδ T cells can be activated by cytokines, molecules induced by stress, and microbes' components, among other molecules (Shiromizu and Jancic, 2018). Once activated, γδ T cells release cytokines, such as IFN-γ and TNF-α, and granules containing granzymes and perforins that lead to the cytotoxicity of target cells. Additionally, they can exert the non-secretory mechanism of cytotoxicity by the interaction between Fas and FasL.

In this work, we aimed to investigate the γδ T cell response to either the presence of human glomerular endothelial cells (HGEC) stimulated with highly purified Stx2a, or its conditioned medium, to elucidate a possible role of γδ T cells during the pathogenesis of HUS.

METHODS

The experimental protocols performed were reviewed and approved by the Biosafety and Research Review boards of the *Instituto de Medicina Experimental–CONICET, Academia Nacional de Medicina* and the Ethical Committee of the *Institutos de la Academia Nacional de Medicina* and the *Universidad de Buenos Aires*. The methods were carried out following the approved guidelines. The participants provided their written informed consent to participate in this study.

Peripheral Blood γδ T Lymphocyte Isolation

γδ T cells were isolated from heparinized human blood from healthy donors, who gave written informed consent, by centrifugation on Ficoll-Hypaque and positive selection using magnetic microspheres covered with anti-TCR γδ antibodies, according to the manufacturer's instructions (Miltenyi Biotec, Germany). After purification, cells were resuspended in RPMI 1640 supplemented with 10% heat-inactivated fetal bovine serum (FBS), penicillin (100 U/ml), and streptomycin (100 μg/ml). Cells were analyzed by flow cytometry (FACSCalibur, Beckton Dickinson, San Jose, CA, USA) to guarantee that γδ T cell purity was >98% and monocyte contamination <2% (**Supplementary Material, Figure 1**). The purification procedure did not affect cell activation; this was evaluated by analyzing the expression of CD69 and the production of TNF-α in the presence or absence of the agonist HMBPP (**Supplementary Material, Figure 2**). The details about donors are listed in **Supplementary Material, Table 1A**.

Human Glomerular Endothelial Cell Culture

HGEC were isolated from healthy areas of kidney fragments from patients undergoing nephrectomies as a consequence of segmental uropathies or tumors in one pole and normal creatinine. The procedure was performed at Hospital Nacional Alejandro Posadas, Buenos Aires, Argentina. Endothelial cells were isolated as was previously described (Amaral et al., 2013). Once obtained, cells were grown in M199 media supplemented with 20% FBS, 3.2 mM L-glutamine, 100 U/ml penicillin/streptomycin, and 25 μg/ml endothelial cell growth supplement. For growth-arrested conditions, a medium with 10% of FBS and without endothelial cell growth supplement was employed. For the experiments, cells were used between 2 and 7 passages, after characterization for von Willebrand factor and platelet/endothelial cell adhesion molecule 1 (PECAM-1) positive expression (Amaral et al., 2013). The details about donors are listed in **Supplementary Material, Table 1B**.

To treat HGEC, highly purified Stx2a (provided by Phoenix Laboratory, Tufts Medical Center, Boston, MA, USA) was used. Lipopolysaccharide content on Stx2a was checked by Limulus amebocyte lysate test (<10 pg/ml).

Reagents and Antibodies

The reagents employed in this work are listed in **Supplementary Material, Table 2**.

The description of the different methodologies employed in this work is in **Supplementary Material**.

RESULTS

Stx2a-Stimulated Human Glomerular Endothelial Cells Promote the Activation of γδ T Lymphocytes

In this study, we focused on the role of circulating γδ T cells in the pathogenesis of the HUS. We speculated that γδ T cells could detect the damages generated by Stx2a on endothelial cells once

accesses to the blood circulation and impacts on kidneys. We propose that γδ T lymphocytes sense cell damage, and then they activate and put in place different mechanisms to exacerbate local inflammation. Therefore, we evaluated the effect of HGEC stimulated or not by Stx2a on the functionality of γδ T cells. For this purpose, we incubated human purified γδ T lymphocytes obtained from peripheral blood with confluent cultures of HGEC, previously treated or not with Stx2a (0.01 ng/ml, overnight). As it is shown in **Figure 1**, the presence of Stx2a-treated HGEC increased the secretion of IFN-γ (**Figure 1A**) and TNF-α (**Figure 1B**) by γδ T cells, supporting their differentiation towards a Th1-like profile. Because HGEC are able to produce TNF-α (see **Figure 3B**), we decided to analyze the production of this cytokine in γδ T cells by intracellular cell staining, in addition to the ELISA quantification. The result obtained confirmed that γδ T cells effectively produce TNF-α (**Figure 1C**). Of note, under our experimental conditions, we did not detect a modulation by Stx2a of the level of the activation marker CD69 on γδ T cells (**Figure 1D**), suggesting that γδ T lymphocytes' responses differ when cultured with Stx2a-stimulated HGEC, compared to IFN-γ and TNF-α secretion.

Then, we speculated that soluble factors released by endothelial cells in the presence or absence of Stx2a could affect the activation of γδ T lymphocytes. To evaluate this hypothesis, we incubated γδ T cells with conditioned media obtained from confluent cultures of HGEC treated or not with Stx2a. As **Figure 2** shows, those supernatants induced the production of IFN-γ (**Figure 2A**) and TNF-α (**Figure 2B**) but did not change the expression of CD69 (**Figure 2C**), similar to that observed in co-culture conditions. This effect was dependent on the activity of Stx2a, since when it was inactivated by heating, the γδ T cells did not change the production of IFN-γ and TNF-α (**Supplementary Figures 3A, B**). Additionally, the conditioned media also prompt an increase in the degranulation of γδ T cells, measured by the expression of CD107a (**Figure 2D**) and intracellular perforin (**Figures 2E, F**). Interestingly, we observed a decrease in the percentage of perforin+ γδ T lymphocytes (**Figure 2E**) and in the median intensity fluorescence for perforin (**Figure 2F**) in the presence of medium coming from Stx2a-stimulated HGEC. To complement the cell degranulation study, we performed an analysis by confocal microscopy by co-culturing γδ T cells with HGEC pretreated or not with Stx2a for 24 h. After co-cultured, cells were intracellularly stained for perforin as described in *Methods* (**Figures 2G–I**). In the samples, we evaluated the capacity of γδ T cells to interact with HGEC pretreated or not with Stx2a, and we analyzed the distribution of perforin in γδ T lymphocytes that were in contact with endothelial cells. As we can observe in **Figure 2G**, there was a high percentage

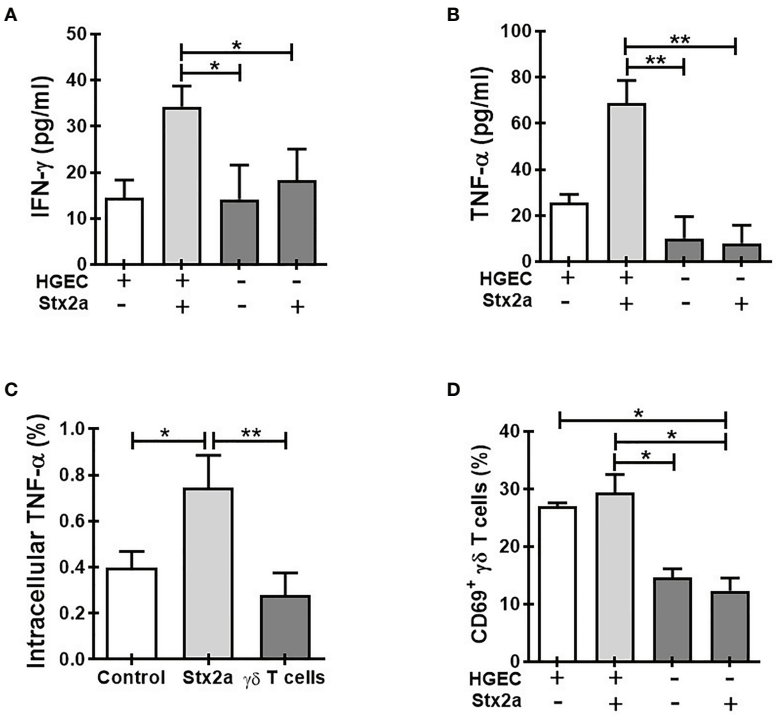

FIGURE 1 | Co-culture of γδ T cells with Stx2a-stimulated HGEC induce its activation. γδ T cells were cultured overnight at 37°C in the absence or presence of HGEC, treated or not previously with Stx2a (0.01 ng/ml, 24 h). γδ T cells were resuspended in M199 supplemented with 10% FBS. After culture, supernatants and cells were collected. **(A)** IFN-γ and **(B)** TNF-α production in supernatants was measured by ELISA, n=7 and n=5, respectively. Biological replicates. Kruskal-Wallis test, with Dunn's multiple comparisons test. **(C)** Intracellular cell staining of TNF-α in γδ T lymphocytes. Control (open bar) represents γδ T cell culture with HGEC non-treated with Stx2a, n=8. Biological replicates. Kruskal-Wallis test, with Dunn's multiple comparisons test. **(D)** CD69 expression in γδ T cells, was analyzed by flow cytometry, n=5. Biological replicates. Kruskal-Wallis test, with Dunn's multiple comparisons test. Results are shown as the mean ± SEM, $*p < 0.05$, $**p < 0.01$.

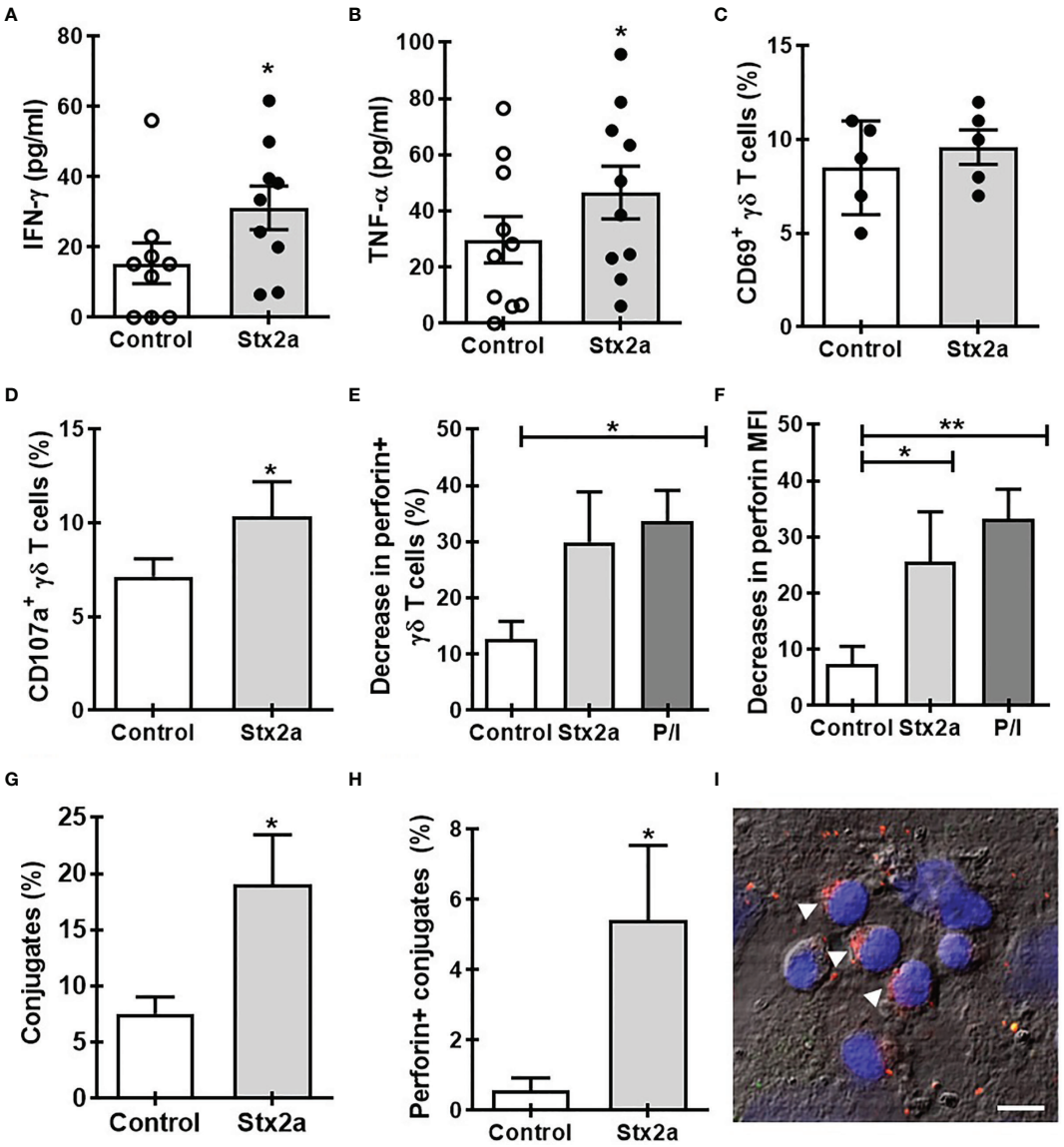

FIGURE 2 | Soluble factors released by Stx2a-stimulated HGEC activate γδ T cells. γδ T cells were cultured overnight at 37°C with conditioned media obtained from confluent monolayers of HGEC, treated (Stx2a) or not (Control) with Stx2a (0.01 ng/ml, 24 h). After overnight incubation, supernatants and cells were collected. **(A, B)** IFN-γ and TNF-α released to the medium determined by ELISA, n=9 and n=10, respectively. Biological replicates. Kruskal-Wallis test, with Dunn's multiple comparisons test. **(C–F)** Flow cytometry analysis of the expression of CD69 **(C)** (n=5), CD107a **(D)** (n=9), and perforin **(E)** (n=5) and **(F)** (n=10) in γδ T cells. PMA and ionomycin (P/I) were used as a positive control. **(G, H)** γδ T cells were seeded on glass slides previously coated with HGEC treated or not (Control) with Stx2a (0.01 ng/ml, 24 h) (for details see the section *Methods*). After incubation, the number of γδ T cells interacting with HGEC (conjugates) and the expression of perforin were evaluated by confocal microscopy. **(G)** Percentage of cell conjugates in non-treated (Control) or Stx2a-stimulates HGEC (Stx2a) (n=10, technical replicates). **(H)** Percentage of perforin+ γδ T cells in interaction with HGEC non-treated (Control) or treated with Stx2a (Stx2) (n=10, technical replicates). **(I)** Representative image of perforin expression (red) in γδ T cells in co-culture with Stx2a-treated HGEC. For nuclear visualization, cells were stained with ToPro-3 (blue). The figure shows one of two independent experiments performed. Bar: 10 μm. Arrows indicate γδ T cells in which perforin are polarized. Results are shown as the mean ± SEM. $^{*}p < 0.05$ and $^{**}p < 0.01$; **(A–D, G, H)** Wilcoxon or Mann-Whitney test. **(E, F)** Kruskal-Wallis with the Dunn's multiple comparisons posttest.

of cell conjugates when HGECs were exposed to Stx2a. Interestingly, γδ T lymphocytes attached to Stx2a-treated endothelial cells display higher levels of perforin compared with those in contact with non-treated HGEC (**Figure 2H**). The image of (**Figure 2I**) shows γδ T lymphocytes with perforin polarized to one side of the cytosol, which is a consequence of the cytoskeleton rearrangement after activation and is the step that takes place before the secretion of perforin towards the target cell in the immunological synapse formed (Trapani and Smyth, 2002; Law et al., 2010).

TNF-α Plays a Critical Role in the Activation of γδ T Lymphocytes by Conditioned Medium From Stx2a-Stimulated Human Glomerular Endothelial Cells

In search for a soluble component responsible for the activation of γδ T cells towards a Th1-like profile, we measured some cytokines secreted by HGEC stimulated with different concentrations of Stx2a (0.01 and 1 ng/ml, 24 h). Because we wanted to evaluate the cross-communication between γδ T cells and HGEC, it is noteworthy that it was a requirement for our work to use a concentration of Stx2a that did not significantly affect the HGEC viability but was sufficient to activate them and promote the secretion of cytokines (Álvarez et al., 2019). For that reason, we chose the concentration of 0.01 ng/ml of Stx2a that induced low and not significant cytotoxicity (86% ± 4) (**Figure 3A**) but stimulated cytokine production. **Figure 3** shows that under Stx2a stimulation, HGEC produced TNF-α (**Figure 3B**), IL-6 (**Figure 3C**), and IL-8 (**Figure 3D**). Among those cytokines, it is well-known that TNF-α has the capacity to activate γδ T cells in autocrine or paracrine ways, and even if their concentration is low, it can act on γδ T cells and modulate their activation (Lahn et al., 1998; Rincon-Orozco et al., 2005; Sabbione et al., 2014). Based on this, we decided to assess a blocking experiment in which by using Etanercept we neutralized TNF-α, and then we evaluated the different activation parameters on γδ T lymphocytes, mentioned before. In **Figure 4**, we can observe that the treatment of cells with Etanercept reversed completely the increase in the IFN-γ (**Figure 4A**) and TNF-α (**Figure 4B**) production; and in the CD107a (**Figures 4C, D**) and perforin (**Figure 4E**) expression. These results demonstrated the role of this cytokine in the activation of several mechanisms of γδ T cells that could be implicated in the pro-inflammatory responses induced by Stx2a-stimulated HGEC.

DISCUSSION

In humans, there are not previous publications reporting the role of γδ T cells during the pathogenesis of HUS, since most of them have studied their role in cattle, calves (Menge et al., 2004), and mice (Obata et al., 2015). In this work, we demonstrated for the first time that Stx2a-stimulated HGEC could modulate the

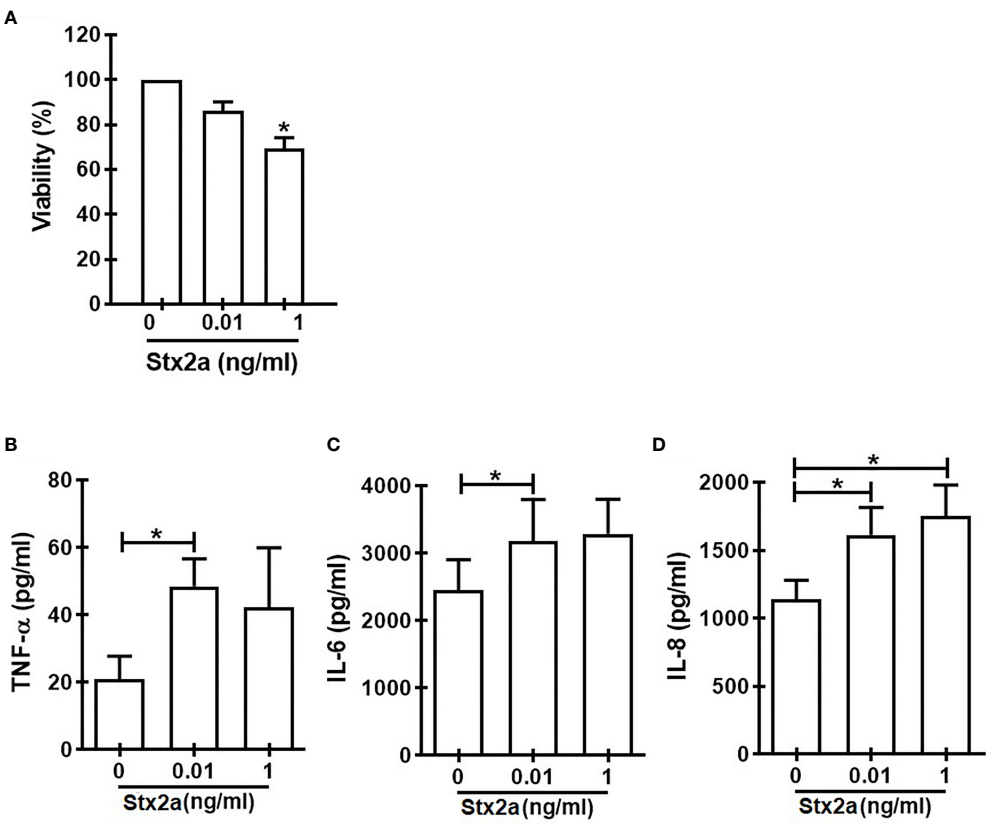

FIGURE 3 | Cytokine secretion by HGEC in response to different concentrations of Stx2a. Confluent monolayers of HGEC were stimulated with different concentrations of Stx2a (0.01 and 1 ng/ml) for 24 h. After incubation, cell supernatants were recovered. **(A)** Percentage of cell viability analyzed by neutral red uptake (n=3, biological replicates). Friedman with the Dunn's multiple comparisons posttest. **(B)** TNF-α, **(C)** IL-6, and IL-8 **(D)** production measured by ELISA in cell supernatants, n=6 (biological replicates). Friedman with the Dunn's multiple comparisons posttest. Results are shown as the mean ± SEM. *$p < 0.05$.

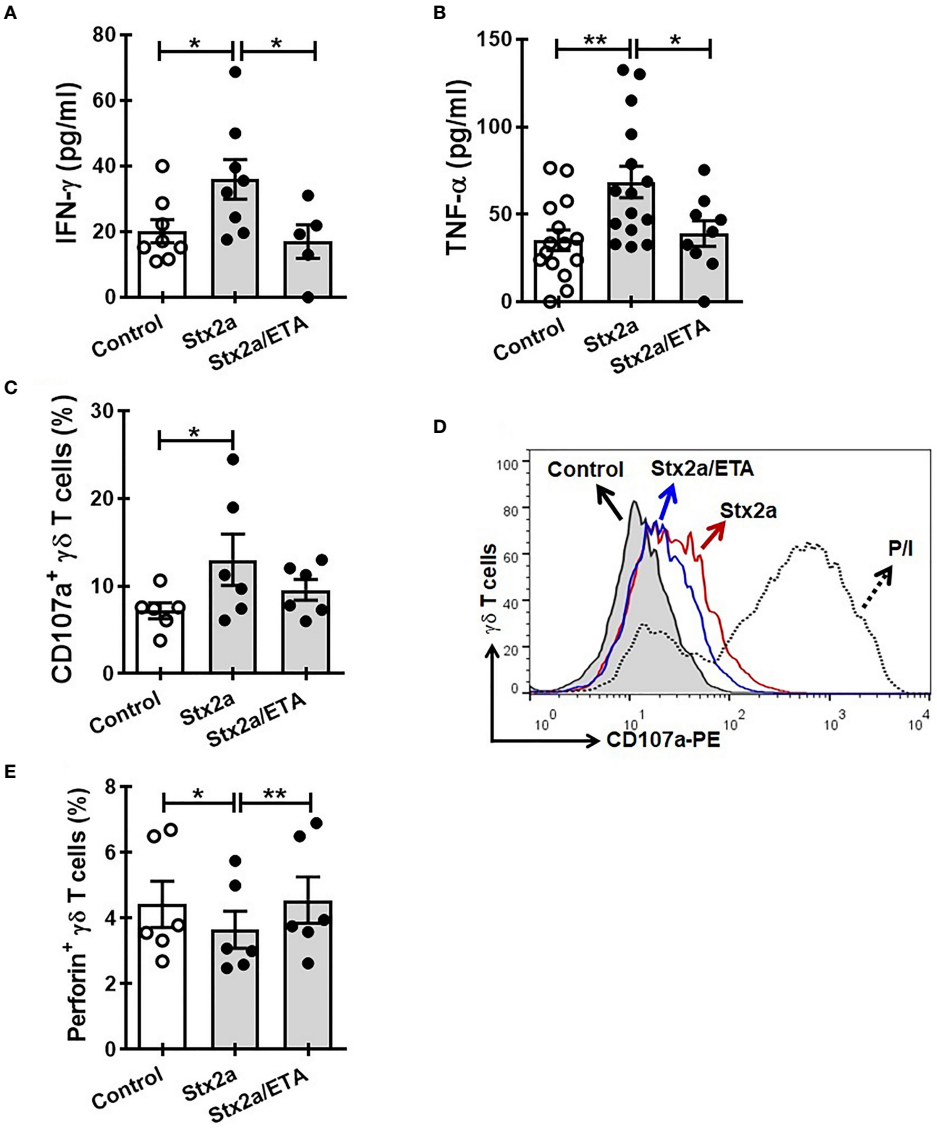

FIGURE 4 | Etanercept impedes the activation of γδ T cells induced by Stx2a-treated HGEC. γδ T cells were cultured overnight at 37°C with a conditioned media obtained from confluent monolayers of HGEC, treated (Stx2) or not (Control) with Stx2a (0.01 ng/ml, 24 h). One group of cells were pre-incubated with Etanercept (ETA: 25 μg/ml, 30 min at 37°C). After overnight incubation, supernatants and cells were collected. **(A, B)** IFN-γ (n=5) and TNF-α (n=9) released to the medium determined by ELISA, respectively. Biological replicates. Kruskal-Wallis test, with Dunn's multiple comparisons test. **(C, D)** Expression of CD107a in γδ T cells, analyzed by flow cytometry. **(C)** Percentage of CD107+ γδ T cells (n=6). Biological replicates. Kruskal-Wallis test, with Dunn's multiple comparisons test. **(D)** Representative histogram of one experiment out of six performed. Gray histogram: γδ T cells cultured with conditioned medium from Stx2a-non-treated HGEC (Control); histogram red: γδ T cells cultured with conditioned medium from Stx2a-treated HGEC (Stx2a); histogram blue: γδ T cells cultured in presence of Etanercept (ETA) and with conditioned medium from Stx2a-treated HGEC (Stx2a/ETA); dot line histogram: γδ T cells incubated with PMA and ionomycin (P/I) (positive control). **(E)** Percentage of perforin+ γδ T cells, analyzed by intracellular staining and flow cytometry (n=6). Biological replicates. Friedman test, witn Dunn's multiple comparison test. Results are shown as the mean ± SEM. $^{*}p < 0.05$ and $^{**}p < 0.01$.

differentiation of γδ T lymphocytes towards a Th1-like profile characterized by the production of IFN-γ and TNF-α. In addition to this phenomenon, there was an increment in the degranulation of γδ T cells, evidenced by the increase in the expression of CD107a (Alter et al., 2004) and the decrease of intracellular perforin. As well, we demonstrated that the interaction of γδ T cells with Stx2a-stimulated HGEC induced the polarization of perforin, which is a key step to allow their posterior secretion together with granzymes towards a target cell (Trapani and Smyth, 2002; Law et al., 2010). This event might contribute to endothelial damage (we are currently studying this hypothesis). Notably, here we demonstrated that the blockage of TNF-α prevents completely the activation of γδ T cells in response to conditioned medium obtained from Stx2a-treated

HGEC. Nevertheless, we cannot dismiss that soluble compounds could act in conjunction with cell-to-cell contact, or have a role in favoring intercellular communication, but we need to perform more experiments to elucidate this hypothesis. However, our results clearly show that γδ T cells respond effectively and efficiently to soluble factors released by HGEC stimulated by low concentrations of Stx2a, mainly TNF-α.

Regarding the role of the other cytokines secreted by HGEC studied in this work, such as IL-6 or IL-8, there are few reports describing their functions on human γδ T cells. Based on the limited data published, it seems that some populations of γδ T cells do not react to IL-8 since it has been reported that peripheral blood γδ T cells respond in dose-dependent transendothelial chemotaxis to the CC chemokines such as RANTES, but not to the CXC chemokines as IL-8 (Roth et al., 1998). Other authors have demonstrated that intraepithelial lymphocytes are able to respond to IL-8, although the presence of other chemokines desensitized these cells to IL-8 (Roberts et al., 1997). Based on our results and on the published data mentioned above, we can speculate that in our experimental model, this molecule has no impact on peripheral blood γδ T cell responses. On the other hand, it has been reported that TNF-α and IL-6 upregulate the expression of the chemokine receptors CCR5 and CXCR3 on Vδ2 T cells in patients suffering from rheumatoid arthritis. Interestingly, this increase was abrogated by the administration of neutralizing antibodies against TNF-α (Mo et al., 2017), assigning a leading role to this cytokine in this process, in accordance with our experimental design. In addition and supporting the role of TNF-α during γδ T cell activation, in a model of bacterial infection done by other authors, it was observed the same behavior as we found, and this may be due to the fact that γδ T cells are very sensitive to the effect of TNF-α (Lahn et al., 1998).

Of mention, and in addition to the study of soluble factors as mediators of γδ T cell activation, it is our aim to evaluate the molecules involved in the cell-to-cell interaction between HGEC and γδ T lymphocytes to go further in the study of the participation of these T cells during the initiation and progression of HUS (ongoing project). Additionally, TNF-α released by γδ T cells could also contribute to tissue sensibility to the toxin as this cytokine upregulates Gb3 expression in HGEC (Stricklett et al., 2002). Interestingly, it has been reported that the chemokine fractalkine (FKN; CX3CL1) is involved in many diseases with renal injury (Cockwell et al., 2002; Durkan et al., 2007) including HUS (Ramos et al., 2007). Remarkably, it has been demonstrated that a fraction of monocytes and NK cells, which express the fractalkine receptor CX3CR1+, are diminished in peripheral blood of HUS patients when compared to healthy donors. Moreover, immunohistochemistry on renal biopsies of children with HUS revealed the presence of CX3CR1+ monocytes infiltrating kidneys (Ramos et al., 2007), contributing to the pathogenesis of HUS promoting inflammation events in the glomeruli endothelium, and increasing the initial damage done by Stx. In this sense, during the Stx-induced damage in the glomeruli, the release of pro-inflammatory cytokines promotes leukocyte recruitment, platelet aggregation, and fibrin deposition. Based on this evidence, we can speculate that in γδ T cells, CX3CR1 could play a role by recruiting them to the glomeruli initially affected by the Stx2a and then to promote the γδ T cell participation in the inflammation process, thus contributing to the exacerbation of the endothelial damage and in the pathogenesis of HUS. Altogether, these events could lead to partial or complete vessel occlusion by microthrombi and the consequent microangiopathic hemolytic anemia (Keir et al., 2012). However, more studies are needed to confirm this hypothesis.

Based on our data presented here, and as a first contribution to the knowledge of the role of human γδ T cells in HUS pathogenesis, our results indicate that γδ T cells could be involved in the exacerbation of the renal tissue damage due to the secretion of pro-inflammatory cytokines and to their degranulation. We speculate that once γδ T cells come into contact with stressed endothelial cells, they might recognize signals that allow their activation, leading to start-up of its cytotoxic function mediated among others by the action of perforins and granzymes. Additionally, the release of pro-inflammatory cytokines as TNF-α and IFN-γ could affect the local microenvironment, contributing to the exacerbation of the initial inflammatory process triggered by Stx2.

DATA AVAILABILITY STATEMENT

The raw data supporting the conclusions of this article will be made available by the authors, without undue reservation.

ETHICS STATEMENT

The studies involving human participants were reviewed and approved by the Biosafety and Research Review Boards of the Instituto de Medicina Experimental–CONICET, Academia Nacional de Medicina and the Ethical Committee of the Institutos de la Academia Nacional de Medicina and the Universidad de Buenos Aires. Written informed consent to participate in this study was provided by the participants or participants' legal guardian/next of kin.

AUTHOR CONTRIBUTIONS

Material preparation and experiments: DR, MR, CS and IK. HGEC culture: FG and RA. Critical revision of the manuscript and results discussion: CI and MA. Experimental design, data interpretation, and manuscript writing: CJ. All authors contributed to the article and approved the submitted version.

FUNDING

This work was supported by grant from Agencia Nacional de Promoción Científica y Tecnológica (PICT2016/700 and PICT2019/255) and Consejo Nacional de Investigaciones Científicas y Técnicas.

ACKNOWLEDGMENTS

The authors thank Dr. Analia Trevani for her helpful discussion on the manuscript and Dr. Federico Fuentes for his support with image acquisition and analysis.

SUPPLEMENTARY MATERIAL

The Supplementary Material for this article can be found online at: https://www.frontiersin.org/articles/10.3389/fcimb.2021.765941/full#supplementary-material

REFERENCES

Alconcher, L. F., Coccia, P. L., Suarez, A. C., Monteverde, M. L., Perez Y Gutiérrez, M. G., Carlopio, P. M., et al (2018). Hyponatremia: A New Predictor of Mortality in Patients With Shiga Toxin-Producing *Escherichia Coli* Hemolytic Uremic Syndrome. *Pediatr. Nephrol.* 33 (10), 1791–1798. doi: 10.1007/s00467-018-3991-6

Alter, G., Malenfant, J. M., and Altfeld, M. (2004). CD107a as a Functional Marker for the Identification of Natural Killer Cell Activity. *J. Immunol. Meth.* 294 (1–2), 15–22. doi: 10.1016/j.jim.2004.08.008

Álvarez, R. S., Jancic, C. C., Garimano, N., Sacerdoti, F., Paton, A. W., Paton, J. C., et al (2019). Crosstalk Between Human Microvascular Endothelial Cells and Tubular Epithelial Cells Modulates Pro-Inflammatory Responses Induced by Shiga Toxin Type 2 and Subtilase Cytotoxin. *Toxins (Basel)* 11 (11), 648. doi: 10.3390/toxins11110648

Amaral, M. M., Sacerdoti, F., Jancic, C. C., Repetto, H. A., Paton, A. W., Paton, J. C., et al (2013). Action of Shiga Toxin Type-2 and Subtilase Cytotoxin on Human Microvascular Endothelial Cells. *PLoS One* 8 (7), e70431. doi: 10.1371/journal.pone.0070431

Arvidsson, I., Ståhl, A. L., Hedström, M. M., Kristoffersson, A. C., Rylander, C., Westman, J. S., et al (2015). Shiga Toxin-Induced Complement-Mediated Hemolysis and Release of Complement-Coated Red Blood Cell-Derived Microvesicles in Hemolytic Uremic Syndrome. *J. Immunol.* 194 (5), 2309–2318. doi: 10.4049/jimmunol.1402470

Bielaszewska, M., Mellmann, A., Zhang, W., Köck, R., Fruth, A., Bauwens, A., et al (2011). Characterisation of the Escherichia Coli Strain Associated With an Outbreak of Haemolytic Uraemic Syndrome in Germany, 2011: A Microbiological Study. *Lancet Infect. Dis.* 11 (9), 671–676. doi: 10.1016/S1473-3099(11)70165-7

Blanco, J. E., Blanco, M., Alonso, M. P., Mora, A., Dahbi, G., Coira, M. A., et al (1992). Serotypes, Virulence Genes, and Intimin Types of Shiga Toxin (Verotoxin)-Producing *Escherichia Coli* Isolates From Human Patients: Prevalence in Lugo, Spain, From 1992 Through 1999. *J. Clin. Microbiol.* 42 (1), 311–319. doi: 10.1128/JCM.42.1.311-319.2004

Boyd, B., and Lingwood, C. (1989). Verotoxin Receptor Glycolipid in Human Renal Tissue. *Nephron* 51 (2), 207–210. doi: 10.1159/000185286

Caprioli, A., and Tozzi, A. E. (1998). "Epidemiology of Shiga Toxin-Producing Escherichia Coli Infections in Continental Europe," in *Escherichia Coli O157: H7 and Other Shiga Toxin-Producing E. Coli Strains*. Eds. J. B. Kaper and A. D. O'Brien (Washington, DC: ASM Press), 38–48.

Carter, M. Q., Pham, A., Du, W. X., and He, X. (2021). Differential Induction of Shiga Toxin in Environmental *Escherichia Coli* O145:H28 Strains Carrying the Same Genotype as the Outbreak Strains. *Int. J. Food Microbiol.* 339, 109029. doi: 10.1016/j.ijfoodmicro.2020.109029

Cockwell, P., Chakravorty, S. J., Girdlestone, J., and Savage, C. O. S. (2002). Fractalkine Expression in Human Renal Inflammation. *J. Pathol.* 196 (1), 85–90. doi: 10.1002/path.1010

Coombes, B. K., Gilmour, M. W., and Goodman, C. D. (2011). The Evolution of Virulence in Non-O157 Shiga Toxin-Producing *Escherichia Coli*. *Front. Microbiol.* 2, 90. doi: 10.3389/fmicb.2011.00090

Durkan, A. M., Alexander, R. T., Liu, G. Y., Rui, M., Femia, G., and Robinson, L. A. (2007). Expression and Targeting of CX3CL1 (Fractalkine) in Renal Tubular Epithelial Cells. *J. Am. Soc Nephrol.* 18 (1), 74–83. doi: 10.1681/ASN.2006080862

Fay, N. S., Larson, E. C., and Jameson, J. M. (2016). Chronic Inflammation and γδ T Cells. *Front. Immunol.* 7, 210. doi: 10.3389/fimmu.2016.00210

Fitzgerald, S. F., Beckett, A. E., Palarea-Albaladejo, J., McAteer, S., Shaaban, S., Morgan, J., et al (2019). Shiga Toxin Sub-Type 2a Increases the Efficiency of *Escherichia Coli* O157 Transmission Between Animals and Restricts Epithelial Regeneration in Bovine Enteroids. *PLoS Pathog.* 15 (10), e1008003. doi: 10.1371/journal.ppat.1008003

Fonseca, S., Pereira, V., Lau, C., Teixeira, M. A., Bini-Antunes, M., and Lima, M. (2020). Human Peripheral Blood Gamma Delta T Cells: Report on a Series of Healthy Caucasian Portuguese Adults and Comprehensive Review of the Literature. *Cells* 9 (3), 729. doi: 10.3390/cells9030729

Frank, C., Faber, M. S., Askar, M., Bernard, H., Fruth, A., Gilsdorf, A., et al (2011). Large and Ongoing Outbreak of Haemolytic Uraemic Syndrome, Germany, May 2011. *Euro Surveill.* 16 (21), 19878. doi: 10.2807/ese.16.21.19878-en

Friedrich, A. W., Bielaszewska, M., Zhang, W. L., Pulz, M., Kuczius, T., Ammon, A., et al (2002). *Escherichia Coli* Harboring Shiga Toxin 2 Gene Variants: Frequency and Association With Clinical Symptoms. *J. Infect. Dis.* 185 (1), 74 ±84. doi: 10.1086/338115

Fujii, J., Wood, K., Matsuda, F., Carneiro-Filho, B. A., Schlegel, K. H., Yutsudo, T., et al (2008). Shiga Toxin 2 Causes Apoptosis in Human Brain Microvascular Endothelial Cells *via* C/EBP Homologous Protein. *Infect. Immun.* 76 (8), 3679–3689. doi: 10.1128/IAI.01581-07

Garred, O., Dubinina, E., Holm, P. K., Olsnes, S., van Deurs, B., Kozlov, J. V., et al (1995). Role of Processing and Intracellular Transport for Optimal Toxicity of Shiga Toxin and Toxin Mutants. *Exp. Cell. Res.* 218 (1), 39–49. doi: 10.1006/excr.1995.1128

Harly, C., Peigné, C. M., and Scotet, E. (2015). Molecules and Mechanisms Implicated in the Peculiar Antigenic Activation Process of Human Vγ9vδ2 T Cells. *Front. Immunol.* 5, 657. doi: 10.3389/fimmu.2014.00657

Hazes, B., and Read, R. J. (1997). Accumulating Evidence Suggests That Several AB-Toxins Subvert the Endoplasmic Reticulum-Associated Protein Degradation Pathway to Enter Target Cells. *Biochemistry* 36 (37), 11051–11054. doi: 10.1021/bi971383p

Johannes, L., and Römer, W. (2010). Shiga Toxins–From Cell Biology to Biomedical Applications. *Nat. Rev. Microbiol.* 8 (2), 105–116. doi: 10.1038/nrmicro2279

Karpman, D., Loos, S., Tati, R., and Arvidsson, I. (2017). Haemolytic Uraemic Syndrome. *J. Intern. Med.* 281 (2), 123–148. doi: 10.1111/joim.12546

Keir, L. S., Marks, S. D., and Kim, J. J. (2012). Shigatoxin-Associated Hemolytic Uremic Syndrome: Current Molecular Mechanisms and Future Therapies. *Drug Des. Devel. Ther.* 6, 195–208. doi: 10.2147/DDDT.S25757

Lahn, M., Kalataradi, H., Mittelstadt, P., Pflum, M., Vollmer, M., Cady, C., et al (1998). Early Preferential Stimulation of Gamma Delta T Cells by TNF-Alpha 160, 11, 5221–5230.

LaPointe, P., Wei, X., and Gariépy, J. (2005). A Role for the Protease-Sensitive Loop Region of Shiga-Like Toxin 1 in the Retrotranslocation of its A1 Domain From the Endoplasmic Reticulum Lumen. *J. Biol. Chem.* 280 (24), 23310–23318. doi: 10.1074/jbc.M414193200

Law, R. H., Lukoyanova, N., Voskoboinik, I., Caradoc-Davies, T. T., Baran, K., Dunstone, M. A., et al (2010). The Structural Basis for Membrane Binding and Pore Formation by Lymphocyte Perforin. *Nature* 468 (7322), 447–451. doi: 10.1038/nature09518

Lee, M. S., Koo, S., Jeong, D. G., and Tesh, V. L. (2016). Shiga Toxins as Multi-Functional Proteins: Induction of Host Cellular Stress Responses, Role in Pathogenesis and Therapeutic Applications. *Toxins (Basel)* 8 (3), 77. doi: 10.3390/toxins8030077

Malyukova, I., Murray, K. F., Zhu, C., Boedeker, E., Kane, A., Patterson, K., et al (2009). Macropinocytosis in Shiga Toxin 1 Uptake by Human Intestinal Epithelial Cells and Transcellular Transcytosis. *Am. J. Physiol. Gastrointest. Liver Physiol.* 296 (1), G78–G92. doi: 10.1152/ajpgi.90347.2008

Menge, C., Stamm, I., van Diemen, P. M., Sopp, P., Baljer, G., Wallis, T., et al (2004). Phenotypic and Functional Characterization of Intraepithelial Lymphocytes in a Bovine Ligated Intestinal Loop Model of Enterohaemorrhagic *Escherichia Coli* Infection. *J. Med. Microbiol.* Pt 6, 573–579. doi: 10.1099/jmm.0.45530-0

Mo, W. X., Yin, S. S., Chen, H., Zhou, C., Zhou, J. X., Zhao, L. D., et al (2017). Chemotaxis of Vδ2 T Cells to the Joints Contributes to the Pathogenesis of Rheumatoid Arthritis. *Ann. Rheumatol. Dis.* 76 (12), 2075–2084. doi: 10.1136/annrheumdis-2016-211069

Nishimura, M., Umehara, H., Nakayama, T., Yoneda, O., Hieshima, K., Kakizaki, M., et al (2002). Dual Functions of Fractalkine/CX3C Ligand 1 in Trafficking of Perforin+/Granzyme B+ Cytotoxic Effector Lymphocytes That are Defined by CX3CR1 Expression. *J. Immunol.* 168 (12), 6173–6180. doi: 10.4049/jimmunol.168.12.6173

Obata, F., Subrahmanyam, P., Vozenilek, A. E., Hippler, L. M., Jeffers, T., Tongsuk, M., et al (2015). Natural Killer T (NKT) Cells Accelerate Shiga Toxin Type 2 (Stx2) Pathology in Mice. *Front. Microbiol.* 8, 262. doi: 10.3389/fmicb.2015.00262

Obrig, O. T. (2010). *Escherichia Coli* Shiga Toxin Mechanisms of Action in Renal Disease. *Toxins (Basel)* 2 (12), 2769–2794. doi: 10.3390/toxins2122769

Persson, S., Olsen, K. E., Ethelberg, S., and Scheutz, F. (2007). Subtyping Method for Escherichia Coli Shiga Toxin (Verocytotoxin) 2 Variants and Correlations to Clinical Manifestations. *J. Clin. Microbiol.* 45 (6), 2020–2024. doi: 10.1128/JCM.02591-06

Poupot, M., and Fournié, J. J. (2004). Non-Peptide Antigens Activating Human Vγ9/Vδ2 T Lymphocytes. *Immunol. Lett.* 95 (2), 129–138. doi: 10.1016/j.imlet.2004.06.013

Ramos, M. V., Fernández, G. C., Patey, N., Schierloh, P., Exeni, R., Grimoldi, I., et al (2007). Involvement of the Fractalkine Pathway in the Pathogenesis of Childhood Hemolytic Uremic Syndrome. *Blood* 15109 (6), 2438–2445. doi: 10.1182/blood-2006-06-026997

Ramos, M. V., Mejias, M. P., Sabbione, F., Fernandez-Brando, R. J., Santiago, A. P., Amaral, M. M., et al (2016). Induction of Neutrophil Extracellular Traps in Shiga Toxin-Associated Hemolytic Uremic Syndrome. *J. Innate Immun.* 8 (4), 400–411. doi: 10.1159/000445770

Rasko, D. A., Webster, D. R., Sahl, J. W., Bashir, A., Boisen, N., Scheutz, F., et al (2011). Origins of the E. Coli Strain Causing an Outbreak of Hemolytic-Uremic Syndrome in Germany. *N. Engl. J. Med.* 365 (8), 709–717. doi: 10.1056/NEJMoa1106920

Repetto, H. A. (1997). Epidemic Hemolytic-Uremic Syndrome in Children. *Kidney Int.* 52, 1708–1719. doi: 10.1038/ki.1997.508

Rincon-Orozco, B., Kunzmann, V., Wrobel, P., Kabelitz, D., Steinle, A., and Herrmann, T. (2005). Activation of Vγ9Vδ2 T Cells by NKG2D. *J. Immunol.* 15 (4), 2144–2151. doi: 10.4049/jimmunol.175.4.2144

Roberts, A. I., Bilenker, M., and Ebert, E. C. (1997). Intestinal Intraepithelial Lymphocytes Have a Promiscuous Interleukin-8 Receptor. *Gut* 40 (3), 333–338. doi: 10.1136/gut.40.3.333

Roth, S. J., Diacovo, T., Brenner, M. B., Rosat, J. P., Buccola, J., Morita, C. T., et al (1998). Transendothelial Chemotaxis of Human Alpha/Beta and Gamma/Delta T Lymphocytes to Chemokines. *Eur. J. Immunol.* 28 (1), 104–113. doi: 10.1002/(SICI)1521-4141(199801)28:01<104::AID-IMMU104>3.0.CO;2-F

Sabbione, F., Gabelloni, M. L., Ernst, G., Gori, M. S., Salamone, G. V., Oleastro, M., et al (2014). Neutrophils Suppress γδ T-Cell Function. *Eur. J. Immunol.* 44, 819–830. doi: 10.1002/eji.201343664

Sandvig, K., Bergan, J., Kavaliauskiene, S., and Skotland, T. (2014). Lipid Requirements for Entry of Protein Toxins Into Cells. *Prog. Lipid Res.* 54, 1–13. doi: 10.1016/j.plipres.2014.01.001

Sandvig, K., Garred, O., Prydz, K., Kozlov, J. V., Hansen, S. H., and van Deurs, B. (1992). Retrograde Transport of Endocytosed Shiga Toxin to the Endoplasmic Reticulum. *Nature* 358 (6386), 510–512. doi: 10.1038/358510a0

Scheutz, F., Teel, L. D., Beutin, L., Piérard, D., Buvens, G., Karch, H., et al (2012). Multicenter Evaluation of a Sequence-Based Protocol for Subtyping Shiga Toxins and Standardizing Stx Nomenclature. *J. Clin. Microbiol.* 50 (9), 2951–2963. doi: 10.1128/JCM.00860-12

Shiromizu, C. M., and Jancic, C. C. (2018). γδ T Lymphocytes: An Effector Cell in Autoimmunity and Infection. *Front. Immunol.* 16, 2389. doi: 10.3389/fimmu.2018.02389

Silva-Santos, B., Serre, K., and Norell, H. (2015). γδ T Cells in Cancer. *Nat. Rev. Immunol.* 15 (11), 683–691. doi: 10.1038/nri3904

Ståhl, A. L., Sartz, L., Nelsson, A., Békássy, Z. D., and Karpman, D. (2009). Shiga Toxin and Lipopolysaccharide Induce Platelet-Leukocyte Aggregates and Tissue Factor Release, a Thrombotic Mechanism in Hemolytic Uremic Syndrome. *PLoS One* 4 (9), e6990. doi: 10.1371/journal.pone.0006990

Stricklett, P. K., Hughes, A. K., Ergonul, Z., and Kohan, D. E. (2002). Molecular Basis for Up-Regulation by Inflammatory Cytokines of Shiga Toxin 1 Cytotoxicity and Globotriaosylceramide Expression. *J. Infect. Dis.* 186 (7), 976–982. doi: 10.1086/344053

Te Loo, D. M. W. M., Hinsbergh, V. W. M. V., Heuvel, L.P.W.J.V.D., and Monnens, L. A. H. (2011). Detection of Verocytotoxin Bound to Circulating Polymorphonuclear Leukocytes of Patients With Hemolytic Uremic Syndrome. *J. Am. Soc Nephrol.* 12 (4), 800–806. doi: 10.1681/ASN.V124800

Terajima, J., Iyoda, S., Ohnishi, M., and Watanabe, H. (2014). Shiga Toxin (Verotoxin)-Producing *Escherichia Coli* in Japan. *Microbiol. Spectr.* 2 (5), 1–9. doi: 10.1128/microbiolspec.EHEC-0011-2013

Trapani, J. A., and Smyth, M. J. (2002). Functional Significance of the Perforin/Granzyme Cell Death Pathway. *Nat. Rev. Immunol.* 2 (10), 735–747. doi: 10.1038/nri911

Conflict of Interest: The authors declare that the research was conducted in the absence of any commercial or financial relationships that could be construed as a potential conflict of interest.

Publisher's Note: All claims expressed in this article are solely those of the authors and do not necessarily represent those of their affiliated organizations, or those of the publisher, the editors and the reviewers. Any product that may be evaluated in this article, or claim that may be made by its manufacturer, is not guaranteed or endorsed by the publisher.

frontiers in Cellular and Infection Microbiology

ORIGINAL RESEARCH
published: 03 December 2021
doi: 10.3389/fcimb.2021.772962

Curcumin β-D-Glucuronide Modulates an Autoimmune Model of Multiple Sclerosis with Altered Gut Microbiota in the Ileum and Feces

Sundar Khadka[1†], *Seiichi Omura*[1†], *Fumitaka Sato*[1†], *Kazuto Nishio*[2], *Hideaki Kakeya*[3] *and Ikuo Tsunoda*[1*]

[1] Department of Microbiology, Kindai University Faculty of Medicine, Osaka, Japan, [2] Department of Genome Biology, Kindai University Faculty of Medicine, Osaka, Japan, [3] Graduate School of Pharmaceutical Sciences, Kyoto University, Kyoto, Japan

OPEN ACCESS

Edited by:
Elias Adel Rahal,
American University of Beirut, Lebanon

Reviewed by:
Shailesh K Shahi,
The University of Iowa, United States
Surya Prakash Pandey,
University of Pittsburgh, United States

***Correspondence:**
Ikuo Tsunoda
itsunoda@med.kindai.ac.jp

[†]*These authors have contributed equally to this work*

Specialty section:
This article was submitted to Microbes and Innate Immunity, a section of the journal Frontiers in Cellular and Infection Microbiology

Received: *09 September 2021*
Accepted: *08 November 2021*
Published: *03 December 2021*

Citation:
Khadka S, Omura S, Sato F, Nishio K, Kakeya H and Tsunoda I (2021) Curcumin β-D-Glucuronide Modulates an Autoimmune Model of Multiple Sclerosis with Altered Gut Microbiota in the Ileum and Feces. Front. Cell. Infect. Microbiol. 11:772962. doi: 10.3389/fcimb.2021.772962

We developed a prodrug type of curcumin, curcumin monoglucuronide (CMG), whose intravenous/intraperitoneal injection achieves a high serum concentration of free-form curcumin. Although curcumin has been reported to alter the gut microbiota and immune responses, it is unclear whether the altered microbiota could be associated with inflammation in immune-mediated diseases, such as multiple sclerosis (MS). We aimed to determine whether CMG administration could affect the gut microbiota at three anatomical sites (feces, ileal contents, and the ileal mucosa), leading to suppression of inflammation in the central nervous system (CNS) in an autoimmune model for MS, experimental autoimmune encephalomyelitis (EAE). We injected EAE mice with CMG, harvested the brains and spinal cords for histological analyses, and conducted microbiome analyses using 16S rRNA sequencing. CMG administration modulated EAE clinically and histologically, and altered overall microbiota compositions in feces and ileal contents, but not the ileal mucosa. Principal component analysis (PCA) of the microbiome showed that principal component (PC) 1 values in ileal contents, but not in feces, correlated with the clinical and histological EAE scores. On the other hand, when we analyzed the individual bacteria of the microbiota, the EAE scores correlated with significant increases in the relative abundance of two bacterial species at each anatomical site: *Ruminococcus bromii* and *Blautia (Ruminococcus) gnavus* in feces, *Turicibacter* sp. and *Alistipes finegoldii* in ileal contents, and *Burkholderia* spp. and *Azoarcus* spp. in the ileal mucosa. Therefore, CMG administration could alter the gut microbiota at the three different sites differentially in not only the overall gut microbiome compositions but also the abundance of individual bacteria, each of which was associated with modulation of neuroinflammation.

Keywords: bioinformatics, animal model, pattern matching, PICRUSt analysis, bacterial taxonomy, Alpha diversity, confidence interval, histology

1 INTRODUCTION

Polyphenol curcumin is the principal active component of turmeric, *Curcuma longa* (Ozawa et al., 2017). Experimentally, curcumin has been reported to have multiple functions, including antioxidant (Lin et al., 2019), antitumor (Ozawa et al., 2017), and anti-inflammatory functions (Xie et al., 2009); curcumin has been shown to be beneficial in several disease conditions including multiple sclerosis (MS) (Mohajeri et al., 2015), cancer (De Velasco et al., 2020), and inflammation (Xie et al., 2009). Clinically, however, the oral administration of free-form curcumin did not provide the desired effects in clinical trials. This can be explained by its rapid metabolism in the body; curcumin is metabolized to an inactive conjugated form after it is taken from the intestine (Asai and Miyazawa, 2000), although only a free-form of curcumin is associated with the pharmacological activity. In addition, the bioavailability of curcumin within the body is inadequate due to the poor absorption from the intestine, insolubility in body fluids, and rapid elimination and clearance from the body through feces (Anand et al., 2007; Ozawa et al., 2017).

Since the low bioavailability of curcumin in the body has limited its application as a therapeutic agent, we developed a prodrug type of curcumin, curcumin β-D-monoglucuronide (curcumin monoglucuronide, CMG). CMG is safe and can be injected intravenously; CMG administration achieved a high concentration of free-form curcumin in the blood of rats (Ozawa et al., 2017). We demonstrated that intravenous CMG administration had an anticancer effect on mice transplanted with human colorectal cancer cells by achieving the blood concentration of free-form curcumin 1000-fold more than oral administration of curcumin (Ozawa et al., 2017). Intraperitoneal CMG administration also had anti-tumor effects on oxaliplatin-resistant colon cancer with less toxicity in mouse xenograft models (Ozawa-Umeta et al., 2020).

Abundant and diverse microbial communities coexist in mammals, including humans and mice. In the gastrointestinal (GI) tract, the microbial communities are composed of microorganisms, including bacteria and archaea, which are collectively referred as the gut "microbiota". Recently, the communications between the gut microbiota and immune system have been shown to contribute to eliminating microbes and cancers by activating systemic immune responses (Lazar et al., 2018). In contrast, dysbiosis, an altered state of microbiota, has been shown to induce uncontrolled excessive immune responses (Park et al., 2017; Gandy et al., 2019), leading to immune-mediated tissue damage, immunopathology, not only in the GI tract but also in other organs, including the central nervous system (CNS) (Braniste et al., 2014). Although curcumin has been reported to potentially alter both the gut microbiota and immune responses, it is unknown which gut microbial communities can be affected by curcumin and whether the altered microbiota could be associated with suppression of immunopathology in immune-mediated diseases, such as MS.

We aimed to determine whether CMG administration could affect the gut microbiota at three anatomical sites: feces, ileal contents, and the ileal mucosa. We also investigated that the altered microbiota by CMG administration could be associated with suppression of immunopathology, using an autoimmune model for MS (Chearwae and Bright, 2008), experimental autoimmune encephalomyelitis (EAE). In MS, the gut microbiota has been proposed to play a role in disease progression and severity. Clinically, MS patients have had increased abundance of some bacteria, including the genera *Akkermansia*, *Pseudomonas*, and *Blautia*, and decreased abundance of some bacteria, such as the genera *Prevotella* and *Parabacteroides*, compared with the healthy controls (Miyake et al., 2015; Chen et al., 2016; Jangi et al., 2016; Park et al., 2017; Tsunoda, 2017). EAE can be induced by sensitizing animals with myelin components, such as myelin oligodendrocyte glycoprotein (MOG) and myelin proteolipid protein (PLP). Anti-myelin autoimmune cells cause inflammatory demyelination in the CNS, resulting in paralysis in EAE animals, which resembles MS (Sato et al., 2018). Pro-inflammatory T helper (Th)1/Th17 cytokines, including interferon (IFN)-γ and interleukin (IL)-17, contribute to the development of EAE; anti-inflammatory Th2/regulatory T (Treg) cytokines, including IL-4 and IL-10, are protective in EAE (Xie et al., 2009; Chaudhry et al., 2011).

Although curcumin has been reported to alter the gut microbiota of rodents and humans (Di Meo et al., 2019; Zam, 2018; Peterson et al., 2018) in healthy and disease conditions, including EAE (Shen et al., 2017; Zhang et al., 2017), the effect of curcumin on the gut microbiota at different anatomical sites and their associations of disease conditions have not been clarified. In the present study, we demonstrated that CMG administration modulated EAE, where the severity was associated with altered overall microbiota composition in ileal contents, but not in feces or the ileal mucosa. On the other hand, when we analyzed the relative abundance of individual bacteria at the three anatomical sites, the EAE severities also correlated with significant increases in the relative abundance of two bacterial species at each anatomical site: *Ruminococcus bromii* and *Blautia (Ruminococcus) gnavus* in feces, *Turicibacter* sp. and *Alistipes finegoldii* in ileal contents, and *Burkholderia* spp. and *Azoarcus* spp. in the ileal mucosa. Therefore, CMG administration could differentially alter the gut microbiota at the three different sites in not only overall gut microbiome compositions, but also the abundance of individual bacterial species, each of which was associated with decreased inflammation in the CNS.

2 MATERIALS AND METHODS

2.1 Mice

Six-week-old female C57BL/6 mice were purchased from CLEA Japan, Inc. (Tokyo, Japan). The mice were maintained under specific-pathogen-free conditions in our animal care facility at Kindai University Faculty of Medicine (Osaka, Japan). All experimental procedures were approved by the Institutional Animal Care and Use Committee of Kindai University Faculty of Medicine and performed according to the criteria outlined by the National Institutes of Health (National Research Council

(US) Committee for the Update of the Guide for the Care and Use of Laboratory Animals, 2011).

2.2 EAE Induction and CMG Administration

For EAE induction, mice were sensitized subcutaneously (s.c.) with 258 μg (=100 nmol) of the MOG_{35-55} peptide (MEVGWYRSPFSRVVHLYRNGK, United BioSystems, Herndon, VA) emulsified in complete Freund's adjuvant (CFA) that is composed of incomplete Freund's adjuvant (BD, Franklin Lakes, NJ) and *Mycobacterium tuberculosis* H37 Ra (BD) on days 0 and 19 (Fernando et al., 2014). The final concentration of *M. tuberculosis* in the MOG_{35-55}/CFA emulsion was 2 mg/mL (400 μg/mouse). The mice were also injected intraperitoneally (i.p.) with 300 ng of pertussis toxin (List Biological Laboratories, Campbell, CA) on days 0 and 2. The clinical scores of EAE were evaluated as follows: 0, no sign; 1, tail paralysis; 2, mild hindlimb paresis; 3, moderate hindlimb paralysis; 4, complete hindlimb paraplegia; and 5, quadriplegia or moribund state (Tsunoda et al., 2007). The cumulative scores were calculated by the area under the EAE score curve that reflects the overall disease severity over the course.

A CMG solution was prepared in phosphate-buffered saline (PBS) at a concentration of 9 mg/mL and stored at −80°C until used (Ozawa et al., 2017; Ozawa-Umeta et al., 2020). The mice were divided into four groups (7–9 mice per group): the Control, Induction, Latent, and Whole groups based on the CMG administration schedule. The mice were injected i.p. with 200 μL of the CMG solution (1.8 mg/mouse) on days 0–4 (Induction group), on days 11–15 (Latent group), or on days 0–4, 6, 8, 9, 11–15, 17, 19, 21, 23, 25, 27, 29, 31, and 33 (Whole group). In the Whole group, the mice were treated daily with CMG on days 0–4 and 11–15 using the same administration schedules as the Induction and Latent groups, respectively, and three times a week in the other time points, based on our previous publications (Ozawa et al., 2017; Ozawa-Umeta et al., 2020). The control mice (Control group) were injected with PBS. To determine the effects of CMG administration on EAE mice, their body weight changes and EAE scores were monitored daily for 5 weeks.

2.3 Neuropathology

The mice were killed with isoflurane (Mylan N.V., Canonsburg, PA) 5 weeks post-induction (p.i.) and perfused with PBS followed by a 4% paraformaldehyde (PFA, FUJIFILM Wako Pure Chemical Corporation, Osaka, Japan) solution in PBS (Sato et al., 2017). After the PFA fixation, the spinal cord and brain were divided into 12 to 15 transversal segments and five coronal slabs, respectively, and were embedded in paraffin. Four-μm-thick CNS sections were made using the HM 325 Rotary Microtome (Thermo Fisher Scientific Inc., Waltham, MA) and stained with Luxol fast blue (Solvent Blue 38; MP Biomedicals, LLC, Irvine, CA) for myelin visualization. The phenotypes of immune cells were determined by immunohistochemistry. The CNS sections were incubated with antibodies against CD3 (T cell marker, 100-fold dilution, Biocare Medical, Pacheco, CA; antigen retrieval: 10 mM citrate buffer pH 6.0 at 120°C for 15 min), B220 (B cell marker, 300-fold dilution, eBioscience, San Diego, CA; no antigen retrieval), F4/80 (macrophage marker, 200-fold dilution, Bio-Rad, Hercules, CA; antigen retrieval: 100 μg/ml proteinase-K for 10 min), Ly-6G (neutrophil marker, 500-fold dilution, BD Bioscience, Franklin Lakes, NJ; no antigen retrieval), Foxp3 (Treg marker, 100-fold dilution, eBioscience; antigen retrieval: 10 mM citrate buffer pH 6.0 at 120°C for 15 min), and goat anti-mouse IgA-UNLB antibody (IgA-producing cell marker, 2000-fold dilution, SouthernBiotech, Birmingham, AL; no antigen retrieval) (Omura et al., 2020). The antibody/antigen complexes were visualized using 3,3'-diaminobenzidine (DAB, FUJIFILM Wako Pure Chemical Corporation).

2.4 Enzyme-Linked Immunosorbent Assays (ELISAs)

When the mice were killed 5 weeks p.i., the spleens and inguinal lymph nodes were harvested and mashed on a metal mesh with 50-μm pores. Splenic mononuclear cells (MNCs) were isolated using Histopaque®-1083 (MilliporeSigma, Burlington, MA). The splenic MNCs and lymph node cells were cultured in RPMI-1640 medium (MilliporeSigma) supplemented with 10% fetal bovine serum (FBS, MilliporeSigma), 2 mM L-glutamine (MilliporeSigma), 50 mM β-mercaptoethanol (FUJIFILM Wako Pure Chemical Corporation), and a 1% antibiotics solution (Thermo Fisher Scientific, Waltham, MA) containing 10,000 U/mL penicillin and 10,000 μg/mL streptomycin at concertation of 8×10^6 cells/well in 6-well plates (Sumitomo Bakelite, Tokyo, Japan) (Martinez et al., 2014). The cells were stimulated with 5 μg/mL of the mitogen concanavalin A (ConA, MilliporeSigma) or 50 μg/mL of the MOG_{35-55} peptide for 2 days. The culture supernatants were harvested and stored at −80°C until examined.

The amounts of IL-4 (BD Biosciences, San Jose, CA), IL-10 (BD Biosciences), IFN-γ (BD Biosciences), and IL-17A (Biolegend, San Diego, CA) in the culture supernatants were quantified using ELISA kits, according to the manufacturers' instructions (Tsunoda et al., 2005). The detection limits of each cytokine were as follows: IL-4, 7.8 pg/mL; IL-10, 31.3 pg/mL; IFN-γ, 31.3 pg/mL; and IL-17A, 15.6 pg/mL. ELISAs were conducted in duplicate, using 96-well plates (Thermo Fisher Scientific).

2.5 Gut Microbiota Sample Collection

After perfusing mice with PBS, for microbiome analyses, the fecal samples (also called "feces" in this manuscript) were collected 5 weeks p.i. from the rectum and/or the anal canal, and the ileal content samples were harvested from the ileum by flushing with distilled water. The flushed ileum was rinsed with Dulbecco's Modified Eagle's Medium (DMEM, MilliporeSigma, Burlington, MA) containing 10% fetal bovine serum (FBS) twice and incubated in DMEM containing 10% FBS and 1 mM dithiothreitol (DTT, MilliporeSigma) with shaking for 40 min. The supernatants were filtered with Falcon® 70-μm cell strainers (Corning Incorporated, Corning, NY) and centrifuged at 5,000*g* for 15 min at 4°C. After centrifugation, the pellets were used as the samples containing the gut microbiota from the ileal mucosa. All samples were frozen in liquid nitrogen and stored at −80°C until examined (Tong et al., 2014).

2.6 DNA Extraction and Sequencing

Bacterial DNA was extracted from feces, ileal contents, and the ileal mucosa using the QIAamp® Fast DNA Stool Mini Kit (Qiagen, Germantown, MD), according to the manufacturer's instructions (Omura et al., 2020). Using the DNA samples, 16S rRNA amplicon sequencing was conducted on MiSeq System (Illumina, San Diego, CA) by MR DNA (Shallowater, TX), a commercially available sequencing service, who processed the sequence data using a MR DNA analysis pipeline (http://www.mrdnalab.com/bioinformatics.html). Primer sequences used for sequencing (515F/806R) were designed against the V4 region of the 16S rRNA as follows: forward (515F), 5'-AATGATACG GCGACCACCGAGATCTACACTATGGTAATTGTGT GCCAGCMGCCGCGGTAA-3'; reverse (806R), 5'-CAAGCAG AAGACGGCATACGAGATCTAGCGTGCGTTAGTCAGT CAGCCGGACTACHVGGGTWTCTAAT-3' (Caporaso et al., 2011). Operational taxonomic units (OTUs) were defined by clustering at 3% divergence (97% similarity). The final OTUs were classified taxonomically using BLASTn against a curated database derived from the Ribosomal Database Project (RDP)-II (http://rdp.cme.msu.edu) and National Center for Biotechnology Information (NCBI, www.ncbi.nlm.nih.gov). Total read count number in our analysis ranged from 22,488 to 29,674 reads (average: 29,245 reads); the number of read counts was similar among the three anatomical sites. The sequencing depth was within this range in all samples. To determine the diversities and conduct PICRUSt (phylogenetic investigation of communities by reconstruction of unobserved states) metagenome prediction analyses, the raw sequence data were denoised, demultiplexed, aligned, and visualized by QIIME 2 (Bolyen et al., 2019). The data generated and analyzed in the current study have been deposited into the Sequence Read Archive (SRA) at NCBI (BioProject ID: PRJNA688384, BioSample accessions: SAMN17174018-SAMN17174101).

2.7 Bioinformatics Analyses

2.7.1 Alpha Diversity

The alpha diversity of microbiomes at the genus level were compared among the three distinct anatomical sites and among the four groups at each anatomical site using QIIME 2 (Bolyen et al., 2019). To determine the bacterial richness, evenness, and combination of richness/evenness, the Faith's phylogenetic diversity, Pielou's evenness, and Shannon indexes were calculated, respectively (Omura et al., 2020).

2.7.2 Principal Component Analysis (PCA)

To compare the overall microbiomes among all samples from the three distinct anatomical sites and among individual samples from each anatomical site, PCA was conducted using an R program "prcomp", as described previously (Chaitanya et al., 2013). Factor loading for principal component (PC) was used to rank individual bacteria whose relative abundance was correlated with PC values. A graph of PCA with ellipses of an 80% confidence interval was drawn, using R packages "dplyr" and "ggplot2".

2.7.3 Pattern Matching

To examine the associations between the EAE severity and gut microbiota, pattern matching was conducted by R, using the clinical and neuropathological scores of EAE versus PC1 values of the microbiome at each anatomical site or versus the relative abundance of individual bacteria at the species level (Omura et al., 2019). The values more than 0.7 or less than −0.7 in the Spearman's rank correlation coefficient (r) with $P < 0.05$ (calculated by functions of Microsoft Excel, Microsoft Corporation, Redmond, WA) were considered as a highly positive or negative correlation, respectively (Mukaka, 2012). The r value, which is from 0.5 to 0.7 or from −0.7 to −0.5 with $P < 0.05$, was considered as a moderate correlation.

2.7.4 Predictive Metagenome Analysis

The functional composition of a metagenome of the microbiota was predicted by running PICRUSt on the Linux operating system, as described previously (Omura et al., 2020). By analyzing 16S rRNA sequencing data of the gut microbiota by PICRUSt (Langille et al., 2013), the following two data files were obtained: 1) a pathway-based prediction data file containing lists of a) the name of pathways, b) the total read count data of all bacteria encoding genes related to each pathway, and c) KEGG pathway names; and 2) an enzyme-based metagenome prediction data file containing lists of a) the enzyme ID number, b) the total read count data of all bacteria encoding the enzyme, and c) KEGG enzyme names. Using the pathway prediction data, the read counts were compared between the Control and CMG-treated groups, and the pathways with significant differences ($P < 0.05$, compared with the Control group, Student's t test) were identified. Using the metagenome prediction data, the read counts of all bacteria encoding β-glucuronidase were also compared between the Control and CMG-treated groups.

2.8 Statistical Analyses

Using the OriginPro 2020 (OriginLab Corporation, Northampton, MA), the Mann–Whitney U test and Student's t test and ANOVA with Fisher's PLSD test as *post hoc* test were conducted for nonparametric and parametric data, respectively.

3 RESULTS

3.1 CMG Administration Modulates EAE

We tested whether CMG administration could affect EAE. Following MOG sensitization, we treated mice with CMG during the induction (Induction group) or latent phase (Latent group), or throughout the whole course (Whole group). We injected the control EAE mice (Control group) with PBS. We monitored the EAE signs (**Figure 1A**) and body weight changes (reflecting the severity of EAE, **Figure 1B**) daily for 5 weeks. All CMG-treated groups (Induction, Latent, and Whole) tended to develop less severe EAE compared with the Control group; less weight loss in the Induction and Latent group (**Figure 1B**) and lower cumulative scores of EAE in the Whole group (**Supplemental Table 1A**). Although CMG-treated groups had lower maximum clinical scores, EAE incidence, and EAE duration compared with the Control

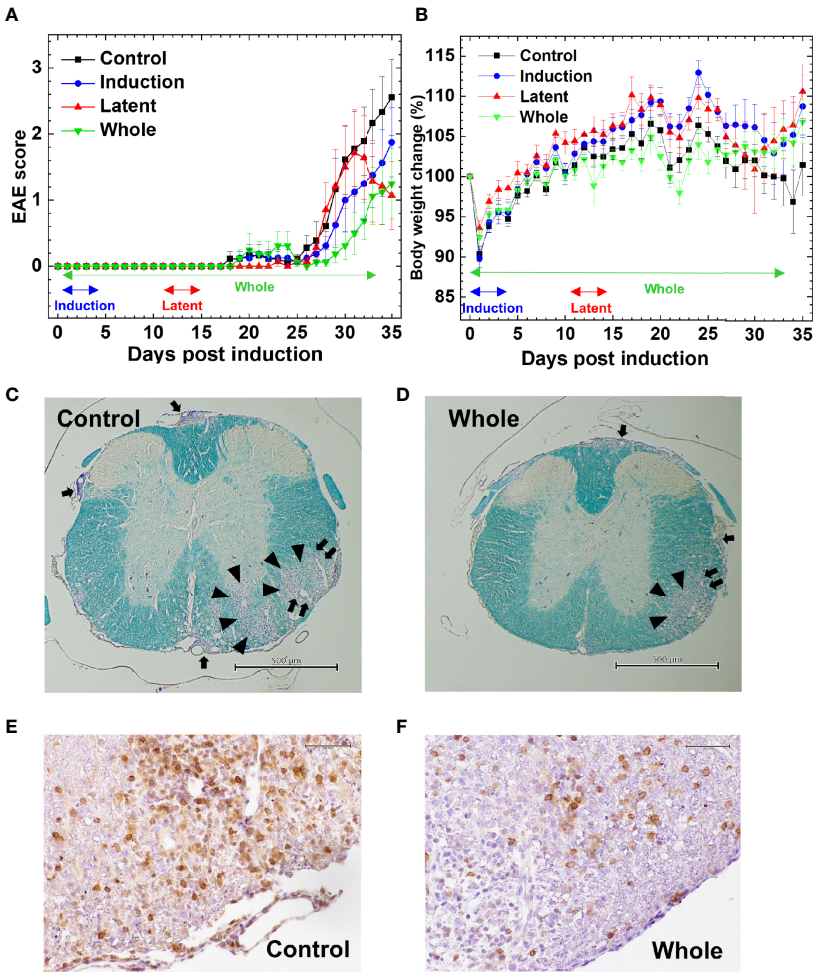

FIGURE 1 | Effects of curcumin monoglucuronide (CMG) in an autoimmune model of multiple sclerosis (MS), experimental autoimmune encephalomyelitis (EAE). **(A)** For EAE induction, we sensitized C57BL/6 mice with the myelin oligodendrocyte glycoprotein $(MOG)_{35-55}$ peptides. We divided the mice into four groups: Control, Induction, Latent, and Whole groups (n = 7–9 per group), and treated the groups with CMG on days 0–4 (Induction), on days 11–15 (Latent), or throughout the course (Whole). We treated the control mice (Control) with phosphate-buffered saline (PBS). All CMG-treated groups had less severe EAE compared with the control group. The Whole group tended to have a lower EAE score than the Control group 30 days post-induction (p.i.) ($P = 0.06$, Mann–Whitney *U* test). The Latent group tended to recover from acute EAE more quickly than the Control group 35 days p.i. ($P = 0.056$, Mann–Whitney *U* test). The clinical score was calculated as the mean ± standard error (SE) of seven to nine mice per group. **(B)** We monitored body weight changes of mice daily. The levels of body weight changes had an inverse relationship to the severity of clinical signs. The Control EAE group had more weight loss compared with the Induction ($P = 0.06$), Latent ($P = 0.07$), and Whole ($P = 0.14$) groups on day 34. Results are the mean ± SE of seven to nine mice per group. **(C–F)** We stained the spinal cord sections (scale bar: C and D = 500 μm, E and F = 50 μm) from EAE mice with Luxol fast blue **(C, D)** or anti-CD3 antibody **(E, F)** to visualize myelin or T cells, respectively, compared the spinal cord pathology between the Control **(C, E)** and CMG-treated Whole groups **(D, F)**. The Whole group had less severe demyelination (arrowhead), meningitis (arrow), and perivascular inflammation (paired arrows) and fewer T cell infiltration, compared with the Control group. The stained sections are representative of seven to nine mice per group.

group, these parameters did not reach statistical differences (**Supplemental Table 1A**).

The severity of EAE correlated with neuropathology; mice from the Latent and Whole groups developed less severe inflammatory demyelinating lesions in the spinal cord (**Figures 1C–F**). Although the neuropathology scores did not reach statistical differences, there were some trends toward lower levels of perivascular inflammation (cuffing) and demyelination in the spinal cord in the Latent and Whole groups compared with the Control group (**Supplemental Figure 1A**). On the other hand, there were no differences in the spinal cord pathology between the Control and Induction groups. We also compared the brain pathology scores among the four groups and found no differences [mean brain pathology scores ± standard error (SE) 5 weeks p.i.: Control, 3.9 ± 0.7; Induction, 4.1 ± 0.9; Latent, 3.6 ± 1.8; Whole, 3.1 ± 0.4]. To further determine the effects of CMG on neuropathology, we conducted hematoxylin and eosin staining to see whether neutrophil infiltration differed among the groups. We found that CNS cellular infiltrates were mainly composed of mononuclear cells (MNCs), but not neutrophils, in all groups

(**Supplemental Figure 1B**); a small number of neutrophil infiltration was confirmed by immunohistochemistry using Ly-6G antibody (**Supplemental Table 1B** and **Supplemental Figure 1E**). Next, we compared the phenotypes of MNCs in the spinal cord by immunohistochemistry using antibodies against CD3 (T cell marker), B220 (B cell marker), and F4/80 (macrophage marker) (**Figures 1E, F**, **Supplemental Figures 1C, D** and **Supplemental Table 1B**). The percentages of $CD3^+$ T cells in CMG-treated groups were lower than the control group: Control, 57.6%; Induction, 52%; Latent, 46%; and Whole, 33%) (**Supplemental Table 1B**). Although we detected a small number of B cells in inflammatory areas and a large number of F4/80 positive macrophage lineage cells in inflammatory areas and demyelinating lesions, B-cell and macrophage infiltrations were similar among the groups (**Supplemental Table 1B**). Since regulatory T (Treg) cells and IgA-producing B cells have been shown to regulate MS and animal models, we compared Treg cells and IgA^+ cells among the groups using Foxp3 and IgA immunohistochemistry (**Supplemental Figures 1F, G**). We found similar levels of $Foxp3^+$ T cells among the groups. We did not find IgA^+ cells in any group in the spinal cord, although IgA was detected in the control intestine sections.

We cultured splenic MNCs and lymph node cells from EAE mice and quantified the amounts of IL-10, IL-4, IFN-γ, and IL-17 in the cultures stimulated with mitogen or MOG by ELISAs. Although splenic MNCs of the Latent group tended to produce larger amounts of IL-10 in mitogen stimulation and IFN-γ in MOG stimulation compared with controls ($P < 0.1$), there were no statistical differences in the cytokine levels among the four groups in the other cultures (**Supplemental Figure 2**). We also examined the levels of MOG-specific lymphoproliferation and found that all groups had substantial MOG-specific lymphoproliferative responses without significant differences among the four groups (**Supplemental Figure 3**).

3.2 Microbiota in EAE Differs Among the Three Anatomical Sites

Since the microbiota has been reported to be different between the luminal contents versus mucosa in the same anatomical site as well as the distinct anatomical sites in humans and mice (Li et al., 2015; Wu et al., 2020), we harvested the microbial samples from feces, ileal contents, and the ileal mucosa of EAE mice. Using 16S rRNA sequencing data, we determined bacterial alpha diversities by the Faith's phylogenetic diversity (species richness), Pielou's evenness (species evenness), and Shannon (combination of richness and evenness) indexes. As expected, the three indexes using the all samples were significantly different among the three anatomical sites ($P < 0.05$, ANOVA, **Supplemental Figure 4**). We also found that the overall microbiome patterns were different between the samples from feces, ileal contents, and the ileal mucosa by PCA of the microbiome data (**Supplemental Figure 5**). PCA separated the ileal mucosal samples from the fecal and ileal content samples by PC1 at all three taxonomical levels: phylum, genus, and species (**Supplemental Figure 6**). PC1 values were significantly higher in the ileal mucosa than in feces and ileal contents at the three taxonomical levels ($P < 0.05$, ANOVA). PC2 values were also significantly different among the three anatomical sites at the genus and species levels, but not the phylum level (**Supplemental Figure 7**).

3.3 CMG Administration Alters the Fecal and Ileal Microbiota

Since a reduced microbial diversity has been associated with some diseases, including inflammatory bowel diseases (IBDs) (Manichanh et al., 2006; Gong et al., 2016), we determined whether CMG administration could alter the diversity of the microbiota at each anatomical site. Using the three indexes, however, we found that the microbial diversity in the CMG-treated groups was similar to that in the Control group (**Figure 2**). There were no differences in the Faith's or Shannon index among the four groups. The Pielou's index was similar in the ileal mucosa between the Control and CMG-treated groups, although it was higher in the Control group compared with the Whole and Induction groups in feces and the Latent groups in ileal contents.

We also tested whether CMG administration could alter the overall microbiota compositions in feces, ileal contents, and the ileal mucosa at the phylum, genus, and species levels. At the three taxonomical levels, PCA of the microbiota data from feces and ileal contents, but not the ileal mucosa, separated the CMG-treated groups from the Control group by PC1 (**Figures 3A–C** and **Supplemental Figures 8A–C**, **9A–C**). PC1 values were significantly higher in the feces and ileal contents of all CMG-treated groups than those of the Control group (**Figures 3D–F** and **Supplemental Figures 8D–F**, **9D–F**). Factor loading for PC1 indicated that, at the species level, increased *Bacteroides acidifaciens* and decreased *Clostridium* sp. and *Alistipes massiliensis* in feces as well as increased *Bacteroides acidifaciens* and decreased *Turcibacter* sp. in ileal contents correlated with PC1 values (**Figures 3G, H**). These results demonstrated that CMG administration affected microbiota in feces and ileal contents, but not in the ileal mucosa.

3.4 CMG Administration Alters the Bacterial Abundance at the Three Anatomical Sites

We prepared naïve, CFA/PT-injected, and EAE mice as the control groups. However, since the relative abundance of naïve and CFA/PT mice was much different from the four EAE groups (**Supplemental Figure 10**), we decided to evaluate the microbiota changes by CMG treatment by comparing the three CMG-treated groups with the control EAE group, but not with the naïve or CFA/PT group (**Figure 4**). We compared the relative abundance of individual bacteria among feces, ileal contents, and the ileal mucosa at the phylum, genus, and species levels (**Figure 4**, **Supplemental Figure 11**, and **Supplemental Tables 2**, **3**). We found significant differences in the bacterial abundance among the three anatomical sites: 7 of total 16 taxa at the phylum levels, 78 of total 252 taxa at the genus levels, and 160 of total 387 taxa at the species level (**Supplemental Table 2**).

Then, we examined whether CMG administration could affect the relative abundance of individual bacteria. We found significant compositional differences of the microbiota between the Control versus CMG-treated groups at the phylum, genus, and species levels (**Figure 4** and **Tables 1–3**). At the phylum and

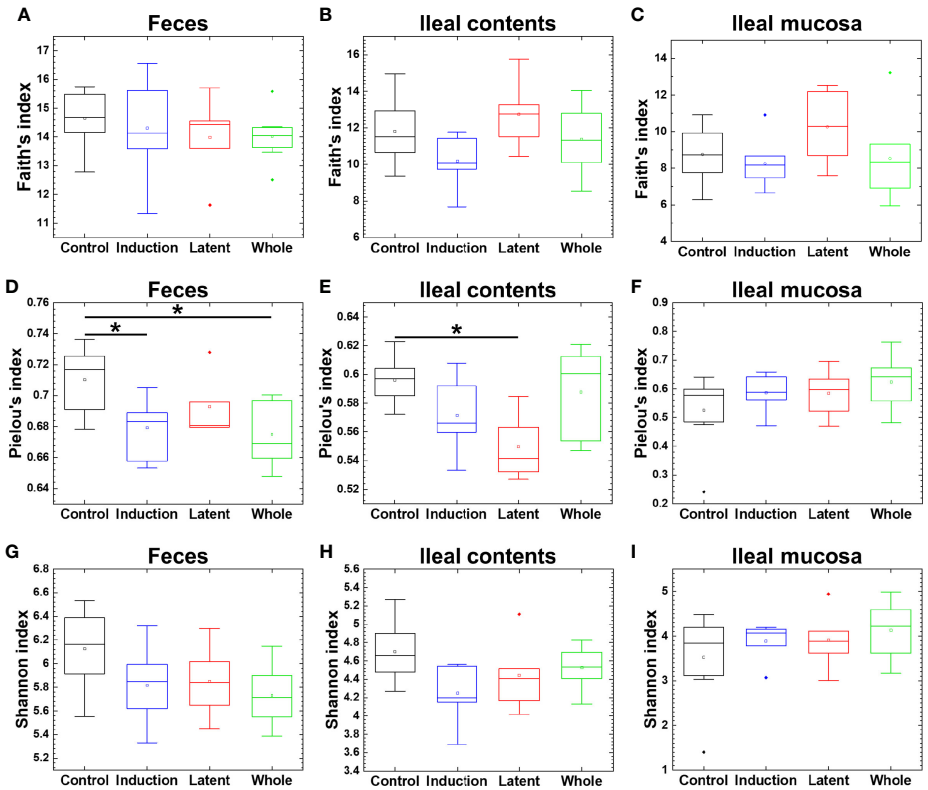

FIGURE 2 | Analyses of bacterial alpha diversities of the microbiome at three anatomical sites from EAE mice with or without CMG administration. Using QIIME 2, we compared the number of genera, evenness, and combination of them by the Faith's phylogenetic diversity **(A–C)**, Pielou's evenness **(D–F)**, and Shannon **(G–I)** indexes, respectively, between the three CMG administration (Induction, blue; Latent, red; and Whole, green) and control groups (Control, black). We found no difference in the Faith's **(A–C)** or Shannon index **(G–I)** among the CMG-treated and Control groups, although the Pielou's index was significantly different between the Control versus Whole, the Control versus Induction groups in feces **(D),** and the Control versus Latent groups in ileal contents **(E)**, all of which had decreased diversity in the CMG-treated groups (*$P < 0.05$, Kruskal-Wallis test) **(D, E)**.

genus levels, CMG administration altered the largest numbers of bacterial taxa in feces and the fewest numbers of bacterial taxa in the ileal mucosa. Among the CMG-treated groups, the Whole group had the largest numbers of altered relative abundance of bacteria compared with the Control group. The changes of the microbiota seemed to depend on the timing of CMG administration; although the numbers of bacteria with altered relative abundance were similar between the Induction and Latent groups, the altered bacterial phyla and genera were different between the two groups. For example, at the phylum level, the decreased abundance of *Firmicutes* in feces and increased abundance of *Proteobacteria* in ileal contents were seen in the Induction and Whole groups, but not in the Latent group, in which the decreased abundance of *Cyanobacteria* was seen (**Table 1**).

Similarly, at the species level, CMG administration resulted in the largest and fewest alterations of the microbiota in feces and the ileal mucosa, respectively; the three CMG-treated groups had common alterations of the relative abundance in limited numbers of bacterial species (**Figure 4B** and **Table 3**). For example, in feces, we found significant changes in 12 species in the Induction group, seven species in the Latent group, and 20 species in the Whole group, among which the relative abundance of *Blautia (Ruminococcus) gnavus* was decreased in all three CMG-treated groups compared with the Control group.

3.5 Ileal Content Microbiota Associates With Clinical and Histological EAE

To determine whether the overall changes in the microbiota by CMG administration could correlate with the severity of EAE, we conducted pattern matching between the clinical and neuropathology scores of EAE versus PC1 values of microbiota data at the species level (**Figure 5**). Although PC1 values of the fecal samples and EAE scores were not correlated (**Figure 5A**), PC1 values of ileal contents and the ileal mucosa correlated moderately with the EAE scores ($P < 0.01$, **Figures 5D, G**). Similarly, there were moderate correlations between PC1 values of ileal contents/mucosa versus the neuropathology scores including inflammation (i.e., perivascular cuffing) and demyelination with statistical differences ($P < 0.01$, **Figures 5E, F, H, I**); we found no correlations between fecal PC1 values versus the neuropathology scores (**Figures 5B, C**). Thus, bacterial PC1 values of ileal contents, but not feces, had significant correlations with the severity of EAE, although

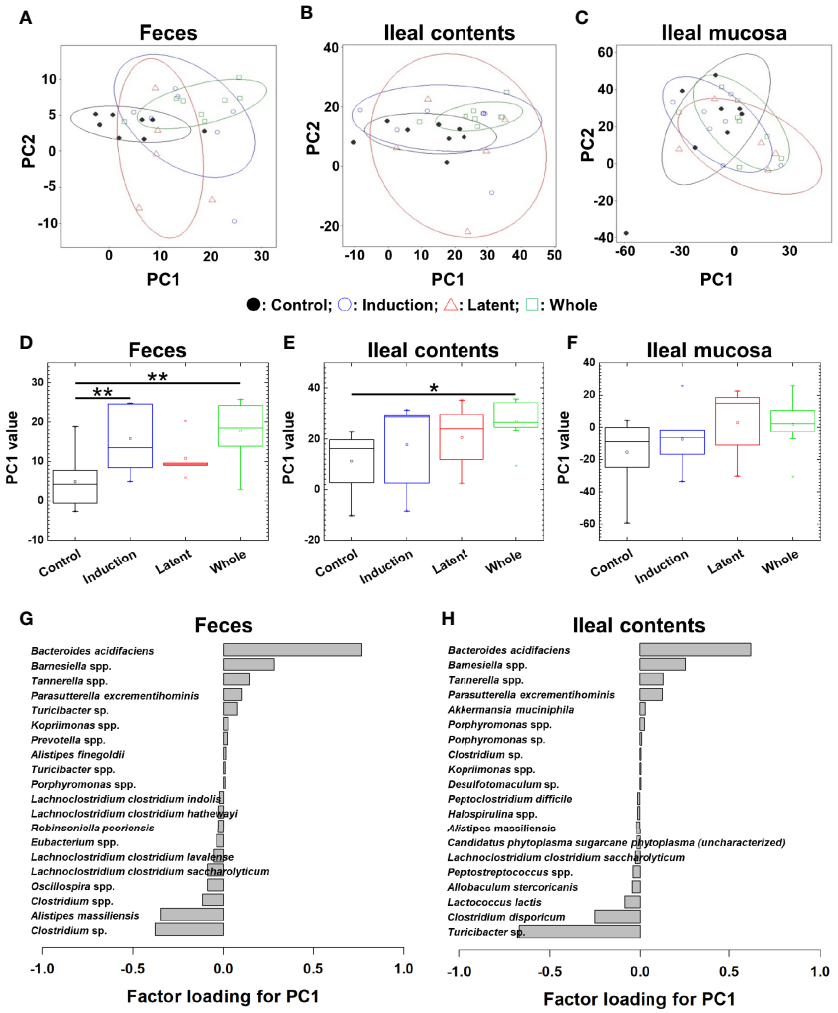

FIGURE 3 | Principal component analysis (PCA) of microbiome data at the species level from the three CMG-treated groups (Induction, blue; Latent, red; and Whole, green) and the control group (Control, black). **(A–C)** We conducted PCA using samples from the three anatomical sites: feces **(A)**, ileal contents **(B)**, and the ileal mucosa **(C)**. Ellipses indicated an 80% confidence interval of each group. Proportion of variance of principal component (PC)1 and PC2 were 47% and 14% in feces, 52% and 27% in ileal contents, and 43% and 37% in the ileal mucosa. **(D)** In feces, PC1 values were significantly different between the Control versus Induction and the Control versus Whole groups (**$P < 0.01$, ANOVA). **(G)** Factor loading for PC1 showed that the relative abundance of the species *Bacteroides acidifaciens* most highly correlated with PC1 values. **(E)** In ileal contents, PC1 values were significantly different between the Control versus Whole groups (*$P < 0.05$, ANOVA). **(H)** Factor loading for PC1 showed that the relative abundance of *Bacteriodes acidifaciens* and *Turcibacter* sp. correlated positively and negatively with PC1 values, respectively. **(F)** In the ileal mucosa, PC1 values were not different among the groups.

CMG administration changed PC1 values of the microbiota in feces and ileal contents (**Figure 3**). This suggests that CMG administration may have beneficial effects in EAE by altering the microbiota in ileal contents. On the other hand, in general, the microbiota in the ileal mucosa may be associated with the EAE severity irrespective of CMG administration.

We also conducted pattern matching between the relative abundance of individual bacterial species and EAE scores (**Figure 6**). Based on the *r* values (Mukaka, 2012), the EAE scores moderately correlated with the relative abundance of several species (five species in feces, five species in ileal contents, and two species in the ileal mucosa) and highly correlated with three species in the ileal mucosa (**Table 4**). Among these species, the relative abundance of *Ruminococcus bromii* and *Blautia (Ruminococcus) gnavus* in feces, *Turicibacter* sp. and *Alistipes finegoldii* in ileal contents, and *Burkholderia* spp. and *Azoarcus* spp. in the ileal mucosa was significantly different between the Control and CMG-treated groups (**Figure 6**, **Table 4**).

3.6 PICRUSt Predicts the CMG Effects on Bacterial Pathways

Lastly, we performed predictive metagenome analyses for microbiome data using the PICRUSt program, which predicts the pathways derived from the read counts of all bacteria in the microbiota involved in the pathways of interest. By comparing the numbers of pathways changed in the three CMG-treated

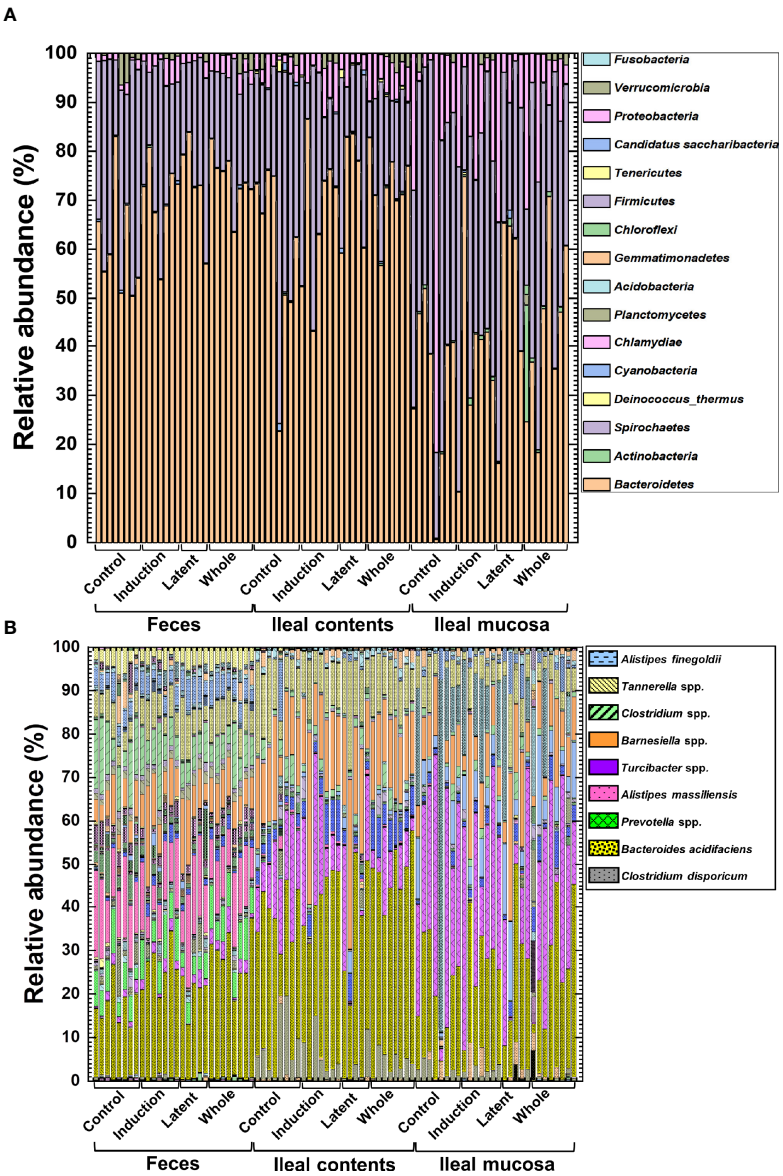

FIGURE 4 | The relative abundance of bacteria from the three anatomical sites: feces, ileal contents, and the ileal mucosa. **(A, B)** Using 16S rRNA sequencing, we analyzed the relative abundance of individual bacteria at the phylum **(A)** and species **(B)** levels. We harvested samples from the three CMG-treated (Induction, Latent, and Whole) and control groups (Control). At both phylum and species levels, compositional differences in the microbiota between the three anatomical sites were larger than the microbiota differences among the CMG-treated and control groups. Each group was composed of five to eight mice.

groups, we did not find changes that were common in all CMG-treated groups or the three anatomical sites. However, we found that changes in the several pathways were common between the two CMG-treated groups and between the two anatomical sites (**Table 5**, **Supplemental Table 4**). CMG administration seemed to affect the bacterial pathways most in ileal contents and least in the ileal mucosa, the latter of which had no upregulated pathways by CMG administration. In fecal samples, five pathways were upregulated commonly in the Induction and Whole groups. In ileal contents, CMG administration upregulated ten pathways commonly in the Latent and Whole groups. By comparing the pathways changed by CMG administration among the three anatomical sites, we found that 14 pathways were commonly upregulated in feces and ileal contents in the Whole group, but not in the Induction or Latent group. In **Table 6**, we listed the pathways that were up- or down-regulated more than 2-fold in the three CMG-treated groups. We found several pathways related to immune response and inflammation, such as "viral myocarditis" and "arachidonic acid metabolism".

We also determined the read counts of bacteria encoding β-glucuronidase between the CMG-treated and Control groups, since β-glucuronidase can be involved in CMG metabolism by

TABLE 1 | Bacterial phyla altered in the curcumin monoglucuronide (CMG)-treated groups compared with the Control group.

Groups	Feces	Ileal contents	Ileal mucosa
Induction	*Firmicutes*↓	*Proteobacteria*↑	(–)
Latent	*Cyanobacteria*↓	(–)	(–)
Whole	*Firmicutes*↓ *Bacteroidetes*↑ *Proteobacteria*↑	*Proteobacteria*↑ *Firmicutes*↓	(–)

↑, *Significant increases compared with the Control group (P < 0.05, ANOVA).*
↓, *Significant decrease compared with the Control group (P < 0.05, ANOVA).*
(–), No differences compared with the Control group.

TABLE 2 | Bacterial genera altered in the CMG-treated groups compared with the Control group.

Groups	Feces		Ileal contents		Ileal mucosa	
	↑	↓	↑	↓	↑	↓
Induction	*Bacteroides* *Enterorhabdus* *Parasutterella*	*Butyricicoccus* *Syntrophococcus* *Marvinbryantia*	*Parasutterella*	*Coprococcus* *Subdoligranulum*	(–)	(–)
Latent	*Enterorhabdus* *Pseudobutyrivibrio* *Bacillus*	*Roseburia* *Ruminiclostridium* *Clostridium* *Alloprevotella* *Gloeobacter*	*Senegalimassilia*	*Parabacteroides*	*Blautia*	(–)
Whole	*Bacteroides* *Parasutterella* *Olsenella* *Kopriimonas* *Turicibacter*	*Dehalobacterium* *Roseburia* *Ruminococcus* *Clostridium* *Lachnoclostridium* *Alloprevotella* *Erysipelatoclostridium* *Butyricicoccus* *Marvinbryantia* *Syntrophococcus* *Ruminiclostridium* *Anaerosporobacter* *Fastidiosipila*	*Parasutterella* *Azoarcus* *Olsenella* *Bacteroides*	*Odoribacter* *Syntrophococcus* *Parabacteroides* *Turicibacter*	*Parasutterella*	*Enterorhabdus* *Azoarcus* *Alistipes*

↑, *Significant increases compared with the Control group (P < 0.05, ANOVA).*
↓, *Significant decrease compared with the Control group (P < 0.05, ANOVA).*
(–), No differences compared with the Control group.

converting CMG to free-form curcumin (Ozawa et al., 2017). We found no significant differences in the read counts of bacteria encoding β-glucuronidase between the CMG-treated and Control groups (**Supplemental Figure 12**).

4 DISCUSSION

Although fecal samples are widely used for microbiome studies as a representative of the gut microbiota throughout the GI tract (Durbán et al., 2011), the microbial compositions have been shown to be different depending on the anatomical sites (Durbán et al., 2011; Durbán et al., 2012; Dieterich et al., 2018; Lee et al., 2018). Bacterial diversities have been reported to increase gradually along the GI tract (Lee et al., 2018) and differ between the GI lumen versus mucosa (Durbán et al., 2011; Durbán et al., 2012). Consistent with these findings, in the current study, we found that bacterial compositions in EAE mice differed not only among the three anatomical sites whose diversities were higher in feces than in ileum contents, but also between ileal contents and the ileal mucosa. This is the first study that compared the microbiota from the three anatomical sites in EAE.

To determine whether CMG administration could affect the microbiota at the three anatomical sites, correlating with the EAE severity, we conducted comparative analyses using the fecal, ileal content, and ileal mucosal samples. Although the reduced bacterial alpha diversity has been associated with the disease severities in many disease conditions (Bosshard et al., 2002; Deng et al., 2019), CMG administration modulated EAE (**Figure 1**) without increased alpha diversities of the microbiota (**Figure 2**). These results were compatible with the previous findings that the reduced bacterial alpha diversity was not observed in MS and its animal models (Cosorich et al., 2017; Omura et al., 2020).

Using PCA, we investigated whether CMG administration could alter the overall microbiome patterns among the three anatomical sites. We found that PC1 values of feces and ileal contents, but not the ileal mucosa, were significantly different

TABLE 3 | Numbers of bacterial species altered in the CMG-treated groups compared with the Control group.

Samples	Feces		Ileal contents		Ileal mucosa	
	↑	↓	↑	↓	↑	↓
Induction	5[a]	7[b]	*Barnesiella* sp., *Parasutterella excrementihominis*	6[c]	*Bifidobacterium choerinum*	3[d]
Latent	*Enterorhabdus mucosicola*, *Pseudobutyrivibrio* spp.	5[e]	*Senegalimassilia anaerobia*	*Parabacteroides distasonis*, *Alistipes putredinis*	*Blautia* sp.	0
Whole	4[f]	16[g]	6[h]	8[i]	*Parasutterella excrementihominis*	8[j]

↑, *increased bacterial species;* ↓, *decreased bacterial species.*

A. Feces

[a]*Induction↑: Pseudobutyrivibrio spp., Enterorhabdus mucosicola, Parasutterella excrementihominis, Barnesiella sp., Bacteroides acidifaciens.*

[b]*Induction↓: Pseudoflavonifractor bacteroides capillosus, Butyricicoccus pullicaecorum, Lachnoclostridium clostridium hathewayi, Lachnoclostridium clostridium aldenense, Marvinbryantia bryantella formatexigens, Blautia (Ruminococcus) gnavus, Syntrophococcus sp.*

[e]*Latent↓: Alloprevotella rava, Gloeobacter spp., Blautia (Ruminococcus) gnavus, Ruminiclostridium eubacterium siraeum, Roseburia faecis.*

[f]*Whole↑: Olsenella spp., Parasutterella excrementihominis, Kopriimonas spp., Bacteroides acidifaciens.*

[g]*Whole↓: Alloprevotella rava, Dehalobacterium spp., Pseudoflavonifractor bacteroides capillosus, Butyricicoccus pullicaecorum, Anaerosporobacter mobilis, Clostridium spp., Roseburia faecis, Lachnoclostridium clostridium hathewayi, Ruminococcus sp., Eubacterium plexicaudatum, Marvinbryantia bryantella formatexigens, Fastidiosipila sanguinis, Ruminococcus bromii, Blautia (Ruminococcus) gnavus, Syntrophococcus sp., Erysipelatoclostridium clostridium innocuum.*

Induction↑ and Latent↑: Enterohabdus mucosicola, Pseudobutyrivibrio spp. (Increases in Enterorhabdus mucosicola and Pseudobutyrivibrio spp. in the Induction and Latent groups, but not in the Whole group).

Induction↓ and Whole↓: Marvinbryantia bryantella formatexigens, Syntrophococcus sp. (Marvinbryantia bryantella formatexigens and Syntrophococcus sp. decreased in the Induction and Whole groups).

Latent↓ and Whole↓: Roseburia faecis (The Latent and Whole groups had a decrease in Roseburia faecis).

Induction↓, Latent↓, and Whole↓: Blautia (Ruminococcus) gnavus [All CMG-treated groups had a decrease in Blautia (Ruminococcus) gnavus].

B. Ileal contents

[c]*Induction↓: Clostridium spp., Ruminiclostridium eubacterium siraeum, Blautia (Ruminococcus) gnavus, Blautia sp., Subdoligranulum spp., Coprococcus catus.*

[h]*Whole↑: Azoarcus spp., Pandoraea sp., Olsenella spp., Eubacterium xylanophilum, Parasutterella excrementihominis, Bacteroides acidifaciens.*

[i]*Whole↓: Turicibacter sp., Parabacteroides distasonis, Alistipes finegoldii, Alistipes putredinis, Odoribacter splanchnicus, Lachnoclostridium clostridium polysaccharolyticum, Clostridium fusiformis, Syntrophococcus sp.*

Induction↑ and Whole↑: Parasutterella excrementihominis.

Latent↓ and Whole↓: Paracteroides distansonis, Alistipes putredinis.

C. Ileal mucosa

[d]*Induction↓: Lachnoclostridium clostridium saccharolyticum, Lachnoclostridium clostridium hathewayi, Clostridium perfringens.*

[j]*Whole↓: Clostridium disporicum, Alistipes massiliensis, Azoarcus spp., Lachnoclostridium clostridium saccharolyticum, Enterorhabdus mucosicola, Burkholderia spp., Clostridium fusiformis, Clostridium perfringens.*

Induction↓ and Whole↓: Lachnoclostridium clostridium saccharolyticum, Clostridium perfringes.

between the CMG-treated versus Control groups (**Figure 3** and **Supplemental Figures 8**, **9**), suggesting that CMG administration altered the microbiota compositions in feces and ileal contents. This could be due to the distinct metabolism of free-form curcumin at the three anatomical sites. In general, following oral administration of free-form curcumin, its conjugation takes place mainly in the liver and some in the intestine; through the enterohepatic circulation, conjugated curcumin reaches the intestine with bile, where deconjugation occurs by β-glucuronidase (Ozawa et al., 2017). Since the β-glucuronidase activity contributes to converting the inactive conjugated curcumin to the active free-form of curcumin, the distribution of free-form curcumin in tissues has been highest in the intestine followed by the spleen and the liver after intraperitoneal administration of free-form curcumin in mice (Pan et al., 1999). On the other hand, in the colon cancer-bearing mouse xenograft models, mice with intraperitoneal CMG administration exhibited the high levels of free-form curcumin in the tumor tissue, comparing with serum and major organs (heart, liver, and spleen) (Ozawa-Umeta et al., 2020). In this study, free-form curcumin either in the GI tract or in the blood derived from CMG could directly affect the gut microbiota. Since CMG altered microbiome of the contents of the GI tract, i.e., feces and ileal contents, but not the ileal mucosa, free-form curcumin in the GI tract, which was likely generated by deconjugation of CMG in the GI luminal site, seemed to directly affect the microbiota present in the lumen; curcumin in the GI lumen may have no contact with mucosal bacteria.

PICRUSt analyses demonstrated that the levels of bacteria encoding β-glucuronidase were higher in fecal samples than in the ileal content/mucosa samples; this is also consistent with the findings that fecal microbiota was affected most by administration with CMG, which can be deconjugated by β-glucuronidase released in the GI lumen. Although we found no differences in bacteria encoding β-glucuronidase between ileal contents and the ileal mucosa in PICRUSt analyses, in the GI tract, free enzymes might be released higher in the lumen than in the mucosa. Thus, the conversion of CMG to free-form curcumin in the GI tract may directly affect the microbiome; the concentration of free-form curcumin may be lowest in the ileal mucosa among the three anatomical sites. Alternatively, free-form curcumin in the blood may also have no contact with mucosal bacteria since the mucus layer is present between the intestinal epithelial surface and mucosal bacteria. In theory, although free-form curcumin in the blood can affect the immune system, influencing the composition of the gut

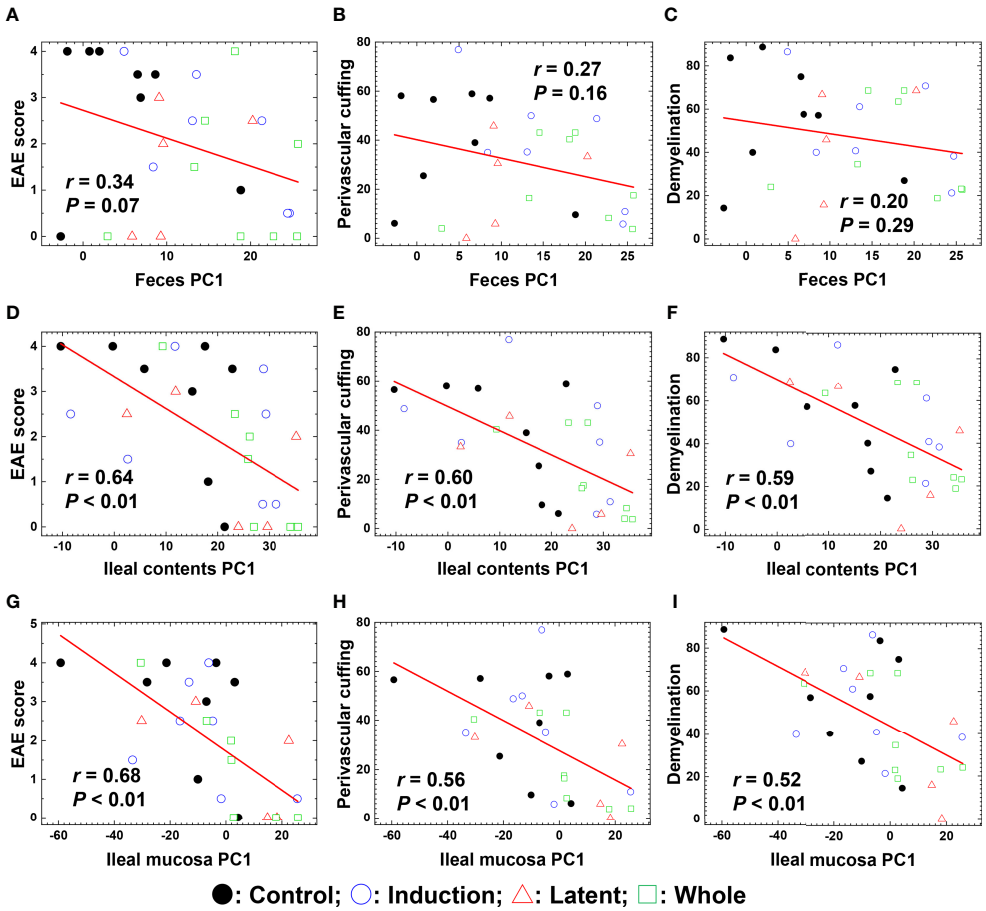

FIGURE 5 | Pattern matching of the microbial PC1 values with the clinical and pathological scores of EAE at the three anatomical sites: feces, ileal contents, and the ileal mucosa. **(A–I)** We harvested samples from the three CMG-treated (Induction, blue circle; Latent, red triangle; and Whole, green square) and control groups (Control, black circle). The microbial PC1 values of ileal contents and the ileal mucosa, but not feces, significantly correlated with the EAE scores **(A, D, G)**, perivascular cuffing (i.e., inflammation) scores **(B, E, H)**, and demyelination scores **(C, F, I)** ($P < 0.01$).

microbiota, this influence seemed to be limited since only a small number of bacterial species changed their relative abundance in the ileal mucosa (**Table 3**) without changes in overall microbiota (**Figure 3** and **Supplemental Figures 8**, **9**).

Associations between the gut microbiomes and disease activities have been reported to differ among the distinct anatomical sites as well as the content versus mucosal samples. For example, in the 2,4,6-trinitrobenzenesulfonic acid (TNBS)-induced colitis model in mice, the alterations in the colonic mucus microbiomes more closely correlated with the disease severity than those in the fecal and cecal microbiomes (Kozik et al., 2019). In the current study, using PCA, we demonstrated that CMG administration altered overall bacterial compositions in feces and ileal contents, but not in the ileal mucosa. Then, using pattern matching, we found that PC1 values of microbiome data in ileal contents and mucosa, but not in feces, correlated with the clinical and neuropathological scores in EAE. Thus, among the three anatomical sites, the altered overall microbiota in ileal contents by CMG administration could contribute to the modulation of EAE. On the other hand, dysbiosis in the ileal mucosa seemed to be associated with the EAE severity regardless of CMG administration. Our results were consistent with previously published observations that the ileal contents/mucosa microbiota direct the differentiation of Th17 cells in mice (Ivanov et al., 2008; Farkas et al., 2015). In human MS, microbiota alterations in the small intestinal mucosa have been reported to correlate with disease activity (Cosorich et al., 2017).

Previously, we demonstrated that, in a viral model for MS, Theiler's murine encephalomyelitis virus (TMEV) infection, alterations in individual bacterial genera, but not changes in the overall gut microbiome, were associated with immune-gene expressions in the CNS (Omura et al., 2020). Similarly, in the current study, although CMG administration affected the overall microbiota patterns in feces and ileal contents, but not the ileal mucosa, pattern matching demonstrated that six bacterial species (two species at each anatomical site, **Table 4**) correlated moderately or highly with the EAE scores among the significantly decreased bacterial species by CMG administration: *Ruminococcus bromii* and

TABLE 4 | Bacterial species correlated with the EAE scores*.

Correlation coefficient (*r*)	Feces		Ileal contents		Ileal mucosa	
	Bacterial species	*r*	Bacterial species	*r*	Bacterial species	*r*
***r* ≥ 0.5**	*Erysipelatoclostridium clostridium innocuum*	0.56	*Turicibacter* sp.**	0.66	*Burkholderia* spp.**	0.75
	*Ruminococcus bromii***	0.55	*Bifidobacterium choerinum*	0.62	*Burkholderia* sp.	0.72
	Porphyromonas sp.	0.54	*Alistipes finegoldii***	0.60	*Burkholderia ubonensis*	0.71
	*Blautia (Ruminococcus) gnavus***	0.52	*Allobaculum stercoricanis*	0.56	*Azoarcus* spp.**	0.54
***r* ≥ –0.5**	*Atopostipes* sp.	–0.50	*Jeotgalicoccus halotolerans*	–0.66	*Barnesiella* spp.	–0.50

*Using pattern matching, we determined correlations between EAE scores and relative abundance of individual bacterial species. $P < 0.01$ (except Barnesiella spp., whose P value was < 0.05). Spearman's rank correlation coefficient (r) = 0.50 to 0.70 (–0.50 to –0.70); moderate positive (negative) correlation and r = 0.70 to 0.90 (–0.70 to –0.90); high positive (negative) correlation (Mukaka, 2012).

**Bacterial species whose relative abundance in the CMG-treated groups was significantly different compared with the Control group by ANOVA, $P < 0.05$.

TABLE 5 | Numbers of pathways changed in the CMG-treated groups by PICRUSt.

Groups		Induction	Latent	Whole
Feces	Increased	5[a, b]	0	36[a, b, d]
	Decreased	0	0	2
Ileal contents	Increased	0	59[a, c]	26[a, c, d]
	Decreased	2	0	4
Ileal mucosa	Increased	0	0	0
	Decreased	0	0	23

Significantly changed pathways compared with the Control group ($P < 0.05$).

[a]*Pathway commonly increased in feces of the Induction and Whole groups, and ileal contents of the Latent and Whole groups (n = 1).*

1. Cell division.

[b]*Pathways commonly increased in feces of the Induction and Whole groups (n = 5).*

1. Cell division; 2. Glycosphingolipid biosynthesis - ganglio series; 3. 1,1,1-Trichloro-2,2-bis(4-chlorophenyl) ethane (DDT) degradation; 4. Toluene degradation; and 5. Glycan biosynthesis and metabolism.

[c]*Pathways commonly increased in ileal contents of the Latent and Whole groups (n = 10).*

1. Cell division; 2. Peroxisome; 3. Primary immunodeficiency; 4. Infectious diseases, pertussis; 5. Oxidative phosphorylation; 6. Biotin metabolism; 7. Folate biosynthesis; 8. Ubiquinone and other terpenoid-quinone biosynthesis; 9. β-Alanine metabolism; and 10. Membrane and intracellular structural molecules.

[d]*Pathways commonly increased in feces and ileal contents of the Whole group (n = 15).*

1. Cell division; 2. Peroxisome; 3. Infectious diseases, pertussis; 4. Citrate cycle (TCA cycle); 5. Oxidative phosphorylation; 6. Lipopolysaccharide biosynthesis; 7. Lipopolysaccharide biosynthesis proteins; 8. Biotin metabolism; 9. Ubiquinone and other terpenoid-quinone biosynthesis; 10. β-Alanine metabolism; 11. 1,1,1-Trichloro-2,2-bis(4-chlorophenyl) ethane (DDT) degradation; 12. Toluene degradation; 13. Adipocytokine signaling pathway; 14. Membrane and intracellular structural molecules; and 15. Glycan biosynthesis and metabolism.

Blautia (Ruminococcus) gnavus in feces, *Turicibacter* sp. and *Alistipes finegoldii* in ileal contents, and *Burkholderia* spp. and *Azoarcus* spp. in the ileal mucosa. Thus, the decreases in individual bacterial species by CMG administration might contribute to suppression of EAE (Shen et al., 2017; Zhang et al., 2017; Peterson et al., 2018; Gandy et al., 2019; Kozik et al., 2019).

Among the six species, *Ruminococcus bromii* belongs to the phylum *Firmicutes*, family *Ruminococcaceae*, and produces short-chain fatty acids (SCFAs) (Park et al., 2019; Yao et al., 2020). SCFAs have been reported to contribute to the pathogenesis of EAE by inducing pro-inflammatory responses, including Th17 cells, depending on the SCFA receptors (Park et al., 2019). On the other hand, SCFAs have also been reported to be protective in EAE by enhancing anti-inflammatory responses, including Tregs (Park et al., 2019; Yao et al., 2020). *Blautia (Ruminococcus) gnavus* belongs to the phylum *Firmicutes*, family *Lachnospiraceae*, and genus *Blautia* (Hansen et al., 2013). The genus *Blautia* has been reported to increase in feces of patients with relapsing-remitting MS (Chen et al., 2016). Furthermore, increased abundance of *Blautia (Ruminococcus) gnavus* positively correlated with disease activity in patients with IBD and systemic lupus erythematosus (Breban et al., 2017; Azzouz et al., 2019).

Turicibacter sp. belongs to the phylum *Firmicutes*, family *Erysipelotrichaceae*, and has been reported as a pro-inflammatory taxon (Bosshard et al., 2002; Ma et al., 2018). For example, Miyauchi et al. demonstrated that a newly isolated bacterium OTU0002 *Erysipelotrichaceae* exacerbated EAE with enhanced MOG_{35-55}-specific Th17 responses by increasing serum amyloid A and IL-23 production (Miyauchi et al., 2020). *Turicibacter sangunis* was isolated from patients with acute appendicitis (Bosshard et al., 2002). *Alistipes finegoldii* belongs to the phylum *Bacteroidetes*, family *Rikenellaceae*, and has been reported to be a potential SCFA producer (Dziarski et al., 2016; Parker et al., 2020). *Alistipes* could play a pro-inflammatory role in cardiovascular disease, although the role of *Alistipes* in IBD is controversial (Parker et al., 2020). *Burkholderia* spp. belongs to the phylum *Proteobacteria*, family *Burkholderiaceae*, and some of the species caused a severe pulmonary disease (Urban et al., 2004; Wiersinga et al., 2008). Experimentally, *Burkholderia* induced inflammation in the lungs due to the production of proinflammatory cytokines in mice (Wiersinga et al., 2008). *Azoarcus* sp. belongs to the phylum *Proteobacteria*, family *Zoogloeaceae*, and has only been reported in antibiotics-induced diarrhea in experimental mice which was associated with dysbiosis in the intestine. Here, antibiotics

TABLE 6 | Predicted pathways up-or down-regulated (> 2-fold) in CMG-treated group.

Pathways	Fold change	Site	Group
1,1,1-Trichloro-2,2-bis(4-chlorophenyl)ethane (DDT) degradation	3.6	Feces	Induction
	4.3	Feces	Whole
	2.4	Ileal content	Whole
Cardiac muscle contraction	3.3	Feces	Whole
Parkinson's disease	3.3	Feces	Whole
Influenza A	3.3	Feces	Whole
p53 signaling pathway	3.3	Feces	Whole
Colorectal cancer	3.3	Feces	Whole
Small cell lung cancer	3.3	Feces	Whole
Toxoplasmosis	3.3	Feces	Whole
Viral myocarditis	3.3	Feces	Whole
G protein-coupled receptors	2.5	Feces	Whole
	0.5	Ileal content	Whole
Photosynthesis - antenna proteins	0.5	Feces	Whole
Calcium signaling pathway	0.5	Feces	Whole
Germination	0.5	Ileal content	Whole
Arachidonic acid metabolism	0.5	Ileal mucosa	Whole
Bacterial chemotaxis	0.4	Ileal mucosa	Whole
Flagellar assembly	0.4	Ileal mucosa	Whole

Pathways listed by a program of Phylogenetic Investigation of Communities by Reconstruction of Unobserved States (PICRUSt) were based on KEGG database (https://www.genome.jp/kegg/).

treatment altered the gut microbiota including the abundance of *Azoarcus* (Long et al., 2017).

In this study, we used PICRUSt analyses to predict whether CMG administration affected multiple bacterial pathways depending on the CMG administration schedule and the anatomical sites. Although we found that changes in the several pathways were common between the CMG-treated groups and between the anatomical sites, we could not find changes that were common in all CMG-treated groups or the three anatomical sites (**Table 5** and **Supplemental Table 4**). Since biological changes in the gut bacteria by polyphenol have been reported to affect the immune system potentially (Kawabata et al., 2018), we examined the biological pathway changes in the CMG-treated groups. Although we did not find bacterial pathways that have been demonstrated to affect the host's systemic immune responses, including the production of SCFAs (Takewaki and Yamamura, 2021), we found several pathways potentially related to immune responses, including "viral myocarditis" and "arachidonic acid metabolism" in the list of upregulated pathways more than 2-fold in the three CMG-treated groups (**Table 6**). We also found that two bacterial pathways related to immune responses ("primary immunodeficiency" and "infectious diseases, pertussis") were commonly increased in the Latent and Whole groups whose EAE scores were less severe than controls. Although PICRUSt predicted neither substantial pathways altered commonly in all CMG-treated groups, nor pathways directly associated with the EAE pathophysiology, more accurate metagenome sequencing analyses may lead to a discovery of metabolome changes by CMG administration.

In EAE using IL-10 transgenic mice and recombinant IL-10 administration, the beneficial effects of IL-10 have been reported, such as inhibition of encephalitogenic T cell responses (Bettelli et al., 1998; Cua et al., 1999); lack of IL-10 exacerbated EAE with larger amounts of pro-inflammatory cytokines, including IFN-γ (Bettelli et al., 1998). IL-10 has been shown to have anti-inflammatory effects in EAE; there have been several reports that curcumin regulated EAE by increasing the levels of IL-10. For example, Mohajeri et al. demonstrated both prophylactic and therapeutic effects of curcumin in an EAE model using Lewis rats with increased IL-10 gene expression (Mohajeri et al., 2015). Kanakasabai et al. reported that curcumin-treated C57BL/6 mice exhibited less severe MOG_{35-55}-induced EAE scores and higher levels of IL-10 expression compared with the control mice (Kanakasabai et al., 2012). Similarly, IL-4 has been demonstrated to play a regulatory role in EAE (Fernando et al., 2014). In this study, we demonstrated the beneficial effects of curcumin in MOG_{35-55}-EAE, where CMG-treated mice, particularly those in the Latent and Whole groups, exhibited lower clinical and neuropathological scores; the Latent and Whole groups had slightly higher levels of anti-inflammatory IL-4 and IL-10 productions (**Supplemental Figure 2**). Thus, the enhanced IL-4 and IL-10 productions by CMG administration may contribute to the modulation of EAE, only to some extent. The poor association between anti-inflammatory IL-4 and IL-10 levels and the severities of EAE by CMG administration could be due to the enhancement of increased levels of pro-inflammatory IFN-γ and IL-17 in these two CMG-treated groups. Here, it should be noted that IFN-γ has been shown to be beneficial in some EAE models by regulating IL-17 production (Martinez et al., 2014); the enhanced IFN-γ production in the Latent and Whole groups might play a protective role in this EAE model.

Immunologically, curcumin has also been known to regulate the proliferation of lymphocytes. When Kanakasabai et al. cultured splenic cells from MOG_{35-55}-EAE mice *in vitro* in the presence of curcumin, the lymphoproliferative responses to the MOG_{35-55} peptide were decreased in a dose-dependent manner (Kanakasabai et al., 2012). On the other hand, splenic cells from EAE mice injected with intraperitoneal curcumin had similar levels of MOG_{35-55}-specific lymphoproliferation to those from the control EAE mice. Consistent with the Kanakasabai's

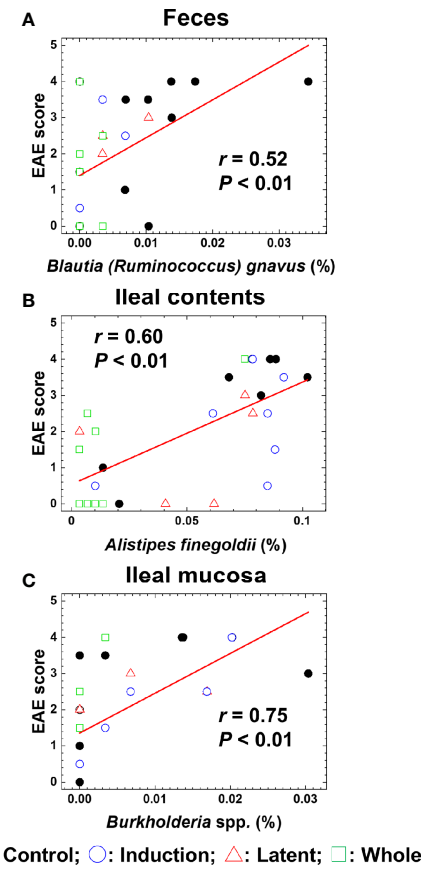

FIGURE 6 | Pattern matching between the EAE scores and relative abundance of bacterial species. **(A–C)** We conducted pattern matching to correlate the EAE scores with the relative abundance of individual bacterial species in feces **(A)**, ileal contents **(B)**, and the ileal mucosa **(C)**. The figures are the representative bacterial species correlated with the EAE scores at the three anatomical sites. These bacterial species significantly decreased in the CMG-treated groups (Induction, blue circle; Latent, red triangle; and Whole, green square), compared with the control group (Control, black circle) (**Table 3**): **(A)** *Blautia (Ruminococcus) gnavus* in feces (Induction, Latent, and Whole < Control), **(B)** *Alistipes finegoldii* in ileal contents (Whole < Control), and **(C)** *Burkholderia* spp. in the ileal mucosa (Whole < Control).

findings, when we tested whether curcumin could directly inhibit the MOG_{35-55}-specific lymphoproliferation using lymphocytes from the spleen or lymph nodes from 2D2 T cell receptor $(TCR)^{MOG}$ transgenic mice in the presence of curcumin, lymphoproliferation was suppressed by curcumin in a dose-dependent manner (**Supplemental Figures 13C, D**) (Tsunoda et al., 2009). Similarly, curcumin directly inhibited the proliferation of a T cell line more efficiently than that of neuronal cells *in vitro* (**Supplemental Figures 13A, B**). On the other hand, we found no differences in the MOG_{35-55}-specific lymphoproliferation among the CMG-treated and Control groups when we used lymphocytes isolated from EAE mice (**Supplemental Figure 3**). These findings suggest that curcumin potentially has direct suppressive effects on lymphocytes; curcumin could directly affect the MOG_{35-55}-specific T cell proliferation *in vivo*, resulting in the modulation of the MOG_{35-55}-EAE model. This may also explain that the efficacy of CMG administration differed depending on the administration schedule; mice receiving CMG throughout the course (Whole group) had the lowest cumulative scores of MOG_{35-55}-induced EAE among the CMG-treated groups. Suppression of CNS inflammation by curcumin has been reported in EAE (Natarajan and Bright, 2002; Xie et al., 2009; Mohajeri et al., 2015); we also demonstrated decreased inflammation and demyelination in the spinal cord of chronic monophasic EAE by CMG administration.

The limitation of the current study is the modest effects of CMG in MOG-induced EAE using C57BL/6 mice. Thus, we investigated whether CMG could modulate another EAE model, by sensitizing a different mouse strain, SJL/J mice, with the $PLP_{139-151}$ peptide. Since PLP-sensitized mice develop relapsing-remitting EAE, this model allowed us to test whether CMG could exert the similar beneficial effects on the different disease courses in the different mouse strains. Unexpectedly, however, we did not find the amelioration of CMG-treated mice with PLP-induced EAE clinically or neuropathologically (**Supplemental Table 5** and **Supplemental Figures 14A, B**). To clarify the discrepancy between MOG-induced EAE and PLP-induced EAE, we examined whether a lack of the treatment effect could be due to a lack of suppression of PLP-specific T cell proliferation by curcumin using lymphocytes isolated from PLP-induced EAE mice. Intriguingly, we found that the PLP-specific lymphoproliferation was suppressed by curcumin in a dose-dependent manner (**Supplemental Figures 14C, D**). Here, although the precise mechanism for the different effects of CMG on the two EAE models is unclear, this was consistent with the previous reports that the efficacy of curcumin was different among the EAE types and animal species (Verbeek et al., 2005; Mohajeri et al., 2015). The different efficacy of CMG in these animal models could be due to several factors including: variation in the microbiota among different mouse strains, i.e., C57BL/6 mice versus SJL/J mice (Verbeek et al., 2005; Mohajeri et al., 2015), whose major bacterial phyla of the gut microbiota are *Verrucomicrobia* and *Tenericutes* phyla, respectively (Gandy et al., 2019). This may also be due to the distinct disease courses and pathomechanisms between the two EAE models. MOG-induced EAE mice develop a monophasic disease course; PLP-induced EAE mice exhibit a relapsing-remitting disease course. Myelin-specific $CD4^+$ T cells, but not $CD8^+$ T cells or antibodies, have been shown to mediate both MOG_{35-55}-induced and $PLP_{139-151}$-induced EAE (Tsunoda et al., 1998; Fernando et al., 2014; Martinez et al., 2014). In the MOG-induced EAE model, autoreactive T cell responses to the sensitized antigen MOG contribute to the pathomechanism. On the other hand, although the first attack in the PLP-induced EAE model is also caused by encephalitogenic T cells against the sensitized antigen PLP, the generation of encephalitogenic T cells that react to different myelin antigens has been proposed as the pathomechanism of relapses (known as "epitope spreading") (McRae et al., 1995).

In the future, CMG treatment is worth testing in MS models, using two different administration schedules. First, we treated mice in the Induction group on days 0–4 to see whether CMG

could affect the priming of MOG-specific T cells. Since there were no differences in MOG-specific lymphoproliferation, CMG treatment seemed not to alter the priming by directly affecting lymphocytes and antigen-presenting cells. Although this induction treatment schedule has often been regarded as a prophylactic treatment in most EAE studies, earlier CMG administration, a few weeks before EAE induction, will give more insight into the beneficial effect of CMG as an alternative prophylactic treatment. Here, if CMG is administered a few weeks before EAE induction, it can change the compositions of gut microbiota, altering the molecules/cells of both humoral and cellular immune effectors, including IgA antibody, Th17 cells, and Tregs. Thus, the early CMG prophylactic treatment might affect MOG-specific immune responses, suppressing EAE more efficiently. Second, we discontinued CMG treatment during the late chronic stage of PLP-induced EAE (**Supplemental Figure 14**); since the second and third relapsing/remissions of PLP-EAE occur randomly in each mouse and do not synchronize among mice, PLP-EAE is often inappropriate to assess the efficacy of drugs. However, CMG can be administered at the late chronic stage of other MS models, such as the TMEV model, in which similar disease progression occurs among most experimental mice.

In conclusion, we found that CMG administration was safe and modulated an autoimmune model of MS by altering the microbiomes in the feces and ileal contents, but not in the ileal mucosa. The microbiome of ileal contents as well as several individual bacterial species in the three anatomical sites correlated with the EAE severities, suggesting that CMG might suppress EAE through alteration of the microbiota. This report would provide insight into how CMG potentially affects the gut microbiota depending on the anatomical sites, which associates with the EAE pathophysiology.

DATA AVAILABILITY STATEMENT

The original contributions presented in the study are publicly available in NCBI using accession number PRJNA688384.

ETHICS STATEMENT

The animal study was reviewed and approved by The Institutional Animal Care and Use Committee of Kindai University Faculty of Medicine.

AUTHOR CONTRIBUTIONS

IT, HK, and KN conceived and supervised the project. IT and HK designed the experiments. SK, SO, and FS conducted the experiments and data analyses. SK, SO, FS, HK, and IT wrote the manuscript. All authors contributed to the article and approved the submitted version.

FUNDING

This work was supported by the Grant-in-Aid for Scientific Research on Innovative Areas "Frontier Research on Chemical Communications" [17H06400 (HK and IT), 17H06401 (HK), and 17H06404 (IT)], Grant-in-Aid for Scientific Research (C) KAKENHI from the Japan Society for the Promotion of Science [JP19K08569 (SO), JP20K07433 (FS), and JP20K07455 (IT)], and Novartis Pharma Research Grants (SO and IT).

ACKNOWLEDGMENTS

We are grateful to Therabiopharma, Inc. (Kanagawa, Japan) for a gift of CMG. We express our acknowledgments to all members of the Department of Microbiology, Kindai University Faculty of Medicine, Dr. Ah-Mee Park, Ph.D., Dr. Mitsugu Fujita, M.D., Ph.D., Mr. Aoshi Katsuki, B.S., Ms. Yumina Nakamura, B.S., and Ms. Namie Sakiyama. We also thank Dr. Kota Moriguchi, M.D., Ph.D., and Dr. Yuta Fukumoto, M.D., Ph.D., the Department of Neurology, Kindai University Faculty of Medicine, Osaka, Japan, and Dr. Felicia Lindeberg, M.D., the Faculty of Medicine and Health Sciences, Linköping University, Linköping, Sweden, for excellent technical assistance, and Dr. Nicholas E. Martinez, Ph.D., M.B.A., Associate Director at UCB, GA, USA, for proofreading the manuscript. This work is supported by the Ministry of Education, Culture, Sports, Science and Technology, Japan, through the Monbukagakusho (MEXT) Scholarship (SK).

SUPPLEMENTARY MATERIAL

The Supplementary Material for this article can be found online at: https://www.frontiersin.org/articles/10.3389/fcimb.2021.772962/full#supplementary-material

REFERENCES

Anand, P., Kunnumakkara, A. B., Newman, R. A., and Aggarwal, B. B. (2007). Bioavailability of Curcumin: Problems and Promises. *Mol. Pharm.* 4, 807–818. doi: 10.1021/mp700113r

Asai, A., and Miyazawa, T. (2000). Occurrence of Orally Administered Curcuminoid as Glucuronide and Glucuronide/Sulfate Conjugates in Rat Plasma. *Life Sci.* 67, 2785–2793. doi: 10.1016/s0024-3205(00)00868-7

Azzouz, D., Omarbekova, A., Heguy, A., Schwudke, D., Gisch, N., Rovin, B. H., et al. (2019). Lupus Nephritis Is Linked to Disease-Activity Associated Expansions and Immunity to a Gut Commensal. *Ann. Rheum. Dis.* 78, 947–956. doi: 10.1136/annrheumdis-2018-214856

Bettelli, E., Das, M. P., Howard, E. D., Weiner, H. L., Sobel, R. A., and Kuchroo, V. K. (1998). IL-10 Is Critical in the Regulation of Autoimmune Encephalomyelitis as Demonstrated by Studies of IL-10- and IL-4-Deficient and Transgenic Mice. *J. Immunol.* 161, 3299–3306.

Bolyen, E., Rideout, J. R., Dillon, M. R., Bokulich, N. A., Abnet, C. C., Al-Ghalith, G. A., et al. (2019). Reproducible, Interactive, Scalable and Extensible Microbiome Data Science Using QIIME 2. *Nat. Biotechnol.* 37, 852–857. doi: 10.1038/s41587-019-0209-9

Bosshard, P. P., Zbinden, R., and Altwegg, M. (2002). Turicibacter Sanguinis Gen. Nov., Sp. Nov., A Novel Anaerobic, Gram-Positive Bacterium. *Int. J. Syst. Evol. Microbiol.* 52, 1263–1266. doi: 10.1099/00207713-52-4-1263

Braniste, V., Al-Asmakh, M., Kowal, C., Anuar, F., Abbaspour, A., Tóth, M., et al. (2014). The Gut Microbiota Influences Blood-Brain Barrier Permeability in Mice. *Sci. Transl. Med.* 6, 263ra158. doi: 10.1126/scitranslmed.3009759

Breban, M., Tap, J., Leboime, A., Said-Nahal, R., Langella, P., Chiocchia, G., et al. (2017). Faecal Microbiota Study Reveals Specific Dysbiosis in Spondyloarthritis. *Ann. Rheum. Dis.* 76, 1614–1622. doi: 10.1136/annrheumdis-2016-211064

Caporaso, J. G., Lauber, C. L., Walters, W. A., Berg-Lyons, D., Lozupone, C. A., Turnbaugh, P. J., et al. (2011). Global Patterns of 16S rRNA Diversity at a Depth of Millions of Sequences Per Sample. *Proc. Natl. Acad. Sci. U.S.A.* 108 (Suppl 1), 4516–4522. doi: 10.1073/pnas.1000080107

Chaitanya, G. V., Omura, S., Sato, F., Martinez, N. E., Minagar, A., Ramanathan, M., et al. (2013). Inflammation Induces Neuro-Lymphatic Protein Expression in Multiple Sclerosis Brain Neurovasculature. *J. Neuroinflamm.* 10, 125. doi: 10.1186/1742-2094-10-125

Chaudhry, A., Samstein, R. M., Treuting, P., Liang, Y., Pils, M. C., Heinrich, J.-M., et al. (2011). Interleukin-10 Signaling in Regulatory T Cells Is Required for Suppression of Th17 Cell-Mediated Inflammation. *Immunity* 34, 566–578. doi: 10.1016/j.immuni.2011.03.018

Chearwae, W., and Bright, J. J. (2008). 15-Deoxy-Delta(12,14)-Prostaglandin J(2) and Curcumin Modulate the Expression of Toll-Like Receptors 4 and 9 in Autoimmune T Lymphocyte. *J. Clin. Immunol.* 28, 558–570. doi: 10.1007/s10875-008-9202-7

Chen, J., Chia, N., Kalari, K. R., Yao, J. Z., Novotna, M., Paz Soldan, M. M., et al. (2016). Multiple Sclerosis Patients Have a Distinct Gut Microbiota Compared to Healthy Controls. *Sci. Rep.* 6, 28484. doi: 10.1038/srep28484

Cosorich, I., Dalla-Costa, G., Sorini, C., Ferrarese, R., Messina, M. J., Dolpady, J., et al. (2017). High Frequency of Intestinal T_H17 Cells Correlates With Microbiota Alterations and Disease Activity in Multiple Sclerosis. *Sci. Adv.* 3, e1700492. doi: 10.1126/sciadv.1700492

Cua, D. J., Groux, H., Hinton, D. R., Stohlman, S. A., and Coffman, R. L. (1999). Transgenic Interleukin 10 Prevents Induction of Experimental Autoimmune Encephalomyelitis. *J. Exp. Med.* 189, 1005–1010. doi: 10.1084/jem.189.6.1005

Deng, F., Li, Y., and Zhao, J. (2019). The Gut Microbiome of Healthy Long-Living People. *Aging (Albany N.Y.)* 11, 289–290. doi: 10.18632/aging.101771

De Velasco, M. A., Lu, Y., Kura, Y., China, T., Inoue, Y., Nakayama, A., et al. (2020). Chemopreventive Effects of Nanoparticle Curcumin in a Mouse Model of *Pten*-Deficient Prostate Cancer. *Hum. Cell* 33, 730–736. doi: 10.1007/s13577-020-00337-7

Dieterich, W., Schink, M., and Zopf, Y. (2018). Microbiota in the Gastrointestinal Tract. *Med. Sci. (Basel)* 6, 116. doi: 10.3390/medsci6040116

Di Meo, F., Margarucci, S., Galderisi, U., Crispi, S., and Peluso, G. (2019). Curcumin, Gut Microbiota, and Neuroprotection. *Nutrients* 11, 2426. doi: 10.3390/nu11102426

Durbán, A., Abellán, J. J., Jiménez-Hernández, N., Ponce, M., Ponce, J., Sala, T., et al. (2011). Assessing Gut Microbial Diversity From Feces and Rectal Mucosa. *Microb. Ecol.* 61, 123–133. doi: 10.1007/s00248-010-9738-y

Durbán, A., Abellán, J. J., Jiménez-Hernández, N., Salgado, P., Ponce, M., Ponce, J., et al. (2012). Structural Alterations of Faecal and Mucosa-Associated Bacterial Communities in Irritable Bowel Syndrome. *Environ. Microbiol. Rep.* 4, 242–247. doi: 10.1111/j.1758-2229.2012.00327.x

Dziarski, R., Park, S. Y., Kashyap, D. R., Dowd, S. E., and Gupta, D. (2016). Pglyrp-Regulated Gut Microflora Prevotella Falsenii, Parabacteroides Distasonis and Bacteroides Eggerthii Enhance and Alistipes Finegoldii Attenuates Colitis in Mice. *PloS One* 11, e0146162. doi: 10.1371/journal.pone.0146162

Farkas, A. M., Panea, C., Goto, Y., Nakato, G., Galan-Diez, M., Narushima, S., et al. (2015). Induction of Th17 Cells by Segmented Filamentous Bacteria in the Murine Intestine. *J. Immunol. Methods* 421, 104–111. doi: 10.1016/j.jim.2015.03.020

Fernando, V., Omura, S., Sato, F., Kawai, E., Martinez, N. E., Elliott, S. F., et al. (2014). Regulation of an Autoimmune Model for Multiple Sclerosis in Th2-Biased GATA3 Transgenic Mice. *Int. J. Mol. Sci.* 15, 1700–1718. doi: 10.3390/ijms15021700

Gandy, K. A. O., Zhang, J., Nagarkatti, P., and Nagarkatti, M. (2019). The Role of Gut Microbiota in Shaping the Relapse-Remitting and Chronic-Progressive Forms of Multiple Sclerosis in Mouse Models. *Sci. Rep.* 9, 6923. doi: 10.1038/s41598-019-43356-7

Gong, D., Gong, X., Wang, L., Yu, X., and Dong, Q. (2016). Involvement of Reduced Microbial Diversity in Inflammatory Bowel Disease. *Gastroenterol. Res. Pract.* 2016, 6951091. doi: 10.1155/2016/6951091

Hansen, S. G. K., Skov, M. N., and Justesen, U. S. (2013). Two Cases of Ruminococcus Gnavus Bacteremia Associated With Diverticulitis. *J. Clin. Microbiol.* 51, 1334–1336. doi: 10.1128/JCM.03382-12

Ivanov, I. I., Frutos R de, L., Manel, N., Yoshinaga, K., Rifkin, D. B., Sartor, R. B., et al. (2008). Specific Microbiota Direct the Differentiation of IL-17-Producing T-Helper Cells in the Mucosa of the Small Intestine. *Cell Host Microbe* 4, 337–349. doi: 10.1016/j.chom.2008.09.009

Jangi, S., Gandhi, R., Cox, L. M., Li, N., von Glehn, F., Yan, R., et al. (2016). Alterations of the Human Gut Microbiome in Multiple Sclerosis. *Nat. Commun.* 7, 12015. doi: 10.1038/ncomms12015

Kanakasabai, S., Casalini, E., Walline, C. C., Mo, C., Chearwae, W., and Bright, J. J. (2012). Differential Regulation of CD4(+) T Helper Cell Responses by Curcumin in Experimental Autoimmune Encephalomyelitis. *J. Nutr. Biochem.* 23, 1498–1507. doi: 10.1016/j.jnutbio.2011.10.002

Kawabata, K., Baba, N., Sakano, T., Hamano, Y., Taira, S., Tamura, S., et al. (2018). Functional Properties of Anti-Inflammatory Substances From Quercetin-Treated Bifidobacterium Adolescentis. *Biosci. Biotechnol. Biochem.* 82, 689–697. doi: 10.1080/09168451.2017.1401916

Kozik, A. J., Nakatsu, C. H., Chun, H., and Jones-Hall, Y. L. (2019). Comparison of the Fecal, Cecal, and Mucus Microbiome in Male and Female Mice After TNBS-Induced Colitis. *PloS One* 14, e0225079. doi: 10.1371/journal.pone.0225079

Langille, M. G. I., Zaneveld, J., Caporaso, J. G., McDonald, D., Knights, D., Reyes, J. A., et al. (2013). Predictive Functional Profiling of Microbial Communities Using 16S rRNA Marker Gene Sequences. *Nat. Biotechnol.* 31, 814–821. doi: 10.1038/nbt.2676

Lazar, V., Ditu, L.-M., Pircalabioru, G. G., Gheorghe, I., Curutiu, C., Holban, A. M., et al. (2018). Aspects of Gut Microbiota and Immune System Interactions in Infectious Diseases, Immunopathology, and Cancer. *Front. Immunol.* 9, 1830. doi: 10.3389/fimmu.2018.01830

Lee, S. M., Kim, N., Park, J. H., Nam, R. H., Yoon, K., and Lee, D. H. (2018). Comparative Analysis of Ileal and Cecal Microbiota in Aged Rats. *J. Cancer Prev.* 23, 70–76. doi: 10.15430/JCP.2018.23.2.70

Lin, X., Bai, D., Wei, Z., Zhang, Y., Huang, Y., Deng, H., et al. (2019). Curcumin Attenuates Oxidative Stress in RAW264.7 Cells by Increasing the Activity of Antioxidant Enzymes and Activating the Nrf2-Keap1 Pathway. *PloS One* 14, e0216711. doi: 10.1371/journal.pone.0216711

Li, G., Yang, M., Zhou, K., Zhang, L., Tian, L., Lv, S., et al. (2015). Diversity of Duodenal and Rectal Microbiota in Biopsy Tissues and Luminal Contents in Healthy Volunteers. *J. Microbiol. Biotechnol.* 25, 1136–1145. doi: 10.4014/jmb.1412.12047

Long, C.-X., He, L., Guo, Y.-F., Liu, Y.-W., Xiao, N.-Q., and Tan, Z.-J. (2017). Diversity of Bacterial Lactase Genes in Intestinal Contents of Mice With Antibiotics-Induced Diarrhea. *World J. Gastroenterol.* 23, 7584–7593. doi: 10.3748/wjg.v23.i42.7584

Manichanh, C., Rigottier-Gois, L., Bonnaud, E., Gloux, K., Pelletier, E., Frangeul, L., et al. (2006). Reduced Diversity of Faecal Microbiota in Crohn's Disease Revealed by a Metagenomic Approach. *Gut* 55, 205–211. doi: 10.1136/gut.2005.073817

Martinez, N. E., Karlsson, F., Sato, F., Kawai, E., Omura, S., Minagar, A., et al. (2014). Protective and Detrimental Roles for Regulatory T Cells in a Viral Model for Multiple Sclerosis. *Brain Pathol.* 24, 436–451. doi: 10.1111/bpa.12119

Martinez, N. E., Sato, F., Omura, S., Kawai, E., Takahashi, S., Yoh, K., et al. (2014). RORγt, But Not T-bet, Overexpression Exacerbates an Autoimmune Model for Multiple Sclerosis. *J. Neuroimmunol.* 276, 142–149. doi: 10.1016/j.jneuroim.2014.09.006

Ma, D., Wang, A. C., Parikh, I., Green, S. J., Hoffman, J. D., Chlipala, G., et al. (2018). Ketogenic Diet Enhances Neurovascular Function With Altered Gut Microbiome in Young Healthy Mice. *Sci. Rep.* 8, 6670. doi: 10.1038/s41598-018-25190-5

McRae, B. L., Vanderlugt, C. L., Dal Canto, M. C., and Miller, S. D. (1995). Functional Evidence for Epitope Spreading in the Relapsing Pathology of Experimental Autoimmune Encephalomyelitis. *J. Exp. Med.* 182, 75–85. doi: 10.1084/jem.182.1.75

Miyake, S., Kim, S., Suda, W., Oshima, K., Nakamura, M., Matsuoka, T., et al. (2015). Dysbiosis in the Gut Microbiota of Patients With Multiple Sclerosis, With a Striking Depletion of Species Belonging to Clostridia XIVa and IV Clusters. *PloS One* 10, e0137429. doi: 10.1371/journal.pone.0137429

Miyauchi, E., Kim, S.-W., Suda, W., Kawasumi, M., Onawa, S., Taguchi-Atarashi, N., et al. (2020). Gut Microorganisms Act Together to Exacerbate Inflammation in Spinal Cords. *Nature* 585, 102–106. doi: 10.1038/s41586-020-2634-9

Mohajeri, M., Sadeghizadeh, M., Najafi, F., and Javan, M. (2015). Polymerized Nano-Curcumin Attenuates Neurological Symptoms in EAE Model of Multiple Sclerosis Through Down Regulation of Inflammatory and Oxidative Processes and Enhancing Neuroprotection and Myelin Repair. *Neuropharmacology* 99, 156–167. doi: 10.1016/j.neuropharm.2015.07.013

Mukaka, M. M. (2012). Statistics Corner: A Guide to Appropriate Use of Correlation Coefficient in Medical Research. *Malawi Med. J.* 24, 69–71.

Natarajan, C., and Bright, J. J. (2002). Curcumin Inhibits Experimental Allergic Encephalomyelitis by Blocking IL-12 Signaling Through Janus Kinase-STAT Pathway in T Lymphocytes. *J. Immunol.* 168, 6506–6513. doi: 10.4049/jimmunol.168.12.6506

National Research Council (US) Committee for the Update of the Guide for the Care and Use of Laboratory Animals (2011) *Guide for the Care and Use of Laboratory Animals* (Washington (DC: National Academies Press (US). Available at: http://www.ncbi.nlm.nih.gov/books/NBK54050/ (Accessed December 1, 2020).

Omura, S., Sato, F., Martinez, N. E., Park, A.-M., Fujita, M., Kennett, N. J., et al. (2019). Bioinformatics Analyses Determined the Distinct CNS and Peripheral Surrogate Biomarker Candidates Between Two Mouse Models for Progressive Multiple Sclerosis. *Front. Immunol.* 10, 516. doi: 10.3389/fimmu.2019.00516

Omura, S., Sato, F., Park, A.-M., Fujita, M., Khadka, S., Nakamura, Y., et al. (2020). Bioinformatics Analysis of Gut Microbiota and CNS Transcriptome in Virus-Induced Acute Myelitis and Chronic Inflammatory Demyelination; Potential Association of Distinct Bacteria With CNS IgA Upregulation. *Front. Immunol.* 11, 1138. doi: 10.3389/fimmu.2020.01138

Ozawa, H., Imaizumi, A., Sumi, Y., Hashimoto, T., Kanai, M., Makino, Y., et al. (2017). Curcumin β-D-Glucuronide Plays an Important Role to Keep High Levels of Free-Form Curcumin in the Blood. *Biol. Pharm. Bull.* 40, 1515–1524. doi: 10.1248/bpb.b17-00339

Ozawa-Umeta, H., Kishimoto, A., Imaizumi, A., Hashimoto, T., Asakura, T., Kakeya, H., et al. (2020). Curcumin β-D-Glucuronide Exhibits Anti–Tumor Effects on Oxaliplatin-Resistant Colon Cancer With Less Toxicity *In Vivo*. *Cancer Sci.* 111, 1785–1793. doi: 10.1111/cas.14383

Pan, M. H., Huang, T. M., and Lin, J. K. (1999). Biotransformation of Curcumin Through Reduction and Glucuronidation in Mice. *Drug Metab. Dispos.* 27, 486–494.

Parker, B. J., Wearsch, P. A., Veloo, A. C. M., and Rodriguez-Palacios, A. (2020). The Genus *Alistipes*: Gut Bacteria With Emerging Implications to Inflammation, Cancer, and Mental Health. *Front. Immunol.* 11, 906. doi: 10.3389/fimmu.2020.00906

Park, A.-M., Omura, S., Fujita, M., Sato, F., and Tsunoda, I. (2017). *Helicobacter Pylori* and Gut Microbiota in Multiple Sclerosis versus Alzheimer's Disease: 10 Pitfalls of Microbiome Studies. *Clin. Exp. Neuroimmunol.* 8, 215–232. doi: 10.1111/cen3.12401

Park, J., Wang, Q., Wu, Q., Mao-Draayer, Y., and Kim, C. H. (2019). Bidirectional Regulatory Potentials of Short-Chain Fatty Acids and Their G-Protein-Coupled Receptors in Autoimmune Neuroinflammation. *Sci. Rep.* 9, 8837. doi: 10.1038/s41598-019-45311-y

Peterson, C. T., Vaughn, A. R., Sharma, V., Chopra, D., Mills, P. J., Peterson, S. N., et al. (2018). Effects of Turmeric and Curcumin Dietary Supplementation on Human Gut Microbiota: A Double-Blind, Randomized, Placebo-Controlled Pilot Study. *J. Evid. Based Integr. Med.* 23, 1–8. doi: 10.1177/2515690X18790725

Sato, F., Kawai, E., Martinez, N. E., Omura, S., Park, A.-M., Takahashi, S., et al. (2017). T-bet, But Not Gata3, Overexpression Is Detrimental in a Neurotropic Viral Infection. *Sci. Rep.* 7, 10496. doi: 10.1038/s41598-017-10980-0

Sato, F., Omura, S., Martinez, N. E., and Tsunoda, I. (2018). "Chapter 3: Animal Models of Multiple Sclerosis," in *Neuroinflammation*. Ed. A. Minagar (Burlington, MA: Elsevier), 37–72.

Shen, L., Liu, L., and Ji, H.-F. (2017). Regulative Effects of Curcumin Spice Administration on Gut Microbiota and Its Pharmacological Implications. *Food Nutr. Res.* 61, 1361780. doi: 10.1080/16546628.2017.1361780

Takewaki, D., and Yamamura, T. (2021). Gut Microbiome Research in Multiple Sclerosis. *Neurosci. Res.* 168, 28–31. doi: 10.1016/j.neures.2021.05.001

Tong, M., Jacobs, J. P., McHardy, I. H., and Braun, J. (2014). Sampling of Intestinal Microbiota and Targeted Amplification of Bacterial 16S rRNA Genes for Microbial Ecologic Analysis. *Curr. Protoc. Immunol.* 107, 7.41.1–7.41.11. doi: 10.1002/0471142735.im0741s107

Tsunoda, I. (2017). Lymphatic System and Gut Microbiota Affect Immunopathology of Neuroinflammatory Diseases, Including Multiple Sclerosis, Neuromyelitis Optica and Alzheimer's Disease. *Clin. Exp. Neuroimmunol.* 8, 177–179. doi: 10.1111/cen3.12405

Tsunoda, I., Kobayashi-Warren, M., Libbey, J. E., and Fujinami, R. S. (2009). "Central Nervous System Degeneration Caused by Autoimmune Cytotoxic $CD8^+$ T Cell Clones and Hybridomas," in *Encyclopedia of Neuroscience*. Eds. M. D. Binder, N. Hirokawa and U. Windhorst (Berlin, Heidelberg: Springer), 619–625. doi: 10.1007/978-3-540-29678-2_894

Tsunoda, I., Kuang, L.-Q., Tolley, N. D., Whitton, J. L., and Fujinami, R. S. (1998). Enhancement of Experimental Allergic Encephalomyelitis (EAE) by DNA Immunization With Myelin Proteolipid Protein (PLP) Plasmid DNA. *J. Neuropathol. Exp. Neurol.* 57, 758–767. doi: 10.1097/00005072-199808000-00005

Tsunoda, I., Libbey, J. E., Kuang, L.-Q., Terry, E. J., and Fujinami, R. S. (2005). Massive Apoptosis in Lymphoid Organs in Animal Models for Primary and Secondary Progressive Multiple Sclerosis. *Am. J. Pathol.* 167, 1631–1646. doi: 10.1016/S0002-9440(10)61247-3

Tsunoda, I., Tanaka, T., Terry, E. J., and Fujinami, R. S. (2007). Contrasting Roles for Axonal Degeneration in an Autoimmune Versus Viral Model of Multiple Sclerosis: When can Axonal Injury be Beneficial? *Am. J. Pathol.* 170, 214–226. doi: 10.2353/ajpath.2007.060683

Urban, T. A., Griffith, A., Torok, A. M., Smolkin, M. E., Burns, J. L., and Goldberg, J. B. (2004). Contribution of *Burkholderia Cenocepacia* Flagella to Infectivity and Inflammation. *Infect. Immun.* 72, 5126–5134. doi: 10.1128/IAI.72.9.5126-5134.2004

Verbeek, R., van Tol, E. A. F., and van Noort, J. M. (2005). Oral Flavonoids Delay Recovery From Experimental Autoimmune Encephalomyelitis in SJL Mice. *Biochem. Pharmacol.* 70, 220–228. doi: 10.1016/j.bcp.2005.04.041

Wiersinga, W. J., de Vos, A. F., de Beer, R., Wieland, C. W., Roelofs, J. J. T. H., Woods, D. E., et al. (2008). Inflammation Patterns Induced by Different Burkholderia Species in Mice. *Cell Microbiol.* 10, 81–87. doi: 10.1111/j.1462-5822.2007.01016.x

Wu, M., Li, P., Li, J., An, Y., Wang, M., and Zhong, G. (2020). The Differences Between Luminal Microbiota and Mucosal Microbiota in Mice. *J. Microbiol. Biotechnol.* 30, 287–295. doi: 10.4014/jmb.1908.08037

Xie, L., Li, X.-K., Funeshima-Fuji, N., Kimura, H., Matsumoto, Y., Isaka, Y., et al. (2009). Amelioration of Experimental Autoimmune Encephalomyelitis by Curcumin Treatment Through Inhibition of IL-17 Production. *Int. Immunopharmacol.* 9, 575–581. doi: 10.1016/j.intimp.2009.01.025

Yao, Y., Yan, L., Chen, H., Wu, N., Wang, W., and Wang, D. (2020). *Cyclocarya Paliurus* Polysaccharides Alleviate Type 2 Diabetic Symptoms by Modulating Gut Microbiota and Short-Chain Fatty Acids. *Phytomedicine* 77, 153268. doi: 10.1016/j.phymed.2020.153268

Zam, W. (2018). Gut Microbiota as a Prospective Therapeutic Target for Curcumin: A Review of Mutual Influence. *J. Nutr. Metab.* 2018, 1367984. doi: 10.1155/2018/1367984

Zhang, Z., Chen, Y., Xiang, L., Wang, Z., Xiao, G. G., and Hu, J. (2017). Effect of Curcumin on the Diversity of Gut Microbiota in Ovariectomized Rats. *Nutrients* 9, 1146. doi: 10.3390/nu9101146

Conflict of Interest: HK owns equity and is a scientific consultant for Therabiopharma.

The remaining authors declare that the research was conducted in the absence of any commercial or financial relationships that could be construed as a potential conflict of interest.

This study received funding from Novartis Pharma. The funder was not involved in the study design, collection, analysis, interpretation of data, the writing of this article or the decision to submit it for publication.

Publisher's Note: All claims expressed in this article are solely those of the authors and do not necessarily represent those of their affiliated organizations, or those of the publisher, the editors and the reviewers. Any product that may be evaluated in this article, or claim that may be made by its manufacturer, is not guaranteed or endorsed by the publisher.

frontiers in Cellular and Infection Microbiology

CORRECTION
published: 01 March 2022
doi: 10.3389/fcimb.2022.855411

Corrigendum: Curcumin β-D-Glucuronide Modulates an Autoimmune Model of Multiple Sclerosis with Altered Gut Microbiota in the Ileum and Feces

Sundar Khadka[1†], Seiichi Omura[1†], Fumitaka Sato[1†], Kazuto Nishio[2], Hideaki Kakeya[3] and Ikuo Tsunoda[1]*

[1] Department of Microbiology, Kindai University Faculty of Medicine, Osaka, Japan, [2] Department of Genome Biology, Kindai University Faculty of Medicine, Osaka, Japan, [3] Graduate School of Pharmaceutical Sciences, Kyoto University, Kyoto, Japan

OPEN ACCESS

Approved by:
Frontiers Editorial Office, Frontiers Media SA, Switzerland

***Correspondence:**
Ikuo Tsunoda
itsunoda@med.kindai.ac.jp

[†]These authors have contributed equally to this work

Specialty section:
This article was submitted to Microbes and Innate Immunity, a section of the journal Frontiers in Cellular and Infection Microbiology

Received: *15 January 2022*
Accepted: *01 February 2022*
Published: *01 March 2022*

Citation:
Khadka S, Omura S, Sato F, Nishio K, Kakeya H and Tsunoda I (2022) Corrigendum: Curcumin β-D-Glucuronide Modulates an Autoimmune Model of Multiple Sclerosis with Altered Gut Microbiota in the Ileum and Feces. Front. Cell. Infect. Microbiol. 12:855411. doi: 10.3389/fcimb.2022.855411

Keywords: bioinformatics, animal model, pattern matching, PICRUSt analysis, bacterial taxonomy, Alpha diversity, confidence interval, histology

A Corrigendum on:

Curcumin β-D-Glucuronide Modulates an Autoimmune Model of Multiple Sclerosis with Altered Gut Microbiota in the Ileum and Feces

By Khadka S, Omura S, Sato F, Nishio K, Kakeya H and Tsunoda I (2021). Front. Cell. Infect. Microbiol. 11:772962. doi: 10.3389/fcimb.2021.772962

Error in Figure/Table

In the published article, there was a mistake in the PDF article as published. **Figure 5** with its legend is missing from the PDF article, although the HTML article has included **Figure 5**. The missing **Figure 5** with its legend appears below.

The authors apologize for this error and state that this does not change the scientific conclusions of the article in any way.

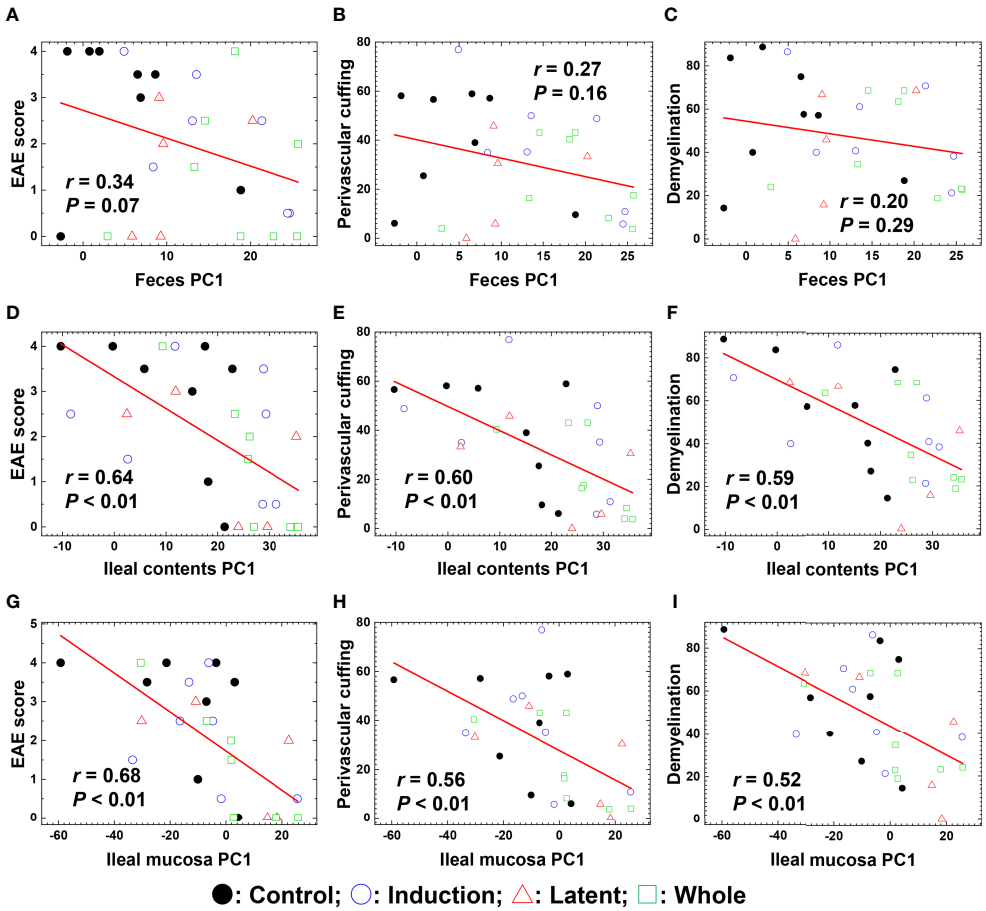

FIGURE 5 | Pattern matching of the microbial PC1 values with the clinical and pathological scores of EAE at the three anatomical sites: feces, ileal contents, and the ileal mucosa. **(A–I)** We harvested samples from the three CMG-treated (Induction, blue circle; Latent, red triangle; and Whole, green square) and control groups (Control, black circle). The microbial PC1 values of ileal contents and the ileal mucosa, but not feces, significantly correlated with the EAE scores **(A, D, G)**, perivascular cuffing (i.e., inflammation) scores **(B, E, H)**, and demyelination scores **(C, F, I)** ($P < 0.01$).

frontiers in Cellular and Infection Microbiology

ORIGINAL RESEARCH
published: 25 January 2022
doi: 10.3389/fcimb.2021.763507

The Gut Microbiome and Metabolites Are Altered and Interrelated in Patients With Rheumatoid Arthritis

Die Yu[1], Juping Du[1], Xia Pu[1], Liyuan Zheng[1], Shuaishuai Chen[1], Na Wang[1], Jun Li[1], Shiyong Chen[1], Shaobiao Pan[2] and Bo Shen[1]**

[1] Department of Clinical Laboratory, Taizhou Hospital of Zhejiang Province Affiliated to Wenzhou Medical University, Taizhou, China, [2] Department of Rheumatology and Immunology, Taizhou Hospital of Zhejiang Province Affiliated to Wenzhou Medical University, Taizhou, China

The relationship among the gut microbiome, global fecal metabolites and rheumatoid arthritis (RA) has not been systematically evaluated. In this study, we performed 16S rDNA sequencing and liquid chromatography-tandem mass spectrometry (LC-MS/MS)-based nontargeted metabolomic profiling on feces of 26 untreated RA patients and 26 healthy controls. Twenty-six genera and forty-one MS2-identified metabolites were significantly altered in the RA patients. *Klebsiella*, *Escherichia*, *Eisenbergiella* and *Flavobacterium* were more abundant in the RA patients, while *Fusicatenibacter*, *Megamonas* and *Enterococcus* were more abundant in the healthy controls. Function prediction analysis demonstrated that the biosynthesis pathways of amino acids, such as L-arginine and aromatic amino acids, were depleted in the RA group. In the metabolome results, fecal metabolites including glycerophospholipids (PC(18:3(9Z,12Z,15Z)/16:1(9Z)), lysoPE 19:1, lysoPE 18:0, lysoPC(18:0/0:0)), sphingolipids (Cer(d18:0/16:0), Cer(d18:0/12:0), Cer(d18:0/14:0)), kynurenic acid, xanthurenic acid and 3-hydroxyanthranilic acid were remarkably altered between the RA patients and healthy controls. Dysregulation of pathways, such as tryptophan metabolism, alpha-linolenic acid metabolism and glycerophospholipid metabolism, may contribute to the development of RA. Additionally, we revealed that the gut microbiome and metabolites were interrelated in the RA patients, while *Escherichia* was the core genus. By depicting the overall landscape of the intestinal microbiome and metabolome in RA patients, our study could provide possible novel research directions regarding RA pathogenesis and targeted therapy.

Keywords: rheumatoid arthritis, autoimmune disease, gut microbiome, metabolome, biomarker, inflammation

OPEN ACCESS

Edited by:
Elias Adel Rahal,
American University of Beirut, Lebanon

Reviewed by:
Matthew Irick Jackson,
Hill's Pet Nutrition, Inc., United States
Margret Shirinian,
American University of Beirut, Lebanon

****Correspondence:***
Shaobiao Pan
pansb@enzemed.com
Bo Shen
shenb@enzemed.com

Specialty section:
This article was submitted to Microbiome in Health and Disease, a section of the journal Frontiers in Cellular and Infection Microbiology

Received: *24 August 2021*
Accepted: *28 December 2021*
Published: *25 January 2022*

Citation:
Yu D, Du J, Pu X, Zheng L, Chen S, Wang N, Li J, Chen S, Pan S and Shen B (2022) The Gut Microbiome and Metabolites Are Altered and Interrelated in Patients With Rheumatoid Arthritis. Front. Cell. Infect. Microbiol. 11:763507. doi: 10.3389/fcimb.2021.763507

INTRODUCTION

Rheumatoid arthritis (RA) is a chronic, complex and systemic autoimmune disease. It is characterized by autoantibody production, synovitis, and long-standing inflammation (Scott et al., 2010). Its pathogenetic mechanism remains obscure. The gut microbiome influences the health of the host, especially with regard to gut immune homeostasis. Mounting evidence has suggested that dysbiosis of the intestinal microbiome is a vital environmental element that triggers

the onset of RA, and dysregulation of the microbiome may result in abnormal immune responses (Kau et al., 2011; Taneja, 2014). It has been reported that mucosal microbes correlate with RA in animal models (van den Broek et al., 1992). In recent years, an increasing number of studies have tried to gain insight into gut microbiome interactions in RA patients. For instance, *Prevotella copri* was enriched and exhibited genomic rearrangement in new-onset untreated RA patients, and one of its 27-kDa proteins could stimulate the Th1 response in 42% of RA patients (Scher et al., 2013; Pianta et al., 2017). Some probiotics, such as *Lactobacillus casei*, significantly attenuate the expression of interferon gamma (IFN-γ), tumor necrosis factor alpha (TNF-α) and interleukin (IL)-1β to prevent joint damage (Pan et al., 2019). On the other hand, evidence indicates that microbial metabolites are crucial intermediate factors connected with the intestinal microbiome and the host. Intestinal microbes ferment food to produce numerous metabolites. Gut metabolites may pass through the mucosal barrier into the circulation to calibrate our immune system. A deficiency of beneficial bacteria and their metabolites may stimulate the inflammatory response (Velasquez-Manoff, 2015).

Combined studies of the gut microbiome and metabolome suggested promising prospects for the development of biomarkers. Unraveling the interactions between the gut microbiome and metabolome could provide new insights to discover novel targets for the treatment of various inflammatory diseases (Yang et al., 2019; Yang and Cong, 2021). Some studies of the interplay between the human gut microbiome and metabolism in RA patients have been conducted. For example, stool butyrate levels were reduced in RA patients compared to healthy controls, and supplementation with butyrate suppressed arthritis severity in an antigen-induced arthritis mouse model (Rosser et al., 2020). However, these studies mainly focused on short-chain fatty acids (SCFAs), with few studies focusing on the full spectrum of fecal metabolites. The association between the intestinal microbiome and metabolites has not been comprehensively evaluated in RA patients to date. Therefore, we performed both 16S rDNA sequencing and liquid chromatography-tandem mass spectrometry (LC-MS/MS)-based nontargeted metabolomic profiling on fecal samples of RA patients to identify potential biomarkers and microbiota-metabolite interactions to provide novel research directions for the pathogenesis of RA.

MATERIALS AND METHODS

Recruitment of Subjects and Collection of Fecal Samples

Twenty-six RA patients were recruited from Taizhou Hospital of Zhejiang Province from July to December 2020. All patients were newly diagnosed with RA based on the RA criteria of the American College of Rheumatology. These patients did not take any disease-modifying antirheumatic drugs, biological agents or steroid drugs three months before the diagnosis. Laboratory parameters and general clinical information were obtained from our diagnosis records. In addition, 26 sex- and age-matched healthy controls (HCs) were enrolled from the medical examination center, and these HCs did not have a history of RA or abnormal inflammatory biomarkers. All patients and HCs were excluded if they (i) received any antibiotic or probiotic therapy within three months before recruitment; (ii) suffered from malignant tumors, diabetes, inflammatory bowel disease (IBD) or other autoimmune diseases; or (iii) were on an extreme diet. Furthermore, an additional 11 RA patients and 11 healthy subjects were included as the validation cohort according to the same criteria from September to October, 2021. Informed consent was obtained from all participants. The study complied with all relevant national regulations and institutional policies and was approved by the Institutional Review Board of the Ethics Committee, Taizhou Hospital of Zhejiang Province. Fecal samples were collected using sterile stool containers. Each sample was split into two tubes and stored at -80°C until subsequent processing.

DNA Extraction and 16S rDNA Sequencing

The omics analysis was supported by LC-Bio Technology Co., Ltd, Hangzhou, Zhejiang Province, China. E.Z.N.A. ®Stool DNA Kit (D4015, Omega, Inc., USA) was applied to extract DNA. Then, the V3-V4 region of the 16S rRNA gene was amplified with primers 341F (5'-CCTACGGGNGGCWGCAG-3') and 805R (5'-GACTACHVGGGTATCTAATCC-3') (Logue et al., 2016). AMPure XT beads (Beckman Coulter Genomics, Danvers, MA, USA) and Qubit (Invitrogen, USA) were used for the purification and quantification of the polymerase chain reaction (PCR) products respectively. Finally, the Illumina NovaSeq platform was used for DNA sequencing.

Analysis of 16S rDNA Gene Sequences

Fast length adjustment of short reads (FLASH) was applied to assign and merge paired-end reads. High-quality clean tags were obtained by FQTrim (V0.94). Operational taxonomic unit (OTU) data were then obtained based on the DADA2 algorithm (Callahan et al., 2016). SILVA and NT-16S databases were used for sequence annotation. Alpha diversity and beta diversity calculations were accomplished by QIIME2 and R (v ;3.6.1). Principal coordinate analysis (PCoA) was based on unweighted UniFrac distance, and the p-value of analysis of similarities (ANOSIM) was obtained by permutation test. Then, we conducted the Wilcoxon test and linear discriminant analysis (LDA) effect size (LEfSe) analysis to determine differential taxa. The validation cohort data were used to validate the biomarkers in LEfSe analysis. Phylogenetic investigation of communities by reconstruction of unobserved states 2 (PICRUST2) was applied to predict the function of the metagenome. Other graphs were produced using R (v 3.6.1).

Metabolite Extraction and LC-MS/MS Analysis

Briefly, 120 μL precooled 50% methanol buffer was added to each 50 mg fecal sample. Then the mixture was vortexed for 1 minute

at room temperature and centrifuged at 4,000 g for 10 minutes (4 °C). The top 200 μL of each supernatant was transferred to 96-well plates. The quality control samples were composed of 10 μL diluent from each sample.

An ultra-performance liquid chromatography system (SCIEX, UK) was applied to achieve chromatographic separations. Reversed-phase separation was performed on an ACQUITY UPLC T3 column (100 mm*2.1 mm, 1.8 μm, Waters, UK). The temperature was set at 35°C, and the flow rate was 0.4 mL/min. The mobile phase was composed of solvent A (water, 0.1% formic acid) and solvent B (acetonitrile, 0.1% formic acid). Gradient elution parameters were set as follows: 0~0.5 min, 5% B; 0.5~7 min, 5% to 100% B; 7~8 min, 100% B; 8~8.1 min, 100% to 5% B; 8.1~10 min, 5% B.

Metabolites were detected by high-resolution tandem mass spectrometer Triple-TOF5600plus (SCIEX, UK) in both negative and positive ion models. The ion source gas 1 was 60 PSI, the ion source gas 2 was 60 PSI, the curtain gas was 30 PSI. The source temperature was 650°C. The ion spray voltage floating of the positive and negative models were set as 5000 V and -4500 V, respectively. The time of flight (TOF) mass ranged from 60 to 1200 Da and was acquired in 150 ms. The 12 most abundant signals were chosen for the MS/MS scan, which exceeded a threshold of 100 counts/s. The total cycle took 0.56 s. Dynamic exclusion was 4 s. We conducted accuracy calibrations every twenty samples and quality control detections every ten samples.

Proteowizard MSConver was applied to transform the raw data files into mzXML format. Then, mzXML files were imported into XCMS software for peak picking and retention time correction. The Human Metabolome Database (HMDB) and online Kyoto Encyclopedia of Genes and Genomes (KEGG) were used to annotate the metabolites. The mass tolerance was set as 10 ppm. The MS/MS fragment data were validated by using an in-house metabolite fragment spectrum library. Metabolite quantification was then performed using metaX. Features were removed if observed in less than 50% of quality control samples or less than 20% of biological samples. The probabilistic quotient normalization (PQN) algorithm was applied for data normalization.

Metabolomic Data Analysis

Multivariate analysis, Student's *t*-test, and fold change (FC) values were used to identify differential features. The heatmap was generated by R (v 3.6.1) with the "ComplexHeatmap" package, and a volcano plot was produced with GraphPad Prism (v 8.0.1). KEGG pathway enrichment analysis was performed on differentially abundant metabolites by using R (v 3.6.1). The co-occurrence network graph was then generated with the igraph package of R (v 3.6.1). Values of $p < 0.05$ were considered significant, and the Benjamini-Hochberg (BH) method was used to obtain false discovery rate (FDR)-adjusted p-values (Q-values).

RESULTS

Characteristics of the Study Participants

The demographic and clinical data of the RA and HC groups are described in **Table 1**. The sex ($p > 0.05$) and age ($p > 0.05$) of the two groups were matched. Body mass index (BMI) values were provided by 19 RA patients and 25 HCs. Based on the available data, no significant difference was found between the two groups ($p > 0.05$). Detailed clinical information of each enrolled subject are shown in **Supplementary Table 1**.

Species Diversity of the Gut Microbiome

In microbiome sequencing, an average of 64,426 reads were obtained from each sample after quality filtering, and no significant difference was found between the RA patients (63,296 ± 6,711) and HCs (65,555 ± 6,340). In total, 5,804 OTUs were obtained by the DADA2 algorithm. A rarefaction curve based on the Observed species specified that the sequencing data were sufficient to detect all species in the samples (**Figure 1A**).

In our results, no significant differences in the Observed species, Shannon, Pielou's Evenness and Simpson index were noted (**Figure 1B**) between the RA and HC groups. To further analyze the microbial composition, beta diversity was evaluated using PCoA and ANOSIM. Although the separation shown in the unweighted three-dimensional PCoA diagram was not

TABLE 1 | Main demographic, clinical, and laboratory data of RA patients and healthy controls.

Characteristic	RA (n = 26)	Healthy controls (n = 26)	P-value
Female n (%)	16 (61.5)	16 (61.5)	0.999
Age, mean (median) years	53.3 (52.0)	52.9 (53.5)	0.917
BMI, mean (median)[a] kg/m^2	21.8 (21.1)	23.5 (23.9)	0.055
Disease course, mean (median) months	8.6 (2.0)	–	
TJC, mean (median)	5.9 (3.5)	–	
SJC, mean (median)	5.3 (2.5)	–	
DAS28-ESR, mean (median)	4.49 (4.16)	–	
RF positive n (%)	17 (65.4)	–	
RF titer, mean (median) IU/ml	93.9 (48.6)	–	
Anti-CCP positive n (%)	16 (61.5)	–	
ESR, mean (median) mm/h	37.8 (37.0)	–	
CRP, mean (median) mg/L	26.8 (14.2)	–	

[a]*19 RA patients and 25 healthy controls provided this data.*

RA, rheumatoid arthritis; BMI, body mass index; TJC, tender joint count; SJC, swollen joint count; DAS28-ESR, disease activity score with 28 joint using erythrocyte sedimentation rate; RF, rheumatoid factor; Anti-CCP, anti-cyclic citrullinated peptide; ESR, erythrocyte sedimentation rate; CRP, C-reactive protein.

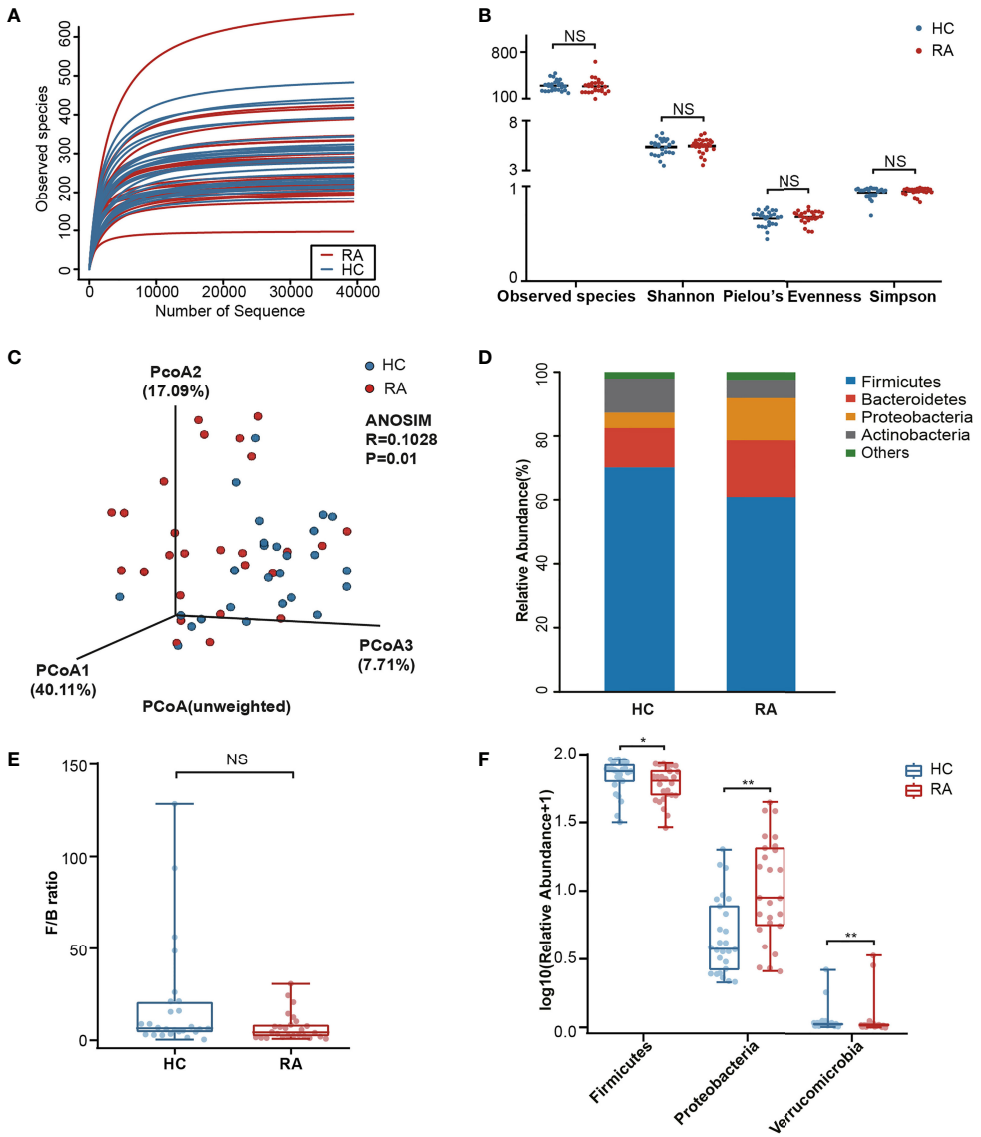

FIGURE 1 | Comparison analysis of species diversity and relative abundance at the phylum level. **(A)** The curve of each sample was nearly smooth, indicating that the sequencing data was sufficient. **(B)** Alpha diversity was measured by the Observed species, Shannon, Pielou's Evenness and Simpson index. NS, not significant. **(C)** Beta diversity was measured by principal coordinate analysis (PCoA) and analysis of similarities (ANOSIM). **(D)** The distribution plot of relative abundance at the phylum level. **(E)** The comparison of F/B ratio between the RA patients and healthy controls. NS, not significant. **(F)** The Wilcoxon test showed that three phyla were significantly altered in RA patients. P-value, *p < 0.05; **p < 0.01.

apparent, ANOSIM revealed differences between RA patients and HCs (R = 0.1028, p < 0.05, **Figure 1C**).

Alterations in Microbial Composition Associated With RA

The differences in the microbial composition between the two groups were evaluated at different taxonomic levels. Among the dominant phyla, Bacteroidetes and Proteobacteria were enriched in the RA patients, while Firmicutes and Actinobacteria were enriched in the HCs (**Figure 1D**). The Firmicutes/Bacteroidetes (F/B) ratio in the RA group was downregulated with no significant difference noted (p = 0.055, **Figure 1E**). The Wilcoxon test was next used to identify the significantly altered taxa. In total, 3 phyla were identified, including Firmicutes (p = 0.044), Proteobacteria (p = 0.001) and Verrucomicrobia (p = 0.006, **Figure 1F**). Among them, Verrucomicrobia was enriched in the RA group. In addition, of the 359 genera, 26 genera (p < 0.05) markedly differed in abundance between the two groups. After p-value adjustment, *Klebsiella* (Q = 0.018), *Enterococcus* (Q = 0.018) and *Eisenbergiella* (Q = 0.036) remained significant (**Supplementary Table 2**). There were 5 genera with significant differences in abundance among the top 30 richest genera.

Specifically, *Escherichia* (p = 0.034) and *Klebsiella* (p < 0.001) were enriched in the RA group, while *Clostridiales_unclassified* (p = 0.034), *Megamonas* (p = 0.028) and *Fusicatenibacter* (p = 0.006) were enriched in the HC group (**Supplementary Figure 1**).

To further determine the specific predominant bacteria associated with RA, LEfSe was used to compare the microbial composition between the two groups. Ultimately, 36 taxa (LDA > 3, p < 0.05) were identified as significantly discriminative. Among them, *Klebsiella*, *Escherichia*, *Flavobacterium* and *Proteobacteria_unclassified* were the main taxa enriched in the RA patients, while *Fusicatenibacter*, *Megamonas*, *Clostridiales_unclassified* and *Coriobacteriaceae* were more abundant in the HCs (**Figures 2A, B**).

The Potential Value of the Gut Microbiota in RA Risk Assessment

To investigate the potential of the gut microbiome in distinguishing the RA patients from the HCs, AUC values of the genera in LEfSe analysis (LDA > 3, p < 0.05) were calculated, and *Klebsiella* and *Fusicatenibacter* were ranked high (**Supplementary Table 3**). Furthermore, according to the validation cohort data (**Supplementary Table 4**), *Fusicatenibacter* was selected as a biomarker, with AUC values of 0.7212 and 0.8595 in the test cohort (**Figure 2C**) and validation cohort (**Figure 2D**), respectively.

Based on Spearman's correlation analysis, a heatmap was generated to show the relationship between the differentially

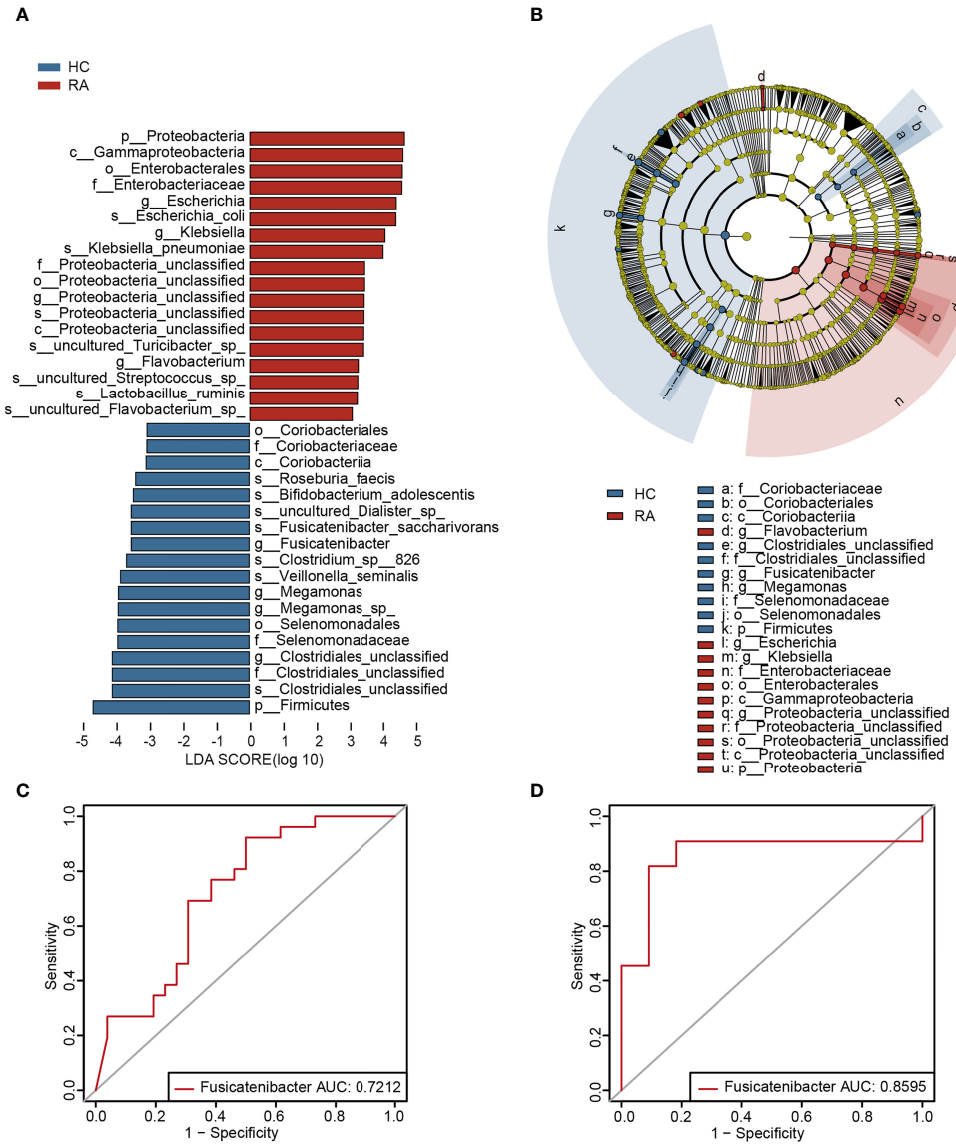

FIGURE 2 | The specific altered taxa were identified by linear discriminant analysis (LDA) effect size (LEfSe) analysis. **(A)** The histogram of taxa with LDA scores more than 3 and p-value less than 0.05. **(B)** The phylogenetic tree in cladogram of the specific differential taxa. **(C)** ROC curve of *Fusicatenibacter* in test cohort. **(D)** ROC curve of *Fusicatenibacter* in validation cohort.

abundant genera and clinical parameters. The main correlations ($r > 0.4$, $p < 0.05$) were further displayed in a co-occurrence network graph (**Figure 3A**). We noticed that BMI, a potential experimental confounder, had minimal effects on most of the genera except *Clostridiales_unclassified* ($r = 0.56$, $p < 0.001$). The rheumatoid factor (RF) level was positively correlated with 3 RA-enriched genera (*Klebsiella*, *Lactobacillus* and *Enterobacter*). In addition, the C-reactive protein (CRP) level was negatively correlated with *Enterobacter* and positively correlated with *Staphylococcus*.

Microbial Function Prediction Analysis

Compared with microbial composition, microbial function seems to be more analogous in homologous environments (Gibbons, 2017). Hence, PICRUSt2 was used to infer the gene function of the microbiota. According to KEGG pathway

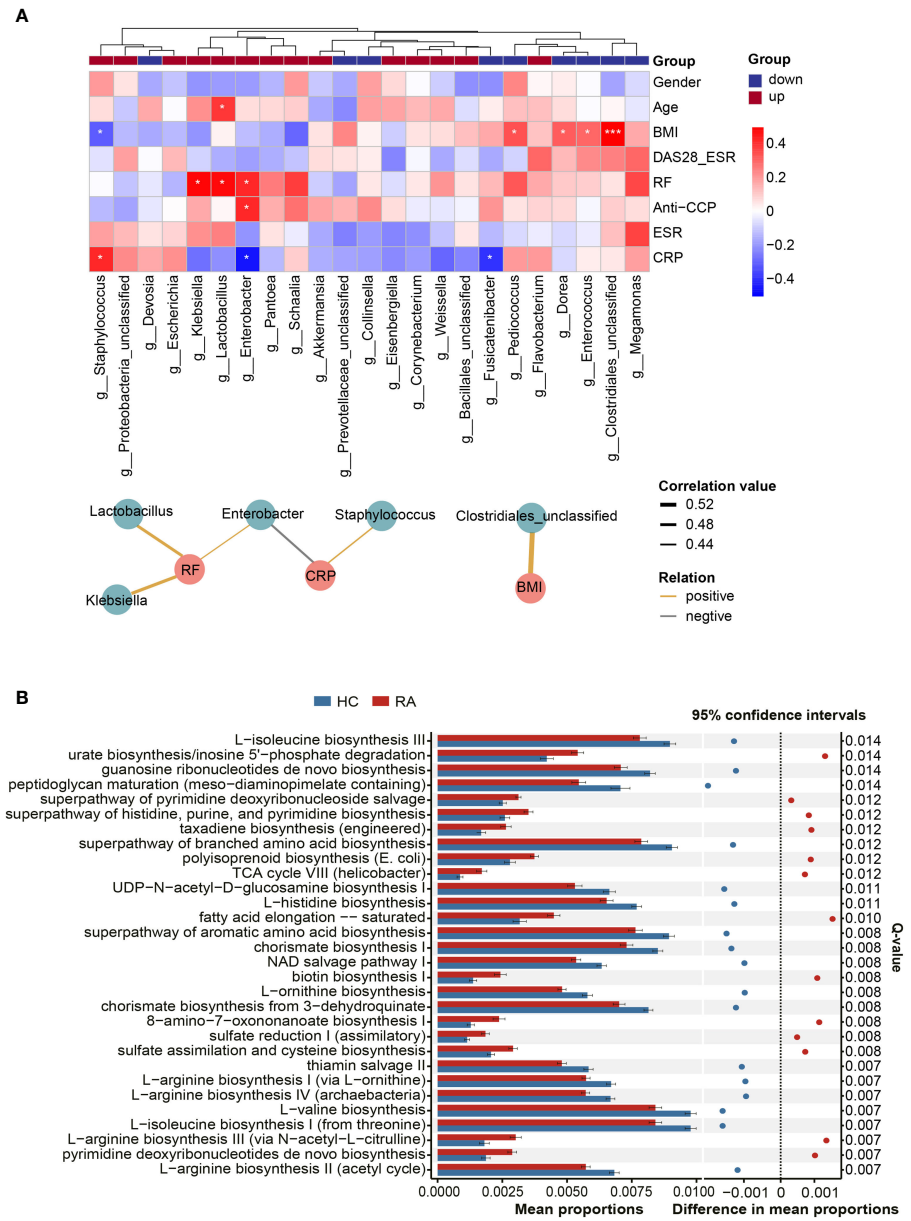

FIGURE 3 | Correlations between microbes and clinical indicators and function prediction analysis. **(A)** The heatmap revealed correlations between differentially abundant genera and clinical indicators, and partial correlations (Spearman's correlation analysis, $r > 0.4$, $p < 0.05$) were shown in co-occurrence networks. *Asaccharobacter*, *Aeromonas* and *Gelria* were excluded because they were only identified in the healthy controls. Genera were divided into two groups based on their alterations in the RA group. P-value, *$p < 0.05$; ***$p < 0.001$. **(B)** The top 30 KEGG pathways with the most significant difference in function prediction.

enrichment analysis, 171 pathways were significantly altered between the RA patients and HCs (Q < 0.05, **Supplementary Table 5**). The top 30 pathways with the most significant differences are illustrated in **Figure 3B**. The results revealed that specific amino acid biosynthesis pathways were depleted in the RA group, and these amino acids included L-arginine, ornithine, aromatic amino acids, and branched amino acids. In addition, pathways such as thiamin salvage II and peptidoglycan maturation were also depleted in the RA group, while some other pathways, such as urate biosynthesis and fatty acid elongation-saturation, were enriched.

General Overview of the Fecal Metabolome

Given that the gut microbiome could affect the immune response by producing metabolites (Krautkramer et al., 2021), LC-MS/MS-based nontargeted metabolomic profiling was performed on fecal samples of all participants. Ultimately, 1,338 features were validated through the MS2 fragment spectrum, of which 1,198 features were quantified. KEGG pathway enrichment analysis was performed, resulting in 35 significantly enriched pathways (FDR< 0.05, **Supplementary Figure 2**, **Supplementary Table 6**).

Differentially Abundant Metabolites Between the RA and HC Groups

Differentially abundant metabolites were identified based on multivariate analysis. The partial least-squares-discriminant analysis (PLS-DA) model displayed a discrimination between the RA patients and HCs according to their metabolic differences (**Figure 4A**). The permutation test indicated that the PLS-DA model was not overfitting (Intercept of Q2 = -0.3514, **Figure 4B**). Finally, 41 differentially abundant metabolites (VIP > 1, FC ≥ 1.5,

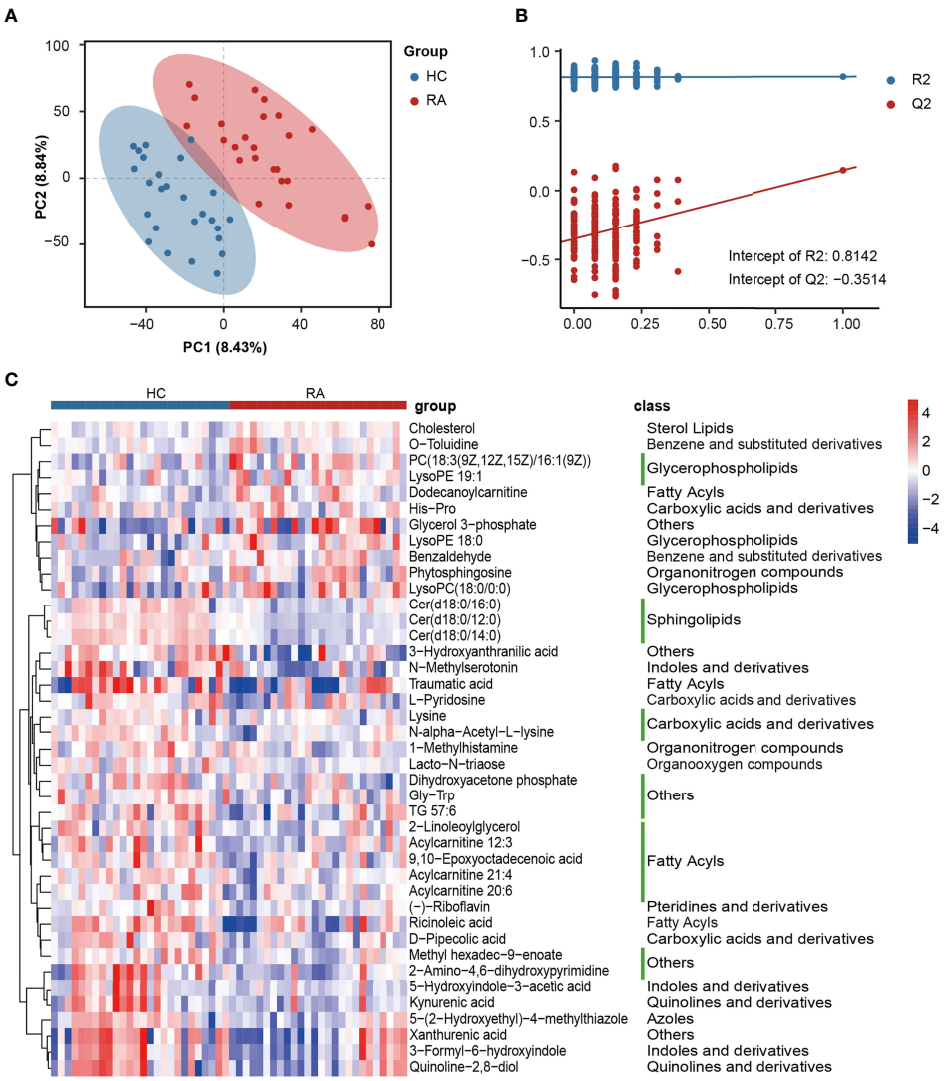

FIGURE 4 | The alterations in fecal metabolites of RA patients. **(A)** PLS-DA score plot of the first two principal components. **(B)** Validation model through 200 permutation tests. **(C)** The heat map of differentially abundant metabolites based on the relative abundance.

$p < 0.05$) between the RA patients and HCs were identified. **Figures 4C** and **5** reveal the alterations of these metabolites. As a result, the RA group showed significantly high levels of glycerophospholipids (PC(18:3(9Z,12Z,15Z)/16:1(9Z)), lysoPE 19:1, lysoPE 18:0, lysoPC(18:0/0:0)), benzene and substituted derivatives (O-toluidine, benzaldehyde), cholesterol, phytosphingosine, His-Pro, glycerol 3-phosphate and dodecanoylcarnitine. In contrast, metabolites enriched in the HC group mainly including sphingolipids (Cer(d18:0/16:0), Cer (d18:0/12:0), Cer(d18:0/14:0)), fatty acyls (traumatic acid, 9,10-epoxyoctadecenoic acid, ricinoleic acid, acylcarnitine 12:3, acylcarnitine 21:4, acylcarnitine 20:6, 2-linoleoylglycerol), indoles and derivatives (N-methylserotonin, 5-hydroxyindole-3-acetic acid (5-HIAA), 3-formyl-6-hydroxyindole), kynurenic acid, xanthurenic acid, 3-hydroxyanthranilic acid (3-HAA), (-)-riboflavin and N-alpha-acetyl-L-lysine. Notably, Cer(d18:0/12:0) and Cer(d18:0/14:0) were the most significantly different molecules, and their differences remained after BH adjustment (**Supplementary Table 7**). To evaluate the possible impact of confounders (gender, age and BMI) on the differentially abundant metabolites, a correlation heat map was applied to show their relationship (**Supplementary Figure 3**). As a result, gender had remarkable associations with 2-linoleoylglycero, Gly-Trp and lacto-N-triaos, age was significantly correlated with 3-hydroxyanthranilic acid and glycerol 3-phosphate, while BMI affected these metabolites little.

KEGG pathway enrichment analysis was then performed on differentially abundant metabolites. As a result, twenty pathways, including unsaturated fatty acid (alpha-linolenic acid, linoleic acid, arachidonic acid) metabolism, tryptophan metabolism, riboflavin metabolism and glycerophospholipid metabolism were the main pathways related to RA (**Figure 6A**). The alterations of eleven differentially abundant metabolites involved in the top five pathways were further illustrated by box maps (**Figure 6B**). We noticed that the RA patients exhibited lower levels of tryptophan metabolites in feces, including N-methylserotonin, 5-HIAA, kynurenic acid, xanthurenic acid and 3-HAA.

Correspondingly, in the validation cohort, pathway enrichment analysis based on significantly altered metabolites also emphasized the importance of glycerophospholipid metabolism, linoleic acid metabolism and arachidonic acid metabolism (**Supplementary Table 8**, **Supplementary Figure 4**).

Multiomics Analysis Revealed Microbiota-Metabolite Interactions of RA

To further investigate the microbiota-metabolite interactions related to RA, we evaluated the correlations between 26 genera and 41 metabolites (**Supplementary Table 9**, **Supplementary Figure 5**). Then a co-occurrence network graph was constructed to illuminate the main interplays (Spearman's correlation analysis, $r > 0.42$, $p < 0.05$, **Figure 7**). From the graph, *Escherichia* seemed to be the core genus given that it was negatively correlated with 8 HC-enriched metabolites (ricinoleic acid, xanthurenic acid, quinoline-2,8-diol, Cer (d18:0/16:0), N-alpha-acetyl-L-lysine, traumatic acid, D-pipecolic acid, 3-formyl-6-hydroxyindole). In addition, *Eisenbergiella* was negatively correlated with HC-enriched Cer (d18:0/12:0), Cer(d18:0/14:0) and xanthurenic acid, while *Fusicatenibacter* was positively correlated with HC-enriched N-alpha-acetyl-L-lysine, traumatic acid and 1-methylhistamine. The above correlations are illustrated in **Supplementary Figure 6** using x-y plots. Other genera, such as *Klebsiella*, were also associated with certain metabolites.

DISCUSSION

In contrast to the metabolome of serum or urine samples, the fecal metabolome could reflect the direct interactions between dietary factors and the gut microbiome (Yang et al., 2019). Previous studies on the intestinal microbiome of RA patients lacked the

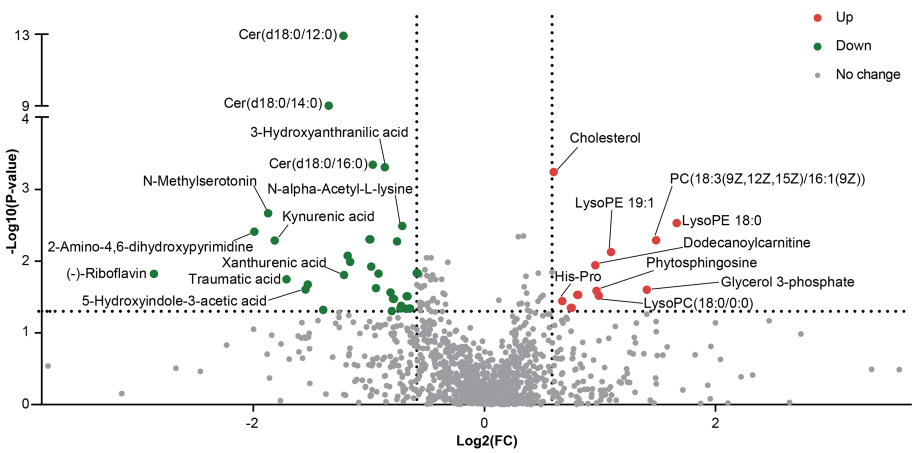

FIGURE 5 | The volcano plot showed the differentially altered metabolites between the two groups.

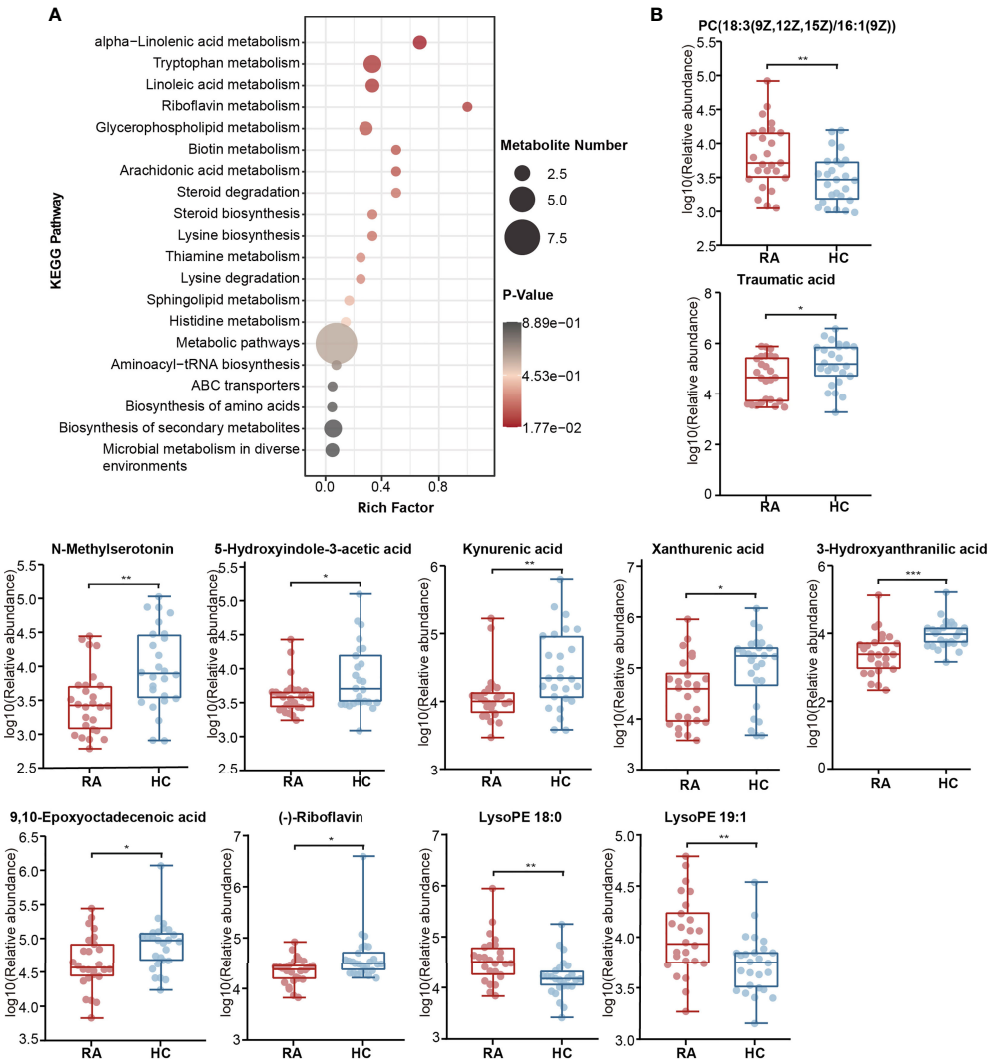

FIGURE 6 | Alterations of KEGG pathway related to RA. **(A)** The KEGG pathway enrichment scatter plot displayed alterations in the intestinal metabolic processes of RA patients. **(B)** Eleven differentially abundant metabolites involved in the mainly altered pathways were further illustrated by box maps. P-value, *p < 0.05; **p < 0.01; ***p < 0.001.

attention of global fecal metabolites. Herein, we performed 16S rDNA sequencing and nontargeted metabolomic profiling to screen for neglected biomarkers and explore microbiota-metabolite interactions. Compared with the HCs, the intestinal microbiome and metabolome of the RA patients exhibited the following characteristics. (1) Microbial composition was altered. Multiple analytical approaches indicated that the main upregulated genera in the RA patients were *Klebsiella*, *Escherichia*, *Eisenbergiella* and *Flavobacterium*, and the main downregulated genera were *Fusicatenibacter*, *Megamonas* and *Enterococcus*. (2) The RA patients displayed high levels of fecal metabolites such as glycerophospholipids, benzene and substituted derivatives and cholesterol, and low levels of metabolites such as sphingolipids and tryptophan downstream metabolites. (3) The gut microbiome and metabolites were interrelated, and *Escherichia* was the core genus.

Evidence from previous studies on RA patients indicated that the alpha diversity of the intestinal microbiome was reduced or unchanged (Chu et al., 2021). Our result was consistent with the latter. Furthermore, beta diversity showed an alteration in microbial composition. We found that Proteobacteria and Verrucomicrobia were remarkably enriched in RA patients, while Firmicutes was depleted. Despite the lack of a significant difference, the RA patients had lower F/B ratios. The aberrant composition of Firmicutes and Bacteroidetes may activate proinflammatory pathways by breaking the intestinal barrier (Khan et al., 2021). We hypothesized that the F/B ratio alteration in RA patients may contribute to the inflammatory status.

In the present study, intestinal microbiota including *Klebsiella*, *Escherichia*, *Eisenbergiella*, *Flavobacterium*, *Lactobacillus*, and *Enterobacter* were more abundant in the RA

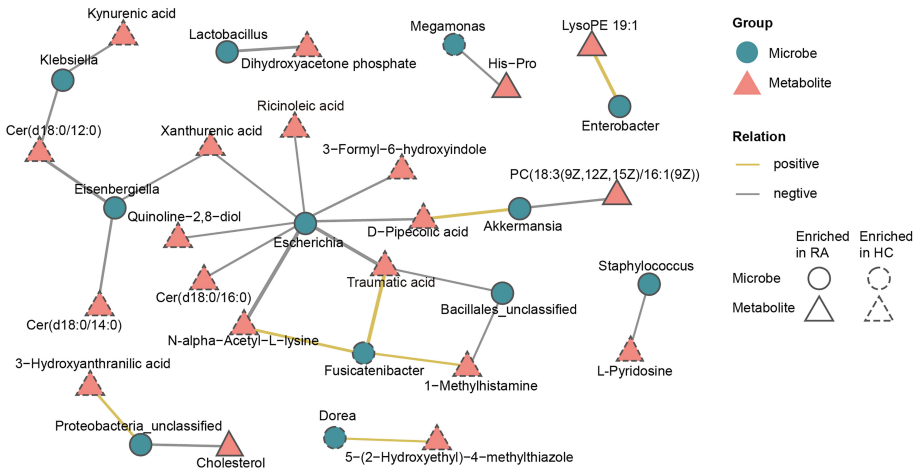

FIGURE 7 | Multiomics approach revealed microbiota-metabolite interactions in RA patients. The co-occurrence network graph showed the main microbiota-metabolite correlations (Spearman's correlation analysis, $r > 0.42$, $P < 0.05$). Microbes were labeled with circles and metabolites with triangles. Solid or dashed borders indicated that the corresponding nodes were enriched in RA patients or healthy controls, respectively. Yellow connecting lines represent positive correlations between two nodes, while gray connecting lines represent negative correlations, and thicker lines indicate greater correlation values.

patients. *Klebsiella* and *Escherichia* belong to the *Enterobacteriaceae* family. Consistent with our results, Li et al. also found an increased proportion of *Escherichia* in fecal samples of the RA patients (Li et al., 2021b). Furthermore, the level of anti-*Klebsiella* IgG antibodies was found increased in the serum of RA patients (Chou et al., 1998). These two kinds of bacteria can produce pathogen-associated molecular patterns (PAMPs) (Feng et al., 2019), and their lipopolysaccharide (LPS) could enhance intestinal permeability to promote inflammation (Chiang et al., 2019). In our results, *Escherichia* was negatively correlated with 8 HC-enriched fecal metabolites, including unsaturated fatty acid (ricinoleic acid and traumatic acid), D-pipecolic acid, xanthurenic acid and Cer(d18:0/16:0). *Klebsiella* was negatively correlated with HC-enriched kynurenic acid and Cer(d18:0/12:0), and exhibited a positive correlation with the serum RF. We hypothesized that the excessive expansion of *Klebsiella* and *Escherichia* contributes to a nonnegligible effect on pathogenicity in RA, which might be partly attributed to the interaction between bacteria and metabolites. *Lactobacillus-ruminis*, which has TNFα stimulatory activity (Taweechotipatr et al., 2009), was enriched in RA patients. Consistent with our results, the increase of *Lactobacillus* in the gut of chronic rheumatic disease patients has been reported previously (Salem et al., 2019). *Eisenbergiella* belongs to the Firmicutes. It was negatively correlated with HC-enriched fecal metabolites including sphingolipids (Cer(d18:0/12:0), Cer(d18:0/14:0)) and xanthurenic acid, indicating a role in promoting the development of RA. However, due to the lack of biological information, the relevant mechanism remains to be further studied.

The RA patients displayed decreases in genera such as *Enterococcus*, *Fusicatenibacter* and *Megamonas*. Enterococcus is a potential probiotic that has a wide range of inhibitory effects on pathogenic and spoilage bacteria by producing bacteriocins (Hanchi et al., 2018). The adjuvant-induced arthritis rat model demonstrated that *Enterococcus_faecium* could enhance the anti-inflammatory and antiarthritic effects of methotrexate (Rovensky et al., 2005). We hypothesized that the decrease of *Enterococcus* in RA patients may relieve the suppression of pathogenic bacteria, thus promoting a gut proinflammatory environment. *Fusicatenibacter* induces IL-10 in intestinal mucosa to exert anti-inflammatory effects (Takeshita et al., 2016). A cirrhosis fecal microbiota study specified that the abundance of *Fusicatenibacter_saccharivorans* was positively correlated with SCFA production (Jin et al., 2019), and SCFAs are beneficial to maintain the integrity of the intestinal mucosa and anti-inflammation (Davila et al., 2013; Morrison and Preston, 2016). Consistent with our study, Lee et al. also found a decrease in *Fusicatenibacter* in feces of RA patients (Lee et al., 2019). In addition, we revealed that *Fusicatenibacter* was positively correlated with HC-enriched metabolites such as traumatic acid and N-alpha-acetyl-L-lysine, and negatively correlated with serum CRP. *Megamonas*, another bacterium decreased in the RA patients, participates in the metabolism of carbohydrate fermentation into SCFAs (Feng et al., 2019). Therefore, we hypothesized that *Fusicatenibacter* and *Megamonas* might antagonize RA by affecting the abundance of SCFAs. The bacteria mentioned above might represent promising targets for RA therapy in the future and deserve further verification experiments.

Our PICRUSt2 analysis specified that the biosynthesis of amino acids, such as L-arginine, ornithine, aromatic amino acids, and branched amino acids, decreased in the RA group. Amino acids, especially branched amino acids, are precursors of SCFA synthesis in the intestinal microbiota. L-arginine has been found to alleviate inflammation in IBD patients (Baier et al., 2020). We consider that the lack of amino acid biosynthesis seems to be the main alteration of microbial function in RA

patients, and this feature might partly induce an imbalance in the immune system.

In the metabolomic results, our study emphasized the crucial role of tryptophan metabolism in RA. We found that the downstream products of tryptophan metabolism, including N-methylserotonin, 5-HIAA, kynurenic acid, xanthurenic acid and 3-HAA, were depleted in the feces of the RA patients. Consistent with our findings, a study on the feces of children with enthesitis-related arthritis found downregulation of tryptophan metabolites (Stoll et al., 2016). Kang et al. also demonstrated a lower level of tryptophan metabolites in the synovial fluid of RA patients than in osteoarthritis patients (Kang et al., 2015). 5-HIAA is derived from the decomposition of serotonin and is an indole derivative. Many indole derivatives are known as ligands for aryl-hydrocarbon receptor (AhR), which can dampen immune responses by activating Treg cells (Agus et al., 2018). Rosser et al. demonstrated that microbiota-derived SCFAs could stimulate Breg cell activity and alleviate arthritis by increasing the level of 5-HIAA (Rosser et al., 2020). Kynurenic acid has an immunosuppressive function (Balog et al., 2021). It is an endogenous component of RA synovial fluid that interferes with synoviocyte proliferation *in vitro* (Parada-Turska et al., 2006). In addition, 3-HAA suppresses the LPS-induced inflammatory response in macrophages through inhibition of the nuclear factor kappa-light-chain enhancer of activated B cells (NF-κB) pathway (Lee et al., 2016). A decrease in 3-HAA was also found in the serum of RA patients (Panfili et al., 2020). Recently, studies have continually appeared suggesting that other autoimmune diseases, including systemic lupus erythematosus and multiple sclerosis, also have an obvious relationship with altered tryptophan metabolism (Brown et al., 2020). However, mechanistic studies on microbiota-derived tryptophan metabolites are lacking. Our multiomics analysis revealed the interactions between tryptophan downstream metabolites (kynurenic acid, xanthurenic acid and 3-HAA) and differential bacteria such as *Klebsiella* and *Escherichia*. The gut microbiota catabolizes tryptophan through tryptophanase and produces diverse metabolites with immune regulatory activity (Agus et al., 2018). We hypothesized that the reduced levels of fecal tryptophan metabolites may be one of the environmental risks of RA. This might be caused by complex inducements such as the redistribution of gut microbial composition and the greater gastrointestinal uptake results from the compromised gut barrier. Microbiota-derived tryptophan catabolites are expected to be developed as biomarkers for dysbiosis and provide new directions for the therapeutic target of RA.

In the present study, we also confirmed that glycerophospholipid and unsaturated fatty acid (alpha-linolenic acid, linoleic acid and arachidonic acid) metabolism pathways were disturbed in the gut of RA patients. Under the catalysis of PLA2, glycerophospholipid is hydrolyzed to generate lysophospholipid and arachidonic acid. Subsequently, arachidonic acid is metabolized to produce inflammatory mediators such as prostaglandins and leukotrienes, which participate in the inflammatory response. Our study revealed that the fecal metabolites of the RA patients displayed significantly high levels of glycerophospholipids including PC(18:3(9Z,12Z,15Z)/16:1(9Z)), lysoPE 19:1, lysoPE 18:0 and lysoPC(18:0/0:0). Consistently, disturbance of the glycerophosphate and arachidonic acid metabolic network was also found in the serum of collagen-induced arthritis (CIA) rats (Ding et al., 2014; Li et al., 2021a). PLA2-deficient mice were not susceptible to arthritis since glycerophospholipid metabolism was restrained (Hegen et al., 2003). In contrast, as an omega-3 polyunsaturated fatty acid, alpha-linolenic acid plays a vital antithrombotic and anti-inflammatory role. Traumatic acid is a little-known beneficial compound derived from alpha-linolenic acid metabolism that has antioxidant and anti-inflammatory potential (Jablonska-Trypuc et al., 2019). In our metabolomic data, traumatic acid was significantly downregulated in the RA patients, indicating a possible antagonistic effect on RA. Furthermore, traumatic acid displayed correlations with the relative abundances of *Escherichia*, *Fusicatenibacter* and *Bacillales-unclassified*. Kindt et al. demonstrated that intestinal microbial colonization degraded dietary fiber to produce acetate, which was a precursor involved in the hepatic synthesis of unsaturated fatty acid and glycerophospholipids (Kindt et al., 2018). We suggested that the dysregulation of glycerophospholipid and unsaturated fatty acid metabolism in RA patients might be partly caused by dysbiosis of the intestinal microbiome. This mechanism may further promote the conversion of the intestinal environment from antiinflammation to proinflammation.

Other differentially abundant metabolites including cholesterol, Cer(d18:0/12:0), Cer(d18:0/14:0), (-)-riboflavin, N-alpha-acetyl-L-lysine, D-pipecolic acid and ricinoleic acid were also identified. Cholesterol is a well-known risk factor for cardiovascular disease. We observed an increase of cholesterol in the feces of RA patients, which was consistent with the results of the study based on serum (Lakatos and Harsagyi, 1988). Cer (d18:0/12:0) and Cer(d18:0/14:0) are ceramides of sphingolipids that are widely found in membranes. Bacteroidetes were the main intestinal bacteria that produce sphingolipids. Bacteroides-derived sphingolipids are beneficial for maintaining intestinal homeostasis and are negatively correlated with inflammation in IBD patients (Brown et al., 2019). Fecal metabolites of Cer(d18:0/12:0) and Cer(d18:0/14:0) was found decreased in the RA patients in our study, suggesting to be possible protective factor for RA. (-)-Riboflavin, i.e., vitamin B2, contributed strongly to maintaining gut microbiota populations. The supply of multiple vitamins is essential for the most abundant butyrate-producing Firmicutes species (Pham et al., 2021). Thus, (-)-riboflavin deficiency may lead to the depletion of SCFAs. N-alpha-acetyl-L-lysine is a lysine acetylated derivative. Lysine acetylation exists in various metabolic processes of the intestinal microbiota, including the production of SCFAs by Firmicutes. Approximately half of the lysine-acetylated derivatives in human feces were derived from Firmicutes (Zhang et al., 2020). We found that N-alpha-acetyl-L-lysine in feces of the RA patients was downregulated and significantly positively correlated with the relative abundance of *Fusicatenibacter* (a genus of Firmicutes). We hypothesized that the decrease in N-alpha-acetyl-L-lysine might be caused by the

depletion of Firmicutes represented by *Fusicatenibacter*. This process may involve a decrease in SCFA production, thus affecting intestinal permeability.

Considering that diet has an essential impact on gut microbial composition, we excluded extreme diets, but we failed to control the diet composition of each participant. In addition, other confounders including gender and BMI were evaluated. Although RA is more prevalent among females than males, this study included male subjects. To eliminate gender bias, the sex ratios between the RA patients and HCs were matched. Furthermore, we checked the gender bias in correlation analyses and found a little impact on the main conclusion. BMI might influence *Clostridiales_unclassified*, which is consistent with previous studies (de La Serre et al., 2010; Kubeck et al., 2016), but has no evident impact on the genera we mainly focused on.

This study was only a cross-sectional study with a small sample size, which did not provide sufficient causality verification. According to the results, no significant difference was found in *Prevotella*, which is a research focus in RA. This finding supported the conclusion of previous studies that *Prevotella copri* increased only in the pre-or early stage of RA rather than the established RA (Vural et al., 2020). In addition, due to the low content or the unsuitable metabolite detection platform, the vital metabolite SCFAs were not identified. Expanding the duration and size of the study and performing an in-depth verification may be beneficial to further study.

Compared with single microbial data set analysis, this study presented more functional insights by introducing global metabolomic profiling, which demonstrated that the gut microbiome and metabolites were altered and interrelated in RA patients compared to HCs. The clinical verification and application of these candidate biomarkers deserve further research and development.

DATA AVAILABILITY STATEMENT

The datasets generated for this study can be found in the SRA of NCBI: https://www.ncbi.nlm.nih.gov/sra/PRJNA753264, and MetaboLights: https://www.ebi.ac.uk/metabolights/MTBLS3233.

ETHICS STATEMENT

The studies involving human participants were reviewed and approved by Institutional Review Board of the Ethics Committee of Taizhou Hospital of Zhejiang Province. The patients/participants provided their written informed consent to participate in this study.

AUTHOR CONTRIBUTIONS

DY, JD, SP, and BS contributed to conception and design of the study. DY, XP, and LZ performed the experiment and statistical analysis. DY wrote the first draft of the manuscript. SSC and NW wrote sections of the manuscript. JL and SYC helped perform the analysis with constructive discussions. All authors contributed to manuscript revision and approved the submitted version.

FUNDING

This work was sponsored by grants from the National Natural Science Foundation of China (No. 81672086), Zhejiang Provincial Natural Science Foundation of China (No. LY19H200001, No. LQ19H100001) and the Science and Technology Plan of Taizhou City (No. 21ywb02).

ACKNOWLEDGMENTS

We thank all the participating patients and healthy volunteers in this study. We thank LC-Bio Technology Co., Ltd, Hangzhou, Zhejiang Province, China for their technical support for this study.

SUPPLEMENTARY MATERIAL

The Supplementary Material for this article can be found online at: https://www.frontiersin.org/articles/10.3389/fcimb.2021.763507/full#supplementary-material

REFERENCES

Agus, A., Planchais, J., and Sokol, H. (2018). Gut Microbiota Regulation of Tryptophan Metabolism in Health and Disease. *Cell Host Microbe* 23 (6), 716–724. doi: 10.1016/j.chom.2018.05.003

Baier, J., Gansbauer, M., Giessler, C., Arnold, H., Muske, M., Schleicher, U., et al. (2020). Arginase Impedes the Resolution of Colitis by Altering the Microbiome and Metabolome. *J. Clin. Invest.* 130 (11), 5703–5720. doi: 10.1172/JCI126923

Balog, A., Varga, B., Fulop, F., Lantos, I., Toldi, G., Vecsei, L., et al. (2021). Kynurenic Acid Analog Attenuates the Production of Tumor Necrosis Factor-Alpha, Calgranulins (S100A 8/9 and S100A 12), and the Secretion of HNP1-3 and Stimulates the Production of Tumor Necrosis Factor-Stimulated Gene-6 in Whole Blood Cultures of Patients With Rheumatoid Arthritis. *Front. Immunol.* 12, 632513. doi: 10.3389/fimmu.2021.632513

Brown, E. M., Ke, X., Hitchcock, D., Jeanfavre, S., Avila-Pacheco, J., Nakata, T., et al. (2019). Bacteroides-Derived Sphingolipids Are Critical for Maintaining Intestinal Homeostasis and Symbiosis. *Cell Host Microbe* 25 (5), 668–680 e667. doi: 10.1016/j.chom.2019.04.002

Brown, J., Robusto, B., and Morel, L. (2020). Intestinal Dysbiosis and Tryptophan Metabolism in Autoimmunity. *Front. Immunol.* 11, 1741. doi: 10.3389/fimmu.2020.01741

Callahan, B. J., McMurdie, P. J., Rosen, M. J., Han, A. W., Johnson, A. J., and Holmes, S. P. (2016). DADA2: High-Resolution Sample Inference From Illumina Amplicon Data. *Nat. Methods* 13 (7), 581–583. doi: 10.1038/nmeth.3869

Chiang, H. I., Li, J. R., Liu, C. C., Liu, P. Y., Chen, H. H., Chen, Y. M., et al. (2019). An Association of Gut Microbiota With Different Phenotypes in Chinese Patients With Rheumatoid Arthritis. *J. Clin. Med.* 8 (11), 1770. doi: 10.3390/jcm8111770

Chou, C. T., Uksila, J., and Toivanen, P. (1998). Enterobacterial Antibodies in Chinese Patients With Rheumatoid Arthritis and Ankylosing Spondylitis. *Clin. Exp. Rheumatol* 16 (2), 161–164.

Chu, X. J., Cao, N. W., Zhou, H. Y., Meng, X., Guo, B., Zhang, H. Y., et al. (2021). The Oral and Gut Microbiome in Rheumatoid Arthritis Patients: A Systematic Review. *Rheumatol. (Oxford)* 60 (3), 1054–1066. doi: 10.1093/rheumatology/keaa835

Davila, A. M., Blachier, F., Gotteland, M., Andriamihaja, M., Benetti, P. H., Sanz, Y., et al. (2013). Intestinal Luminal Nitrogen Metabolism: Role of the Gut Microbiota and Consequences for the Host. *Pharmacol. Res.* 68 (1), 95–107. doi: 10.1016/j.phrs.2012.11.005

de La Serre, C. B., Ellis, C. L., Lee, J., Hartman, A. L., Rutledge, J. C., and Raybould, H. E. (2010). Propensity to High-Fat Diet-Induced Obesity in Rats is Associated With Changes in the Gut Microbiota and Gut Inflammation. *Am. J. Physiol. Gastrointest Liver Physiol.* 299 (2), G440–G448. doi: 10.1152/ajpgi.00098.2010

Ding, X., Hu, J., Li, J., Zhang, Y., Shui, B., Ding, Z., et al. (2014). Metabolomics Analysis of Collagen-Induced Arthritis in Rats and Interventional Effects of Oral Tolerance. *Anal. Biochem.* 458, 49–57. doi: 10.1016/j.ab.2014.04.035

Feng, J., Zhao, F., Sun, J., Lin, B., Zhao, L., Liu, Y., et al. (2019). Alterations in the Gut Microbiota and Metabolite Profiles of Thyroid Carcinoma Patients. *Int. J. Cancer* 144 (11), 2728–2745. doi: 10.1002/ijc.32007

Gibbons, S. M. (2017). Microbial Community Ecology: Function Over Phylogeny. *Nat. Ecol. Evol.* 1 (1), 32. doi: 10.1038/s41559-016-0032

Hanchi, H., Mottawea, W., Sebei, K., and Hammami, R. (2018). The Genus Enterococcus: Between Probiotic Potential and Safety Concerns-An Update. *Front. Microbiol.* 9, 1791. doi: 10.3389/fmicb.2018.01791

Hegen, M., Sun, L., Uozumi, N., Kume, K., Goad, M. E., Nickerson-Nutter, C. L., et al. (2003). Cytosolic Phospholipase A2alpha-Deficient Mice are Resistant to Collagen-Induced Arthritis. *J. Exp. Med.* 197 (10), 1297–1302. doi: 10.1084/jem.20030016

Jablonska-Trypuc, A., Wydro, U., Wolejko, E., and Butarewicz, A. (2019). Toxicological Effects of Traumatic Acid and Selected Herbicides on Human Breast Cancer Cells: *In Vitro* Cytotoxicity Assessment of Analyzed Compounds. *Molecules* 24 (9), 1710. doi: 10.3390/molecules24091710

Jin, M., Kalainy, S., Baskota, N., Chiang, D., Deehan, E. C., McDougall, C., et al. (2019). Faecal Microbiota From Patients With Cirrhosis has a Low Capacity to Ferment non-Digestible Carbohydrates Into Short-Chain Fatty Acids. *Liver Int.* 39 (8), 1437–1447. doi: 10.1111/liv.14106

Kang, K. Y., Lee, S. H., Jung, S. M., Park, S. H., Jung, B. H., and Ju, J. H. (2015). Downregulation of Tryptophan-Related Metabolomic Profile in Rheumatoid Arthritis Synovial Fluid. *J. Rheumatol* 42 (11), 2003–2011. doi: 10.3899/jrheum.141505

Kau, A. L., Ahern, P. P., Griffin, N. W., Goodman, A. L., and Gordon, J. I. (2011). Human Nutrition, the Gut Microbiome and the Immune System. *Nature* 474 (7351), 327–336. doi: 10.1038/nature10213

Khan, R., Sharma, A., Ravikumar, R., Parekh, A., Srinivasan, R., George, R. J., et al. (2021). Association Between Gut Microbial Abundance and Sight-Threatening Diabetic Retinopathy. *Invest. Ophthalmol. Vis. Sci.* 62 (7), 19. doi: 10.1167/iovs.62.7.19

Kindt, A., Liebisch, G., Clavel, T., Haller, D., Hormannsperger, G., Yoon, H., et al. (2018). The Gut Microbiota Promotes Hepatic Fatty Acid Desaturation and Elongation in Mice. *Nat. Commun.* 9 (1), 3760. doi: 10.1038/s41467-018-05767-4

Krautkramer, K. A., Fan, J., and Backhed, F. (2021). Gut Microbial Metabolites as Multi-Kingdom Intermediates. *Nat. Rev. Microbiol.* 19 (2), 77–94. doi: 10.1038/s41579-020-0438-4

Kubeck, R., Bonet-Ripoll, C., Hoffmann, C., Walker, A., Muller, V. M., Schuppel, V. L., et al. (2016). Dietary Fat and Gut Microbiota Interactions Determine Diet-Induced Obesity in Mice. *Mol. Metab.* 5 (12), 1162–1174. doi: 10.1016/j.molmet.2016.10.001

Lakatos, J., and Harsagyi, A. (1988). Serum Total, HDL, LDL Cholesterol, and Triglyceride Levels in Patients With Rheumatoid Arthritis. *Clin. Biochem.* 21 (2), 93–96. doi: 10.1016/s0009-9120(88)80094-8

Lee, K., Kwak, J. H., and Pyo, S. (2016). Inhibition of LPS-Induced Inflammatory Mediators by 3-Hydroxyanthranilic Acid in Macrophages Through Suppression of PI3K/NF-kappaB Signaling Pathways. *Food Funct.* 7 (7), 3073–3082. doi: 10.1039/c6fo00187d

Lee, J. Y., Mannaa, M., Kim, Y., Kim, J., Kim, G. T., and Seo, Y. S. (2019). Comparative Analysis of Fecal Microbiota Composition Between Rheumatoid Arthritis and Osteoarthritis Patients. *Genes (Basel)* 10 (10), 748. doi: 10.3390/genes10100748

Li, Y., Lv, D., Liu, R., Shi, Y., Wang, R., Zhu, Z., et al. (2021a). Non-Target Metabolomic Analysis Reveals the Therapeutic Effect of Saposhnikovia Divaricata Decoction on Collagen-Induced Arthritis Rats. *J. Ethnopharmacol* 271, 113837. doi: 10.1016/j.jep.2021.113837

Li, Y., Zhang, S. X., Yin, X. F., Zhang, M. X., Qiao, J., Xin, X. H., et al. (2021b). The Gut Microbiota and Its Relevance to Peripheral Lymphocyte Subpopulations and Cytokines in Patients With Rheumatoid Arthritis. *J. Immunol. Res.* 2021, 6665563. doi: 10.1155/2021/6665563

Logue, J. B., Stedmon, C. A., Kellerman, A. M., Nielsen, N. J., Andersson, A. F., Laudon, H., et al. (2016). Experimental Insights Into the Importance of Aquatic Bacterial Community Composition to the Degradation of Dissolved Organic Matter. *ISME J.* 10 (3), 533–545. doi: 10.1038/ismej.2015.131

Morrison, D. J., and Preston, T. (2016). Formation of Short Chain Fatty Acids by the Gut Microbiota and Their Impact on Human Metabolism. *Gut Microbes* 7 (3), 189–200. doi: 10.1080/19490976.2015.1134082

Panfili, E., Gerli, R., Grohmann, U., and Pallotta, M. T. (2020). Amino Acid Metabolism in Rheumatoid Arthritis: Friend or Foe? *Biomolecules* 10 (9), 1280. doi: 10.3390/biom10091280

Pan, H., Guo, R., Ju, Y., Wang, Q., Zhu, J., Xie, Y., et al. (2019). A Single Bacterium Restores the Microbiome Dysbiosis to Protect Bones From Destruction in a Rat Model of Rheumatoid Arthritis. *Microbiome* 7 (1), 107. doi: 10.1186/s40168-019-0719-1

Parada-Turska, J., Rzeski, W., Zgrajka, W., Majdan, M., Kandefer-Szerszen, M., and Turski, W. (2006). Kynurenic Acid, an Endogenous Constituent of Rheumatoid Arthritis Synovial Fluid, Inhibits Proliferation of Synoviocytes In Vitro. *Rheumatol Int.* 26 (5), 422–426. doi: 10.1007/s00296-005-0057-4

Pham, V. T., Fehlbaum, S., Seifert, N., Richard, N., Bruins, M. J., Sybesma, W., et al. (2021). Effects of Colon-Targeted Vitamins on the Composition and Metabolic Activity of the Human Gut Microbiome- a Pilot Study. *Gut Microbes* 13 (1), 1–20. doi: 10.1080/19490976.2021.1875774

Pianta, A., Arvikar, S., Strle, K., Drouin, E. E., Wang, Q., Costello, C. E., et al. (2017). Evidence of the Immune Relevance of Prevotella Copri, a Gut Microbe, in Patients With Rheumatoid Arthritis. *Arthritis Rheumatol* 69 (5), 964–975. doi: 10.1002/art.40003

Rosser, E. C., Piper, C. J. M., Matei, D. E., Blair, P. A., Rendeiro, A. F., Orford, M., et al. (2020). Microbiota-Derived Metabolites Suppress Arthritis by Amplifying Aryl-Hydrocarbon Receptor Activation in Regulatory B Cells. *Cell Metab.* 31 (4), 837–851 e810. doi: 10.1016/j.cmet.2020.03.003

Rovensky, J., Svik, K., Matha, V., Istok, R., Kamarad, V., Ebringer, L., et al. (2005). Combination Treatment of Rat Adjuvant-Induced Arthritis With Methotrexate, Probiotic Bacteria Enterococcus Faecium, and Selenium. *Ann. N Y Acad. Sci.* 1051, 570–581. doi: 10.1196/annals.1361.101

Salem, F., Kindt, N., Marchesi, J. R., Netter, P., Lopez, A., Kokten, T., et al. (2019). Gut Microbiome in Chronic Rheumatic and Inflammatory Bowel Diseases: Similarities and Differences. *U Eur. Gastroenterol. J.* 7 (8), 1008–1032. doi: 10.1177/2050640619867555

Scher, J. U., Sczesnak, A., Longman, R. S., Segata, N., Ubeda, C., Bielski, C., et al. (2013). Expansion of Intestinal Prevotella Copri Correlates With Enhanced Susceptibility to Arthritis. *Elife* 2, e01202. doi: 10.7554/eLife.01202

Scott, D. L., Wolfe, F., and Huizinga, T. W. (2010). Rheumatoid Arthritis. *Lancet* 376 (9746), 1094–1108. doi: 10.1016/S0140-6736(10)60826-4

Stoll, M. L., Kumar, R., Lefkowitz, E. J., Cron, R. Q., Morrow, C. D., and Barnes, S. (2016). Fecal Metabolomics in Pediatric Spondyloarthritis Implicate Decreased Metabolic Diversity and Altered Tryptophan Metabolism as Pathogenic Factors. *Genes Immun.* 17 (7), 400–405. doi: 10.1038/gene.2016.38

Takeshita, K., Mizuno, S., Mikami, Y., Sujino, T., Saigusa, K., Matsuoka, K., et al. (2016). A Single Species of Clostridium Subcluster XIVa Decreased in Ulcerative Colitis Patients. *Inflammation Bowel Dis.* 22 (12), 2802–2810. doi: 10.1097/MIB.0000000000000972

Taneja, V. (2014). Arthritis Susceptibility and the Gut Microbiome. *FEBS Lett.* 588 (22), 4244–4249. doi: 10.1016/j.febslet.2014.05.034

Taweechotipatr, M., Iyer, C., Spinler, J. K., Versalovic, J., and Tumwasorn, S. (2009). Lactobacillus Saerimneri and Lactobacillus Ruminis: Novel Human-Derived Probiotic Strains With Immunomodulatory Activities. *FEMS Microbiol. Lett.* 293 (1), 65–72. doi: 10.1111/j.1574-6968.2009.01506.x

van den Broek, M. F., van Bruggen, M. C., Koopman, J. P., Hazenberg, M. P., and van den Berg, W. B. (1992). Gut Flora Induces and Maintains Resistance

Against Streptococcal Cell Wall-Induced Arthritis in F344 Rats. *Clin. Exp. Immunol.* 88 (2), 313–317. doi: 10.1111/j.1365-2249.1992.tb03079.x

Velasquez-Manoff, M. (2015). Gut Microbiome: The Peacekeepers. *Nature* 518 (7540), S3–11. doi: 10.1038/518S3a

Vural, M., Gilbert, B., Ustun, I., Caglar, S., and Finckh, A. (2020). Mini-Review: Human Microbiome and Rheumatic Diseases. *Front. Cell Infect. Microbiol.* 10, 491160. doi: 10.3389/fcimb.2020.491160

Yang, W., and Cong, Y. (2021). Gut Microbiota-Derived Metabolites in the Regulation of Host Immune Responses and Immune-Related Inflammatory Diseases. *Cell Mol. Immunol.* 18 (4), 866–877. doi: 10.1038/s41423-021-00661-4

Yang, Y., Misra, B. B., Liang, L., Bi, D., Weng, W., Wu, W., et al. (2019). Integrated Microbiome and Metabolome Analysis Reveals a Novel Interplay Between Commensal Bacteria and Metabolites in Colorectal Cancer. *Theranostics* 9 (14), 4101–4114. doi: 10.7150/thno.35186

Zhang, X., Ning, Z., Mayne, J., Yang, Y., Deeke, S. A., Walker, K., et al. (2020). Widespread Protein Lysine Acetylation in Gut Microbiome and its Alterations in Patients With Crohn's Disease. *Nat. Commun.* 11 (1), 4120. doi: 10.1038/s41467-020-17916-9

Conflict of Interest: The authors declare that the research was conducted in the absence of any commercial or financial relationships that could be construed as a potential conflict of interest.

Publisher's Note: All claims expressed in this article are solely those of the authors and do not necessarily represent those of their affiliated organizations, or those of the publisher, the editors and the reviewers. Any product that may be evaluated in this article, or claim that may be made by its manufacturer, is not guaranteed or endorsed by the publisher.

frontiers in Cellular and Infection Microbiology

ORIGINAL RESEARCH
published: 28 January 2022
doi: 10.3389/fcimb.2021.787667

Dysregulation of the Intestinal Microbiome in Patients With Haploinsufficiency of A20

Etsushi Toyofuku[1,2†], Kozue Takeshita[3†], Hidenori Ohnishi[4], Yuko Kiridoshi[5], Hiroaki Masuoka[6], Tomonori Kadowaki[4], Ryuta Nishikomori[7,8], Kenichi Nishimura[9], Chie Kobayashi[10], Takasuke Ebato[11], Tomonari Shigemura[12], Yuzaburo Inoue[13], Wataru Suda[6], Masahira Hattori[6,14], Tomohiro Morio[1], Kenya Honda[3] and Hirokazu Kanegane[15]*

[1] Department of Pediatrics and Developmental Biology, Graduate School of Medical and Dental Sciences, Tokyo Medical and Dental University (TMDU), Tokyo, Japan, [2] Graduate School of Medicine and Faculty of Medicine, The University of Tokyo, Tokyo, Japan, [3] Department of Microbiology and Immunology, Keio University School of Medicine, Tokyo, Japan, [4] Department of Pediatrics, Gifu University Graduate School of Medicine, Gifu, Japan, [5] JSR-Keio University Medical and Chemical Innovation Center (JKiC), JSR Corporation, Tokyo, Japan, [6] Laboratory for Microbiome Sciences, RIKEN Center for Integrative Medical Sciences, Yokohama, Japan, [7] Department of Pediatrics, Kyoto University Hospital, Kyoto, Japan, [8] Department of Pediatrics and Child Health, Kurume University School of Medicine, Kurume, Japan, [9] Department of Pediatrics, Yokohama City University Graduate School of Medicine, Yokohama, Japan, [10] Department of Child Health, Faculty of Medicine, University of Tsukuba, Tsukuba, Japan, [11] Department of Pediatrics, Kitasato University Hospital, Sagamihara, Japan, [12] Department of Pediatrics, Shinshu University School of Medicine, Matsumoto, Japan, [13] Department of Allergy and Rheumatology, Chiba Children's Hospital, Chiba, Japan, [14] Graduate School of Advanced Science and Engineering, Waseda University, Tokyo, Japan, [15] Department of Child Health and Development, Graduate School of Medical and Dental Sciences, Tokyo Medical and Dental University (TMDU), Tokyo, Japan

OPEN ACCESS

Edited by:
Elias Adel Rahal, American University of Beirut, Lebanon

Reviewed by:
Daniel Alford Powell, University of Arizona, United States
Melhem Bilen, Stanford University, United States

***Correspondence:**
Hirokazu Kanegane
hkanegane.ped@tmd.ac.jp

[†]These authors have contributed equally to this work

Specialty section:
This article was submitted to Microbiome in Health and Disease, a section of the journal Frontiers in Cellular and Infection Microbiology

Received: *01 October 2021*
Accepted: *28 December 2021*
Published: *28 January 2022*

Citation:
Toyofuku E, Takeshita K, Ohnishi H, Kiridoshi Y, Masuoka H, Kadowaki T, Nishikomori R, Nishimura K, Kobayashi C, Ebato T, Shigemura T, Inoue Y, Suda W, Hattori M, Morio T, Honda K and Kanegane H (2022) Dysregulation of the Intestinal Microbiome in Patients With Haploinsufficiency of A20. Front. Cell. Infect. Microbiol. 11:787667. doi: 10.3389/fcimb.2021.787667

Introduction: Haploinsufficiency of A20 (HA20) is a form of inborn errors of immunity (IEI). IEIs are genetically occurring diseases, some of which cause intestinal dysbiosis. Due to the dysregulation of regulatory T cells (Tregs) observed in patients with HA20, gut dysbiosis was associated with Tregs in intestinal lamina propria.

Methods: Stool samples were obtained from 16 patients with HA20 and 15 of their family members. Infant samples and/or samples with recent antibiotics use were excluded; hence, 26 samples from 13 patients and 13 family members were analyzed. The 16S sequencing process was conducted to assess the microbial composition of samples. Combined with clinical information, the relationship between the microbiome and the disease activity was statistically analyzed.

Results: The composition of gut microbiota in patients with HA20 was disturbed compared with that in healthy family members. Age, disease severity, and use of immunosuppressants corresponded to dysbiosis. However, other explanatory factors, such as abdominal symptoms and probiotic treatment, were not associated. The overall composition at the phylum level was stable, but some genera were significantly increased or decreased. Furthermore, among the seven operational taxonomic units (OTUs) that increased, two OTUs, *Streptococcus mutans* and *Lactobacillus salivarius*, considerably increased in patients with autoantibodies than those without autoantibodies.

Discussion: Detailed interaction on intestinal epithelium remains unknown; the relationship between the disease and stool composition change helps us understand the mechanism of an immunological reaction to microorganisms.

Keywords: haploinsufficiency of A20, intestinal microbiome, regulatory T cells, inborn errors of immunity, *Streptococcus mutans*, *Lactobacillus salivarius*

INTRODUCTION

A20, which is encoded by the tumor necrosis factor alpha-induced protein 3 (*TNFAIP3*) gene, is a negative regulator of the TNF-nuclear factor-κB (NF-κB) signaling pathway. Haploinsufficiency of A20 (HA20) causes autoinflammatory and autoimmune disorders (Kadowaki et al., 2018). Dysbiosis of the intestinal microbiome has been observed in some inborn errors of immunities (IEIs)/primary immunodeficiency disease, such as chronic granulomatous disease (CGD) (Sokol et al., 2016), X-linked inhibitor of apoptosis (XIAP) deficiency (Sokol et al., 2016; Ono et al., 2021), tetratricopeptide repeat domain 7A (TTC7A) deficiency (Sokol et al., 2016), common variable immunodeficiency (CVID) (Jørgensen et al., 2016; Varricchi et al., 2021), and Wiskott–Aldrich syndrome (Zhang et al., 2020). Despite IEIs having a monogenetic nature, they vary in severity relating to the microbiome (Liu et al., 2021). Little is known about the mechanism of dysbiosis in patients with IEI, but the association of gut microbiota and regulatory T cells (Tregs) was reported (Liu et al., 2021). Tregs regulate A20 (Kadowaki et al., 2020); as a result, the gut microbiota of patients with HA20 plays a vital role in association with Tregs. Alternatively, the mouse lacking A20 expression in dendritic cells showed intestinal dysbiosis (Talpin et al., 2019). This is the first report of the microbiome in patients with HA20.

MATERIALS AND METHODS

Research Participants and Samples

Kadowaki et al. (2018) previously reported that there were 22 patients with HA20 from nine families in Japan. Thirty-six individuals from nine families, including 18 patients, 17 healthy family members living together, and a sibling whose genetic information is unknown, agreed to participate in this study. Next, fecal samples were obtained from 16 patients and 15 healthy relatives from eight corresponding families. Clinical characteristics of the patients were previously reported (patients 3–5, 7–13, and 17–22), and additional information, such as sex, age at the sample collection, symptoms, and medication, was collected (**Supplementary Table 1**).

The Classification of the Disease Severity of Haploinsufficiency of A20

We proposed the classification of disease severity for clinical manifestations of patients with HA20. The mild type was defined as asymptomatic or minor phenotype (e.g., mild recurrent stomatitis and/or rash). The moderate type was defined as paroxysmal symptoms (e.g., recurrent fever and/or abdominal pain). The frequency of symptoms is once or more for at least 3 months. The severe type was defined as persistent inflammation (e.g., fever, central nerve lesion, vascular lesion, ocular lesion, intestinal lesion, and/or arthritis) sustained over 2 weeks.

Detection of the Microbiome

Fecal samples were collected and stored at 4°C under anaerobic conditions until preparation. Fecal samples were stirred until completely homogenized and suspended in phosphate-buffered saline (PBS) containing 20% glycerol (1 g of feces per 5 ml) and poured through a filter to remove large-sized food-derived debris. The fecal suspension was added to EDTA (final concentration of 10 mM, Nacalai) and stored at −80°C until use. After thawing, 100 µl of fecal suspension was gently mixed and incubated in 800 µl of TE10 (10 mM of Tris-HCl and 10 mM of EDTA) buffer containing RNase A (final concentration of 100 µg/ml, Invitrogen) and lysozyme (final concentration of 15 mg/ml, Sigma) for 1 h at 37°C. Purified achromopeptidase (final concentration of 2,000 U/ml, Wako) was added and further incubated for 30 min at 37°C. Sodium dodecyl sulfate (SDS) (final concentration of 1%) and proteinase K (final concentration of 1 mg/ml, Roche) were further added to the mixture and incubated for 1 h at 55°C. High-molecular-weight DNA was extracted with phenol:chloroform:isoamyl alcohol (25:24:1 at pH 7.9), precipitated with isopropanol (equal volume to the aqueous phase), washed with 1 ml of 70% ethanol, and gently resuspended in 30 µl of TE buffer. We used 40 ng of DNA per sample for the sequence.

The sequencing of the 16S ribosomal RNA gene from fecal samples was performed as previously described (Kim et al., 2013; Kakihana et al., 2016). The hypervariable V1–2 region of the 16S rRNA gene was amplified by PCR using barcoded 27Fmod and 338R primers. DNA extracted from *Escherichia coli* Strain SE 11 (isolated from a healthy adult) was used as the positive control template, whereas a DNA-free sample was used as the negative control. The electrophoresis procedure confirmed the PCR amplicons and negative reaction. Then, an equal amount of purified PCR amplicons was sequenced on a MiSeq platform (Illumina, San Diego, CA). Next, 3,000 high-quality reads were randomly selected per sample and analyzed to minimize the overestimation of species richness during clustering associated with the sequencing error (Kim et al., 2013). Good's coverage index (Singleton et al., 2001) for the 3,000 reads per sample in the current study was 0.980, indicating a high degree of coverage and a sufficient read number for the fecal microbiome analysis. Furthermore, the reads were sorted into operational taxonomic units (OTUs) using the UCLUST algorithm, at a sequence identity threshold of 97% (Stackebrandt and Goebel, 1994;

Konstantinidis and Tiedje, 2005). Taxonomic assignments of each OTU were made by similarity searching against the publicly available 16S (RDP v.10.27 and CORE) and National Center for Biotechnology Information genome database, using GLSEARCH. OTU-based microbial diversity was estimated using the Shannon index with Scikit-bio (v.0.5.5). A comparison of each group (family, HA20) in the unweighted and weighted UniFrac principal coordinate analysis (PCoA) was evaluated by using permutational multivariate ANOVA (PERMANOVA) with Scikit-bio (v.0.5.5) (Anderson, 2017).

Statistical Analysis

Statistical analysis of OTUs and Shannon index was performed using the Wilcoxon rank-sum test. Values are represented as median (minimum–maximum). The threshold for significance was $p < 0.05$. Also, stratified analysis was performed using the two-tailed t-test for ordinal scale or regression analysis for continuous scale. Statistical analyses were conducted using R package (exactRankTests) or JMP Pro v.16.0.0 (SAS Institute Inc., NC, USA). The linear discriminant analysis (LDA) effect size (LEfSe) method was performed on the Huttenhower lab Galaxy server (https://huttenhower.sph.harvard.edu/galaxy/) by importing the bacterial relative abundance values at the genus level with Kruskal–Wallis test $p < 0.05$ and LDA score (log10) > 2 (Segata et al., 2011).

RESULTS

Thirty-one fecal samples from 16 patients and 15 healthy family members were sequenced. However, samples from three patients who received antibiotic treatment within 4 weeks of stool collection were excluded from statistical analysis. Also, two samples from children under the age of 3 years were excluded from statistical analysis because their gut microbiome is naturally different from the older's microbiome (Yatsunenko et al., 2012). Nobody but an excluded younger brother (P22-sib) has food allergies. The median (min–max) age of 13 patients with HA20 and their healthy family members of 13 individuals were 19 (3–43) and 36 (4–49) years ($p = 0.09$, Wilcoxon rank-sum test), respectively. Patients with HA20 consist of four mild, four moderate, and five severe patients. Eleven of 13 patients and eight of 13 presented with stomatitis and abdominal symptoms, respectively. One patient was treated with probiotics and 5 with immunosuppressants (**Supplementary Table 1**).

Ten thousand reads were used from an average (and SD) of 53,935 (± 9,383) raw reads. An average of 9,848 reads passed the filter, and every 3,000 Passed Filter reads were used for OTU analysis. The number of OTUs in patients' samples was considerably less than their healthy members (median 123 *vs.* 150, $p = 0.049$, Wilcoxon rank-sum test) (**Figure 1A**). Likewise, the Shannon index in patients' samples was significantly less than their healthy members (median 4.68 *vs.* 5.26, $p = 0.009$, Wilcoxon rank-sum test) (**Figure 1B**), whereas the principal component analysis showed a significant difference in the composition of the intestinal microbiome in unweighted UniFrac analysis ($p = 0.008$, PERMANOVA) (**Figure 2A**), although not significant in weighted UniFrac analysis ($p = 0.059$) (**Figure 2B**). Thus, the stratified analysis suggested that any sex, stomatitis, abdominal symptoms, and use of probiotics do not affect the microbiome diversity (**Tables 1** and **2**). Lower age was significantly associated with a lower Shannon index although insignificantly with OTUs. Both disease severity and immunosuppressant use were associated with a lower number of OTUs with significance, and they showed lower Shannon index although not significantly.

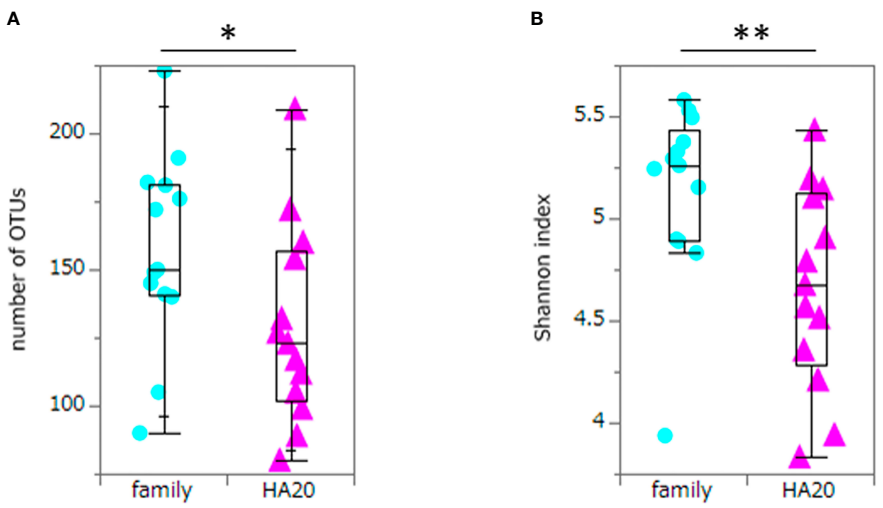

FIGURE 1 | The numbers of OTUs and Shannon index. The numbers of OTUs (median 123 *vs.* 150, $p = 0.049$) **(A)** and Shannon index (median 4.68 *vs.* 5.26, $p = 0.009$) **(B)** of patients with HA20 and their family members. Box plot indicates median value, and lower and upper quartiles. *p*-Value is calculated using the Wilcoxon rank-sum test. *$p < 0.05$, **$p < 0.01$. OTU, operational taxonomic unit; HA20, haploinsufficiency of A20.

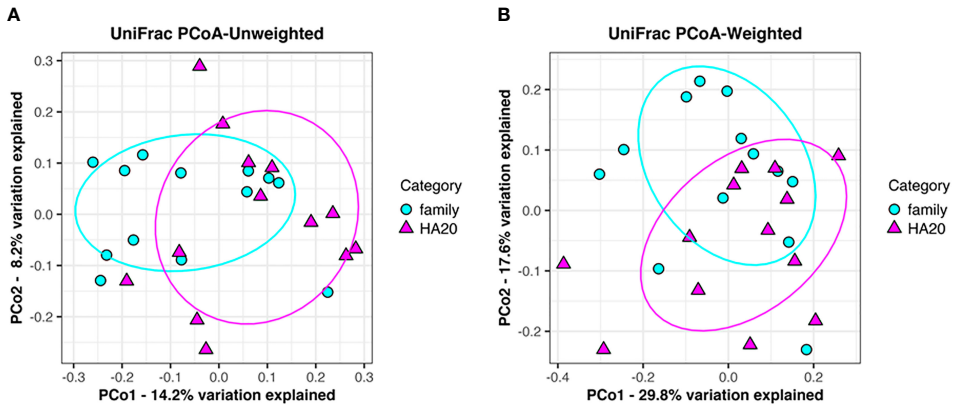

FIGURE 2 | Principal component analysis of gut flora. Clustering of patients (red triangle) and their families (blue circle) following unweighted UniFrac analysis (p = 0.008). **(A)** Weighted UniFrac analysis (p = 0.059). **(B)** Explained variation is represented as a percentage.

At the phylum level, there was no significant difference between patients with HA20 and their family members (**Figure 3** and **Supplementary Table 2**). Conversely, at the genus level, five genera (*Streptococcus*, *Lactobacillus*, *Butyricicoccus*, *Haemophilus*, and *Enterococcus*) increased, and another four (*Ruminococcus*, *Clostridium*, *Parabacteroides*, and *Alistipes*) decreased in patients with HA20 compared with their family members (LDA score greater than two at $p < 0.05$ with LEfSe analysis) (**Figure 4A**). At the OTU level, seven OTUs significantly increased in patients with HA20 compared with their family members ($p < 0.001$: closest species/strain name *Haemophilus parainfluenzae*, *Streptococcus mutans*, and *Veillonella* sp. oral taxon 158, $p < 0.05$: *Bifidobacterium dentium*, *Lactobacillus salivarius*, *Enterococcus avium*, and *Eubacterium eligens*, Wilcoxon rank-sum test). Most of these OTUs are indigenous bacteria and are undetected in the intestinal microbiota. As a representative, only one of two healthy child siblings under 10 years and none of 11 healthy adult members had *H. parainfluenzae*, when all six child patients with HA20 and two of seven adult patients with HA20 had it (**Figure 4B**). None of these seven OTUs showed a significant correlation with either stomatitis or abdominal symptoms. However, two of seven OTUs showed a significant difference between patients with and without autoantibodies (four and five patients, respectively; four patients were not analyzed) (**Figure 4C**).

DISCUSSION

This study demonstrated that patients with HA20 show intestinal dysbiosis. Despite HA20 being a genetically occurring disease, previous studies report bacterial composition changes in other IEIs. XIAP deficiency is a rare IEI, and it is characterized by recurrent hemophagocytic lymphohistiocytosis and refractory inflammatory bowel disease (IBD) similar to Crohn's disease. Furthermore, patients with XIAP deficiency showed intestinal dysbiosis and IBD, which are rescued by allogeneic hematopoietic cell transplantation (Ono et al., 2021). These data further establish the hypothesis that monogenic disease is the cause of gut dysbiosis. From previous studies, there are 118 of 354 IEIs that exhibit gastrointestinal symptoms (Hartono et al., 2019), and the interaction between bacteria and the immune system might vary with the disease. For instance, immunoglobulin A secreted at the mucosal surface of the gastrointestinal tract was associated with selective IgA deficiency (Berbers et al., 2019), and the absence of various

TABLE 1 | Univariable analysis of Shannon index.

Parameter	Median (IQR) or N (percentage)	Risk difference (95% CIs)	*p*-Value
Age	19 (6.5–33.5)	0.020 (0.0030 to 0.0370)	**0.03**
Sex (male or female)	8 (62%)	0.25 (–0.38 to 0.87)	0.41
Severity (severe or not)	5 (28%)	–0.39 (–0.98 to 0.20)	0.18
Stomatitis	11 (85%)	0.49 (–0.32 to 1.30)	0.21
Abdominal symptoms	8 (62%)	0.18 (–0.46 to 0.81)	0.56
Probiotics	1 (8%)	0.13 (–1.04 to 1.31)	0.81
Immunosuppressants	5 (28%)	–0.18 (–0.82 to 0.45)	0.53

Statistical analyses were performed using the two-tailed t-test for ordinal scale or regression analysis for continuous scale. Bold indicates a significant difference. IQR, interquartile range.

TABLE 2 | Univariable analysis of OTUs.

Parameter	Median (IQR) or N (percentage)	Risk difference (95% CIs)	*p*-Value
Age	19 (6.5–33.5)	0.64 (–0.88 to 2.17)	0.37
Sex (male or female)	8 (62%)	21.5 (–55.3 to 39.2)	0.36
Severity (severe or not)	5 (28%)	–36.3 (–77.3 to 4.7)	**0.04**
Stomatitis	11 (85%)	27.9 (–34.1 to 88.8)	0.35
Abdominal symptoms	8 (62%)	21.2 (–33.5 to 60.0)	0.55
Probiotics	1 (8%)	11.3 (–72.4 to 95.0)	0.61
Immunosuppressants	5 (28%)	–41.0 (–78.0 to –3.9)	**0.02**

Statistical analyses were performed using the two-tailed t-test for ordinal scale or regression analysis for continuous scale. Bold indicates a significant difference. OTU, operational taxonomic unit; IQR, interquartile range.

subsets of T cells in intestinal lamina propria was associated with X-linked severe combined immunodeficiency (Clarke et al., 2018).

The mechanism that causes dysbiosis in patients with HA20 is mediated by Tregs because it is a key factor of immunoregulatory disorders in patients with HA20 (Liu et al., 2021), and in the mouse model of Treg-associated monogenic autoimmune disorders, *Aire* knockout mouse showed significant dysbiosis (Dobeš et al., 2015). Mouse models, *Aire*-deficient mice (Gray et al., 2007), and *Foxp3* knockout mice (Chinen et al., 2010) exhibit an autoimmune phenotype even in germ-free conditions, and it was concluded that these diseases are independent of commensal microbial regulation (Liu et al., 2021). Conversely, the Treg-depleted model showed more severe inflammation in the small intestine of specific pathogen-free mice than germ-free mice, which indicates that the disease severity is associated with the microbiome (Liu et al., 2021). These findings indicate the possible association between disease severity and gut dysbiosis. Additionally, data from this study showed a significant correlation between disease severity and dysbiosis. The use of immunosuppressants, an alternative indicator of disease severity, also correlated with dysbiosis.

Another possible mechanism of dysbiosis is metabolism. A mouse model lacking A20 in specific dendritic cells reported aberrant expression of antibacterial peptides and luminal dysbiosis (Talpin et al., 2019).

Ten of 18 patients with HA20 were treated with immunosuppressants (Kadowaki et al., 2020), and one refractory patient successfully received hematopoietic cell transplantation (Shiraki et al., 2021). However, less invasive therapy would be required. Successful fecal microbiota transplantation (FMT) is reported in patients with HIV (Serrano-Villar et al., 2021) and the mouse model of Behcet's disease (Ye et al., 2018), while there is no evidence of FMT in patients with IEIs including HA20. Further study is required to clarify the mechanism of dysbiosis in patients with HA20 and IEIs, to determine the biomarker of the disease, and to discover if FMT works or not.

Several monogenic IEIs inform us how the disease-specific immune dysfunction causes disease-specific dysbiosis.

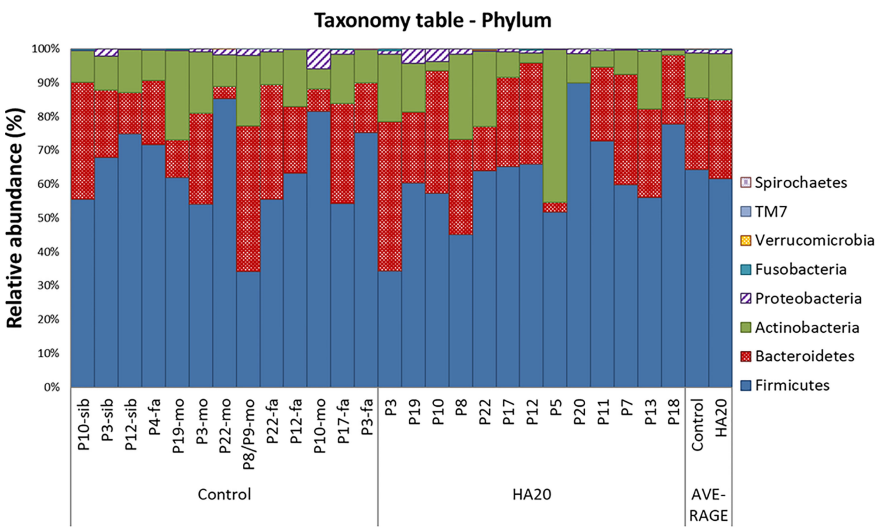

FIGURE 3 | The composition of gut bacterial microbiota. The global composition of bacterial microbiota at the phylum level for the indicated groups. The healthy family members (left) and patients (middle) are represented in order of age. The two bars on the right are average values. P, patient; fa, Father; mo, mother; sib, sibling.

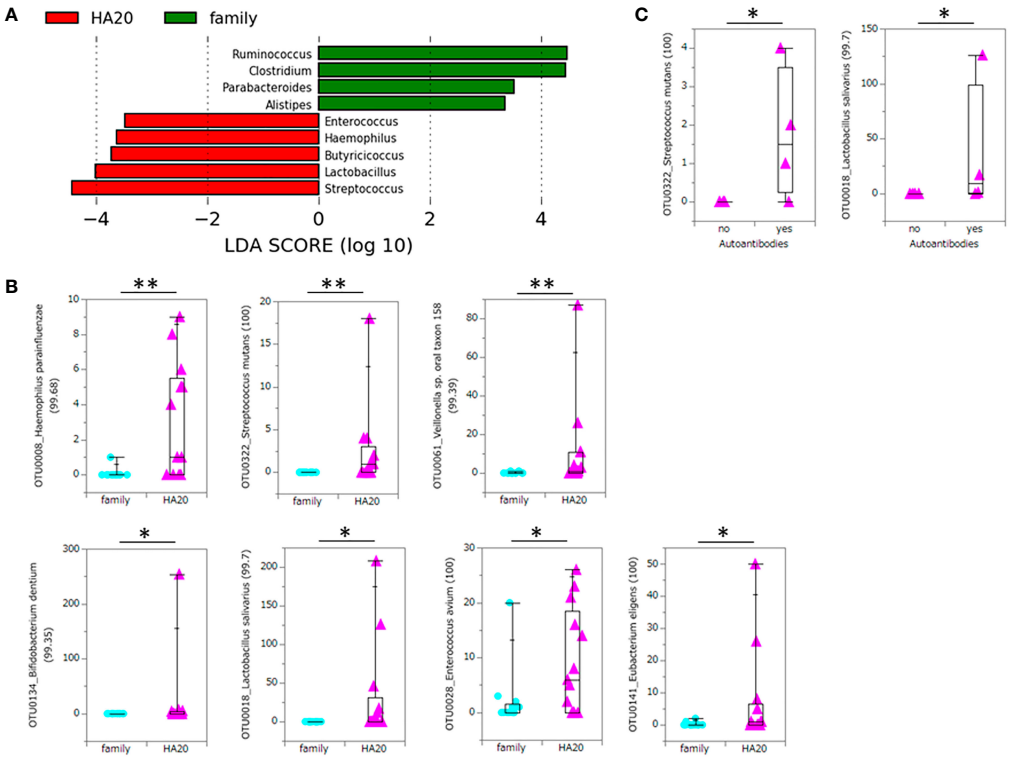

FIGURE 4 | Significant increase or decrease of bacteria at the genus level and increase at the OTU level. The LDA score of patients with HA20 compared with their family members (Kruskal–Wallis test $p < 0.05$ and LDA score (log10) > 2) are represented. **(A)** The increased OTUs in patients with HA20 compared with their family members. **(B)** and the increased OTUs in patients with autoantibodies compared with those without antibodies. **(C)** Their closest species or strain and percentage similarity (%) in the Ribosomal Database Project (RDP) database are indicated. Box plot indicates the median value, and lower and upper quartiles. p-Values are calculated using the Wilcoxon rank-sum test. *$p < 0.05$, **$p < 0.01$. OTU, operational taxonomic unit; LDA, linear discriminant analysis; HA20, haploinsufficiency of A20.

Collectively, we can easily understand how the complex immune systems respond to various microorganisms. This study showed that *S. mutans* and *L. salivarius* significantly increased in both patients with HA20, those with autoantibodies compared with family members and patients without autoantibodies, respectively. Since the sample size was small for statistical analysis (13 *vs.* 13, and 4 *vs.* 5, respectively), statistical significance in two manners was rare enough to reject the null hypothesis. Also, although the close mechanism remains unclear, it was suggested that these two OTUs might be associated with autoimmune onset.

In the context of statistical analysis, we excluded patients younger than 3 years and/or patients with antibiotics use because they present a confounding bias for microbiota (Hopkins et al., 2002; Yatsunenko et al., 2012; Ramirez et al., 2020). However, our data suggested that lower age is the explanatory variable for lower Shannon index, not for OTU numbers. This potential confounding bias is statistically a problem but not clinically crucial. Considering clinical management, both lower age and antibiotics use affect disease severity as well as microbiome diversity. Indeed, the excluded patients based on antibiotics use [previously described as P4, P9, and P21 (Kadowaki et al., 2018)] were relatively younger (4, 1, and 3 years old, respectively) and more severe (P4 and P9 are moderate; P21 is severe) than the included patients. Early-onset patients could be regarded as more strongly influenced by genetics and so potentially more severe than late-onset patients.

This study has several limitations. Firstly, clinical heterogeneity exists among medications, such as probiotics and antibiotics. The potential confounding factor is underestimated because of the small sample size. Secondly, because of rare diseases, it is difficult to collect more fecal samples for statistical analysis of the potential confounding factor described. Multivariate analysis was unfeasible due to small samples. Thirdly, not all patients with HA20 received gastrointestinal endoscopy, and so alternative indicators such as the disease severity or abdominal symptoms do not necessarily reflect the exact intestinal condition.

CONCLUDING REMARKS

We investigated the intestinal microbiome composition in patients with HA20 and identified that seven OTUs significantly increased in the patients. In particular, *S. mutans* and *L. salivarius* significantly increased in patients with HA20 and autoantibodies, and these OTUs were associated with autoimmune onset.

DATA AVAILABILITY STATEMENT

The datasets for this article are not publicly available as regards participant/patient anonymity. Requests to access the datasets should be forwarded to the corresponding author.

ETHICS STATEMENT

Written informed consent was obtained from patients or their parents. This study was conducted following the Declaration of Helsinki and approved by the ethics boards of Tokyo Medical and Dental University and Keio University.

AUTHOR CONTRIBUTIONS

ET, KT, and YK contributed to data management. KT, YK, WS, HM, WS, and MH conducted DNA sequencing and bioinformatics analysis. HO and HK managed sample recruitment. HO, TK, RN, KN, CK, TE, TS, and YI contributed to sample collection. ET, KT, and HK wrote the manuscript. TM and KH provided critical discussion. HK designed and managed the project. All authors read and approved the final manuscript.

FUNDING

This work was partly supported by MEXT/JSPS KAKENHI (Grant Number: JP17K10099) and Naoki Tsuchida Research Grant to HK.

ACKNOWLEDGMENTS

We appreciate the patients and their families for their participation in this study. We express gratitude to Mayako Asakawa for technical support and members of the JSR-Keio University Medical and Chemical Innovation Center for conducting the meta-16S rRNA gene sequencing. We also express gratitude to Kazushi Izawa at the Department of Pediatrics, Kyoto University Hospital, for collecting clinical information for revision.

SUPPLEMENTARY MATERIAL

The Supplementary Material for this article can be found online at: https://www.frontiersin.org/articles/10.3389/fcimb.2021.787667/full#supplementary-material

REFERENCES

Anderson, M. J. (2017). *Permutational Multivariate Analysis of Variance (PERMANOVA)* (Wiley StatsRef), 1–15. Stat Ref Online. doi: 10.1002/9781118445112.stat07841

Berbers, R. M., Franken, I. A., and Leavis, H. L. (2019). Immunoglobulin A and Microbiota in Primary Immunodeficiency Diseases. *Curr. Opin. Allergy Clin. Immunol.* 19, 563–570. doi: 10.1097/ACI.0000000000000581

Chinen, T., Volchkov, P. Y., Chervonsky, A. V., and Rudensky, A. Y. (2010). A Critical Role for Regulatory T Cell-Mediated Control of Inflammation in the Absence of Commensal Microbiota. *J. Exp. Med.* 207, 2323–2330. doi: 10.1084/jem.20101235

Clarke, E. L., Connell, A. J., Six, E., Kadry, N. A., Abbas, A. A., Hwang, Y., et al. (2018). T Cell Dynamics and Response of the Microbiota After Gene Therapy to Treat X-Linked Severe Combined Immunodeficiency. *Genome Med.* 10, 70. doi: 10.1186/s13073-018-0580-z

Dobeš, J., Neuwirth, A., Dobešová, M., Vobořil, M., Balounová, J., Ballek, O., et al. (2015). Gastrointestinal Autoimmunity Associated With Loss of Central Tolerance to Enteric α-Defensins. *Gastroenterology* 149, 139–150. doi: 10.1053/j.gastro.2015.05.009

Gray, D. H. D., Gavanescu, I., Benoist, C., and Mathis, D. (2007). Danger-Free Autoimmune Disease in Aire-Deficient Mice. *Proc. Natl. Acad. Sci. U. S. A.* 104, 18193–18198. doi: 10.1073/pnas.0709160104

Hartono, S., Ippoliti, M. R., Mastroianni, M., Torres, R., and Rider, N. L. (2019). Gastrointestinal Disorders Associated With Primary Immunodeficiency Diseases. *Clin. Rev. Allergy Immunol.* 57, 145–165. doi: 10.1007/s12016-018-8689-9

Hopkins, M. J., Sharp, M., and Macfarlane, G. T. (2002). Variation in Human Intestinal Microbiota With Age. *Dig. Liver Dis.* 24, S12–S18. doi: 10.1016/s1590-8658(02)80157-8

Jørgensen, S. F., Trøseid, M., Kummen, M., Anmarkrud, J. A., Michelsen, A. E., Osnes, L. T., et al. (2016). Altered Gut Microbiota Profile in Common Variable Immunodeficiency Associates With Levels of Lipopolysaccharide and Markers of Systemic Immune Activation. *Mucosal Immunol.* 9, 1455–1465. doi: 10.1038/mi.2016.18

Kadowaki, T., Ohnishi, H., Kawamoto, N., Hori, T., Nishimura, K., Kobayashi, C., et al. (2018). Haploinsufficiency of A20 Causes Autoinflammatory and Autoimmune Disorders. *J. Allergy Clin. Immunol.* 141, 1485–1488.e11. doi: 10.1016/j.jaci.2017.10.039

Kadowaki, T., Ohnishi, H., Kawamoto, N., Kadowaki, S., Hori, T., Nishimura, K., et al. (2020). Immunophenotyping of A20 Haploinsufficiency by Multicolor Flow Cytometry. *Clin. Immunol.* 216, 108441. doi: 10.1016/j.clim.2020.108441

Kakihana, K., Fujioka, Y., Suda, W., Najima, Y., Kuwata, G., Sasajima, S., et al. (2016). Fecal Microbiota Transplantation for Patients With Steroid-Resistant Acute Graft-Versus-Host Disease of the Gut. *Blood* 128, 2083–2088. doi: 10.1182/blood-2016-05-717652

Kim, S. W., Suda, W., Kim, S., Oshima, K., Fukuda, S., Ohno, H., et al. (2013). Robustness of Gut Microbiota of Healthy Adults in Response to Probiotic Intervention Revealed by High-Throughput Pyrosequencing. *DNA Res.* 20, 241–253. doi: 10.1093/dnares/dst006

Konstantinidis, K. T., and Tiedje, J. M. (2005). Genomic Insights That Advance the Species Definition for Prokaryotes. *Proc. Natl. Acad. Sci. U. S. A.* 102, 2567–2572. doi: 10.1073/pnas.0409727102

Liu, Y., Freeborn, J., Armbrister, S. A., Tran, D. Q., and Rhoads, J. M. (2021). Treg-Associated Monogenic Autoimmune Disorders and Gut Microbial Dysbiosis. *Pediatr. Res.* 91(1), 35–43. doi: 10.1038/s41390-021-01445-2

Liu, Y., Tran, D. Q., Lindsey, J. W., and Rhoads, J. M. (2021). The Association of Gut Microbiota and Treg Dysfunction in Autoimmune Diseases. *Adv. Exp. Med. Biol.* 1278, 191–203. doi: 10.1007/978-981-15-6407-9_10

Ono, S., Takeshita, K., Kiridoshi, Y., Kato, M., Kamiya, T., Hoshino, A., et al. (2021). Hematopoietic Cell Transplantation Rescues Inflammatory Bowel Disease and Dysbiosis of Gut Microbiota in XIAP Deficiency. *J. Allergy Clin. Immunol. Pract.* 9 (10), 3767–3780. doi: 10.1016/j.jaip.2021.05.045

Ramirez, J., Guarner, F., Bustos Fernandez, L. B., Maruy, A., Sdepanian, V. L., and Cohen, H. (2020). Antibiotics as Major Disruptors of Gut Microbiota. *Front. Cell. Infect. Microbiol.* 10, 572912. doi: 10.3389/fcimb.2020.572912

Segata, N., Izard, J., Waldron, L., Gevers, D., Miropolsky, L., Garrett, W. S., et al. (2011). Metagenomic Biomarker Discovery and Explanation. *Genome Biol.* 12, R60. doi: 10.1186/gb-2011-12-6-r60

Serrano-Villar, S., Talavera-Rodríguez, A., Gosalbes, M. J., Madrid, N., Pérez-Molina, J. A., Elliott, R. J., et al. (2021). Fecal Microbiota Transplantation in HIV: A Pilot Placebo-Controlled Study. *Nat. Commun.* 12, 1139. doi: 10.1038/s41467-021-21472-1

Shiraki, M., Williams, E., Yokoyama, N., Shinoda, K., Nademi, Z., Matsumoto, K., et al. (2021). Hematopoietic Cell Transplantation Ameliorates Autoinflammation in A20 Haploinsufficiency. *J. Clin. Immunol.* 41 (8), 1954–1956. doi: 10.1007/s10875-021-01124-1

Singleton, D. R., Furlong, M. A., Rathbun, S. L., and Whitman, W. B. (2001). Quantitative Comparisons of 16S rRNA Gene Sequence Libraries From Environmental Samples. *Appl. Environ. Microbiol.* 67, 4374–4376. doi: 10.1128/AEM.67.9.4374-4376.2001

Sokol, H., Mahlaoui, N., Aguilar, C., Bach, P., Lambert, O. J., Garraffo, A., et al. (2016). Intestinal Dysbiosis in Inflammatory Bowel Disease Associated With Primary Immunodeficiency. *J. Allergy Clin. Immunol.* 143, 775–778.e6. doi: 10.1016/j.jaci.2018.09.021

Stackebrandt, E., and Goebel, B. M. (1994). Taxonomic Note: A Place for DNA-DNA Reassociation and 16S rRNA Sequence Analysis in the Present Species Definition in Bacteriology. *Int. J. Syst. Bacteriol.* 44, 846–849. doi: 10.1099/00207713-44-4-846

Talpin, A., Kattah, M. G., Advincula, R., Fadrosh, D., Lynch, K., LaMere, B., et al. (2019). A20 in Dendritic Cells Restrains Intestinal Anti-Bacterial Peptide Expression and Preserves Commensal Homeostasis. *PloS One* 14, e0218999. doi: 10.1371/journal.pone.0218999

Varricchi, G., Poto, R., Ianiro, G., Punziano, A., Marone, G., Gasbarrini, A., et al. (2021). Gut Microbiome and Common Variable Immunodeficiency: Few Certainties and Many Outstanding Questions. *Front. Immunol.* 12, 712915. doi: 10.3389/fimmu.2021.712915

Yatsunenko, T., Rey, F. E., Manary, M. J., Trehan, I., Dominguez-Bello, M. G., Contreras, M., et al. (2012). Human Gut Microbiome Viewed Across Age and Geography. *Nature* 486, 222–227. doi: 10.1038/nature11053

Ye, Z., Zhang, N., Wu, C., Zhang, X., Wang, Q., Huang, X., et al. (2018). A Metagenomic Study of the Gut Microbiome in Behcet's Disease. *Microbiome* 6, 135. doi: 10.1186/s40168-018-0520-6

Zhang, L., Li, Y. Y., Tang, X., and Zhao, X. (2020). Faecal Microbial Dysbiosis in Children With Wiskott–Aldrich Syndrome. *Scand. J. Immunol.* 91, e12805. doi: 10.1111/sji.12805

Conflict of Interest: KH is a scientific advisory board member of Vedanta Biosciences and 4BIO CAPITAL. YK is an employee of JSR Corporation.

The remaining author declares that the research was conducted in the absence of any commercial or financial relationships that could be construed as a potential conflict of interest.

Publisher's Note: All claims expressed in this article are solely those of the authors and do not necessarily represent those of their affiliated organizations, or those of the publisher, the editors and the reviewers. Any product that may be evaluated in this article, or claim that may be made by its manufacturer, is not guaranteed or endorsed by the publisher.

frontiers in Cellular and Infection Microbiology

ORIGINAL RESEARCH
published: 31 January 2022
doi: 10.3389/fcimb.2022.759077

ASB17 Facilitates the Burst of LPS-Induced Inflammation Through Maintaining TRAF6 Stability

Pin Wan[1†], Ge Yang[2†], Simeng Zhang[1], Yaru Zhang[1], Yaling Jia[1], Xu Che[1], Zhen Luo[1,3], Pan Pan[4], Geng Li[1,3], Xulin Chen[1,3], Qiwei Zhang[1,3], Wen Zhang[5], Qiuping Tan[5], Yongkui Li[1,3] and Jianguo Wu[1,2,3,4*]*

[1] Guangdong Provincial Key Laboratory of Virology, Institute of Medical Microbiology, Jinan University, Guangzhou, China, [2] State Key Laboratory of Virology, College of Life Sciences, Wuhan University, Wuhan, China, [3] Foshan Institute of Medical Microbiology, Foshan, China, [4] The First Affiliated Hospital of Jinan University, Jinan University, Guangzhou, China, [5] Guangdong Longfan Biological Science and Technology, Foshan, China

OPEN ACCESS

Edited by:
Daniele Dessì,
University of Sassari, Italy

Reviewed by:
Donna A. MacDuff,
University of Illinois at Chicago, United States
Maria Foti,
University of Milano-Bicocca, Italy

***Correspondence:**
Yongkui Li
lyk070@jnu.edu.cn
Jianguo Wu
jwu898@jnu.edu.cn

[†]These authors have contributed equally to this work and share first authorship

Specialty section:
This article was submitted to Microbes and Innate Immunity, a section of the journal Frontiers in Cellular and Infection Microbiology

Received: 15 August 2021
Accepted: 06 January 2022
Published: 31 January 2022

Citation:
Wan P, Yang G, Zhang S, Zhang Y, Jia Y, Che X, Luo Z, Pan P, Li G, Chen X, Zhang Q, Zhang W, Tan Q, Li Y and Wu J (2022) ASB17 Facilitates the Burst of LPS-Induced Inflammation Through Maintaining TRAF6 Stability. Front. Cell. Infect. Microbiol. 12:759077. doi: 10.3389/fcimb.2022.759077

ASB17, a member of the ankyrin repeat and SOCS box-containing protein (ASB) family, has been supposed to act as an E3 ubiquitin ligase. Actually, little is known about its biological function. In this study, we found that ASB17 knocking-out impaired the expression of the pro-inflammatory cytokines CCL2 and IL-6 in bone marrow-derived dendritic cells (BMDCs) stimulated by lipopolysaccharide (LPS), indicating an inflammation-promoting role of this gene. We reveal that ASB17 promotes LPS-induced nuclear factor kappa B (NF-κB) signal activation through interacting with TNF receptor-associated factor 6 (TRAF6) which is a crucial adaptor protein downstream of toll-like receptors (TLR). ASB17 *via* its aa177–250 segment interacts with the Zn finger domain of TRAF6. The interaction of ASB17 stabilizes TRAF6 protein through inhibiting K48-linked TRAF6 polyubiquitination. Therefore, we suggest that ASB17 facilitates LPS-induced NF-κB activation by maintaining TRAF6 protein stability. The inflammation enhancer role of ASB17 is recognized here, which provides new understanding of the activation process of inflammation and immune response.

Keywords: ASB17, NF-κB, TRAF6, K48-linked polyubiquitination, inflammatory cytokine

INTRODUCTION

The ankyrin repeat and suppressor of cytokine signaling (SOCS) box-containing protein (ASB) family containing 18 members has been identified as an E3 ubiquitin ligase family (Kohroki et al., 2005; Liu et al., 2019). ASB1, ASB2, and ASB12 have been found to form complexes respectively with Cullin5–Rbx2 and have E3 Ub ligase activity (Kohroki et al., 2005). ASB7 ubiquitinates DDA3 for degradation to regulate spindle dynamics and genome integrity (Uematsu et al., 2016). ASB9 targets ubiquitous mitochondrial creatine kinase (uMtCK) and negatively regulates cell growth (Kwon et al., 2010). ASB11 mediates BIK ubiquitination and degradation to determine cell fate during different cellular stresses (Chen et al., 2019). Like other members of the ASB family, ASB17 protein contains two ankyrin repeats and one SOCS box (Guo et al., 2004). We recently reported that ASB17 mediates cell apoptosis in the testis by ubiquitylating and degrading BCLW and MCL1 (Yang et al., 2021). Through a study with ASB17 KO mice, we found that ASB17 was involved in cytokine regulation, so its

biological function in inflammatory signaling was investigated in this work. Importantly, here we report a novel distinguishing activity of ASB17 showing that it functions as a ubiquitination inhibitor in regulation of the NF-κB signal pathway.

Cellular inflammatory signals are generally activated by microbial components *via* pattern recognition receptors (PRRs) such as toll-like receptors (TLRs), retinoid acid-inducible gene-I (RIG-I)-like receptors, and DNA-recognizing receptors (Kawai and Akira, 2010). TNF receptors and the interleukin-1 receptor (IL-1R) activate the subsequent downstream signaling of inflammation when cytokine ligands are induced (Gabay et al., 2010; Hayden and Ghosh, 2014). Tumor necrosis factor (TNF) receptor-associated factor 6 (TRAF6) functions as a crucial adaptor protein that mediates signaling events from the TLR family, IL-1 receptor, and TNF receptor superfamily (Cao et al., 1996; Chung et al., 2007). Thus, TRAF6 play important roles in the activation process of inflammation and immune response. When these receptors are triggered by their ligands, they activate TRAF6 to exert its E3 Ub ligase activity. TRAF6 forms a ubiquitin-binding enzyme complex with Ubc13 and Uev1A to attach lysine 63 (K63)–linked polyubiquitin chains to the substrates (Deng et al., 2000). TRAF6 also attaches K63-linked polyubiquitin chains to itself, which is required for triggering the activation of canonical NF-κB (Lamothe et al., 2008). TRAF6 attached with K63-linked polyubiquitin can recruit TAK1 and phosphorylate the IkB kinase complex IKKα/β/γ, leading to NF-κB activation (Deng et al., 2000). The TRAF6-mediated NF-κB signal pathway is involved in multiple pathological processes and especially essential for inflammatory diseases, which makes TRAF6 become a key modulating target of inflammation (Dainichi et al., 2019). TRAF6 can be ubiquitylated by a K48-linked polyubiquitin form, which leads to its proteasomal degradation. BICP0 and TRIM38 negatively regulate TRAF6-mediated NF-κB by promoting the K48-linked ubiquitination and degradation of TRAF6 (Zhao et al., 2012; Cao et al., 2019). Given the significant relevance of TRAF6-mediated NF-κB in inflammation activation, the modulation on TRAF6 can determine the pathological process of many inflammatory diseases (Du et al., 2017; Lv et al., 2018; Matsumoto et al., 2018; Wu et al., 2020). In this study, we recognize ASB17 as a TRAF6-stabilizing factor which enhances LPS-induced NF-κB activation. ASB17 facilitates the induction of pro-inflammatory cytokines *via* suppressing TRAF6 K48-linked ubiquitination. These will provide more knowledge about the TRAF6-mediated NF-κB signal pathway.

MATERIALS AND METHODS

Animal Study

Asb17 deficiency mice with the *Asb17* Exon 1 (1,595 bp) deleted were reserved by our laboratory (Yang et al., 2021). All animal experiments were approved by the Institutional Animal Care and Use Committee (IACUC) of the College of Life Sciences, Wuhan University (permit number: WDSKY0201901).

Cells

THP-1 (human myeloid leukemia mononuclear cell line) and HEK293T (human embryonic kidney cell line) were purchased from the China Center of Type Culture Collection (CCTCC) (Wuhan, China). HEK293T cells were cultured in DMEM purchased from Gibco (Grand Island, NY, USA) supplemented with 10% fetal bovine serum (FBS), 100 U/ml penicillin, and 100 μg/ml streptomycin sulfate. THP-1 cells were cultured in RPMI 1640 and purchased from Gibco supplemented with 10% FBS, 100 U/ml penicillin, and 100 μg/ml streptomycin sulfate. Bone marrow-derived dendritic cells (BMDCs) were isolated from the femoral and tibia bone marrow of 6–8-week-old mice. Briefly, the bone marrow was flushed with RPMI 1640. Extracted cells were resuspended and passed through a 200-pore-sized mesh. Collected cells were resuspended in BMDC culture medium, which was made from RPMI 1640 medium containing 10% FBS, 100 U/ml streptomycin, 100 U/ml penicillin, and 20 ng/ml recombinant mouse granulocyte macrophage-colony stimulating factor (GM-CSF) in a 100-mm Petri dish. On the third day, 10 ml BMDC culture medium was added into the Petri dish. On the sixth and eighth days, the medium was changed in half: the old culture medium was collected and centrifuged, and the cell pellet was resuspended in the complete medium containing 20 ng/ml recombinant mouse GM-CSF, and then the cell suspension was returned to the original dish. On the tenth day, the culture medium was gently pipetted to collect the suspended cells and centrifuged at room temperature. The supernatant was discarded, while the cell pellet was resuspended in complete medium containing 10 ng/ml recombinant mouse GM-CSF and then spread on a cell culture plate at 37°C and 5% CO_2.

Bone marrow-derived macrophages (BMDMs) were isolated from the bone marrow of 6–8-week-old mice; these experiments were performed as described previously (Wan et al., 2019). Briefly, the bone marrow was flushed with RPMI 1640. Collected cells were resuspended and passed through a 200-pore sized mesh. Collected cells were resuspended with Red Blood Cell Lysis Buffer for 5 min, then collected cells were cultured in DMEM complemented with 10% FBS, 10%–20% L929 cell-conditioned medium, 100 μg/ml streptomycin sulfate, and 100 U/ml penicillin for 5–6 days.

Reagents

Lipopolysaccharide (LPS) (Cat# L2630) and polybrene (Cat# TR-1003-G) were purchased from Sigma-Aldrich (St. Louis, MO, USA). Puromycin (Cat# ant-pr-1) was purchased from InvivoGene Biotech Co., Ltd. (San Diego, CA, USA). Cycloheximide (CHX) was purchased from Selleck (Houston, TX, USA). Protease Inhibitor Cocktail Tablets were purchased from Roche (Indianapolis, IN, USA). TRIzol reagent and Lipofectamine 2000 transfection reagent (Cat# 11668019) were purchased from Invitrogen (Carlsbad, CA, USA). Mouse GM-CSF (Cat#315-03) were purchased from PeproTech (Rocky Hill, NJ, USA).

Antibodies

Anti-IRAK1 (D51G7) (Cat#4504), anti-TRAF6 (D21G3) (Cat#8028), anti-Myc (9B11) (Cat#2276), anti-ubiquitin

(P4D1) (Cat#3936), anti-K48-linkage-specific polyubiquitin (D9D5) (Cat#8081), anti-K63-linkage-specific polyubiquitin (D7A11) (Cat#5621), anti-p65 (Cat#8242), and anti-phospho-p65 (Ser536) (Cat#3033) were purchased from Cell Signaling Technology (Beverly, MA, USA).Anti-TRAF6 (Cat#ab137452) was purchased from Abcam (Cambridge, MA, USA). Anti-Flag (Cat# F3165) and anti-HA (Cat# H6908) antibodies were purchased from Sigma-Aldrich. Anti-TRAF6 (Cat# 66498-1-lg) and anti-GAPDH (Cat# 60004-1-lg) were purchased from Proteintech (Wuhan, Hubei, China). Anti-Rabbit IgG FITC (Cat# A22120) and anti-Mouse IgG DyLight 649 (Cat# A23610) antibodies were purchased from Abbkine.

Plasmids and Constructions

Candidate genes were cloned into pcDNA3.1(+)-3Flag vector or pCAGGS-HA vector. TRAF2, TRAF3, TRAF5, TRAF6, IRF7, STING, IRF3, TBK1, and ASB17 were cloned into the pcDNA3.1 (+)-3Flag vector. NLRP3-PYD, ASB17, and NLRP3 were cloned into the pCAGGS-HA vector. NLRP3 point mutant and truncated ASB17 genes were cloned into the pcDNA3.1-3Flag vector. All recombinant plasmids were confirmed by DNA sequencing.

Western Blot Analysis

For Western blot analysis, cells were lysed in lysis buffer. Cell lysates were separated by 7.5%–10% SDS-polyacrylamide gel electrophoresis (SDS-PAGE) and then transferred onto a nitrocellulose (NC) membrane. The membranes were sealed in phosphate-buffered saline with 0.1% Tween 20 (TBST) containing 5% non-fat dried milk for 45 min at room temperature (RT) and then were incubated with first antibodies at 4°C overnight. Next, the membranes were incubated with second antibodies for 45 min at RT. Finally, the membranes were detected with the Clarity™ Western ECL Substrate (Bio-Rad).

Co-Immunoprecipitation

The cells were washed with pre-cold PBS for three times and lysed in RIPA lysis buffer (50 mM Tris–HCl (pH 7.4), 150 mM NaCl, 1% (vol/vol) NP-40, 1 mM EDTA, and 5% (vol/vol) glycerol) containing protease inhibitor cocktails. After 20 min, the lysed samples were centrifuged for 10 min at 4°C. A part of the lysates was saved as control. For immunoprecipitation, the rest of the lysates were incubated with the indicated antibodies at 4°C overnight and then incubated with protein G agarose for 2 h. The beads were washed for 5–7 times by RIPA washing buffer (50 mM Tris–HCl (pH 7.4), 300 mM NaCl, 1% (vol/vol) NP-40, 1 mM EDTA, and 5% (vol/vol) glycerol) and then reconstituted in 50 μl 2× SDS loading buffer. All targeted protein bands were immunoblotted with the indicated antibodies.

Quantitative PCR

Total RNA was extracted with TRIzol reagent, following the manufacturer's instructions. The mRNA was then used to create cDNA by using the M-MLV Reverse Transcriptase (Promega). Real-time quantitative RT-PCR was performed by using SYBR Green PCR Master Mix in the Roche LC480 following the manufacturer's instructions. All real-time PCR primers were designed in Nucleotide of National Center for Biotechnology Information (NCBI). The following primers were used:

human GAPDH-F: 5′-AAGGCTGTGGGCAAGG-3′;
human GAPDH-R: 5′-TGGAGGAGTGGGTGTCG-3′;
human ASB17-F: 5′-CTGGGTTTTTGCCAGAAAAGGT-3′;
human ASB17-R: 5′-TGCCACTTAATGGGCTTGGA-3′;
human CCL2-F: 5′-GCTCAGCCAGATGCAATCAA-3′;
human CCL2-R: 5′-GACACTTGCTGCTGGTGATTC-3′;
human IL-6-F: 5′-ACCCCTGACCCAACCACAAAT-3′;
human IL-6-R: 5′-AGCTGCGCAGAATGAGATGAGTT-3′;
human IL-1β-F: CACGATGCACCTGTACGATCA;
human IL-1β-R: GTTGCTCCATATCCTGTCCCT;
human IP-10-F: GCCATTCTGATTTGCTGCCT;
human IP-10-R: TTGATGGCCTTCGATTCTGGA;
mouse GAPDH-F: 5′-TTCACCACCATGGAGAAGGC-3′;
mouse GAPDH-R: 5′-GGCATCGACTGTGGTCATGA-3′;
mouse CCL2-F: 5′-GACCCCAAGAAGGAATGGGT-3′;
mouse CCL2-R: 5′-ACCTTAGGGCAGATGCAGTT-3′;
mouse IL-6-F: 5′-CAACGATGATGCACTTGCAGA-3′;
mouse IL-6-R: 5′-TGACTCCAGCTTATCTCTTGGT-3′;
mouse ASB17-F: 5′-TAGTTAAGCGGCCCTCTCTG-3′;
mouse ASB17-R: 5′-GTCAAAGCCGTCCAAGTCAAC-3′;
Mouse IL-1β-F: CTGGTGTGTGACGTTCCCAT;
Mouse IL-1β-R:GTGGGTGTGCCGTCTTTCAT;
Mouse IP-10-F: ATGACGGGCCAGTGAGAATG;
Mouse IP-10-R:CGGATTCAGACATCTCTGCTCAT.

Lentiviral Production and Infection

The pLenti-CMV vector was derived from the pLenti-CMV-GFP-Puro vector (Addgene, 17448). 3Flag-ASB17 (human) and 3Flag-Asb17 (mouse) were cloned and constructed into pLenti-CMV to generate lentiviruses. pLenti-3Flag-ASB17 (or pLenti-3Flag-Asb17), pMD2.G, and psPAX2 plasmids were co-transfected into HEK293T cells to generate lentivirus. HEK293T cell culture supernatants were harvested at 36 and 48 h after transfection. The culture supernatants were filtered through a 0.45-μm filter. THP-1 cells were infected with the lentivirus plus 8 μg/ml polybrene for 24–36 h. Next, 1 μg/ml puromycin was added into the culture supernatants for selection of THP-1 stably expressing ASB17 cells. After 5–7 days, THP-1 stably expressing ASB17 cells were identified by qPCR and immunoblot analysis.

Immunofluorescence Microscopy

For immunofluorescence staining, the cells were washed three times with pre-cold PBS and fixed with 4% paraformaldehyde for 15 min. Then, the cells were permeabilized with PBS containing 0.5% Triton X-100 for 5 min and then blocked with PBS containing 5% bovine serum albumin (BSA) for 45 min at room temperature. Then, the cells were incubated with the indicated antibody at 4°C overnight, followed by incubation with anti-Mouse IgG DyLight 649 and anti-Rabbit IgG FITC at room temperature for 2 h. After washing three times, the cells were incubated with DAPI for 5 min in 37°C. Finally, the cells were analyzed using a confocal laser scanning microscope (FluoView FV1000; Olympus, Tokyo, Japan).

In Vivo Ubiquitination Assay

Cells were lysed with 100 μl lyses buffer. After heating at 95°C for 5 min, lysates were diluted 10-fold with dilution buffer containing protease inhibitors. A part of the lysates was saved as input, and the rest of the lysates were immunoprecipitated with indicated antibodies. The rest of the procedures followed the Co-IP assays.

Statistical Analyses

All experiments were reproducible and each set was repeated at least three times. For data with a normal distribution and homogeneity of variance, differences between two groups were statistically analyzed by a two-tailed Student's *t*-test. Statistical significance was valued based on the *p* value. * indicates $p < 0.05$; ** indicates $p < 0.01$; and *** indicates $p < 0.001$. $p < 0.05$ was considered statistically significant.

RESULTS

ASB17 Deficiency Inhibits LPS-Mediated NF-κB Activation in BMDCs

The detection of Asb17 in mouse organs displayed that it mainly expressed in testis (Kim et al., 2004). However, the expression of this gene was detectable in bone marrow-derived macrophages (BMDMs) and dendritic cells (BMDCs) (**Figure 1A**). Especially,

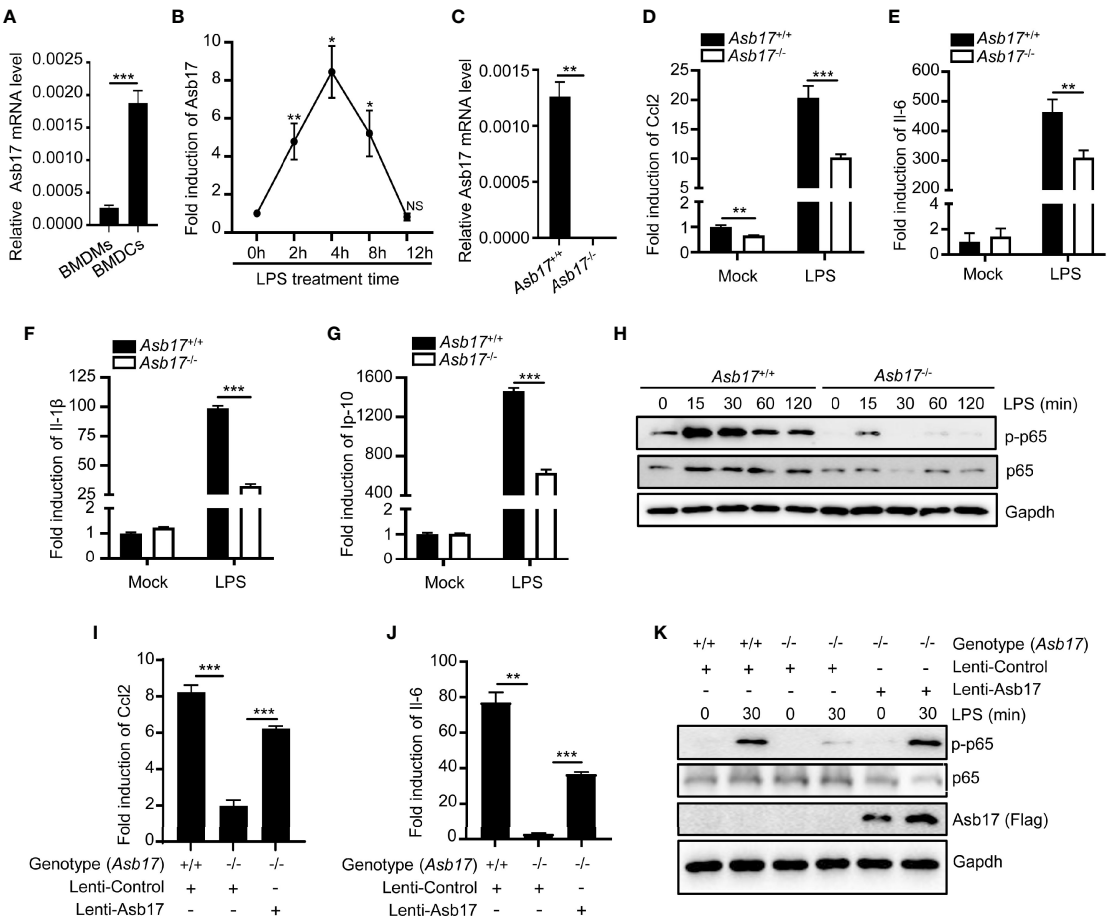

FIGURE 1 | ASB17 deficiency inhibits LPS-mediated NF-κB activation in BMDCs. **(A)** BMDMs and BMDCs were isolated from wild-type mice; the mRNA expression of ASB17 in BMDMs and BMDCs were analyzed by qPCR. **(B)** BMDCs were isolated from wild-type mice and were stimulated by LPS (1 μg/ml) in different timepoints (0, 2, 4, 8, and 12 h), and the mRNA expression of ASB17 in BMDCs were analyzed by qPCR. **(C)** BMDCs were isolated from *ASB17*$^{+/+}$ and *ASB17*$^{-/-}$ mice, the mRNA expression of ASB17 in BMDCs were analyzed by qPCR. **(D–G)** BMDCs were isolated from *ASB17*$^{+/+}$ and *ASB17*$^{-/-}$ mice and were stimulated by LPS (1 μg/ml) for 0 and 2 h; the mRNA expression of CCL2 **(D)**, IL-6 **(E)**, IL-1β **(F)**, and IP-10 **(G)** in BMDCs were analyzed by qPCR. **(H)** BMDCs were isolated from *ASB17*$^{+/+}$ and *ASB17*$^{-/-}$ mice and were stimulated by LPS (1 μg/ml) in different timepoints (0, 15, 30, 60, and 120 min); the protein levels of p65 and phosph-p65 in BMDCs were analyzed by Western blotting. **(I, J)** BMDCs were isolated from *ASB17*$^{+/+}$ and *ASB17*$^{-/-}$ mice, and ASB17 was overexpressed in *ASB17*$^{-/-}$ BMDCs by infecting with the recombinant lentivirus. All cells were stimulated by LPS (1 μg/ml) for 0 or 2 h; the mRNA expressions of CCL2 and IL-6 in BMDCs were analyzed by qPCR. **(K)** BMDCs were isolated from *ASB17*$^{+/+}$ and *ASB17*$^{-/-}$ mice, and ASB17 was overexpressed in *ASB17*$^{-/-}$ BMDCs by infecting with the recombinant lentivirus. All cells were stimulated by LPS (1 μg/ml) for two timepoints (0 and 30 min); the protein levels of phosph-p65 in BMDCs were analyzed by Western blotting. Data are shown as means ± SD. *$p < 0.05$; **$p < 0.01$; ***$p < 0.001$.

its expression level in BMDCs could be induced by LPS which was an important pyrogen derived from gram-negative bacteria (**Figure 1B**). These results indicated that ASB17 might have participated in pathological processes of infectious inflammation. We isolated BMDCs from *Asb17*$^{-/-}$ and wild-type mice (**Figure 1C**). We found that *Asb17* knocking-out significantly impaired the expression of the LPS-induced pro-inflammatory cytokines Ccl2, Il-6, Il-1β, and Ip-10 in BMDCs (**Figures 1D–G**). The NF-κB signal pathway plays a critical role in the production of the pro-inflammatory cytokines when TLR4 was activated by LPS (Guha and Mackman, 2001). By detecting this pathway, we found that Asb17 deficiency obviously decreased the phosphorylation of NF-κB p65 when BMDCs were stimulated with LPS (**Figure 1H**), indicating an impairment of NF-κB activation. In addition, we checked the induction of pro-inflammatory cytokines and the phosphorylation of NF-κB p65 when Asb17 was overexpressed in *Asb17*$^{-/-}$ BMDCs to verify its specificity. Asb17 overexpression in *Asb17*$^{-/-}$ BMDCs recovered the LPS-induced Ccl2 and Il-6 expression and NF-κB p65 activation (**Figures 1I–K**). Our results suggested that ASB17 was important for LPS-mediated NF-κB activation.

Overexpression ASB17 Promotes LPS-Mediated NF-κB Activation in THP-1 Cells

To further examine the role of ASB17 in NF-κB signaling, we constructed THP-1 cells stably expressing ASB17 protein (**Figure 2A**). Overexpression of ASB17 significantly promoted the expression of *IL-6*, *CCL2*, *IL-1β*, and *IP-10* whether with LPS stimulation or not (**Figures 2B–E**). Besides, ASB17 overexpression obviously enhanced the p65 and IKKα phosphorylation induced by LPS (**Figure 2F**). Overall, ASB17 could enhance LPS-mediated NF-κB activation.

ASB17 Interacts With TRAF6

To study how ASB17 regulated the NF-κB signal pathway, we screened key molecules involved in or related to this pathway including IRF7, STING, TBK1, IRF3, IκBα, IKKε, RIP1, TRAF6, P50, and P65 by immunoprecipitation to identify which of them might interact with ASB17. Among these molecules, we found that only TRAF6 was associated with ASB17 (**Figure 3A**). To assure that TRAF6 was associated with ASB17 truly and specifically, we also constructed TRAF family-related genes, TRAF2, TRAF3, and TRAF5, to perform the immunoprecipitation. The results indicated that TRAF6 could be precipitated by ASB17 specifically (**Figure 3B**). The further co-immunoprecipitation (Co-IP) and reciprocal Co-IP assays confirmed the interaction of ASB17 and TRAF6 (**Figures 3C–E**). To further confirm the interaction between ASB17 and TRAF6, we identified the interaction in THP-1 cells stably expressing ASB17 protein. The results indicated that ASB17 could interact with endogenous TRAF6 (**Figure 3F**). This interaction was enhanced by LPS treatment

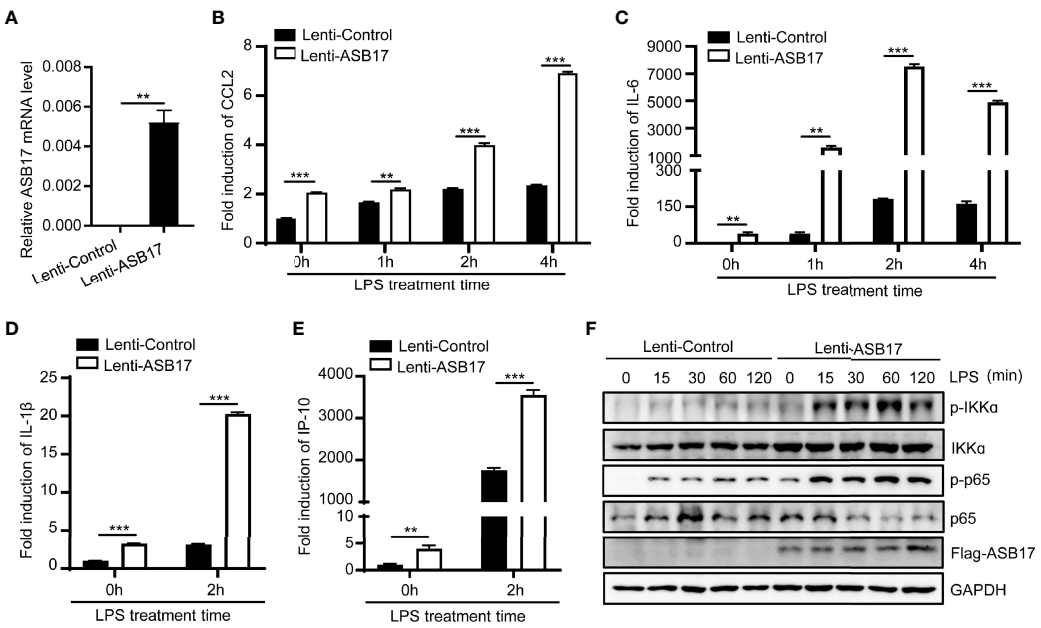

FIGURE 2 | Overexpression ASB17 promotes LPS-mediated NF-κB activation in THP-1 cells. **(A)** Total RNAs were isolated from THP-1 stably expressing Flag-ASB17 and its control; mRNA levels of ASB17 in these cells were quantified by RT-PCR. **(B, C)** THP-1 stably expressing Flag-ASB17 and its control were stimulated by LPS (1 μg/ml) in different timepoints (0, 1, 2, and 4 h). The mRNA levels of IL-6 and CCL2 in these cells were quantified by RT-PCR. **(D, E)** THP-1 stably expressing Flag-ASB17 and its control were stimulated by LPS (1 μg/ml) in different timepoints (0 and 2 h). The mRNA levels of IL-1β and IP-10 in these cells were quantified by RT-PCR. **(F)** THP-1 stably expressing Flag-ASB17 and its control were stimulated by LPS (1 μg/ml) in different timepoints (0, 15, 30, 60, and 120 min); the protein levels of IKKα, phosph-IKKα, p65, and phosph-p65 in these cells were quantified by Western blotting. Data are shown as means ± SD. $^{**}p < 0.01$; $^{***}p < 0.001$.

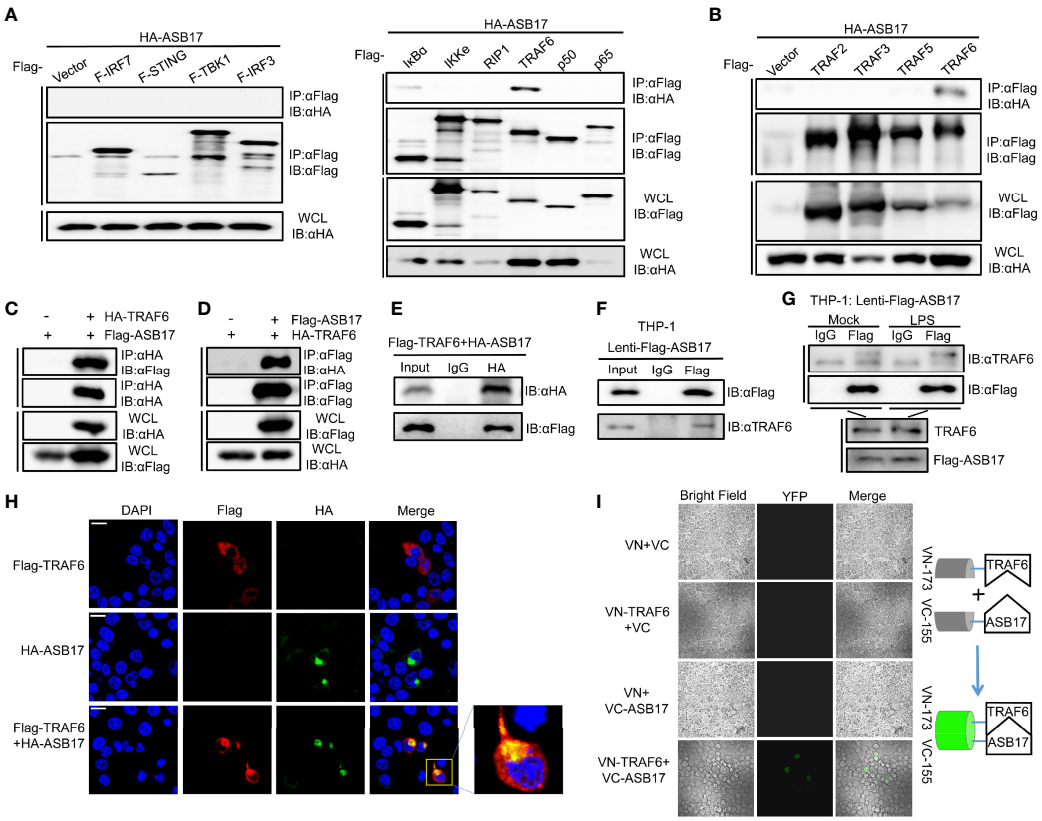

FIGURE 3 | ASB17 interacts with TRAF6. ***(A)*** HEK293T cells were co-transfected with HA-ASB17 and Flag-IRF7, Flag-STING, Flag-TBK1, Flag-IRF3, Flag-IkBα, Flag-IKKe, Flag-RIP1, Flag-TRAF6, Flag-p50, or Flag-p65 in 6-cm cell dishes for 24–36 h, respectively. A part of the cell lysates as input and remaining cell lysates were immunoprecipitated with anti-Flag antibodies. **(B)** HEK293T cells were co-transfected with HA-ASB17 and Flag-TRAF2, Flag-TRAF3, Flag-TRAF5, or Flag-TRAF6 in 6-cm cell dishes for 24–36 h A part of the cell lysates as input and remaining cell lysates were immunoprecipitated with anti-Flag antibodies. **(C, D)** HEK293T cells were co-transfected with HA-TRAF6 and Flag-ASB17 in 10-cm cell dishes for 24–36 h A part of the cell lysates as input and remaining cell lysates were immunoprecipitated with anti-HA antibody **(C)** or anti-Flag antibody **(D)**. **(E)** HEK293T cells were co-transfected with Flag-TRAF6 and HA-ASB17 in 6-cm cell dishes for 24–36 h. A part of the cell lysates as input and remaining cell lysates were immunoprecipitated with IgG or anti-HA antibodies. **(F)** A part of THP-1 stably expressing ASB17 cell lysates as input and remaining cell lysates were immunoprecipitated with IgG or anti-Flag antibodies. **(G)** THP-1 stably expressing ASB17 cells were stimulated with LPS (1 μg/ml) in different timepoints (0 and 2 h) in 10-cm cell dishes. A part of the cell lysates as input and remaining cell lysates were immunoprecipitated with IgG or anti-Flag antibodies. **(H)** HEK293T cells were co-transfected with plasmids as indicated. Subcellular localizations of HA-ASB17 (green), Flag-TRAF6 (red), and nucleus marker DAPI (blue) were analyzed under confocal microscopy. Scale bar, 20 μm. **(I)** HEK293T cells were co-transfected with plasmids as indicated, biomolecular fluorescence complementation (BiFC) assays for detection of interactions between ASB17 and TRAF6. All bands were immunoblotted with the indicated antibodies.

(**Figure 3G**). Confocal microscopy showed that ASB17 co-localized with TRAF6 in cells (**Figure 3H**). We also used the bimolecular fluorescence complementation (BiFC) analysis system to detect this protein–protein interaction. We constructed the VN-173-TRAF6 and VC-155-ASB17 plasmids and transfected them into cells. Fluorescence was not observed in control groups but was obviously observed in the experimental group in which VN-173-TRAF6 and VC-155-ASB17 were both transfected. The result suggests that ASB17 directly interacted with TRAF6 (**Figure 3I**). Overall, these results demonstrated that ASB17 was physically associated with TRAF6. Given that TRAF6 plays a key role in NF-κB signal transduction, we hypothesize that ASB17 regulated the NF-κB signal pathway *via* the interaction with TRAF6.

ASB17 Suppresses TRAF6 Polyubiquitination and Stabilizes TRAF6 Protein

To explore how ASB17 affected the function of TRAF6, we investigated the TRAF6 protein levels. HEK293T were quantitatively transfected with TRAF6, EGFP (set as control), and different doses of ASB17. The Western-blotting analysis displayed that ASB17 increased the TRAF6 protein level but did not affect the EGFP (**Figure 4A**). To study the stability of TRAF6 protein, we performed a protein decay assay with cycloheximide (CHX) which blocked cellular protein synthesis. The results showed that ASB17 overexpression markedly reduced the decay rate of TRAF6 protein, indicating that ASB17 stabilized the TRAF6 protein (**Figure 4B**).

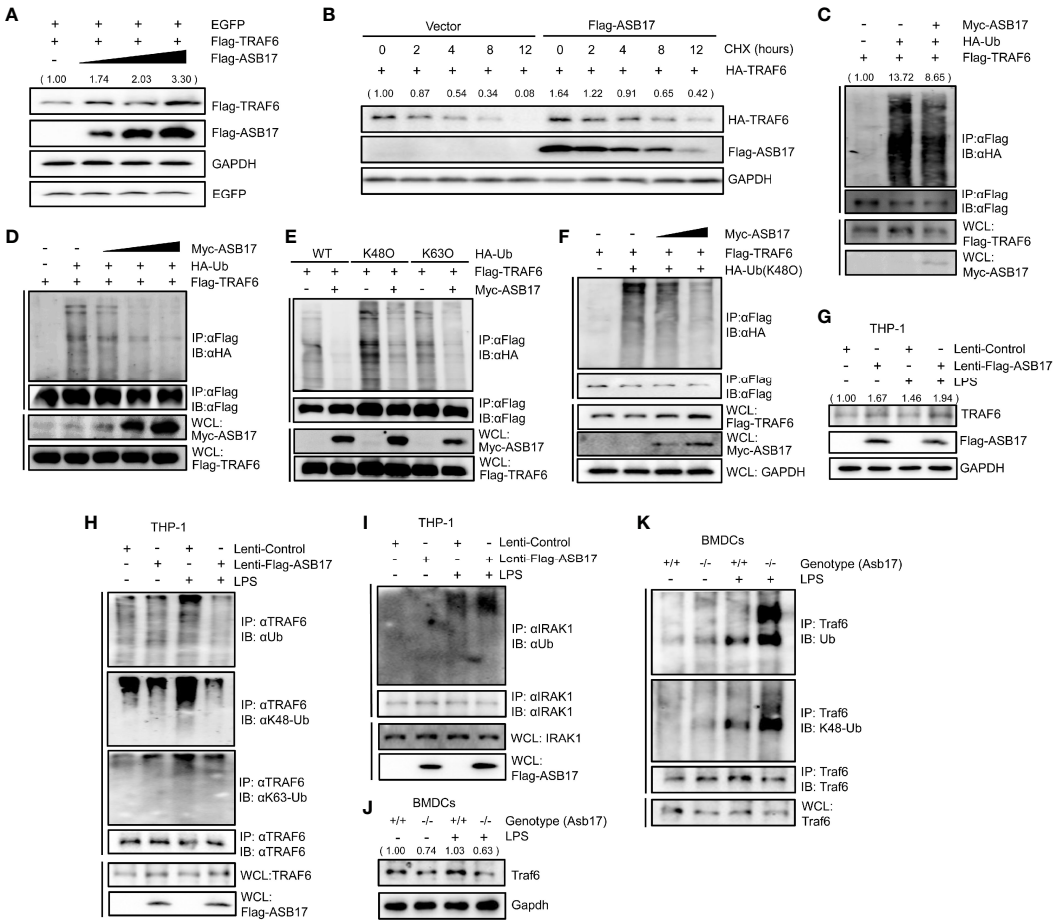

FIGURE 4 | ASB17 suppresses TRAF6 polyubiquitination and stabilizes TRAF6 protein. **(A)** HEK293T cells were co-transfected with TRAF6, EGFP, and ASB17; the cell lysates were immunoblotted with indicated antibodies. **(B)** HEK293T cells were co-transfected with TRAF6 or ASB17, then were treated with CHX (50 μg/ml) in different timepoints; the cell lysates were immunoblotted with indicated antibodies. **(C)** HEK293T cells were transfected with TRAF6, Ub, or Flag-ASB17. A part of the cell lysates as input and remaining cell lysates were immunoprecipitated with anti-Flag antibody. **(D)** HEK293T cells were transfected with TRAF6, Ub, or a series of increasing amounts of Myc-ASB17 plasmids (0.5, 1, and 2 μg). A part of the cell lysates as input and remaining cell lysates were immunoblotted with anti-Flag antibodies. **(E)** HEK293T cells were transfected with TRAF6, ASB17, or Ub (WT, K48O, and K63O). A part of the cell lysates as input and remaining cell lysates were immunoprecipitated with anti-Flag antibody. **(F)** HEK293T cells were transfected with TRAF6, Ub (K48O), or a series of increasing amounts of Myc-ASB17 plasmids (1 and 2 μg). A part of the cell lysates as input and remaining cell lysates were immunoprecipitated with anti-Flag antibody and then immunoblotted with indicated antibodies. **(G–I)** THP-1 cells stably expressing ASB17 and control; the indicated THP-1 cells were stimulated by LPS for 0 and 2 h, and the cell lysates were immunoblotted with indicated antibodies **(G)**. A part of the cell lysates as input and the remaining cell lysates were immunoprecipitated with anti-TRAF6 antibody **(H)**. A part of the cell lysates as input and the remaining cell lysates were immunoprecipitated with anti-IRAK1 antibody **(I)**. **(J, K)** BMDCs were isolated from *ASB17*$^{+/+}$ and *ASB17*$^{-/-}$ mice, and cells were stimulated by LPS for 0 and 2 h. The cell lysates were immunoprecipitated with indicated antibody **(J)**. A part of the cell lysates as input and and remaining cell lysates were immunoprecipitated with anti-TRAF6 antibody **(K)**.

Then, we examined whether polyubiquitination of TRAF6 was regulated by ASB17. In HEK293T cells, ASB17 could markedly suppress the polyubiquitination of TRAF6 (**Figure 4C**). Moreover, ASB17 suppressed the polyubiquitination of TRAF6 in an ASB17 dose-dependent manner (**Figure 4D**). It had been reported that many E3 ubiquitin ligases targeted ubiquitin chains of linkages (K48-linked or K63-linked) to TRAF6 (Zhang et al., 2013; Wu et al., 2017). We constructed ubiquitin mutant vectors K48O and K63O (all lysine residues become arginine residues except its lysine residues at positions 48 and 63, respectively). The ubiquitin detection displayed that ASB17 could markedly suppress K48-linked polyubiquitination (**Figure 4E**). To further assure that ASB17 inhibited the K48-linked polyubiquitination of TRAF6, we showed the result that ASB17 could suppress K48-linked polyubiquitination of TRAF6 in an ASB17 dose-dependent manner (**Figure 4F**). Additionally, overexpression of ASB17 also elevated the endogenous TRAF6 protein level in THP-1 (**Figure 4G**). Overexpression of ASB17 significantly inhibited the TRAF6 polyubiquitination and K48-linked polyubiquitination in LPS-stimulated THP-1, but no obvious inhibition on the K63-linked polyubiquitination was observed when THP-1 was stimulated with LPS (**Figure 4H**). In order to confirm the specificity of ASB17-mediated TRAF6 deubiquitination by LPS stimulation, we verified whether the ubiquitination of IRAK1 could be altered by ASB17

after LPS stimulation. The results indicated that ASB17 did not reduce the ubiquitination of IRAK1 (**Figure 4I**). Consistent with this, Asb17 knocking-out reduced the endogenous Traf6 protein level and increased the Traf6 polyubiquitination in BMDCs (**Figures 4J, K**). Together, ASB17 could suppress the polyubiquitination of TRAF6, indicating that ASB17 protected TRAF6 from degradation to promote NF-kB activation.

The aa177-250 Segment of ASB17 Is Required for the Interaction With the Zn Finger Domain of TRAF6 and Polyubiquitination Suppression of TRAF6

TRAF6 contains an RF domain, a ZnF domain, and a TRAF-C domain (**Figure 5A**). The Co-IP assay indicated that ASB17 could interact with the ZnF domain of TRAF6 (**Figure 5B**). In order to identify the interaction between ASB17 and the specific domain of TRAF6, we constructed more detailed domains (**Figure 5C**). The Co-IP assay also indicated that ASB17 could interact with the ZnF domain of TRAF6 (**Figure 5D**). It had been reported that ASB17 mainly contains the ANK box domain and SOCS box domain (**Figure 5E**). Co-IP assay indicated that the aa177–250 segment of ASB17 between the ANK box domain and the SOCS box domain was required for the interaction with TRAF6 (**Figure 5F**). To further study the effect of the ASB17 interaction on TRAF6 polyubiquitination, we performed the ubiquitin detecting assay with the ASB17 truncation. The results indicated that the truncation of the aa177–250 segment removed the polyubiquitination-suppressing activity of ASB17 on TRAF6

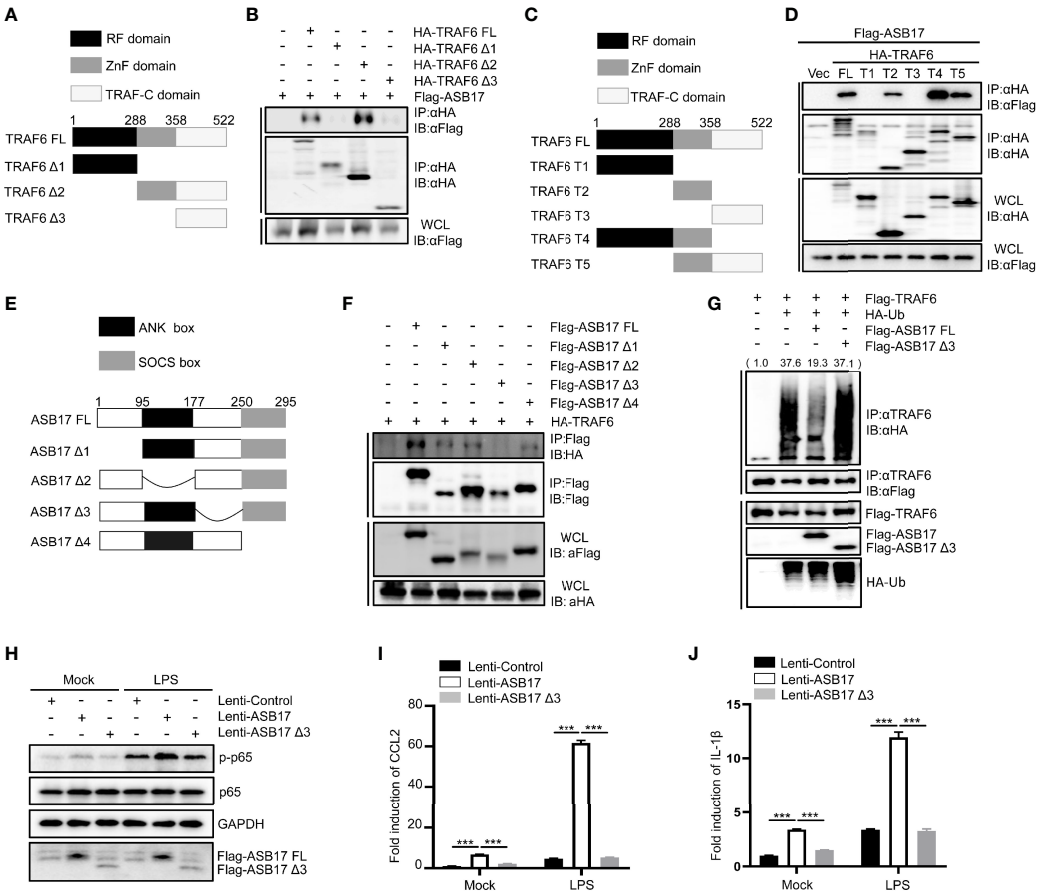

FIGURE 5 | The aa177-250 segment of ASB17 is required for the interaction with the Zn finger domain of TRAF6 and polyubiquitination suppression of TRAF6. **(A)** Schematic diagram of TRAF6 and its truncated mutants (TRAF6 FL, TRAF6 Δ1, TRAF6 Δ2, and TRAF6 Δ3). **(B)** HEK293T cells were transfected with ASB17 and TRAF6 or its truncated mutants. A part of the cell lysates as input and remaining cell lysates were immunoprecipitated with anti-HA antibody. **(C)** Schematic diagram of TRAF6 and its truncated mutants (TRAF6 FL, TRAF6 T1, TRAF6 T2, TRAF6 T3, TRAF6 T4, and TRAF6 T5). **(D)** HEK293T cells were transfected with ASB17 and TRAF6 or its truncated mutants. A part of the cell lysates as input and remaining cell lysates were immunoprecipitated with anti-HA antibody. **(E)** Schematic diagram of TRAF6 and its truncated mutants (ASB17 FL, ASB17 Δ1, ASB17 Δ2, ASB17 Δ3, and ASB17 Δ4). **(F)** HEK293T cells were transfected with TRAF6 and ASB17 or its truncated mutants. A part of the cell lysates as input and remaining cell lysates were immunoblotted with anti-Flag antibodies. **(G)** HEK293T cells were transfected with TRAF6, Ub, ASB17, or ASB17 Δ3. A part of the cell lysates as input and remaining cell lysates were immunoprecipitated with anti-TRAF6 antibody. **(H)** THP-1 stably expressing ASB17, ASB17Δ3, and its control were stimulated by LPS (1 μg/ml) in different timepoints (0 and 2 h), and p65 and phosph-p65 in these cells were quantified by western blotting. **(I, J)** THP-1 stably expressing ASB17, ASB17Δ3, and its control were stimulated by LPS (1 μg/ml) in different timepoints (0 and 2 h). The mRNA levels of CCL2 and IL-1β in these cells were quantified by RT-PCR. Data are shown as means ± SD. ***$p < 0.0001$.

(**Figure 5G**). We also found that ASB17 could significantly enhance LPS-mediated NF-κB activation and LPS-induced pro-inflammatory cytokines CCL2 and IL-1β, but ASB17 Δ3 could not (**Figures 5H–J**). These data revealed that ASB17 *via* its aa177–250 segment interacted with TRAF6 to inhibit TRAF6 polyubiquitination.

Hypothetical Model for the Role of ASB17 in the TRAF6-Mediated NF-κB Signal Pathway

ASB17 knocking-out in BMDCs impaired LPS-induced inflammatory cytokine expressions and markedly inhibited the activation of the NF-κB signal pathway. Overexpression of ASB17 elevated the levels of LPS-mediated NF-κB activation and the cytokine expressions in THP-1 cells. We found that ASB17 interacted with TRAF6 and suppressed K48-linked polyubiquitination of TRAF6, by which it stabilizes the TRAF6 protein. The TRAF6 partner role of ASB17 is crucial for LPS-mediated NF-κB activation and the burst of inflammation (**Figure 6**).

DISCUSSION

It is reported that ASB17 is mainly expressed in the testis, and we have found that ASB17 promotes testis cell apoptosis through specifically degrading BCLW and MCL1 (Yang et al., 2021). ASB17 may be a necessary gene for testis development and physiology. However, we found that ASB17 could be induced by LPS in dendritic cells. These indicated that ASB17 might be involved in immune and inflammatory responses. ASB17 promotes NF-κB activation and facilitated the expression of CCL2 and IL-6 when dendritic cells were stimulated with LPS. Thus, we screened the related factors involved in NF-κB signaling to search the target that ASB17 interacts with. We found that ASB17 was associated with TRAF6 and it significantly suppressed the K48-linked linked polyubiquitin of TRAF6. We suggested that ASB17 facilitates NF-κB activation through maintaining the TRAF6 protein stability.

Although ASB17 has E3 ubiquitin ligase activity like other members of the ASB family (Kohroki et al., 2005; Liu et al., 2019; Yang et al., 2021), our data reveal that it also functions as a ubiquitin-inhibiting factor. Therefore, its function is much more than ubiquitin ligase. It is suggested that ASB17 exerts bilateral functions in protein ubiquitination. We speculate that the function of ASB17 may be determined by the interaction site with the target protein. We previously reported that ASB17 induced the ubiquitination of BCLW and MCL1 for proteasomal degradation through its SOCS domain interaction with the two targets (Yang et al., 2021). The segment aa177–aa250 of ASB17 is required for the association with TRAF6 in the immunoprecipitation assay. The biological function of this segment is unclear before. It is between ankyrin repeat and SOCS domains. We define it as a TRAF6-associated domain and speculate that it mediates the ubiquitination-inhibiting activity of ASB17. In fact, it is not surprising that a protein has both deubiquitination and ubiquitination activities. The amino-terminal domain of A20,

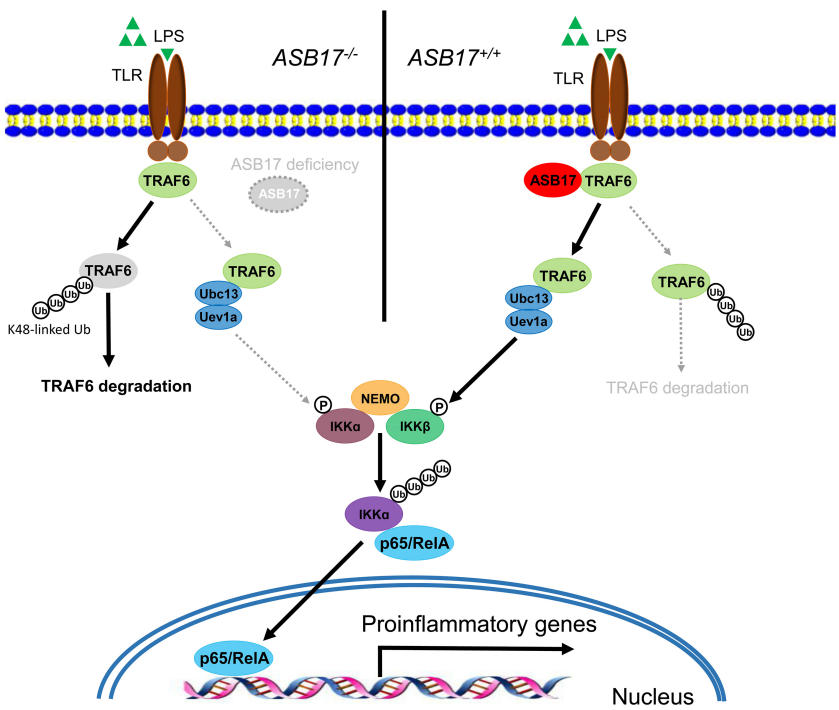

FIGURE 6 | Hypothetical model for the role of ASB17 in the TRAF6-mediated NF-κB signal pathway. ASB17 interacts with TRAF6 and suppresses its K48-linked linked polyubiquitin, which protects TRAF6 from degradation. LPS activates NF-κB signaling through TRAF6 more effectively in wild-type DCs than in ASB17-knocking-out DCs.

as a de-ubiquitinating enzyme, removes lysine-63 (K63)-linked ubiquitin chains from the receptor-interacting protein (RIP), while the carboxy-terminal domain of A20 functions as a ubiquitin ligase by promoting RIP K48-linked polyubiquitination for proteasomal degradation (Wertz et al., 2004). Although ASB17 does not contain a DUB domain, it may regulate ubiquitination of other protin by recruiting an E3 ligase to block ubiquitination of TRAF6, or recruit a de-ubiquitinase to de-ubiquitinate TRAF6.

Actually, there is faultiness in this study. Because of TRAF6 as the target of ASB17 we screened out from a few candidates which was not a global screening, ASB17 might regulate NF-κB signaling through other targets. Thus, it is necessary to knock out TRAF6 in mice or immune cell lines in the future to look into this possibility. Besides, we did not study the role of ASB17 in certain infectious inflammation models, as we focused on the cellular mechanism of NF-κB activation involved in pro-inflammatory cytokine induction. We revealed the biological role of ASB17 in TRAF6/NF-κB signaling. Given the importance of its target TRAF6 in cells, it is worth to study the functions of ASB17 in physiology and pathology by using clinical or animal models.

Therefore, we report a novel function of ASB17 that it targets TRAF6 to suppress its K48-linked polyubiquitination and proteasomal degradation. Besides, we recognize the important role of ASB17 in inflammation that it enhances NF-κB activation by maintaining TRAF6 stability.

DATA AVAILABILITY STATEMENT

The original contributions presented in the study are included in the article/supplementary material. Further inquiries can be directed to the corresponding authors.

ETHICS STATEMENT

The animal study was reviewed and approved by the Institutional Animal Care and Use Committee (IACUC) of the College of Life Sciences, Wuhan University.

AUTHOR CONTRIBUTIONS

Conceptualization, PW, GY, YL, and JW. Data curation, GY and SZ. Formal analysis, PW, GY, SZ, YZ, YJ, XC, ZL, and PP. Funding acquisition, YL and JW. Investigation, GL, XlC, QZ, WZ, and QT. Methodology, PW, GY, and SZ. Project administration, YL and JW. Software, ZL, PP, GL, XlC, and QZ. Supervision, JW. Validation, ZL, PP, GL, XlC, and QZ. Visualization, PW, GY, and SZ. Writing—original draft, PW, GY, and SZ. Writing—review and editing, YL and JW. All authors contributed to the article and approved the submitted version.

FUNDING

This work was supported by the National Natural Science Foundation of China (81730061, 32070148, and 81471942), the Guangdong Province "Pearl River Talent Plan" Innovation and Entrepreneurship Team Project (2017ZT07Y580), the Guangdong Basic and Applied Basic Research Foundation (2020A1515010369, 2019A1515011073), and the Fundamental Research Funds for the Central Universities (21620401).

REFERENCES

Cao, C., An, R., Yu, Y., Dai, H., Qu, Z., Gao, M., et al. (2019). BICP0 Negatively Regulates TRAF6-Mediated NF-kappaB and Interferon Activation by Promoting K48-Linked Polyubiquitination of TRAF6. *Front. Microbiol.* 10, 3040. doi: 10.3389/fmicb.2019.03040

Cao, Z., Xiong, J., Takeuchi, M., Kurama, T., and Goeddel, D. V. (1996). TRAF6 Is a Signal Transducer for Interleukin-1. *Nature* 383, 443–446. doi: 10.1038/383443a0

Chen, F. Y., Huang, M. Y., Lin, Y. M., Ho, C. H., Lin, S. Y., Chen, H. Y., et al. (2019). BIK Ubiquitination by the E3 Ligase Cul5-ASB11 Determines Cell Fate During Cellular Stress. *J. Cell Biol.* 218, 3002–3018. doi: 10.1083/jcb.201901156

Chung, J. Y., Lu, M., Yin, Q., Lin, S. C., and Wu, H. (2007). Molecular Basis for the Unique Specificity of TRAF6. *Adv. Exp. Med. Biol.* 597, 122–130. doi: 10.1007/978-0-387-70630-6_10

Dainichi, T., Matsumoto, R., Mostafa, A., and Kabashima, K. (2019). Immune Control by TRAF6-Mediated Pathways of Epithelial Cells in the EIME (Epithelial Immune Microenvironment). *Front. Immunol.* 10, 1107. doi: 10.3389/fimmu.2019.01107

Deng, L., Wang, C., Spencer, E., Yang, L., Braun, A., You, J., et al. (2000). Activation of the IkappaB Kinase Complex by TRAF6 Requires a Dimeric Ubiquitin-Conjugating Enzyme Complex and a Unique Polyubiquitin Chain. *Cell* 103, 351–361. doi: 10.1016/S0092-8674(00)00126-4

Du, M., Yuan, L., Tan, X., Huang, D., Wang, X., Zheng, Z., et al. (2017). The LPS-Inducible lncRNA Mirt2 Is a Negative Regulator of Inflammation. *Nat. Commun.* 8, 2049. doi: 10.1038/s41467-017-02229-1

Gabay, C., Lamacchia, C., and Palmer, G. (2010). IL-1 Pathways in Inflammation and Human Diseases. *Nat. Rev. Rheumatol.* 6, 232–241. doi: 10.1038/nrrheum.2010.4

Guha, M., and Mackman, N. (2001). LPS Induction of Gene Expression in Human Monocytes. *Cells Signal.* 13, 85–94. doi: 10.1016/S0898-6568(00)00149-2

Guo, J. H., Saiyin, H., Wei, Y. H., Chen, S., Chen, L., Bi, G., et al. (2004). Expression of Testis Specific Ankyrin Repeat and SOCS Box-Containing 17 Gene. *Arch. Androl.* 50, 155–161. doi: 10.1080/01485010490425485

Hayden, M. S., and Ghosh, S. (2014). Regulation of NF-kappaB by TNF Family Cytokines. *Semin. Immunol.* 26, 253–266. doi: 10.1016/j.smim.2014.05.004

Kawai, T., and Akira, S. (2010). The Role of Pattern-Recognition Receptors in Innate Immunity: Update on Toll-Like Receptors. *Nat. Immunol.* 11, 373–384. doi: 10.1038/ni.1863

Kim, K. S., Kim, M. S., Kim, S. K., and Baek, K. H. (2004). Murine Asb-17 Expression During Mouse Testis Development and Spermatogenesis. *Zygote* 12, 151–156. doi: 10.1017/S0967199404002722

Kohroki, J., Nishiyama, T., Nakamura, T., and Masuho, Y. (2005). ASB Proteins Interact With Cullin5 and Rbx2 to Form E3 Ubiquitin Ligase Complexes. *FEBS Lett.* 579, 6796–6802. doi: 10.1016/j.febslet.2005.11.016

Kwon, S., Kim, D., Rhee, J. W., Park, J. A., Kim, D. W., Kim, D. S., et al. (2010). ASB9 Interacts With Ubiquitous Mitochondrial Creatine Kinase and Inhibits Mitochondrial Function. *BMC Biol.* 8, 23. doi: 10.1186/1741-7007-8-23

Lamothe, B., Campos, A. D., Webster, W. K., Gopinathan, A., Hur, L., and Darnay, B. G. (2008). The RING Domain and First Zinc Finger of TRAF6 Coordinate Signaling by Interleukin-1, Lipopolysaccharide, and RANKL. *J. Biol. Chem.* 283, 24871–24880. doi: 10.1074/jbc.M802749200

Liu, P., Verhaar, A. P., and Peppelenbosch, M. P. (2019). Signaling Size: Ankyrin and SOCS Box-Containing ASB E3 Ligases in Action. *Trends Biochem. Sci.* 44, 64–74. doi: 10.1016/j.tibs.2018.10.003

Lv, Y., Kim, K., Sheng, Y., Cho, J., Qian, Z., Zhao, Y. Y., et al. (2018). YAP Controls Endothelial Activation and Vascular Inflammation Through Traf6. *Circ. Res.* 123, 43–56. doi: 10.1161/CIRCRESAHA.118.313143

Matsumoto, R., Dainichi, T., Tsuchiya, S., Nomura, T., Kitoh, A., Hayden, M. S., et al. (2018). Epithelial TRAF6 Drives IL-17-Mediated Psoriatic Inflammation. *JCI Insight* 3 (15), e121175. doi: 10.1172/jci.insight.121175

Uematsu, K., Okumura, F., Tonogai, S., Joo-Okumura, A., Alemayehu, D. H., Nishikimi, A., et al. (2016). ASB7 Regulates Spindle Dynamics and Genome Integrity by Targeting DDA3 for Proteasomal Degradation. *J. Cell Biol.* 215, 95–106. doi: 10.1083/jcb.201603062

Wan, P., Zhang, Q., Liu, W., Jia, Y., Ai, S., Wang, T., et al. (2019). Cullin1 Binds and Promotes NLRP3 Ubiquitination to Repress Systematic Inflammasome Activation. *FASEB J.* 33, 5793–5807. doi: 10.1096/fj.201801681R

Wertz, I. E., O'rourke, K. M., Zhou, H., Eby, M., Aravind, L., Seshagiri, S., et al. (2004). De-Ubiquitination and Ubiquitin Ligase Domains of A20 Downregulate NF-KappaB Signalling. *Nature* 430, 694–699. doi: 10.1038/nature02794

Wu, Y., Hu, Y., Wang, B., Li, S., Ma, C., Liu, X., et al. (2020). Dopamine Uses the DRD5-ARRB2-PP2A Signaling Axis to Block the TRAF6-Mediated NF-KappaB Pathway and Suppress Systemic Inflammation. *Mol. Cell* 78, 42–56.e46. doi: 10.1016/j.molcel.2020.01.022

Wu, C., Su, Z., Lin, M., Ou, J., Zhao, W., Cui, J., et al. (2017). NLRP11 Attenuates Toll-Like Receptor Signalling by Targeting TRAF6 for Degradation via the Ubiquitin Ligase RNF19A. *Nat. Commun.* 8, 1977. doi: 10.1038/s41467-017-02073-3

Yang, G., Wan, P., Xiang, Q., Huang, S., Huang, S., Wang, J., et al. (2021). E3 Ubiquitin Ligase ASB17 Promotes Apoptosis by Ubiquitylating and Degrading BCLW and MCL1. *Biol. (Basel)* 10 (3), 234. doi: 10.3390/biology10030234

Zhang, X., Zhang, J., Zhang, L., Van Dam, H., and Ten Dijke, P. (2013). UBE2O Negatively Regulates TRAF6-Mediated NF-KappaB Activation by Inhibiting TRAF6 Polyubiquitination. *Cell Res.* 23, 366–377. doi: 10.1038/cr.2013.21

Zhao, W., Wang, L., Zhang, M., Yuan, C., and Gao, C. (2012). E3 Ubiquitin Ligase Tripartite Motif 38 Negatively Regulates TLR-Mediated Immune Responses by Proteasomal Degradation of TNF Receptor-Associated Factor 6 in Macrophages. *J. Immunol.* 188, 2567–2574. doi: 10.4049/jimmunol.1103255

Conflict of Interest: The authors declare that the research was conducted in the absence of any commercial or financial relationships that could be construed as a potential conflict of interest.

Publisher's Note: All claims expressed in this article are solely those of the authors and do not necessarily represent those of their affiliated organizations, or those of the publisher, the editors and the reviewers. Any product that may be evaluated in this article, or claim that may be made by its manufacturer, is not guaranteed or endorsed by the publisher.

frontiers in Cellular and Infection Microbiology

ORIGINAL RESEARCH
published: 07 February 2022
doi: 10.3389/fcimb.2022.805302

Curdlan, a Microbial β-Glucan, Has Contrasting Effects on Autoimmune and Viral Models of Multiple Sclerosis

*Fumitaka Sato[1,2], Yumina Nakamura[1], Aoshi Katsuki[1], Sundar Khadka[1], Ijaz Ahmad[1], Seiichi Omura[1,2], Nicholas E. Martinez[2] and Ikuo Tsunoda[1,2]**

[1] Department of Microbiology, Kindai University Faculty of Medicine, Osakasayama, Osaka, Japan, [2] Department of Microbiology and Immunology, Center for Molecular and Tumor Virology, Louisiana State University Health-Shreveport, Shreveport, LA, United States

OPEN ACCESS

Edited by:
Elias Adel Rahal,
American University of Beirut, Lebanon

Reviewed by:
Pushpa Pandiyan,
Case Western Reserve University, United States
Staley Brod,
Medical College of Wisconsin, United States
Eytan R. Barnea,
BioIncept, LLC, United States

***Correspondence:**
Ikuo Tsunoda
itsunoda@med.kindai.ac.jp

Specialty section:
This article was submitted to Microbes and Innate Immunity, a section of the journal Frontiers in Cellular and Infection Microbiology

Received: 30 October 2021
Accepted: 06 January 2022
Published: 07 February 2022

Citation:
Sato F, Nakamura Y, Katsuki A, Khadka S, Ahmad I, Omura S, Martinez NE and Tsunoda I (2022) Curdlan, a Microbial β-Glucan, Has Contrasting Effects on Autoimmune and Viral Models of Multiple Sclerosis. Front. Cell. Infect. Microbiol. 12:805302. doi: 10.3389/fcimb.2022.805302

Multiple sclerosis (MS) is an immune-mediated disease characterized by inflammatory demyelination and axonal degeneration in the central nervous system (CNS). Bacterial and fungal infections have been associated with the development of MS; microbial components that are present in several microbes could contribute to MS pathogenesis. Among such components, curdlan is a microbial 1,3-β-glucan that can stimulate dendritic cells, and enhances T helper (Th) 17 responses. We determined whether curdlan administration could affect two animal models for MS: an autoimmune model, experimental autoimmune encephalomyelitis (EAE), and a viral model, Theiler's murine encephalomyelitis virus (TMEV)-induced demyelinating disease (TMEV-IDD). We induced relapsing-remitting EAE by sensitizing SJL/J mice with the myelin proteolipid protein (PLP) $_{139\text{-}151}$ peptide and found that curdlan treatment prior to PLP sensitization converted the clinical course of EAE into hyperacute EAE, in which the mice developed a progressive motor paralysis and died within 2 weeks. Curdlan-treated EAE mice had massive infiltration of T cells and neutrophils in the CNS with higher levels of Th17 and Th1 responses, compared with the control EAE mice. On the other hand, in TMEV-IDD, we found that curdlan treatment reduced the clinical scores and axonal degeneration without changes in inflammation or viral persistence in the CNS. In summary, although curdlan administration exacerbated the autoimmune MS model by enhancing inflammatory demyelination, it suppressed the viral MS model with reduced axonal degeneration. Therefore, microbial infections may play contrasting roles in MS depending on its etiology: autoimmunity versus viral infection.

Keywords: animal models, CNS demyelinating diseases, neuropathology, persistent virus infections, *Picornaviridae* infections, fungal infections, principal component analysis, bioinformatics

INTRODUCTION

Multiple sclerosis (MS) is an immune-mediated disease characterized by inflammatory demyelination and axonal degeneration in the central nervous system (CNS) (Trapp and Nave, 2008). Although the etiology of MS is unclear, there are two major effector mechanisms that have been proposed as a cause/trigger of MS: autoimmune responses against myelin sheaths (autoimmune theory) and CNS viral infections (viral theory) (Sato et al., 2018). The autoimmune theory has been supported by clinical findings. For example, some MS patients have higher immune responses to CNS antigens than the healthy controls; immune cell infiltration and antibody deposition have been observed in demyelinating lesions (Lucchinetti et al., 2000). Immunomodulatory drugs, such as interferon (IFN)-β and anti-very late antigen (VLA)-4 antibody, have therapeutic efficacy in MS patients (Minagar et al., 2003). Experimentally, experimental autoimmune encephalomyelitis (EAE) has been widely used as an autoimmune model of MS, since EAE mimics human MS, clinically, histologically, and immunologically (Sato et al., 2016). EAE can be induced by sensitization with CNS antigens including myelin proteolipid protein (PLP), myelin oligodendrocyte glycoprotein (MOG), and myelin basic protein (MBP) (Miyamoto et al., 2006). In most EAE models, demyelination is mediated by pro-inflammatory myelin-specific $CD4^+$ T helper (Th) 1 and Th17 cells; axonal degeneration occurs secondary following severe demyelination (Tsunoda and Fujinami, 2002).

The viral theory of MS has also been supported clinically and experimentally (Libbey et al., 2014). For example, some viruses including human herpesvirus 6 have been isolated from the serum and brain samples of MS patients; increased anti-viral immune responses have also been detected in cerebrospinal fluid of MS patients (Omura et al., 2018). Experimental infections of neurotropic viruses, including Theiler's murine encephalomyelitis virus (TMEV) and mouse hepatitis virus, can induce MS-like CNS diseases in animals (Trandem et al., 2010; Kulcsar et al., 2014). TMEV is a non-enveloped, positive-sense, single-stranded RNA virus that belongs to the family *Picornaviridae* (Hertzler et al., 2000) and has been widely used as a viral model of MS. TMEV-infected mice develop chronic inflammatory demyelination and axonal degeneration in the CNS with viral persistence in macrophages and glial cells, including myelin-forming oligodendrocytes (Sato et al., 2017). TMEV-induced demyelinating disease (TMEV-IDD) has two components in the pathogenesis: 1) direct lytic viral infection (viral pathology) and 2) immunopathology, in which $CD4^+$ and $CD8^+$ T cells, antibody, and macrophages have been demonstrated to play pathogenic roles. In TMEV-IDD, axonal degeneration has been shown to precede demyelination (Tsunoda et al., 2003).

In addition to viral infections, bacterial and fungal infections have been associated with MS, since the higher levels of antibody responses to certain bacteria and fungi, such as *Chlamydia pneumoniae* and *Candida albicans*, have been detected in some MS patients than in the healthy controls (Alonso et al., 2018; Cossu et al., 2018). Experimentally, in the MOG_{35-55}-induced EAE, injection of *Streptococcus pneumoniae* during the latent stage exacerbated the clinical signs (Herrmann et al., 2006). *C. albicans*-injected mice prior to MOG sensitization also developed more severe EAE than the control mice (Fraga-Silva et al., 2015). Despite the previous reports supporting the role of bacterial and fungal infections, no single microbe has been identified to cause/trigger MS consistently. This raises the hypothesis that, instead of one single microbes, microbial components commonly present in several bacteria and fungi may contribute to MS pathogenesis.

One of such candidate microbial components is curdlan, one of the β-glucans that are components of a variety of bacteria/fungi, which are not synthesized in humans; β-glucans can be detected in human sera during fungal infections, as shown in a case report of MS (Pisa et al., 2011). Curdlan is a high molecular weight microbial 1,3-β-glucan with linear polymer of 1,3-β-glycosidic linkages; curdlan is recognized by the C-type lectin receptor dectin-1, a pattern recognition receptor, expressed on various myeloid cells including dendritic cells (DCs), monocytes, macrophages, B cells, and neutrophils (LeibundGut-Landmann et al., 2007; Isnard et al., 2021). Following curdlan stimulation, DCs enhance interleukin (IL)-17-producing Th17 cell responses. Although Th17 cells play a beneficial role in host defense against bacteria and fungi, such as *Klebsiella pneumoniae* and *C. albicans* (Curtis and Way, 2009), pro-inflammatory Th17 cells could play an effector role in inflammatory demyelination of MS (Hussman et al., 2016), EAE (Hofstetter et al., 2005; Komiyama et al., 2006), and TMEV-IDD (Hou et al., 2009; Martinez et al., 2015). Curdlan has also been reported to enhance IL-10 production and favor IgA antibody responses (LeibundGut-Landmann et al., 2007; Kawashima et al., 2012; Fujimoto et al., 2019). In addition to acquired immunity, β-glucans can induce a long-lasting change in innate immune cells (i.e., monocytes, macrophages, and microglia) (Haley et al., 2019), as a result of complex regulation including epigenetic reprogramming; the phenomenon is referred to as "trained innate immunity" or "innate immunity memory" (Rusek et al., 2018). The trained immunity independent of T or B cells has been shown to be beneficial in various microbial infections including bacteria, fungi, and viruses by diverse mechanisms, such as changes in cytokine and nitric oxide production; the anti-microbial protection can last for several weeks (Quintin et al., 2012). On the other hand, innate immunity stimulated by β-glucans could be deleterious, exacerbating immune-mediated diseases (Quintin, 2019).

In the current study, we investigated whether curdlan, a component present in many microbes, could affect autoimmune and viral models for MS, EAE and TMEV-IDD. We hypothesized that immune modulation by curdlan may result in different outcomes in the two MS models, whose immune effectors and neuropathology have been shown to be different. We first determined the effects of curdlan in EAE, where we injected mice with curdlan prior to sensitization with the $PLP_{139-151}$ peptide. We found that curdlan-treated EAE mice developed a fatal hyperacute EAE, in which mice had progressive

motor paralysis with massive infiltration of T cells and neutrophils in the CNS, although the control EAE mice developed relapsing-remitting (RR) EAE with mild to moderate CNS inflammation. We also found sustained higher levels of Th17 and Th1 responses in curdlan-treated EAE mice, compared with the control EAE mice. In contrast, curdlan treatment ameliorated TMEV-IDD with less severe clinical signs and lower levels of axonal degeneration in the CNS, compared with the control TMEV-infected group, although curdlan treatment did not alter inflammatory demyelination or viral persistence in the CNS. Thus, our findings suggested that microbial infections could result in different outcomes in MS depending on its etiology: autoimmunity versus viral infection.

MATERIALS AND METHODS

Animal Experiments

We purchased 5-week-old SJL/J mice (JAX® Mice Strain) from Charles River Laboratories Japan, Inc. (Yokohama, Japan) and maintained the mice under specific pathogen-free conditions in the animal care facility at Kindai University Faculty of Medicine (Osaka, Japan) or Louisiana State University Health-Shreveport (LSUHS, Shreveport, LA). All experimental procedures were reviewed and approved by the Institutional Animal Care and Use Committee of Kindai University Faculty of Medicine or LSUHS and performed according to the criteria outlined by the National Institutes of Health (NIH).

For EAE induction, we sensitized 6 to 7-week-old SJL/J mice subcutaneously (s.c.) with 100 nmol of the $PLP_{139\text{-}151}$ peptide (United BioSystems Inc., Herndon, VA) emulsified in complete Freund's adjuvant (CFA) composed of incomplete Freund's adjuvant [Becton, Dickinson and Company (BD), Tokyo, Japan] and *Mycobacterium tuberculosis* H37 Ra (BD) (Tsunoda et al., 2007). The final concentration of *M. tuberculosis* in the $PLP_{139\text{-}151}$/CFA emulsion was 2 mg/mL (400 μg/mouse). Clinical scores of EAE were evaluated as follows: 0, no signs; 1, paralyzed tail; 2, mild hind limb paresis; 3, moderate hind limb paralysis; 4, complete hind limb paraplegia; and 5, moribund or death (Omura et al., 2019).

For TMEV-IDD induction, we infected 6 to 7-week-old SJL/J mice intracerebrally (i.c.) with 2×10^5 plaque forming units (PFUs) of the Daniels (DA) strain of TMEV (Kawai et al., 2015). Clinical signs of TMEV-IDD were evaluated by measuring impairment of righting reflex: the proximal end of the mouse's tail was grasped and twisted to the right and then to the left (0, a healthy mouse resists being turned over; 1, the mouse is flipped onto its back but immediately rights itself on one side; 1.5, the mouse is flipped onto its back but immediately rights itself on both sides; 2, the mouse rights itself in 1 to 5 seconds; 3, righting takes more than 5 seconds; and 4, the mouse cannot right itself) (Tsunoda et al., 2008).

In both EAE and TMEV-IDD models, mice were injected intraperitoneally (i.p.) with 5 mg of curdlan (FUJIFILM Wako Pure Chemical Corporation, Osaka, Japan) in 200 μL of phosphate-buffered saline (PBS) one day prior to PLP sensitization or TMEV infection. Mice in the control group had PBS injection or no treatment.

Neuropathology

We perfused EAE or TMEV-infected mice with PBS followed by a 4% paraformaldehyde (FUJIFILM Wako Pure Chemical Corporation) solution in PBS, harvested the spinal cord and brain, which were divided into 10 to 14 transversal segments and five coronal slabs, respectively, and embedded in paraffin. We stained 4-μm-thick sections with Luxol fast blue (Solvent blue 38; MP Biomedicals, LLC, Irvine, CA) for myelin visualization and performed histological scoring of the CNS, as described previously (Sato et al., 2013). For scoring of spinal cord sections, each spinal cord section was divided into four quadrants: the ventral funiculus, the dorsal funiculus, and each lateral funiculus. Any quadrant containing meningitis, perivascular cuffing (inflammation), or demyelination was given a score of 1 in that pathological class. The total number of positive quadrants for each pathological class was determined and then divided by the total number of quadrants present on the slide and multiplied by 100 to give the percent involvement for each pathological class. An overall pathology score was also determined as the percent involvement by giving a positive score if any pathology was seen in the quadrant (Martinez et al., 2014).

T cells, neutrophils, TMEV antigens, damaged axons, activated microglia/macrophages, and plasma cells were visualized by immunohistochemistry against CD3 (Biocare Medical, Pacheco, CA) (Sato et al., 2017), Ly-6G (BD Biosciences, San Jose, CA) (Park et al., 2020), TMEV (Nitayaphan et al., 1985), nonphosphorylated neurofilaments (SMI 311, BioLegend) (Sato et al., 2013), Iba1 (GeneTex, Inc., Irvine, CA) (Wang et al., 2021), and CD138 (BD Biosciences) (Tsunoda et al., 2005), respectively, using a Histofine MAX-PO kit (Nichirei Biosciences Inc., Tokyo, Japan) or Vector Blue Substrate kit (Vector Laboratories, Inc., Burlingame, CA). For CD3, nonphosphorylated neurofilaments, Iba1, and CD138 staining, the spinal cord sections were pretreated with a citrate buffer pH 6 (Agilent Technologies Japan, Ltd., Tokyo, Japan) for 15 minutes at 95°C using an MI-77 temperature controllable microwave (Azumaya Medical Devices Inc., Tokyo, Japan) for antigen retrieval (Sato et al., 2017). To quantify the levels of damaged axons and TMEV antigens, each spinal cord section was divided into four quadrants: the ventral funiculus, the dorsal funiculus, and each lateral funiculus. The number of SMI 311- and TMEV antigen-positive cells in each quadrant was counted under a light microscope using 10 to 14 transverse spinal cord segments per mouse, as described previously (Martinez et al., 2014).

Lymphoproliferative Assays

In EAE, mice were killed 8–9 days post sensitization (a few days before the expected onset of disease) or 13–14 days post sensitization (the disease peak), using isoflurane (Viatris Inc., Canonsburg, PA). The inguinal lymph nodes were harvested and mashed on metal mesh with 50-μm pores using a plunger of 5-mL syringes to make single-cell suspensions. The lymph node

cells were cultured in RPMI-1640 medium (Sigma-Aldrich, Co., St. Louis, MO) supplemented with 10% fetal bovine serum (FBS, Sigma-Aldrich, Co.), 2 mM L-glutamine (Sigma-Aldrich, Co.), 50 mM β-mercaptoethanol (FUJIFILM Wako Pure Chemical Corporation), 1% antibiotics (Thermo Fisher Scientific Inc., Waltham, MA) at 2×10^5 cells/well in 96-well plates (Sumitomo Bakelite Co., Ltd., Tokyo, Japan) and stimulated with 50 μg/mL of the $PLP_{139-151}$ peptide in the presence or absence of a blocking antibody against CD4 [GK1.5, American Type Culture Collection (ATCC), Rockville, MD] or CD8 (Ly2.43, ATCC) at 37°C for 5 days (Tsunoda et al., 2005). To assess the levels of $PLP_{139-151}$-specific lymphoproliferation, we added 3 μl/well of the Cell Counting Kit-8 (CCK-8) solution (Dojindo Laboratories, Kumamoto, Japan) in the culture system for the last 24 hours (Miyamoto et al., 2002). The absorbance was measured at 450 nm using the Synergy H1 Hybrid Multi-Mode Microplate Reader (BioTek Instruments, Inc., Winooski, VT). All cultures were performed in triplicate, and the data were expressed as stimulation indexes: (mean absorbance in $PLP_{139-151}$ stimulation)/(mean absorbance without stimulation).

In TMEV-IDD, 5–6 weeks p.i., we isolated splenic mononuclear cells (MNCs) using Histopaque®-1083 (Sigma-Aldrich, Co.), cultured them at 2×10^5 cells/well in 96-well plates with 1×10^5 cells/well of TMEV-infected antigen-presenting cells (TMEV-APCs) or mock-infected antigen-presenting cells (control-APCs) at 37°C for 5 days (Omura et al., 2018). TMEV-APCs were made from whole spleen cells infected *in vitro* with TMEV at a multiplicity of infection (MOI) of 1; control-APCs were made from mock-infected whole spleen cells (Kawai et al., 2015). Both TMEV-APCs and control-APCs were incubated overnight and irradiated with 20 Gy using an irradiator. The levels of lymphoproliferative responses to TMEV were assessed using the Carboxyfluorescein succinimidyl ester (CFSE) Cell Division Tracker Kit (BioLegend, Inc., San Diego, CA) (Barsheshet et al., 2017). All cultures were performed in triplicate, and the data were expressed as Δ% CFSE: (mean CFSE-positive cell % in TMEV-APC stimulation) − (mean CFSE-positive cell % in control-APC stimulation).

Enzyme-Linked Immunosorbent Assays (ELISAs)

To quantify cytokines, we cultured lymph node cells from EAE mice or splenic MNCs from TMEV-infected mice at 8×10^6 cells/well in 6-well plates (Sumitomo Bakelite Co.) and stimulated with 50 μg/mL of the $PLP_{139-151}$ peptide or 5 μg/mL of concanavalin A (conA), respectively for 2 days. The culture supernatants were harvested and stored at −80°C until examined. We quantified IL-17A (BioLegend, Inc.), IFN-γ (BD Biosciences), IL-4 (BD Biosciences), and IL-10 (BD Biosciences) by ELISAs according to the manufacturers' instructions (Martinez et al., 2014).

Using ELISAs, we also quantified serum anti-$PLP_{139-151}$ and anti-TMEV antibody titers, as described previously (Sato et al., 2017). We coated 96-well flat-bottom Nunc-Immuno plates (Thermo Fisher Scientific Inc.) with 10 μg/ml of the $PLP_{139-151}$ peptide or TMEV antigen. The serum samples were diluted by means of serial two-fold dilutions from 2^7 to 2^{28} and added to the plates followed by a peroxidase-conjugated anti-mouse immunoglobulin (Ig) G1 (Thermo Fisher Scientific Inc.), IgG2c (Southern Biotechnology Associates, Inc., Birmingham, AL), IgA (Thermo Fisher Scientific Inc.), or IgM (Enzo Biochem, Inc., Farmingdale, NY) antibody (Omura et al., 2018). Immunoreactive complexes were detected with *o*-phenylendiamine dihydrochloride (FUJIFILM Wako Pure Chemical Corporation). The absorbance was measured at 492 nm using the Synergy H1 Hybrid Multi-Mode Microplate Reader. An absorbance higher than the mean + two standard deviations of naïve serum samples at a 2^7-fold dilution was used as the standard for evaluating anti-$PLP_{139-151}$ and anti-TMEV antibody titers.

Real-time Polymerase Chain Reaction (Real-Time PCR)

Following perfusion with PBS, the brain and spinal cord were harvested, frozen with liquid nitrogen, and then homogenized with the TRIzol® Reagent (Thermo Fisher Scientific Inc.) using a Polytron PT1200E homogenizer (Kinematica AG, Luzern, Switzerland) (Sato et al., 2017). RNA was isolated from the homogenate using the Qiagen RNeasy Mini Kit (Qiagen, Inc., Valencia, CA), according to the manufacturer's instruction (Omura et al., 2014). We reverse-transcribed 1 μg of total RNA into cDNA using the SuperScript® II Reverse Transcriptase (Thermo Fisher Scientific Inc.) (Omura et al., 2020). Using 10 ng of cDNA, real-time PCR was conducted with the THUNDERBIRD® SYBR® qPCR Mix (TOYOBO Co., LTD., Osaka, Japan) and the StepOnePlus® Real-Time PCR System (Thermo Fisher Scientific Inc.). To determine the levels of viral replication and gene expression related to cellular and humoral immunities, adhesion molecules, and chemokines in the brain and spinal cord, we used the following primer pairs (**Table 1**): *Cxcl2*, *Cxcl9*, *Cxcl10*, *Cxcr3*, *Foxp3*, *Icam1*, *Igha*, *Il10*, *Itga4*, *Itgb2*, *Vcam1* (Eurofins Genomics, Tokyo, Japan); and *Gzmb*, *Ifng*, *Il17a* (Real Time Primers, LLC, Elkins Park, PA). A primer pair for *Pgk1* (Real Time Primers) was used as a housekeeping gene for normalization (Omura et al., 2019).

Principal Component Analysis (PCA)

To compare the overall clinical and immunopathological profiles between the control and curdlan treatment groups in TMEV-IDD, we conducted PCA using the clinical scores, neuropathology data, and serum anti-TMEV IgG1 and IgG2c titers 5 weeks p.i. using the "prcomp" program of R version 4.1.0, as described previously (Chaitanya et al., 2013; R Core Team, 2021). We also calculated the proportion of variance and factor loadings to determine the percentage of variance among the samples explained by each principal component (PC) and to rank the potential effectors contributing to the distribution of samples on each PC value, respectively.

Statistical Analyses

Using the OriginPro 2020 (OriginLab Corporation, Northampton, MA), the Student's *t*-test and Mann-Whitney *U* test were conducted for parametric data and nonparametric data, respectively. The χ^2 test was conducted for categorical data using

TABLE 1 | The primer sets for real-time polymerase chain reaction.

Gene name	Forward primer	Reverse primer
Cxcl2	CCAACCACCAGGCTACAGG	GCGTCACACTCAAGCTCTG
Cxcl9	GGAGTTCGAGGAACCCTAGTG	GGGATTTGTAGTGGATCGTGC
Cxcl10	CCAAGTGCTGCCGTCATTTTC	GGCTCGCAGGGATGATTTCAA
Cxcr3	GGTTAGTGAACGTCAAGTGCT	CCCCATAATCGTAGGGAGAGGT
Foxp3	AGAGCCCTCACAACCAGCTA	CCAGATGTTGTGGGTGAGTG
Gzmb	TGGCCTTACTTTCGATCA AG	CAGCATGATGTCATTGGAGA
Icam1	GTGATGCTCAGGTATCCATCCA	CACAGTTCTCAAAGCACAGCG
Ifng	CAAAAGGATGGTGACATGAA	TTGGCAATACTCATGAATGC
Igha	TGCACAGTTACCCATCCTGA	GCACCAGCACTTCTTTAGGG
Il10	CTTACTGACTGGCATGAGGATCA	GCAGCTCTAGGAGCATGTGG
Il17a	CGCAAACATGAGTCCAGGGAGAGC	TCAGGGTCTTCATTGCGGTGGAG
Itga4	AACCGGGCACTCCTACAAC	CACCACCGAGTAGCCAAACAG
Itgb2	CAGGAATGCACCAAGTACAAAGT	GTCACAGCGCAAGGAGTCA
Pgk1	GCAGATTGTTTGGAATGGTC	TGCTCACATGGCTGACTTTA
Vcam1	TTGGGAGCCTCAACGGTACT	GCAATCGTTTTGTATTCAGGGGA

Cxcl2 [chemokine (C-X-C motif) ligand 2]; Cxcl9; Cxcl10; Cxcr3 [chemokine (C-X-C motif) receptor 3]; Foxp3 (forkhead box P3); Gzmb (granzyme B); Icam1 (intracellular adhesion molecule 1); Ifng [interferon (IFN)-γ]; Igha [immunoglobulin (Ig) heavy chain α]; Il10 [interleukin (IL)-10]; Il17a (IL-17a); Itga4 (integrin α4); Itgb2 (integrin β2); Pgk1 (phosphoglycerate kinase 1); and Vcam1 (vascular cell adhesion molecule 1).

the GraphPad QuickCalcs (GraphPad Software, San Diego, CA, https://www.graphpad.com/quickcalcs/contingency1.cfm) (Sato et al., 2017).

RESULTS

Curdlan Injection Converts RR-EAE Into Fatal Hyperacute EAE

We determined whether curdlan injection could affect the clinical course of EAE, an autoimmune model of MS. One day prior to subcutaneous sensitization with the $PLP_{139-151}$/CFA, SJL/J mice were treated i.p. with curdlan or PBS. We monitored the clinical signs for 6 weeks and found that the incidence of EAE was similar between the control and curdlan treatment groups (**Table 2**). As described previously (Tsunoda et al., 1998), most $PLP_{139-151}$-sensitized control mice developed RR-EAE; the control EAE mice developed hind limb paralysis around 2 weeks after EAE induction (mean onset day, 11.8 ± 0.7), recovered within 10 days (remission), and had relapses once or twice during the 6-week observation period (**Figure 1A**). Although the curdlan-treated EAE mice had the disease onset with hind limb paralysis (mean onset day, 12.8 ± 1.1) similar to the control EAE mice, most mice developed progressive motor paralysis without remission and became moribund or died within 20 days of EAE induction (**Table 2** and **Figure 1B**). Thus, the disease was defined as hyperacute EAE with a progressive disease course. A few mice in each group were asymptomatic or developed secondary progressive EAE (SP-EAE, **Table 2**). We also monitored the body weight changes and found that mice with RR-EAE exhibited substantial weight loss only during the first attack of EAE and gained weight thereafter regardless of relapses (**Figure 1C**). In contrast, mice with hyperacute EAE had severe progressive weight loss following the disease onset (**Figure 1D**).

Curdlan Injection Induces Hyperacute EAE With Severe Demyelination and Massive T-Cell and Neutrophil Infiltration

To clarify the cause of fatal hyperacute EAE following curdlan injection, we compared the neuropathology between the control and curdlan treatment groups. In the spinal cord, we found more severe inflammatory demyelination in hyperacute EAE than in RR-EAE. The spinal cord pathology scores of demyelination, perivascular cuffing, meningitis, and overall pathology were significantly higher in hyperacute EAE than in RR-EAE ($P < 0.01$, Student's *t*-test, **Figure 2B**). In RR-EAE, immune cell infiltrates, mostly composed of MNCs, were observed in the

TABLE 2 | Incidence, mortality, and disease forms of the control mice and curdlan-treated mice in experimental autoimmune encephalomyelitis (EAE)[a].

Group[b]	Incidence[c]	Mortality[d]	Disease forms[e]		
			Relapsing-remitting	Hyperacute	Secondary progressive
Control	10/12	2/10	8/10	1/10	1/10
Curdlan	11/12	9/11*	2/11	8/11	1/11

[a]*For EAE induction, SJL/J mice were sensitized subcutaneously with the myelin proteolipid protein $(PLP)_{139-151}$ peptide emulsified in complete Freund's adjuvant (CFA).*
[b]*One day prior to $PLP_{139-151}$ sensitization, mice from the control and curdlan treatment groups were injected intraperitoneally with phosphate-buffered saline (PBS) and curdlan, respectively.*
[c]*Number of symptomatic mice/total number of mice sensitized with the $PLP_{139-151}$/CFA emulsion.*
[d]*Number of dead mice/total number of symptomatic mice. *$P < 0.05$, χ^2 test, compared with controls.*
[e]*Number of mice with each disease form/total number of symptomatic mice.*

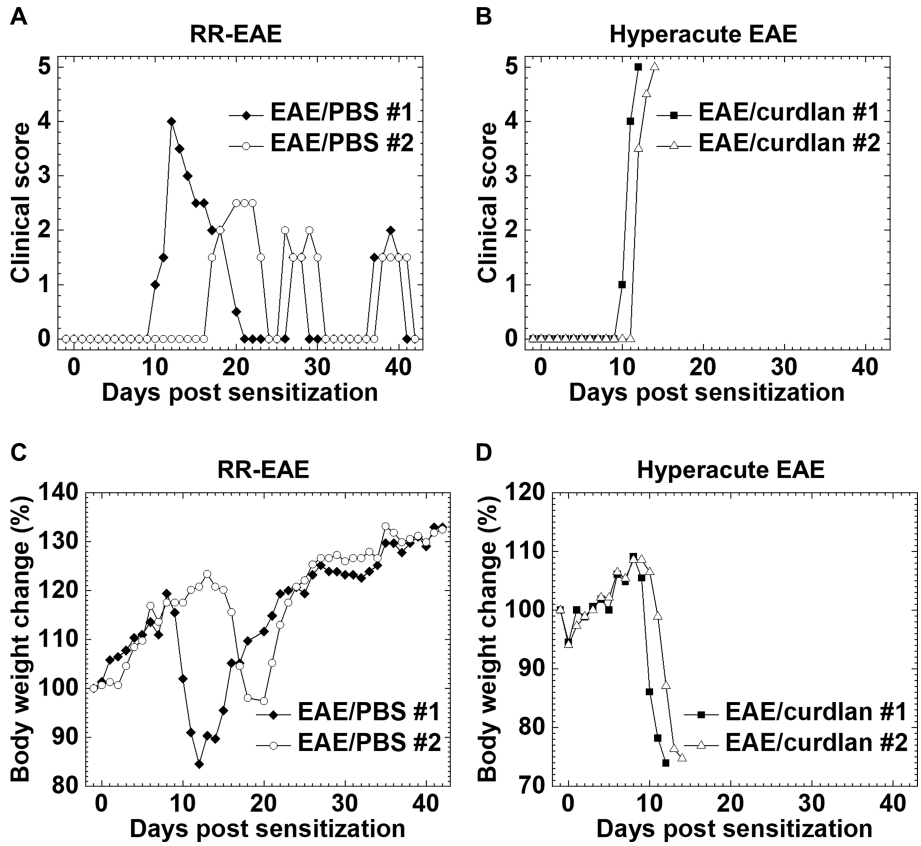

FIGURE 1 | Two clinical courses of experimental autoimmune encephalomyelitis (EAE) induced with myelin proteolipid protein $(PLP)_{139\text{-}151}$. One day prior to EAE induction, SJL/J mice were injected intraperitoneally (i.p.) with phosphate-buffered saline (PBS) (EAE/PBS, **A, C**) or curdlan (EAE/curdlan, **B, D**). Mice were observed for clinical signs **(A, B)** and weight changes **(C, D)** for 6 weeks. In the EAE/PBS group, mice developed relapsing-remitting (RR)-EAE; the mice had hind limb paralysis around 2 weeks post sensitization, recovered within 10 days (remission), and had relapses once or twice during the 6-week observation period. In the EAE/curdlan group, mice develop hyperacute EAE; the mice had progressive motor paralysis without remission and died within 1 week following the disease onset. Results are the two representative mice of 12 mice per group from three independent experiments.

meninges and perivascular areas (perivascular cuffing) (**Figure 2A** top panels). In contrast, in hyperacute EAE, severe demyelinating lesions contained both MNCs and neutrophils were observed not only around perivascular spaces but also in deep parenchymal areas of the spinal cord white matter. Using immunohistochemistry against CD3 (T cell marker) and Ly-6G (neutrophil marker), we found massive parenchymal infiltration of T cells (**Figure 2A** middle panels) and neutrophils (**Figure 2A** bottom panels) in hyperacute EAE. On the other hand, both RR-EAE and hyperacute EAE mice had a small number of $CD138^+$ plasma cells in the meninges of the spinal cord (**Supplementary Figure 1A**). Using immunohistochemistry against nonphosphorylated neurofilaments, we also found no differences in the number of damaged axons between the two EAE forms (**Supplementary Figure 1B**). In the brain, the anatomic distribution and severity of lesions were similar between the control RR-EAE and hyperacute EAE; inflammation with or without mild demyelination was observed in the cerebellum and hippocampal fissure in both EAE forms (data not shown).

Curdlan Injection Ameliorates Chronic TMEV-IDD, But Does Not Alter Acute Polioencephalomyelitis

Next, we determined whether curdlan treatment could alter TMEV-IDD, a viral model of MS. We injected curdlan one day prior to TMEV infection and monitored the clinical signs and body weight changes for 5 weeks (**Figure 3A**). TMEV infection causes a biphasic disease: acute polioencephalomyelitis 1 week p.i. (acute phase) and TMEV-IDD 1 month p.i. (chronic phase). During the acute phase, TMEV infects and replicates in neurons mainly in the gray matter of the brain, leading to polioencephalomyelitis; tissue damage is induced by viral pathology, not immunopathology. During the acute phase of TMEV infection, both groups had similar impaired righting reflex scores (**Figure 3A**) and weight loss (data not shown), reflecting acute polioencephalomyelitis.

During the chronic phase, TMEV-infected mice with curdlan treatment exhibited lower clinical scores than the control TMEV-infected mice without treatment (e.g., days 34 and 35, $P < 0.05$, Mann-Whitney U test, **Figure 3A**). The curdlan

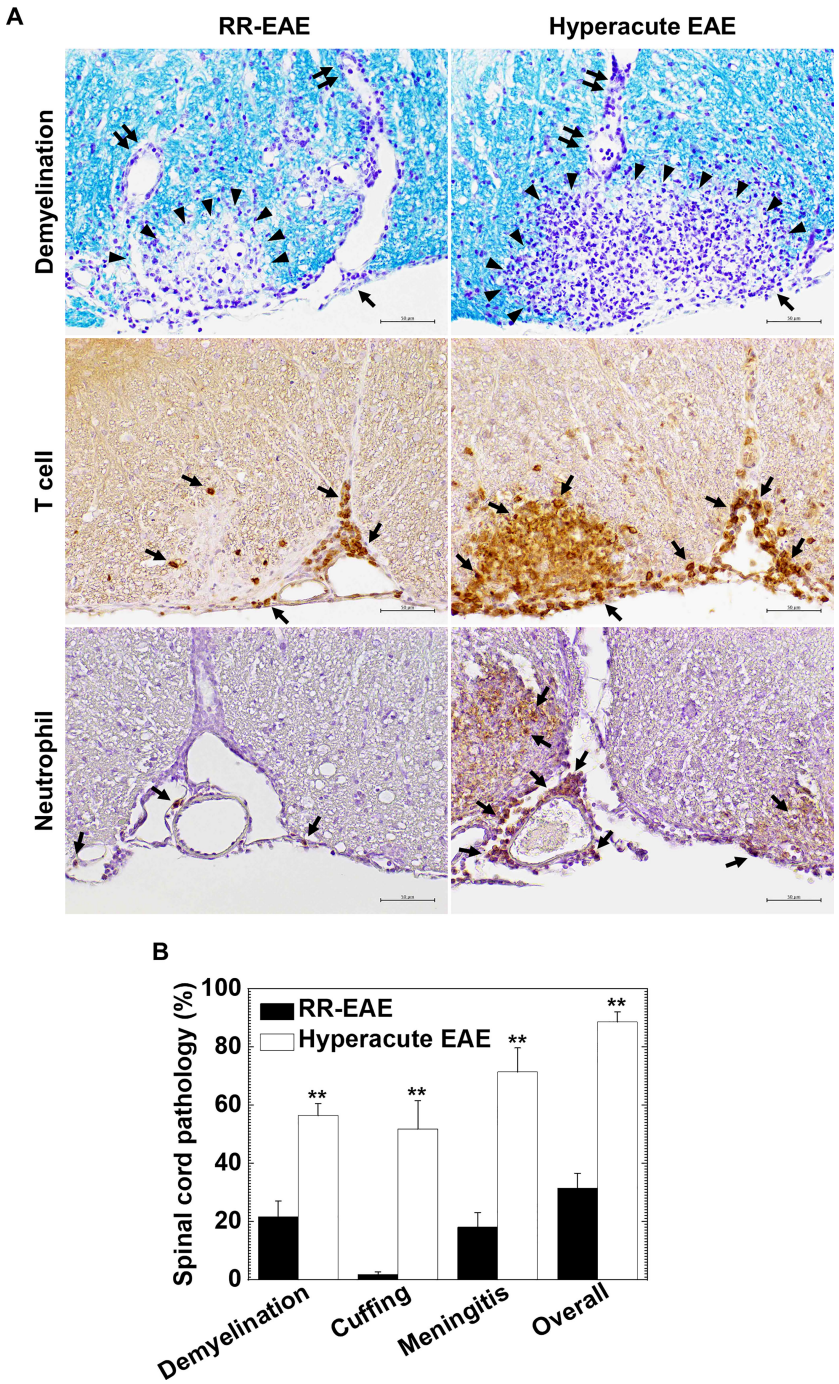

FIGURE 2 | Curdlan-induced hyperacute EAE mice developed more severe demyelinating lesions with massive infiltration of T cells and neutrophils in the spinal cord. **(A)** We visualized myelin by Luxol fast blue stain (top panels) and infiltration of T cells and neutrophils by immunohistochemistry against CD3 (middle panels) and Ly-6G (bottom panels), respectively, in RR-EAE (left) and hyperacute EAE (right). In RR-EAE, we observed mild to moderate demyelination around perivascular spaces or subpial areas with infiltration of mononuclear cells (MNCs), mainly composed of $CD3^+$ T cells; only a few neutrophils were observed in the meninges. In hyperacute EAE, we found severe demyelination with massive parenchymal infiltration of MNCs and polymorphonuclear cells (PMNs), which were composed of $CD3^+$ T cells and Ly-6G neutrophils, respectively. In Luxol fast blue staining, arrowheads, paired arrows, and arrows indicate demyelination, perivascular cuffing (inflammation), and meningitis, respectively. In immunostaining, arrows indicate $CD3^+$ T cells (middle panels) and Ly-$6G^+$ neutrophils (bottom panels). Tissue sections are representative of five to eight mice per group. Scale bar = 50 μm. **(B)** Neuropathology scores of the spinal cords in RR-EAE (black bar) and hyperacute EAE (white bar). Hyperacute EAE mice had significantly higher pathology scores than RR-EAE in all pathology classes: demyelination, perivascular cuffing (inflammation), meningitis, and overall pathology. Values are the mean + standard error of the mean (SEM) of six to eight mice per group. $^{**}P < 0.01$, Student's *t*-test.

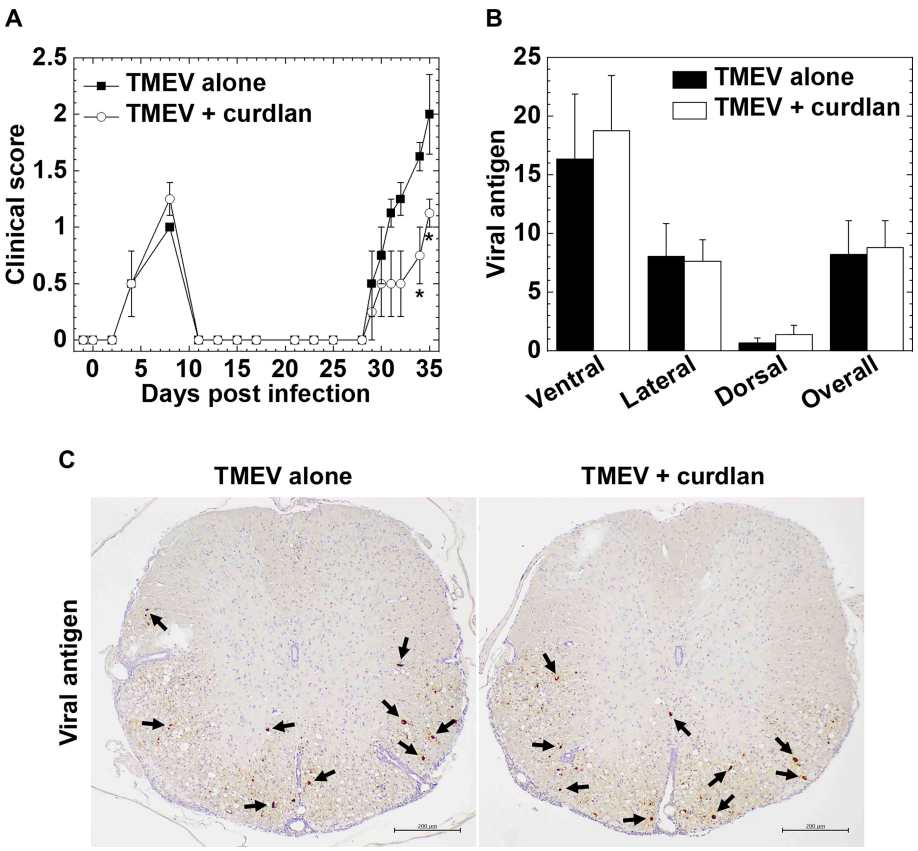

FIGURE 3 | Curdlan treatment suppressed chronic Theiler's murine encephalomyelitis virus (TMEV)-induced demyelinating disease (TMEV-IDD). **(A)** We evaluated the clinical signs by impaired righting reflex scores in the control mice (closed boxes) and curdlan-treated mice (open circles) following TMEV infection. One day prior to TMEV infection, mice were injected with curdlan (TMEV + curdlan); the control mice had no treatment (TMEV alone). The curdlan treatment group had a delayed disease onset and less severe clinical signs during the chronic phase, 1 month post infection (p.i.), but not during the acute phase, 1 week, p.i. Results are representative of three independent experiments (four mice per group per experiment). *$P < 0.05$, Mann-Whitney U test. **(B)** Numbers of viral antigen-positive cells of the spinal cord tissue sections from the control mice (black bar) and curdlan-treated mice (white bar) 5 weeks after TMEV infection. Values are the mean + SEM of four mice per group. **(C)** Immunohistochemistry against viral antigens of the spinal cord tissue sections from the control mice and curdlan-treated mice 5 weeks after TMEV infection. Arrows indicate viral antigen-positive cells (scale bar = 200 μm). Tissue sections were representative of four mice per group.

treatment group had also delayed onset, compared with the control group [mean onset days ± standard error of the mean (SEM) of the combined data of three individual experiments: TMEV alone (n = 12), 29.5 ± 0.7; TMEV + curdlan (n = 12), 32.8 ± 0.9; $P < 0.01$, Student's t-test]. In both groups, TMEV-IDD did not result in body weight loss during the chronic phase (data not shown), as described previously (Martinez et al., 2014).

Curdlan Injection Suppresses Axonal Degeneration, But Not Inflammatory Demyelination, in TMEV-IDD

To investigate how curdlan treatment ameliorated TMEV-IDD, we compared neuropathology between the control and curdlan treatment groups. Since β-glucan treatment has been shown to play beneficial effects on several viral infections, reducing the number of viral antigen-positive cells (Jung et al., 2004; Quintin, 2019), we compared the levels of TMEV-infected cells between the two groups by immunohistochemistry with anti-TMEV antibody and quantified the viral antigen-positive cells (**Figures 3B, C**). In both groups, TMEV antigen-positive cells were mainly localized in the white matter of the ventral and lateral funiculi of the spinal cord; the numbers of TMEV antigen-positive cells were comparable.

In TMEV-IDD, axonal degeneration and inflammatory demyelination in the white matter of the spinal cord develop 1 month p.i (Tsunoda et al., 2003); axonal degeneration has been shown to contribute to clinical signs more than demyelination (Rivera-Quiñones et al., 1998; Martinez et al., 2015). Using immunohistochemistry against nonphosphorylated neurofilaments, we visualized damaged axons in the white matter of the spinal cord and compared the levels of axonal degeneration between the control and curdlan-treated mice (**Figures 4A** top panels and **4B**). TMEV-infected mice from both groups developed axonal degeneration in the white matter of the spinal cord, particularly in the ventral and lateral funiculi of the spinal cord, as described previously (Tsunoda et al., 2003). Consistent with the clinical scores, curdlan-treated mice had significantly less severe axonal degeneration in the spinal cord, particularly in the ventral funiculus, compared with the control

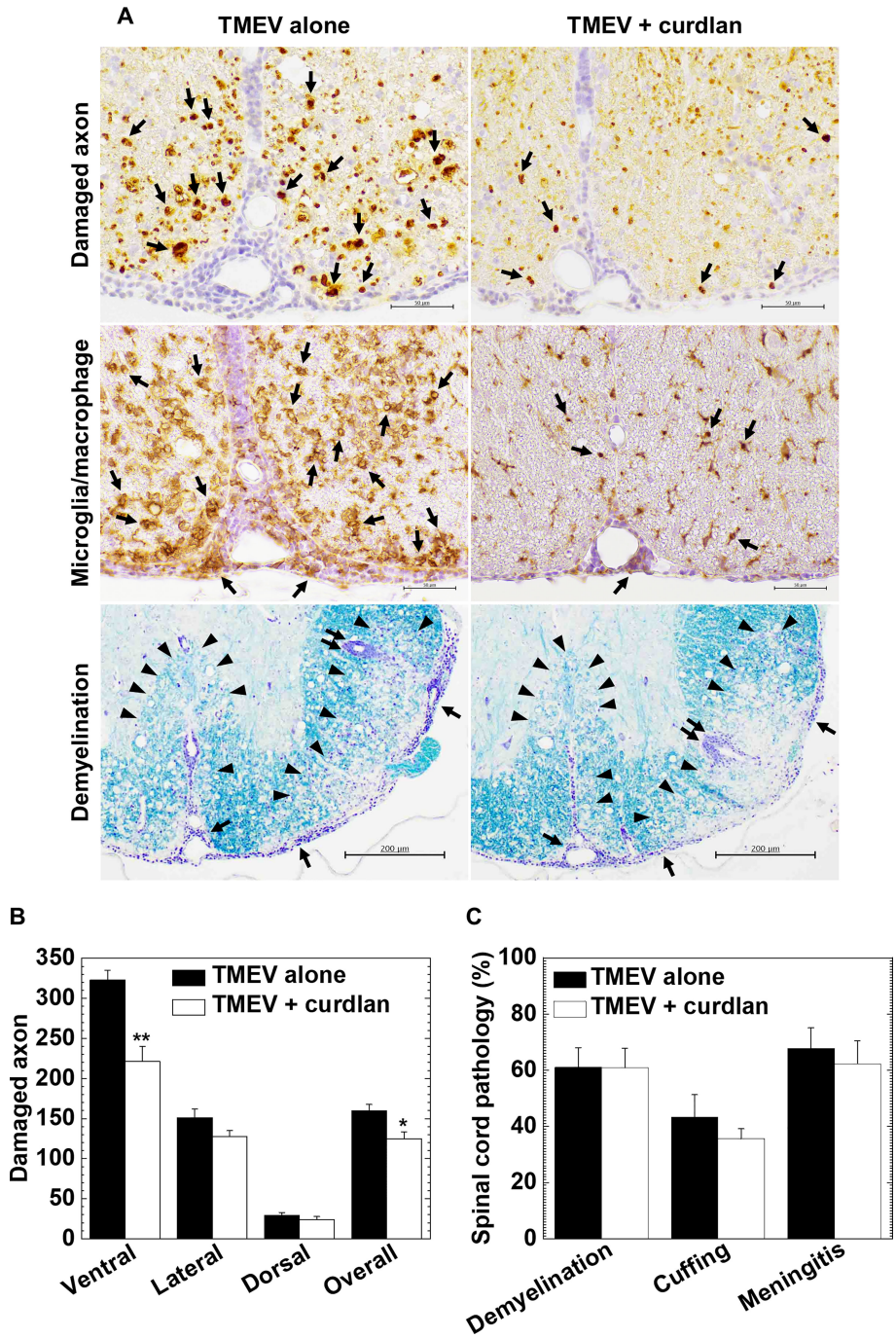

FIGURE 4 | Curdlan treatment suppressed axonal damage, but not inflammatory demyelination, in TMEV-IDD. **(A)** In the curdlan treatment group, we observed fewer damaged axons (top panels) and activated macrophages/microglia (middle panels), compared with the control group. On the other hand, the levels of inflammation and demyelination were similar between the two groups (bottom panels). Immunohistochemistry against non-phosphorylated neurofilaments (top panels) and Iba1 (middle panels), and myelin stain by Luxol fast blue (bottom panels), using spinal cord sections from the control mice and curdlan-treated mice 5 weeks p.i. In immunohistochemistry (scale bar = 50 μm), arrows indicate damaged axons (top panels) and microglia/macrophage activation (middle panels). In Luxol fast blue stain (scale bar = 200 μm), arrowheads, paired arrows, and arrows indicate demyelination, perivascular cuffing (inflammation), and meningitis, respectively. Tissue sections are representative from three independent experiments (four mice per group per experiment). **(B, C)** We quantified the number of damaged axons per spinal cord quadrant **(B)** and neuropathology scores **(C)** of the spinal cord in the TMEV alone (black bar) and TMEV + curdlan groups (white bar) 5 weeks p.i. The TMEV + curdlan group had less damaged axons in the spinal cord, particularly in the ventral funiculus, compared with the TMEV alone group, although the pathology scores of demyelination, perivascular cuffing (inflammation), and meningitis were similar between the two groups. Values are the mean + SEM of four mice per group. $^{*}P < 0.05$ and $^{**}P < 0.01$, Student's *t*-test.

mice (**Figure 4B**). We also visualized microglia/macrophage activation in the spinal cord by immunohistochemistry against Iba1 (microglia/macrophage marker) and found lower levels of microglia/macrophage activation in the spinal cord, particularly in the ventral funiculus (**Figure 4A** middle panels), in the curdlan treatment group than in the control group. To further determine the associations between damaged axons and activated microglia/macrophages, we conducted double-immunostaining with antibodies against nonphosphorylated neurofilaments and Iba1. We observed damaged axons adjacent to activated microglia/macrophages; TMEV-infected mice from the curdlan treatment group had fewer damaged axons and activated macrophages than the control group (**Supplementary Figure 2** top panels).

Using Luxol fast blue stain, we compared inflammation and demyelination between the control and curdlan treatment groups (**Figures 4A** bottom panels and **4C**). In both groups, we found similar levels of demyelination, perivascular cuffing (inflammation), and meningitis in the spinal cord; CNS immune infiltrates were composed of MNCs, not neutrophils, in both groups. Using immunohistochemistry against CD3, we found similar levels of T-cell infiltration in the spinal cord between the two groups (**Supplementary Figure 2** bottom panels), which was consistent with the inflammation scores in **Figure 4C**.

Curdlan Injection Enhances Pro-inflammatory Cytokine Productions, But Not Antigen-Specific Lymphoproliferation, in EAE

We determined the effects of curdlan injection on antigen-specific cellular and humoral immune responses as well as cytokine productions. In EAE, we found no differences in the levels of $PLP_{139\text{-}151}$-specific lymphoproliferation between the control and curdlan treatment groups (**Figure 5A**). The lymphoproliferative responses were suppressed in the presence of a blocking antibody against CD4, but not CD8, in the two groups; we confirmed the previous findings (Tsunoda and Fujinami, 1996) that $PLP_{139\text{-}151}$ sensitization primed only $CD4^+$ T cells. Similarly, curdlan injection did not alter serum anti-$PLP_{139\text{-}151}$ IgG1 or IgG2c antibody titers (**Figure 5B**). Furthermore, we examined whether curdlan injection could affect antigen-specific cytokine profiles in the periphery using the regional lymph node cells a few days before the disease onset (day 8 or 9) and at the disease peak (day 13 or 14). We quantified the amounts of pro-inflammatory IL-17/IFN-γ and anti-inflammatory IL-4/IL-10 cytokines by cytokine ELISAs (**Figures 5C, D**). Before the onset of EAE, the levels of IL-17, IFN-γ, and IL-10 production were higher in the curdlan treatment group than in the control group. At the disease peak, IL-17 and IFN-γ levels, but not IL-10, remained high in the curdlan group, although IL-17 and IFN-γ levels were decreased substantially in the control group. IL-4 was undetectable in both groups. We also determined the effects of curdlan on major immune-related gene expressions, including cytokines/chemokines, transcription factors, and adhesion molecules, in the spinal cord at the disease peak by real-time PCR. Compared with the control EAE mice, the curdlan-treated EAE mice had significantly higher levels of IL-10, IgA, and CXCL9 gene expressions in the spinal cord ($P < 0.05$, Student's *t*-test); the levels of IFN-γ, VCAM-1, ICAM-1, and CXCR3 gene expressions tended to be higher in the spinal cord of curdlan-treated mice ($P < 0.1$, Student's *t*-test, **Figures 5E, F**).

Curdlan Injection Does Not Alter TMEV-Specific Lymphoproliferation or Expressions of Cytokine/Adhesion Molecules in TMEV Infection

In TMEV-IDD, we compared the levels of TMEV-specific lymphoproliferative responses between the TMEV alone and TMEV + curdlan groups and found that both TMEV-specific $CD4^+$ and $CD8^+$ T cell responses were comparable between the two groups (**Figure 6A**). We also compared serum anti-TMEV antibody titers and cytokine profiles by ELISAs between the two groups. The curdlan treatment group had significantly reduced anti-TMEV IgG1 (induced by IL-4) titers, compared with the TMEV alone group, although there were no differences in anti-TMEV IgG2c (induced by IFN-γ), IgA, or IgM titers (**Figure 6B**). On the other hand, curdlan injection enhanced the amounts of IL-17 and IFN-γ, but not the amounts of IL-4 or IL-10, although there were no statistical differences between the two groups (**Figure 6C**).

We also determined the effects of curdlan on immune cells/molecules in the CNS during the acute and chronic phases of TMEV infection by real-time PCR analyses of gene expressions of T-cell related molecules, cytokines/chemokines, and adhesion molecules. We found no differences in the levels of cellular/humoral immunity-related gene expressions or chemokine/adhesion molecule gene expressions during the acute phase (**Figures 7A, B**), or during the chronic phase of TMEV infection between the control and curdlan treatment groups (**Figures 7C, D**).

Although we found no differences in immune-related gene expressions between the control and curdlan treatment groups, we found statistical differences in clinical signs, damaged axons, and immunoglobulin titers. PCA has been used to characterize the overall pathophysiology of disease conditions from multivariate data that can be composed of a different set of metrics (Sato et al., 2014; Omura et al., 2019). By calculating factor loading for PC values, one can rank the multivariate data based on the extent of which components contribute to each PC value. Thus, we used the clinical, neuropathological, and immunological data to characterize the overall pathophysiology associated with curdlan treatment. PCA clearly separated the two groups into two distinct populations by PC2 values, which seemed to reflect the disease severity; the proportion of variance of PC1 and PC2 were 49.8% and 21.1%, respectively (**Figure 7E**). Factor loading for PC2 showed that the clinical and axonal damage scores contributed to PC2 values, although viral persistence and inflammatory demyelination were not associated with PC2 values (**Figure 7F**). This was consistent with the previous findings that axonal damage, rather than the extent of viral persistence or inflammatory demyelination, contributed to clinical disability in TMEV-IDD (Yamada et al., 1990; Rivera-Quiñones et al., 1998).

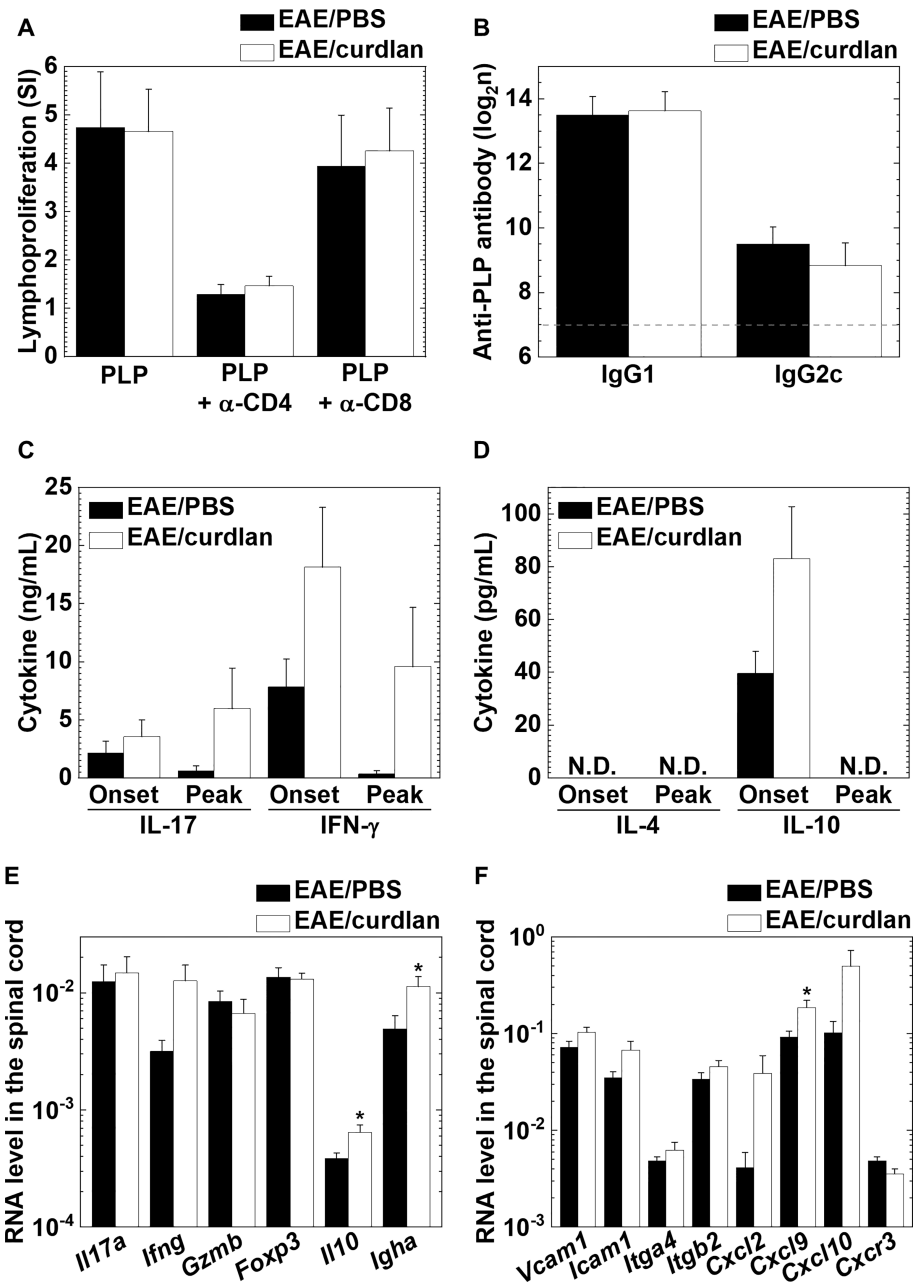

FIGURE 5 | Curdlan injection enhanced the production of interleukin (IL)-17 and interferon (IFN)-γ, but not antigen-specific lymphoproliferation or antibody responses in EAE. **(A)** $PLP_{139-151}$-specific lymphoproliferative responses of lymph node cells from the control (EAE/PBS, black bar) and curdlan-treated (EAE/curdlan, white bar) EAE mice a few days before the disease onset, 8–9 days post sensitization. Inguinal lymph node cells were stimulated with the $PLP_{139-151}$ peptide in the presence or absence of a blocking antibody against CD4 or CD8. Levels of lymphoproliferation were expressed as stimulation indexes (SI): (mean absorbance in $PLP_{139-151}$ stimulation)/(mean absorbance without stimulation). **(B)** Enzyme-linked immunosorbent assays (ELISAs) of serum anti-$PLP_{139-151}$ immunoglobulin (Ig) G1 and IgG2c antibodies in sera from the control EAE and curdlan-treated EAE mice 13–14 days post sensitization. The dotted line indicates the detection limit. **(C, D)** ELISAs of IL-17, IFN-γ **(C)**, IL-4, and IL-10 **(D)** production from lymph node cells of the control EAE and curdlan-treated EAE mice harvested a few days before onset (Onset) or at the disease peak (Peak). Cells isolated from the inguinal lymph nodes were cultured with the $PLP_{139-151}$ peptide. The four cytokines in the culture supernatants were quantified using ELISA kits. N.D., not detectable. **(E, F)** Real-time polymerase chain reaction (PCR) analyses of T cell-related **(E)** and immune cell migration/infiltration-related **(F)** genes in the spinal cord from the control and curdlan-treated EAE mice at the disease peak. *Il17a* (IL-17), *Ifng* (IFN-γ), *Gzmb* (granzyme B), *Foxp3* (forkhead box P3, regulatory T cell marker), *Il10* (IL-10), *Igha* (Ig heavy chain α, IgA marker), *Vcam1* (vascular cell adhesion molecule 1), *Icam1* (intracellular adhesion molecule 1), *Itga4* (integrin α4), *Itgb2* (integrin β2), *Cxcl2* [chemokine (C-X-C motif) ligand 2, CXCL2], *Cxcl9* (CXCL9), *Cxcl0* (CXCL10, also known as IFN-γ-inducible protein 10), and *Cxcr3* [chemokine (C-X-C motif) receptor 3, CXCR3]. *Pgk1* expression was used as a housekeeping gene for normalization. **(A–F)** Values are the mean + SEM from six to eight mice per group. $^*P < 0.05$, Student's *t*-test.

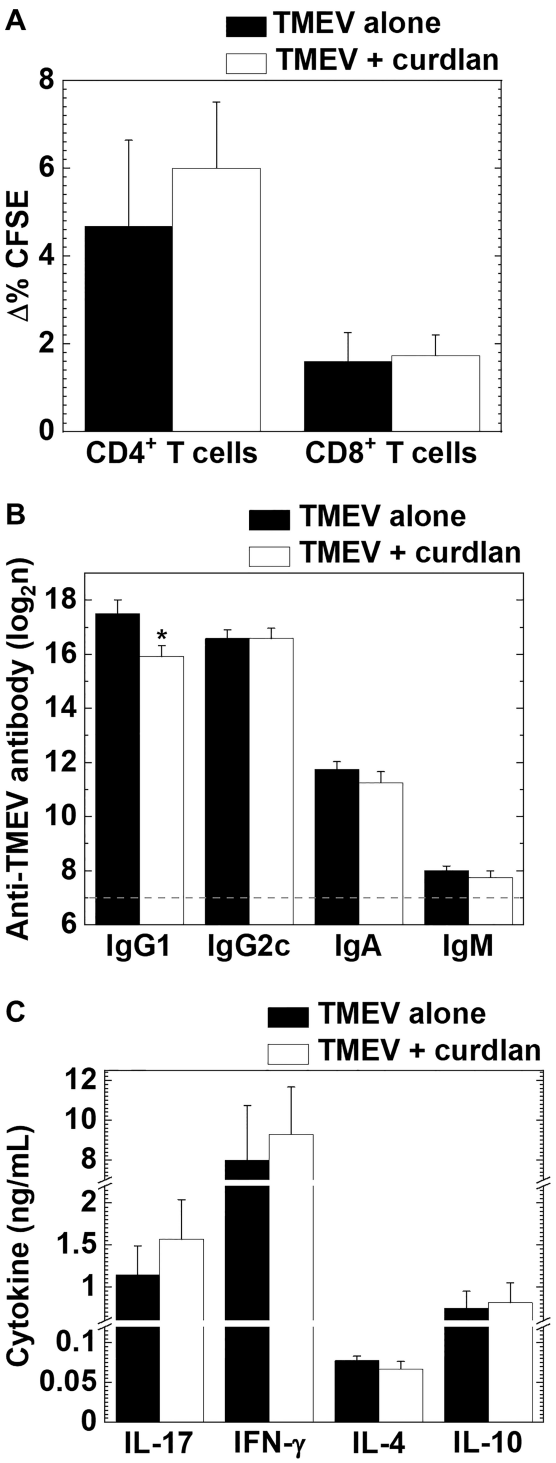

FIGURE 6 | TMEV-specific T cell proliferation and antibody responses, and cytokine productions in TMEV-IDD with or without curdlan treatment. **(A)** We found similar levels of TMEV-specific $CD4^+$ T cell and $CD8^+$ T cells responses between the control (TMEV alone, black bar) and curdlan-treated (TMEV/curdlan, white bar) mice 5–6 weeks p.i. Values of TMEV-specific lymphoproliferative responses were expressed as Δ% CFSE: (mean CFSE-positive cell % in TMEV-APC stimulation) – (mean CFSE-positive cell % in control-APC stimulation). **(B)** Although the curdlan treated group had lower serum anti-TMEV IgG1 titers compared with the control group, anti-TMEV IgG2c, IgA, and IgM titers were similar between the two groups 5–6 weeks p.i. The dotted line indicates the detection limit. $^*P < 0.05$, Student's *t*-test. **(C)** IL-17, IFN-γ, IL-4, and IL-10 production from splenic MNCs of the control and curdlan-treated mice 5–6 weeks p.i. Antibody titers and cytokine concentrations were determined by ELISAs. **(A–C)** Values are the mean + SEM from eight to twelve mice per group.

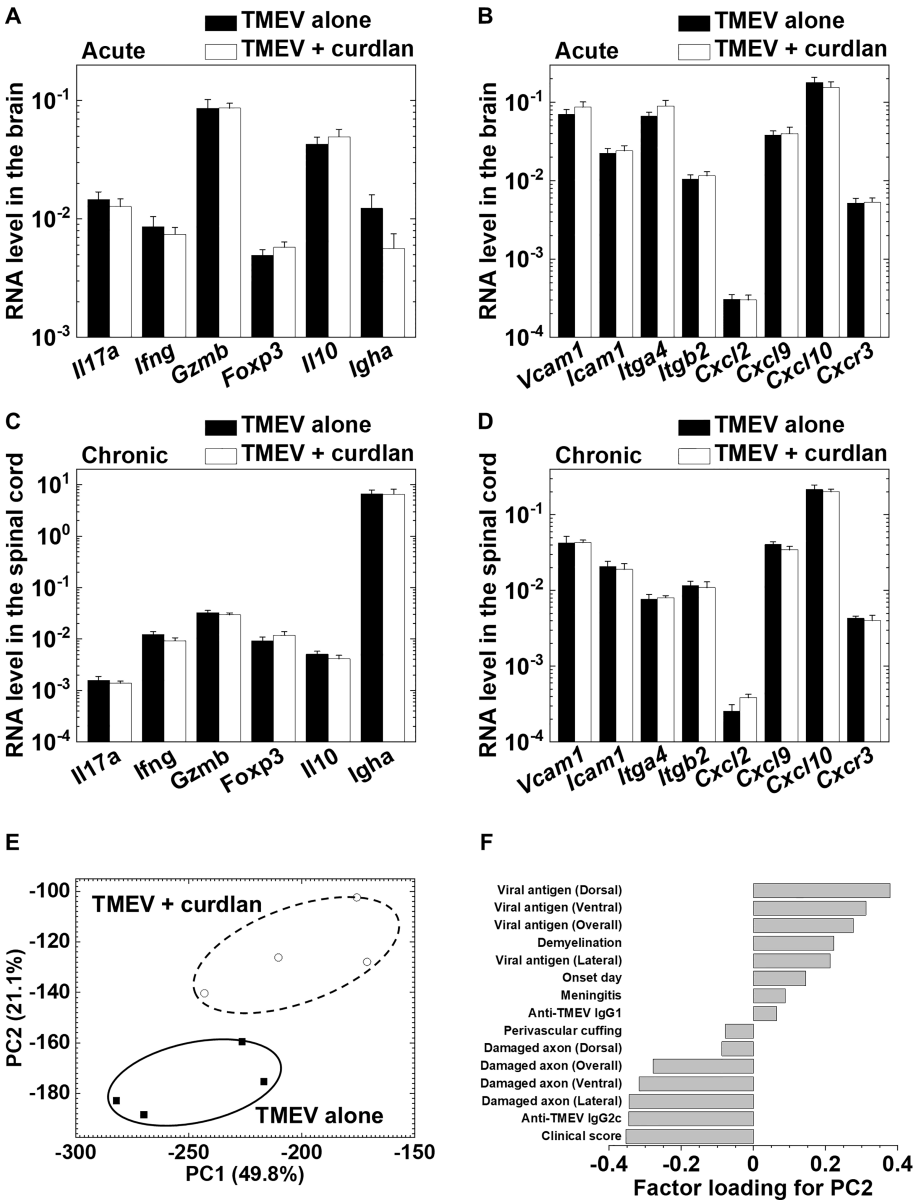

FIGURE 7 | Curdlan injection did not alter immune-related gene expressions in the central nervous system (CNS) during the acute and chronic phases of TMEV infection between the control and curdlan treatment groups. **(A–D)** Real-time PCR analyses of T cell-related and immune cell migration/infiltration-related genes in the brain 8 days p.i. **(A, B)** and in the spinal cord 5 weeks p.i. **(C, D)**. **(A, C)** mRNA levels of *Il17a*, *Ifng*, *Gzmb*, *Foxp3*, *Il10*, and *Igha*. **(B, D)** mRNA levels of *Vcam1*, *Icam1*, *Itga4*, *Itgb2*, *Cxcl2*, *Cxcl9*, *Cxcl0*, and *Cxcr3*. *Pgk1* expression was used as a housekeeping gene for normalization. Values are the mean + SEM of four mice per group. **(E)** Principal component analysis (PCA) separated TMEV-infected control and curdlan-treated mice as two distinct populations by the principal component (PC) 2 values. We conducted PCA, using 15 immunopathology data: neuropathology (demyelination, perivascular cuffing, meningitis, viral-antigen positive cells, damaged axons), antibody titers, clinical scores, and the disease onset day from the two groups 5 weeks p.i. Each group was composed of four mice. **(F)** Factor loading for PC2 showed that clinical scores and damaged axon numbers contributed to the PC2 distribution.

DISCUSSION

In this study, we demonstrated that microbial component curdlan injection in the autoimmune and viral models for MS resulted in disease exacerbation and amelioration, respectively. In the $PLP_{139-151}$-induced RR-EAE model, a pure $CD4^+$ T cell-mediated disease, curdlan injection prior to PLP sensitization induced hyperacute EAE and the mice died around 2 weeks after EAE induction. In TMEV-IDD, curdlan injection prior to TMEV infection delayed the disease onset and reduced the severity of chronic disease, around 1 month p.i. On the other hand, we previously reported that curdlan injection exacerbated MOG_{92-106}-induced EAE in SJL/J mice, who died around 1 month after EAE induction, where enhancement of $CD4^+$ T-cell and anti-

MOG demyelinating antibody responses converted RR-EAE into chronic primary progressive (PP)-EAE (Omura et al., 2019). Thus, the effects of curdlan injection on MS models seemed to be different, depending on several factors such as the etiology (autoimmune versus viral), disease onset (acute versus chronic disease), and effector mechanism (myelin-specific $CD4^+$ T cells, anti-myelin antibodies, or anti-viral immune responses). We also found that curdlan injection on day 21 after the onset of $PLP_{139-151}$-induced RR-EAE (**Supplementary Figure 3**) or on day 53 after the onset of MOG_{92-106}-induced EAE (Libbey et al., 2010) converted the RR disease course into a progressive course in more than 50% of EAE mice. On the other hand, using C57BL/6 mice, we determined the effects of curdlan in MOG_{35-55}-induced EAE, in which EAE mice have a monophasic disease course without relapsing (Fernando et al., 2014). Although curdlan injection in the MOG_{35-55}-induced EAE model developed hyperacute EAE with similar neuropathology to what was observed in the $PLP_{139-151}$-induced EAE model, the incidence of hyperacute EAE was lower in MOG_{35-55}-induced EAE mice than in $PLP_{139-151}$-EAE mice (**Supplementary Table 1**). On the other hand, most curdlan-injected C57BL/6 mice developed monophasic EAE without differences in the clinical signs or the mortality, compared with PBS-injected control EAE mice. Thus, the effects of curdlan injection differed between the two classic EAE models: the MOG_{35-55}-induced EAE and $PLP_{139-151}$-induced EAE models. Although it is unclear what factors contribute to the different outcomes between the two EAE models, both models have several differences that may play a role. For example, to induce EAE, injection of pertussis toxin, which has been proposed to act as an adjuvant and break the blood-brain barrier, is required for C57BL/6 mice, but not SJL/J mice. C57BL/6 mice develop monophasic EAE without relapses; SJL/J mice develop RR-EAE. SJL/J mice have several immunological and genetical deficits, including the absence of one major histocompatibility complex class II molecule, several TCR repertoire, and natural killer (NK) cells (Kaminsky et al., 1985; Friedmann et al., 1987; Bahk et al., 1997); both mouse strains also have different compositions of the gut microbiota that has been shown to modulate immune responses (Gandy et al., 2019). These findings give insight into the inconsistent and anecdotal reports on the involvement of bacterial and fungal infections in MS published previously; immunomodulation by microbial components likely depends on the immunological and etiological background of each MS patient.

In this study, to gain mechanistic insight, we tested whether curdlan could directly stimulate encephalitogenic effector cells, conferring the ability to induce hyperacute EAE. We used two passive EAE models, where MOG_{35-55}- or $PLP_{139-151}$-specific T cells were activated *in vitro* in the presence or absence of curdlan and then transferred into naive C57BL/6 or SJL/J mice, respectively. In the two passive EAE models, however, *in vitro* direct stimulation of encephalitogenic effector cells with curdlan neither increased the incidence of EAE nor induced hyperacute EAE (**Supplementary Table 2**). Thus, the direct stimulation of effector encephalitogenic cells with curdlan alone was not sufficient for hyperacute EAE induction.

In curdlan-induced hyperacute EAE, we found massive infiltration of both T cells and neutrophils in the spinal cord, not in the brain. The heavy neutrophil infiltration in the CNS was similar to the classical hyperacute EAE model in rats (Levine and Wenk, 1965), although the hemorrhage observed in the classical hyperacute EAE was rare in the curdlan-induced hyperacute EAE. Neutrophil infiltration has also been observed in other PP-EAE models, including MOG_{92-106}-induced PP-EAE, where IL-17-producing Th17 cells play a role in the neutrophil recruitment in the CNS (Omura et al., 2019). In this study, we found that the levels of IL-17 and IFN-γ production remained high at the peak of hyperacute EAE, but not RR-EAE, suggesting the pathogenic roles of pro-inflammatory Th17 cells and Th1 cytokines in disease progression. This was consistent with the findings that curdlan has been known as a Th17 inducer; curdlan has also been shown to enhance Th1 responses (LeibundGut-Landmann et al., 2007; Kim et al., 2016). Although the precise pathomechanism of curdlan-mediated Th1 responses is still controversial, curdlan has been shown to be recognized by toll-like receptor 4, resulting in the increased production of IL-12, which contributes to Th1 differentiation (Kim et al., 2016). Alternatively, Th17 cells have been reported to trigger the recruitment of Th1 cells by inducing chemokines, such as CXCL9, CXCL10, and CXCL11. In this study, we found that the expression levels of *Cxcl9*, *Cxcl10*, and *Ifng* in the spinal cord were higher in the curdlan-treated EAE mice than in the control EAE mice. Furthermore, curdlan treatment enhanced the gene expressions of adhesion molecules including *Vcam1* and *Icam1*; PCA showed that the increased expressions of *Cxcl9* and *Cxcl10* as well as *Cxcl2* (neutrophil chemokine) in the spinal cord could contribute to immunopathology of the curdlan treatment group (data not shown). These results were consistent with the neuropathological findings that the curdlan treatment EAE group had more severe CNS inflammation and higher levels of myelin-specific Th17 and Th1 responses than the control EAE group. On the other hand, we found no changes in anti-PLP antibody responses or axonal degeneration in hyperacute EAE mice, suggesting that these factors have no roles in disease exacerbation in the curdlan treatment group.

Curdlan has also been reported to enhance IL-10 production and favor IgA antibody responses (LeibundGut-Landmann et al., 2007; Kawashima et al., 2012; Fujimoto et al., 2019). Recently, IgA^+ cells have been detected in the active demyelinating lesions of MS patients (Probstel et al., 2020); IgA-secreting plasma cells have been shown to play protective roles in EAE by producing IL-10 (Rojas et al., 2019). Thus, we had anticipated that curdlan treatment might be beneficial in our EAE model. However, this was not the case. Although we found significantly increased levels of IL-10 and IgA gene expression in the spinal cord of curdlan-treated EAE mice, we did not see increases in IgA-producing cells (data not shown) or $CD138^+$ plasma cells (**Supplementary Figure 1**) in the spinal cord by immunohistochemistry in the curdlan treatment group.

In contrast to EAE, curdlan injection ameliorated TMEV-IDD with reduced axonal degeneration in the spinal cord,

although it did not alter the levels of inflammation/demyelination or viral persistence. This was consistent with the previous findings by Rivera-Quiñones et al. (1998) that the clinical signs of TMEV-IDD were associated with axonal degeneration rather than inflammatory demyelination. Previously, we also demonstrated that, although TMEV-infected SJL/J and RORγt transgenic mice had similar levels of inflammatory demyelination, only TMEV-infected SJL/J mice had neurological signs with severe axonal damage. Here, TMEV-infected RORγt transgenic mice had no clinical signs because of significantly reduced axonal degeneration (Martinez et al., 2015).

Several factors have been suggested to contribute to axonal degeneration in TMEV-IDD, for example, activation of microglia/macrophages, $CD8^+$ T cells, and neuronal damage during the acute phase of TMEV infection. In this study, we found that $Iba1^+$ activated microglia/macrophages accumulated around the lesions with damaged axons in the spinal cord. Since β-glucan treatment has been shown to induce a long-lasting immunomodulatory effect on innate immune cells including microglia (Haley et al., 2019), curdlan may affect microglia/macrophages by binding to the specific receptor dectin-1 during the early phase of TMEV infection, which influences the activation status of microglia/macrophages during the chronic phase of TMEV infection, 1 month p.i. Using immunohistochemistry against dectin-1 (Dong et al., 2014), we examined the expression levels of dectin-1 in the spinal cord as well as in the spleen as the positive control. Consistent with previously published data (Dong et al., 2014), we found a small number of dectin-1-positive cells in the spleen, but not in the spinal cord (data not shown). This could be due to the low sensitivity limit used in the current study; the associations between dectin-1 expression and activated microglia and macrophages remain unknown. Although $CD8^+$ T cells have also been proposed to damage axons in TMEV infection, this seemed not to be the case in the curdlan treatment group; we did not find increased levels of $CD8^+$ T cell responses to TMEV or the upregulation of *Cd8a* (data not shown) and *Gzmb* in the spinal cord. Alternatively, the early neuronal damage by lytic TMEV infection during the acute phase can alter the levels of axonal degeneration later on; neuronal and axonal damage can be followed by Wallerian degeneration of axons. This is also unlikely since we found no difference in the severity of acute polioencephalomyelitis or CNS viral replication during the acute phase (data not shown) between the control and curdlan treatment groups.

In TMEV-IDD, TMEV-specific $CD4^+$ and $CD8^+$ T cells, as well as anti-TMEV antibodies, have been demonstrated to contribute to inflammatory demyelination (Sato et al., 2018). In this study, we did not see differences in TMEV-specific $CD4^+$ and $CD8^+$ T cell proliferation or anti-TMEV isotype responses between the control and curdlan treatment groups, except for the mild reduction of IgG1 titers in the curdlan treatment group. Since Th2 responses help immunoglobulin class switching to IgG1 in mice, the reduced anti-TMEV IgG1 titers in the curdlan treatment group can be due to the increased IFN-γ (Th1 cytokine)/IL-4 (Th2 cytokine) ratios (mean IFN-γ/IL-4 ± SEM: TMEV alone, 108.0 ± 39.5; TMEV + curdlan, 151.6 ± 46.2), although it did not reach statistical difference. We also found similar expression levels of Th-related cytokines, *Il17*, *Ifng*, and *Il10*, adhesion molecules, *Vcam1*, *Icam1*, *Itga4*, and *Itgb2*, and chemokines/chemokine receptor, *Cxcl2*, *Cxcl9*, *Cxcl10*, and *Cxcr3*, in the spinal cord between the control and curdlan treatment groups. These immune profiles were consistent with similar levels of inflammatory demyelination between the two groups.

In summary, we demonstrated that curdlan injection was detrimental in an autoimmune model for MS by converting it into a fatal hyperacute EAE with massive infiltration of T cells and neutrophils. On the other hand, curdlan injection ameliorated a viral model for MS with decreased CNS axonal degeneration, although it did not alter inflammation or demyelination. Since human MS has been suggested to be heterogenous with different etiology and immunopathology depending on each patient, the effects of microbial immunomodulating components, including curdlan, in human MS may differ. This could reflect diverse and often conflicting etiological reports of human MS following bacterial and fungal infections. It has been reported that, depending on the disease stage or subtype of MS, neuropathology of MS can be predominantly composed of axonal degeneration with microglia/macrophage activation; curdlan-like microbial components might be useful to treat such MS neuropathology. Lastly, our study supports the view that MS is a heterogeneous disease whose treatment needs to be tailored on a more individual basis, rather than considering only whether MS patients have an RR or progressive course. Our study also raises the issue that the clinical courses of MS may depend on the type of exposure (bacteria/virus/fungus), although it should be clarified whether other microbial components, such as *Mycobacterium smegmatis* (Kannan et al., 2020), also affect the clinical courses of MS, as a single modulator or together with other microbial components. In the future, these experimental and clinical approaches would lead to develop a basis for therapy, for example, to determine the levels of β-glucan as a biomarker in circulation might be beneficial once its role is clarified.

DATA AVAILABILITY STATEMENT

The raw data supporting the conclusions of this article will be made available by the authors, without undue reservation.

ETHICS STATEMENT

The animal study was reviewed and approved by Institutional Animal Care and Use Committee of Kindai University Faculty of Medicine and LSUHS.

AUTHOR CONTRIBUTIONS

FS and IT designed the experiments and prepared the manuscript. FS, YN, AK, SK, and IA performed the experiments. NEM and SO

aided in the experiments and manuscript preparation. IT supervised the experiments. All authors read and approved the final manuscript.

FUNDING

This work was supported by the Institutional Development Award (IDeA) from the National Institute of General Medical Sciences of the NIH (5P30GM110703, IT), the fellowships (FS and SO) from the Malcolm Feist Cardiovascular Research Endowment, LSUHS, the Research Program on Emerging and Re-emerging Infectious Diseases from the Japan Agency for Medical Research and Development (AMED, 21fk0108084h0803, IT), the All-Kindai University Support Project against COVID-19 (IT), and the KAKENHI from the Japan Society for the Promotion of Science [Grant-in-Aid for Scientific Research (C): JP20K07433, FS; JP19K08569, SO; and JP20K07455, IT].

ACKNOWLEDGMENTS

We thank Dr. Ah-Mee Park, Dr. Kota Moriguchi, Ms. Erina Kawashima, and Ms. Namie Sakiyama, Kindai University Faculty of Medicine, for helpful discussions and excellent technical assistance.

SUPPLEMENTARY MATERIAL

The Supplementary Material for this article can be found online at: https://www.frontiersin.org/articles/10.3389/fcimb.2022.805302/full#supplementary-material

REFERENCES

Alonso, R., Fernández-Fernández, A. M., Pisa, D., and Carrasco, L. (2018). Multiple Sclerosis and Mixed Microbial Infections. Direct Identification of Fungi and Bacteria in Nervous Tissue. *Neurobiol. Dis.* 117, 42–61. doi: 10.1016/j.nbd.2018.05.022

Bahk, Y. Y., Kappel, C. A., Rasmussen, G., and Kim, B. S. (1997). Association Between Susceptibility to Theiler's Virus-Induced Demyelination and T-Cell Receptor *Jβ1-Cβ1* Polymorphism Rather Than *Vβ* Deletion. *J. Virol.* 71, 4181–4185. doi: 10.1128/jvi.71.5.4181-4185.1997

Barsheshet, Y., Wildbaum, G., Levy, E., Vitenshtein, A., Akinseye, C., Griggs, J., et al. (2017). $CCR8^{+}FOXp3^{+}$ T_{reg} Cells as Master Drivers of Immune Regulation. *Proc. Natl. Acad. Sci. U. S. A.* 114, 6086–6091. doi: 10.1073/pnas.1621280114

Chaitanya, G. V., Omura, S., Sato, F., Martinez, N. E., Minagar, A., Ramanathan, M., et al. (2013). Inflammation Induces Neuro-Lymphatic Protein Expression in Multiple Sclerosis Brain Neurovasculature. *J. Neuroinflamm.* 10, 125. doi: 10.1186/1742-2094-10-125

Cossu, D., Yokoyama, K., and Hattori, N. (2018). Bacteria-Host Interactions in Multiple Sclerosis. *Front. Microbiol.* 9, 2966. doi: 10.3389/fmicb.2018.02966

Curtis, M. M., and Way, S. S. (2009). Interleukin-17 in Host Defence Against Bacterial, Mycobacterial and Fungal Pathogens. *Immunology* 126, 177–185. doi: 10.1111/j.1365-2567.2008.03017.x

Dong, B., Li, D., Li, R., Chen, S. C.-A., Liu, W., Liu, W., et al. (2014). A Chitin-Like Component on Sclerotic Cells of *Fonsecaea Pedrosoi* Inhibits Dectin-1-Mediated Murine Th17 Development by Masking β-Glucans. *PloS One* 9, e114113. doi: 10.1371/journal.pone.0114113

Fernando, V., Omura, S., Sato, F., Kawai, E., Martinez, N. E., Elliott, S. F., et al. (2014). Regulation of an Autoimmune Model for Multiple Sclerosis in Th2-Biased GATA3 Transgenic Mice. *Int. J. Mol. Sci.* 15, 1700–1718. doi: 10.3390/ijms15021700

Fraga-Silva, T. F. C., Mimura, L. A. N., Marchetti, C. M., Chiuso-Minicucci, F., Franca, T. G. D., Zorzella-Pezavento, S. F. G., et al. (2015). Experimental Autoimmune Encephalomyelitis Development Is Aggravated by *Candida Albicans* Infection. *J. Immunol. Res.* 2015, 635052. doi: 10.1155/2015/635052

Friedmann, A., Frankel, G., Lorch, Y., and Steinman, L. (1987). Monoclonal Anti-I-A Antibody Reverses Chronic Paralysis and Demyelination in Theiler's Virus-Infected Mice: Critical Importance of Timing of Treatment. *J. Virol.* 61, 898–903. doi: 10.1128/jvi.61.3.898-903.1987

Fujimoto, K., Kawaguchi, Y., Shimohigoshi, M., Gotoh, Y., Nakano, Y., Usui, Y., et al. (2019). Antigen-Specific Mucosal Immunity Regulates Development of Intestinal Bacteria-Mediated Diseases. *Gastroenterology* 157, 1530–1543.e4. doi: 10.1053/j.gastro.2019.08.021

Gandy, K. A. O., Zhang, J., Nagarkatti, P., and Nagarkatti, M. (2019). The Role of Gut Microbiota in Shaping the Relapse-Remitting and Chronic-Progressive Forms of Multiple Sclerosis in Mouse Models. *Sci. Rep.* 9, 6923. doi: 10.1038/s41598-019-43356-7

Haley, M. J., Brough, D., Quintin, J., and Allan, S. M. (2019). Microglial Priming as Trained Immunity in the Brain. *Neuroscience* 405, 47–54. doi: 10.1016/j.neuroscience.2017.12.039

Herrmann, I., Kellert, M., Schmidt, H., Mildner, A., Hanisch, U. K., Brück, W., et al. (2006). *Streptococcus Pneumoniae* Infection Aggravates Experimental Autoimmune Encephalomyelitis via Toll-Like Receptor 2. *Infect. Immun.* 74, 4841–4848. doi: 10.1128/IAI.00026-06

Hertzler, S., Luo, M., and Lipton, H. L. (2000). Mutation of Predicted Virion Pit Residues Alters Binding of Theiler's Murine Encephalomyelitis Virus to BHK-21 Cells. *J. Virol.* 74, 1994–2004. doi: 10.1128/JVI.74.4.1994-2004.2000

Hofstetter, H. H., Ibrahim, S. M., Koczan, D., Kruse, N., Weishaupt, A., Toyka, K. V., et al. (2005). Therapeutic Efficacy of IL-17 Neutralization in Murine Experimental Autoimmune Encephalomyelitis. *Cell Immunol.* 237, 123–130. doi: 10.1016/j.cellimm.2005.11.002

Hou, W., Kang, H. S., and Kim, B. S. (2009). Th17 Cells Enhance Viral Persistence and Inhibit T Cell Cytotoxicity in a Model of Chronic Virus Infection. *J. Exp. Med.* 206, 313–328. doi: 10.1084/jem.20082030

Hussman, J. P., Beecham, A. H., Schmidt, M., Martin, E. R., McCauley, J. L., Vance, J. M., et al. (2016). GWAS Analysis Implicates NF-κB-Mediated Induction of Inflammatory T Cells in Multiple Sclerosis. *Genes Immun.* 17, 305–312. doi: 10.1038/gene.2016.23

Isnard, S., Lin, J., Bu, S., Fombuena, B., Royston, L., and Routy, J. P. (2021). Gut Leakage of Fungal-Related Products: Turning Up the Heat for HIV Infection. *Front. Immunol.* 12, 656414. doi: 10.3389/fimmu.2021.656414

Jung, K., Ha, Y., Ha, S. K., Han, D. U., Kim, D. W., Moon, W. K., et al. (2004). Antiviral Effect of *Saccharomyces Cerevisiae* β-Glucan to Swine Influenza Virus by Increased Production of Interferon-γ and Nitric Oxide. *J. Vet. Med. B Infect. Dis. Vet. Public Health* 51, 72–76. doi: 10.1111/j.1439-0450.2004.00732.x

Kaminsky, S. G., Nakamura, I., and Cudkowicz, G. (1985). Genetic Control of the Natural Killer Cell Activity in SJL and Other Strains of Mice. *J. Immunol.* 135, 665–671.

Kannan, N., Haug, M., Steigedal, M., and Flo, T. H. (2020). Mycobacterium Smegmatis Vaccine Vector Elicits $CD4^{+}$ Th17 and $CD8^{+}$ Tc17 T Cells With Therapeutic Potential to Infections With Mycobacterium Avium. *Front. Immunol.* 11, 1116. doi: 10.3389/fimmu.2020.01116

Kawai, E., Sato, F., Omura, S., Martinez, N. E., Reddy, P. C., Taniguchi, M., et al. (2015). Organ-Specific Protective Role of NKT Cells in Virus-Induced Inflammatory Demyelination and Myocarditis Depends on Mouse Strain. *J. Neuroimmunol.* 278, 174–184. doi: 10.1016/j.jneuroim.2014.11.003

Kawashima, S., Hirose, K., Iwata, A., Takahashi, K., Ohkubo, A., Tamachi, T., et al. (2012). β-Glucan Curdlan Induces IL-10-Producing $CD4^{+}$ T Cells and Inhibits Allergic Airway Inflammation. *J. Immunol.* 189, 5713–5721. doi: 10.4049/jimmunol.1201521

Kim, H. S., Park, K. H., Lee, H. K., Kim, J. S., Kim, Y. G., Lee, J. H., et al. (2016). Curdlan Activates Dendritic Cells Through Dectin-1 and Toll-Like Receptor 4 Signaling. *Int. Immunopharmacol.* 39, 71–78. doi: 10.1016/j.intimp.2016.07.013

Komiyama, Y., Nakae, S., Matsuki, T., Nambu, A., Ishigame, H., Kakuta, S., et al. (2006). IL-17 Plays an Important Role in the Development of Experimental Autoimmune Encephalomyelitis. *J. Immunol.* 177, 566–573. doi: 10.4049/jimmunol.177.1.566

Kulcsar, K. A., Baxter, V. K., Greene, I. P., and Griffin, D. E. (2014). Interleukin 10 Modulation of Pathogenic Th17 Cells During Fatal Alphavirus Encephalomyelitis. *Proc. Natl. Acad. Sci. U. S. A.* 111, 16053–16058. doi: 10.1073/pnas.1418966111

LeibundGut-Landmann, S., Groß, O., Robinson, M. J., Osorio, F., Slack, E. C., Tsoni, S. V., et al. (2007). Syk- and CARD9-Dependent Coupling of Innate Immunity to the Induction of T Helper Cells That Produce Interleukin 17. *Nat. Immunol.* 8, 630–638. doi: 10.1038/ni1460

Levine, S., and Wenk, E. J. (1965). A Hyperacute Form of Allergic Encephalomyelitis. *Am. J. Pathol.* 47, 61–88.

Libbey, J. E., Cusick, M. F., and Fujinami, R. S. (2014). Role of Pathogens in Multiple Sclerosis. *Int. Rev. Immunol.* 33, 266–283. doi: 10.3109/08830185.2013.823422

Libbey, J. E., Tsunoda, I., and Fujinami, R. S. (2010). Studies in the Modulation of Experimental Autoimmune Encephalomyelitis. *J. Neuroimmune Pharmacol.* 5, 168–175. doi: 10.1007/s11481-010-9215-x

Lucchinetti, C., Brück, W., Parisi, J., Scheithauer, B., Rodriguez, M., and Lassmann, H. (2000). Heterogeneity of Multiple Sclerosis Lesions: Implications for the Pathogenesis of Demyelination. *Ann. Neurol.* 47, 707–717. doi: 10.1002/1531-8249(200006)47:6<707::AID-ANA3>3.0.CO;2-Q

Martinez, N. E., Karlsson, F., Sato, F., Kawai, E., Omura, S., Minagar, A., et al. (2014). Protective and Detrimental Roles for Regulatory T Cells in a Viral Model for Multiple Sclerosis. *Brain Pathol.* 24, 436–451. doi: 10.1111/bpa.12119

Martinez, N. E., Sato, F., Kawai, E., Omura, S., Takahashi, S., Yoh, K., et al. (2015). Th17-Biased RORγt Transgenic Mice Become Susceptible to a Viral Model for Multiple Sclerosis. *Brain Behav. Immun.* 43, 86–97. doi: 10.1016/j.bbi.2014.07.008

Minagar, A., Long, A., Ma, T., Jackson, T. H., Kelley, R. E., Ostanin, D. V., et al. (2003). Interferon (IFN)-β1a and IFN-β1b Block IFN-γ-Induced Disintegration of Endothelial Junction Integrity and Barrier. *Endothelium* 10, 299–307. doi: 10.1080/10623320390272299

Miyamoto, T., Min, W., and Lillehoj, H. S. (2002). Lymphocyte Proliferation Response During Eimeria Tenella Infection Assessed by a New, Reliable, Nonradioactive Colorimetric Assay. *Avian Dis.* 46, 10–16. doi: 10.1637/0005-2086(2002)046[0010:LPRDET]2.0.CO;2

Miyamoto, K., Miyake, S., Mizuno, M., Oka, N., Kusunoki, S., and Yamamura, T. (2006). Selective COX-2 Inhibitor Celecoxib Prevents Experimental Autoimmune Encephalomyelitis Through COX-2-Independent Pathway. *Brain* 129, 1984–1992. doi: 10.1093/brain/awl170

Nitayaphan, S., Toth, M. M., and Roos, R. P. (1985). Neutralizing Monoclonal Antibodies to Theiler's Murine Encephalomyelitis Viruses. *J. Virol.* 53, 651–657. doi: 10.1128/jvi.53.2.651-657.1985

Omura, S., Kawai, E., Sato, F., Martinez, N. E., Chaitanya, G. V., Rollyson, P. A., et al. (2014). Bioinformatics Multivariate Analysis Determined a Set of Phase-Specific Biomarker Candidates in a Novel Mouse Model for Viral Myocarditis. *Circ. Cardiovasc. Genet.* 7, 444–454. doi: 10.1161/CIRCGENETICS.114.000505

Omura, S., Sato, F., Martinez, N. E., Park, A.-M., Fujita, M., Kennett, N. J., et al. (2019). Bioinformatics Analyses Determined the Distinct CNS and Peripheral Surrogate Biomarker Candidates Between Two Mouse Models for Progressive Multiple Sclerosis. *Front. Immunol.* 10, 516. doi: 10.3389/fimmu.2019.00516

Omura, S., Sato, F., Martinez, N. E., Range, T., Ekshyyan, L., Minagar, A., et al. (2018). Immunoregulation of Theiler's Virus-Induced Demyelinating Disease by Glatiramer Acetate Without Suppression of Antiviral Immune Responses. *Arch. Virol.* 163, 1279–1284. doi: 10.1007/s00705-018-3729-6

Omura, S., Sato, F., Park, A.-M., Fujita, M., Khadka, S., Nakamura, Y., et al. (2020). Bioinformatics Analysis of Gut Microbiota and CNS Transcriptome in Virus-Induced Acute Myelitis and Chronic Inflammatory Demyelination; Potential Association of Distinct Bacteria With CNS IgA Upregulation. *Front. Immunol.* 11, 1138. doi: 10.3389/fimmu.2020.01138

Park, A.-M., Khadka, S., Sato, F., Omura, S., Fujita, M., Hsu, D. K., et al. (2020). Galectin-3 as a Therapeutic Target for NSAID-Induced Intestinal Ulcers. *Front. Immunol.* 11, 550366. doi: 10.3389/fimmu.2020.550366

Pisa, D., Alonso, R., and Carrasco, L. (2011). Fungal Infection in a Patient With Multiple Sclerosis. *Eur. J. Clin. Microbiol. Infect. Dis.* 30, 1173–1180. doi: 10.1007/s10096-011-1206-1

Pröbstel, A.-K., Zhou, X., Baumann, R., Wischnewski, S., Kutza, M., Rojas, O. L., et al. (2020). Gut Microbiota-Specific IgA$^+$ B Cells Traffic to the CNS in Active Multiple Sclerosis. *Sci. Immunol.* 5, eabc7191. doi: 10.1126/sciimmunol.abc7191

Quintin, J. (2019). Fungal Mediated Innate Immune Memory, What Have We Learned? *Semin. Cell Dev. Biol.* 89, 71–77. doi: 10.1016/j.semcdb.2018.05.023

Quintin, J., Saeed, S., Martens, J. H. A., Giamarellos-Bourboulis, E. J., Ifrim, D. C., Logie, C., et al. (2012). *Candida Albicans* Infection Affords Protection Against Reinfection via Functional Reprogramming of Monocytes. *Cell Host Microbe* 12, 223–232. doi: 10.1016/j.chom.2012.06.006

R Core team (2021). *R: A Language and Environment for Statistical Computing* (Vienna, Austria: R Foundation for Statistical Computing). Available at: https://www.R-project.org.

Rivera-Quiñones, C., McGavern, D., Schmelzer, J. D., Hunter, S. F., Low, P. A., and Rodriguez, M. (1998). Absence of Neurological Deficits Following Extensive Demyelination in a Class I-Deficient Murine Model of Multiple Sclerosis. *Nat. Med.* 4, 187–193. doi: 10.1038/nm0298-187

Rojas, O. L., Pröbstel, A. K., Porfilio, E. A., Wang, A. A., Charabati, M., Sun, T., et al. (2019). Recirculating Intestinal IgA-Producing Cells Regulate Neuroinflammation via IL-10. *Cell* 176, 610–624.e18. doi: 10.1016/j.cell.2018.11.035

Rusek, P., Wala, M., Druszczyńska, M., and Fol, M. (2018). Infectious Agents as Stimuli of Trained Innate Immunity. *Int. J. Mol. Sci.* 19, 456. doi: 10.3390/ijms19020456

Sato, F., Kawai, E., Martinez, N. E., Omura, S., Park, A.-M., Takahashi, S., et al. (2017). T-bet, But Not Gata3, Overexpression is Detrimental in a Neurotropic Viral Infection. *Sci. Rep.* 7, 10496. doi: 10.1038/s41598-017-10980-0

Sato, F., Martinez, N. E., Shahid, M., Rose, J. W., Carlson, N. G., and Tsunoda, I. (2013). Resveratrol Exacerbates Both Autoimmune and Viral Models of Multiple Sclerosis. *Am. J. Pathol.* 183, 1390–1396. doi: 10.1016/j.ajpath.2013.07.006

Sato, F., Omura, S., Jaffe, S. L., and Tsunoda, I. (2016). "Role of CD4$^+$ T Cells in the Pathophysiology of Multiple Sclerosis," in *Multiple Sclerosis: A Mechanistic View*. Ed. A. Minagar (Waltham, MA: Academic Press), 41–69.

Sato, F., Omura, S., Kawai, E., Martinez, N. E., Acharya, M. M., Reddy, P. C., et al. (2014). Distinct Kinetics of Viral Replication, T Cell Infiltration, and Fibrosis in Three Phases of Myocarditis Following Theiler's Virus Infection. *Cell Immunol.* 292, 85–93. doi: 10.1016/j.cellimm.2014.10.004

Sato, F., Omura, S., Martinez, N. E., and Tsunoda, I. (2018). "Animal Models of Multiple Sclerosis," in *Neuroinflammation*. Ed. A. Minagar (Cambridge, MA: Academic Press), 37–72.

Trandem, K., Anghelina, D., Zhao, J., and Perlman, S. (2010). Regulatory T Cells Inhibit T Cell Proliferation and Decrease Demyelination in Mice Chronically Infected With a Coronavirus. *J. Immunol.* 184, 4391–4400. doi: 10.4049/jimmunol.0903918

Trapp, B. D., and Nave, K.-A. (2008). Multiple Sclerosis: An Immune or Neurodegenerative Disorder? *Annu. Rev. Neurosci.* 31, 247–269. doi: 10.1146/annurev.neuro.30.051606.094313

Tsunoda, I., and Fujinami, R. S. (1996). Two Models for Multiple Sclerosis: Experimental Allergic Encephalomyelitis and Theiler's Murine Encephalomyelitis Virus. *J. Neuropathol. Exp. Neurol.* 55, 673–686. doi: 10.1097/00005072-199606000-00001

Tsunoda, I., and Fujinami, R. S. (2002). Inside-Out Versus Outside-In Models for Virus Induced Demyelination: Axonal Damage Triggering Demyelination. *Springer Semin. Immunopathol.* 24, 105–125. doi: 10.1007/s00281-002-0105-z

Tsunoda, I., Kuang, L.-Q., Igenge, I. Z. M., and Fujinami, R. S. (2005). Converting Relapsing Remitting to Secondary Progressive Experimental Allergic Encephalomyelitis (EAE) by Ultraviolet B Irradiation. *J. Neuroimmunol.* 160, 122–134. doi: 10.1016/j.jneuroim.2004.11.007

Tsunoda, I., Kuang, L.-Q., Libbey, J. E., and Fujinami, R. S. (2003). Axonal Injury Heralds Virus-Induced Demyelination. *Am. J. Pathol.* 162, 1259–1269. doi: 10.1016/S0002-9440(10)63922-3

Tsunoda, I., Kuang, L.-Q., Tolley, N. D., Whitton, J. L., and Fujinami, R. S. (1998). Enhancement of Experimental Allergic Encephalomyelitis (EAE) by DNA Immunization With Myelin Proteolipid Protein (PLP) Plasmid DNA. *J. Neuropathol. Exp. Neurol.* 57, 758–767. doi: 10.1097/00005072-199808000-00005

Tsunoda, I., Libbey, J. E., Kuang, L.-Q., Terry, E. J., and Fujinami, R. S. (2005). Massive Apoptosis in Lymphoid Organs in Animal Models for Primary and Secondary Progressive Multiple Sclerosis. *Am. J. Pathol.* 167, 1631–1646. doi: 10.1016/S0002-9440(10)61247-3

Tsunoda, I., Tanaka, T., and Fujinami, R. S. (2008). Regulatory Role of CD1d in Neurotropic Virus Infection. *J. Virol.* 82, 10279–10289. doi: 10.1128/JVI.00734-08

Tsunoda, I., Terry, E. J., Marble, B. J., Lazarides, E., Woods, C., and Fujinami, R. S. (2007). Modulation of Experimental Autoimmune Encephalomyelitis by VLA-2 Blockade. *Brain Pathol.* 17, 45–55. doi: 10.1111/j.1750-3639.2006.00042.x

Wang, M., Feng, L.-R., Li, Z.-L., Ma, K.-G., Chang, K.-W., Chen, X.-L., et al. (2021). Thymosin β4 Reverses Phenotypic Polarization of Glial Cells and Cognitive Impairment via Negative Regulation of NF-κB Signaling Axis in APP/PS1 Mice. *J. Neuroinflamm.* 18, 146. doi: 10.1186/s12974-021-02166-3

Yamada, M., Zurbriggen, A., and Fujinami, R. S. (1990). Monoclonal Antibody to Theiler's Murine Encephalomyelitis Virus Defines a Determinant on Myelin and Oligodendrocytes, and Augments Demyelination in Experimental Allergic Encephalomyelitis. *J. Exp. Med.* 171, 1893–1907. doi: 10.1084/jem.171.6.1893

Conflict of Interest: The authors declare that the research was conducted in the absence of any commercial or financial relationships that could be construed as a potential conflict of interest.

Publisher's Note: All claims expressed in this article are solely those of the authors and do not necessarily represent those of their affiliated organizations, or those of the publisher, the editors and the reviewers. Any product that may be evaluated in this article, or claim that may be made by its manufacturer, is not guaranteed or endorsed by the publisher.

Advantages of publishing in Frontiers

OPEN ACCESS
Articles are free to read for greatest visibility and readership

FAST PUBLICATION
Around 90 days from submission to decision

HIGH QUALITY PEER-REVIEW
Rigorous, collaborative, and constructive peer-review

TRANSPARENT PEER-REVIEW
Editors and reviewers acknowledged by name on published articles

Frontiers
Avenue du Tribunal-Fédéral 34
1005 Lausanne | Switzerland

Visit us: www.frontiersin.org
Contact us: frontiersin.org/about/contact

REPRODUCIBILITY OF RESEARCH
Support open data and methods to enhance research reproducibility

DIGITAL PUBLISHING
Articles designed for optimal readership across devices

FOLLOW US
@frontiersin

IMPACT METRICS
Advanced article metrics track visibility across digital media

EXTENSIVE PROMOTION
Marketing and promotion of impactful research

LOOP RESEARCH NETWORK
Our network increases your article's readership